TECHNISCHE UNIVERSITÄT MÜNCHEN

Institut für Siliciumchemie,
WACKER-Lehrstuhl für Makromolekulare Chemie

Silicon Containing Mesogen Building Blocks -

Synthesis, Characterization and Application in Silane and Siloxane Self-Assembly

Dipl.-Chem. Paul Heinz

Vollständiger Abdruck der von der Fakultät für Chemie der Technischen Universität München zur Erlangung des akademischen Grades eines Doktors der Naturwissenschaften genehmigten Dissertation.

Vorsitzende: Univ.-Prof. Dr. Sevil Weinkauf

Prüfer der Dissertation:

1. Univ.-Prof. Dr. Dr. h.c. Bernhard Rieger
2. Univ.-Prof. Dr. Klaus Köhler

Die Dissertation wurde am 14.02.2012 bei der Technischen Universität München eingereicht und durch die Fakultät für Chemie am 08.05.2012 angenommen.

“If I would have asked them what they want, they would have said faster horses”

(Henry Ford, 1863-1947)

Acknowledgements

This dissertation was prepared at the Institute of Silicon Chemistry and the WACKER-Chair of Macromolecular Chemistry at the Technische Universität München in the period between August 2007 and March 2011 under the supervision of *Prof. Dr. Dr. h.c. Bernhard Rieger*.

Prior to describing the topic and the results, I would like to express my deepest gratitude to all people who contributed to the success of this work. In particular, I would like to thank *Prof. Rieger* for the opportunity to pursue my research at his working group and giving me every 'degree of freedom' in defining the topic and following new ideas. I also want to thank him for his patience, numerous fruitful discussions, and for his open door and attentive ear to any kind of questions.

Furthermore I want to thank WACKER Chemie AG for financial support through granting me the WACKER Presidential Science Award.

This work would not have been possible without various internal and external cooperation partners. Therefore I would like to thank the following people:

- *Prof. Dr. Christine M. Papadakis* from the Physics Department of the TU München for providing the possibility to perform SAXS and GISAXS measurements at the synchrotron radiation source HASYLAB at the 'Deutsches Elektronen Synchrotron' (DESY) in Hamburg and also for many discussions and her invaluable contribution to our publication in *ChemPhysChem*.
- *Prof. Dr. Sevil Weinkauf* and *Dr. Marianne Hanzlik* from the Electron Microscopy Department of the TU München, for many TEM and SEM measurements, valuable discussions and especially for hosting our STM device at their premises.
- *Dr. Jürgen Heindl* and *Dr. Matthias Rodewald* from JEOL Germany for SEM and TEM measurements.
- *PD Dr. Hubert Rauscher*, *Dr. Giacomo Ceccone* and *Dr. Douglas Gilliland* from the Institute for Health and Consumer Protection, DG Joint Research Centre, European Commission in Ispra (VA, Italy) for their assistance in XPS, DLS, and Ellipsometry measurements. Also many thanks to *Francesco Fumagalli* for hosting me during two visits in Ispra and for lots of experiments on the plasma reactor.

Natürlich möchte ich mich auch bei meinen Kollegen am Institut für Siliciumchemie und am WACKER-Lehrstuhl für die tolle Zeit, die ich mit Ihnen in den letzten Jahren verbringen durfte, bedanken. Ganz besonders bedanke ich mich bei *Dr. Carsten Troll* und *Dr. Sergei Vagin* für ihre Unterstützung in technischen, administrativen und wissenschaftlichen Fragen. Weiterhin danke ich *Aleksandra Jonovich*, *Katia Rodewald* und *Dr. Uwe B. Seemann* für zahllose Messungen an der GPC. *Sanna Zimmer* gilt mein besonderer Dank für ihre Hilfe beim Drucken, Binden und Einreichen der Arbeit. Und schließlich auch vielen Dank an meine ehemaligen Laborkollegen *Dr. Robert Luxenhofer, Dr. Michael Reif*, *Tobi van Deisner*, *Abdussalam Qaroush* und *Konrad Hindelang* für die tolle Arbeitsatmosphäre im Labor.

Auch bei meinen ‚Masteranden' und ‚Diplomanden' sowie bei meinen Forschungspraktikanten möchte ich mich für die gute Zusammenarbeit und ihre zahlreichen Resultate, ohne die weder diese Arbeit, noch die Publikationen möglich waren. Im Einzelnen waren das (in chronologischer Reihenfolge): *Sascha Erhardt*, *Annemarie Frey*, *Linus Schulz*, *Michael Wegener*, *Konrad Hindelang*, *Christian Anger* und *Florian Golling*. Ich wünsche Euch alles Gute auf dem weiteren Weg!

Ganz besonderer Dank gilt einer ganz speziellen Kollegin und gleichzeitig meiner Partnerin. Danke *Moni* für Deine Unterstützung und für Deine unendliche Geduld in allen Lebenssituationen. Deine Liebe und Treue bedeutet mir alles! Vielen Dank auch für die vielen Wochenenden die Du während dem Schreiben der Arbeit geopfert hast um mir den Rücken freizuhalten - wir werden alles nachholen! Natürlich auch vielen Dank fürs Lesen und Korrigieren.

Zuletzt bedanke ich mich ganz herzlich bei meiner Familie. Ganz besonders möchte ich meinen Eltern danken die mich all die Jahre - nicht nur finanziell - unterstützt haben. Vielen Dank auch meiner Schwester dass Sie mir zwei so tolle Patenkinder geschenkt hat. Ich wollte nie etwas anderes als Euch stolz zu machen!

Table of Contents

Abbreviations

(in alphabetical order)

AFM	Atomic force microscopy
b.p.	boiling point
BP	*BAYER*-process
Bu	Butyl
BuLi	Butyl lithium
CMC	Critical micelle concentration
d	Diameter
δ	Chemical shift in NMR
DBS	Diffuse *Bragg* sheets
DLS	Dynamic light scattering
DP	Degree of polymerization
DSC	Differential scanning calorimetry
EDX	Energy dispersive X-ray spectroscopy
Eq.	Equation
Et	Ethyl
et al.	And coworkers (*lat.: et alii*)
etc.	And so on (*lat: et cetera*)
FTIR	Fourier transform infrared spectroscopy
GISAXS	Grazing incidence small angle X-ray scattering
GPC	Gel permeation chromatography

HOMO	Highest occupied molecular orbital
IBX	2-Iodoxy benzoic acid
ICP	Inductively coupled plasma
IR	Infrared spectroscopy
LB	*Langmuir-Blodgett*
LUMO	Lowest unoccupied molecular orbital
m	Mass
M	Molecular mass
Me	Methyl
MMA	Methyl methacrylate
M_n	Number average molecular weight
m.p.	melting point
M_w	Weight average molecular weight
MRP	*Müller-Rochow*-Process
NHC	N-heterocyclic carbene
NMR	Nuclear magnetic resonance
OFET	Organic field effect transistor
OLED	Organic light emitting diode
PDI	Polydispersity index
Ph	Phenyl
POM	Polarized optical microscopy
POSS	Polyhedral oligomeric silsesquioxane
pPhS	polyphenylsilane
ppm	parts per million
prim.	Primary
PV	Photovoltaic
RF	Radio frequency
RI	Refractive index
rms	Root mean square
RT	Room temperature
SAXS	Small angle X-ray scattering
sec.	Secondary

SLS	Static light scattering
TBAF	Tetrabutyl ammoniumflouride
TCB	1,2,4-Trichloro benzene
TEM	Transmission electron microscopy
tert.	Tertiary
TGA	Thermogravimetric analysis
THF	Tetrahydrofurane
TMS	Tetramethylsilane
TMS-Ac	Trimethylsilyl-protected acetylene
TMV	Tobacco mosaic virus
WLI	White light interferometry
WP	*WACKER*-process

1 Introduction

While carbon is the most important building block of ‘organic life’, silicon can be considered to be the eminent building block of ‘inorganic life’.[1] With a mass fraction of 27%, silicon is the second most abundant element in the earth crust (*Figure 1.1*) and the eighth most abundant element in the whole universe.[2] But in contrast to carbon and due to its high oxophilicity, it only occurs in different forms of silicates where it is bound to oxygen. In its bound form, it is even the most important component of the earth crust, since 90% of the earth’s minerals are composed of silicates. Its ability to form a broad variety of meso-, soro-, cyclo-, ino-, phyllo-, or tectosilicates is the basis of its broad usability and the today’s importance in scientific research and industrial products.

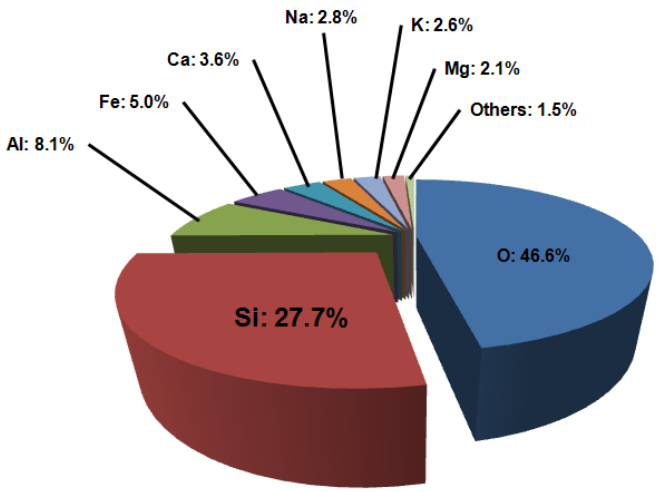

Figure 1.1 *Abundance of elements in the earth crust.*[2]

In the mineral world, the most important silicates are the tectosilicates feldspar ($KAlSi_3O_8$/$NaAlSi_3O_8$) and quartz (SiO_2). While feldspar is mostly used in glass and ceramics fabrication, quartz is the main industrial source material for manifold silicon containing compounds. Here the most important form is of course metallic silicon in metallurgical grade (~98% Si), which is on the one hand the main source material for the production of silicones, and on the other hand is a superior blend component for metals, such as aluminum, iron, or calcium, to obtain high-performance alloys. Furthermore, the metallurgical silicon can also be converted to higher purity grades, such as polycrystalline silicon for photovoltaics (PV) and other electronic components. The worldwide production of metallurgical silicon in variable purities amounts to more than 6,000,000 t per year, and is driven mostly by three different regions in the world (*Figure 1.2*), namely China (55%), Americas (20%), and Western Europe (17%).[3-4]

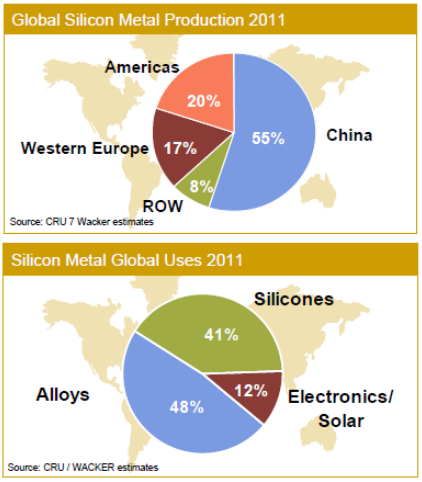

Figure 1.2 *Global view on Si production and its uses in 2011.*[4]

The importance of silicon in the development of semiconducting materials arose in the mid of the last century and is continuously growing since the foundation of microelectronics in the late 1940's, when Bardeen, Shockley and Brattain developed the first bipolar transistor at the BELL laboratories in Murray Hill (USA).[5] For this discovery they were awarded with the Nobel Prize in 1956. Although the first discoveries in the field of transistors were based on germanium as semiconducting material, the development of a method for ultra-pure monocrystalline silicon, the so-

called zone melting process, in 1954 by Eberhard Spenke at SIEMENS AG in Munich (Germany), caused a breakthrough of silicon based semiconductors in the microelectronics technology.[6] In the same year, once again at the BELL laboratories, Chapin, Fuller, and Pearson developed the first silicon based PV-cells, which already provided an efficiency factor of 4%.[7] This discovery was a second boost for the demand of silicon metal. Thenceforward the developments in the PV technology went on steadily, until in the 1960s the first solar panels were used in satellites and other aerospace applications. Since the 1970 the demand of silicon in the semiconductor and photovoltaic industry is continuously growing. Nowadays the world's leading silicon producing companies still tend to constantly increase their production capacities. The WACKER AG for instance, plans to increase its production capacities of polycrystalline silicon from 2006 to 2014 by a factor of 10 (*Figure 1.3*).[4] This expansion is based on a worldwide extremely high public demand for alternative energies implicated by recent regulations of manifold national administrations, such as USA, Japan, or Germany. Although today's PV devices, which are equipped with monocrystalline silicon, provide much higher efficiencies (28%) than the ones with polycrystalline silicon (18%), the market share for polycrystalline silicon in the PV industry is much higher than for monocrystalline silicon (*Figure 1.3*). This tendency reflects the global business trend towards increasing demand of low-cost production methods.

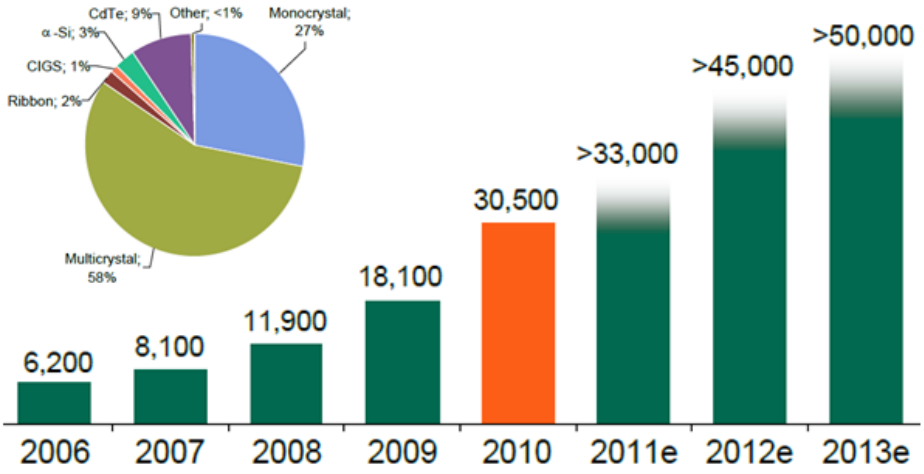

Figure 1.3 *Polysilicon production of WACKER AG (in t) between 2006 and 2013 (from 2011 on: estimated values) and photovoltaic technology world market shares in 2010.[4]*

In the periodic table, silicon can be found in the same main group as carbon. Although these two elements therefore exhibit some analogies concerning the nature of bonding and the chemistry, the discrepancies between the elements are predominant. The most peculiar discrepancy is the lacking of structural varieties in the case of silicon compared to the diverse allotropes of carbon. Until the 1960s only two different modifications of carbon, two-dimensional graphite and three-dimensional diamond, were known. But the development of novel synthesis methods and powerful analysis tools facilitated the discovery of other carbon allotropes, such as fullerenes, nanotubes, or graphenes. These allotropes are built up from C-C p_π-p_π-bonds and therefore exhibit outstanding electronic properties. Hence they are considered to be the revolutionary materials for emerging electronic compounds.[8] For this reason, in the last decades many efforts have been undertaken to find similar regular silicon based structures, for which even more interesting electronic properties can be expected. But owing to the low stability of the p_π-p_π-bond between two Si atoms and the highly reactive nature of silicon based intermediate compounds, the discovery of analogous silicon allotropes was not possible up to date.

Despite the apparent hurdles towards the formation of regular hierarchically structured silicon architectures, the motivation to find a material with exceptional electronic and mechanic properties and possible applications in future electronic and photovoltaic components legitimates further efforts in research and development.

In the present work, a novel approach towards the development of a construction kit based on silicon containing building blocks is presented. Within this construction kit, classical polysilane synthesis is combined with modern concepts of molecular self-assembly, to obtain novel hierarchically structured silicon based architectures.

2 Theoretical Background

2.1 Supramolecular Chemistry and Self-Assembly Phenomena

Although the concepts and roots of supramolecular chemistry are found in the early 19th century, the discovery of the scientific field as we know it today can be dated back to the late 1960s. Therefore supramolecular chemistry, the so called 'chemistry beyond the molecule' is a relatively young discipline.[9] The pioneering work in this area has been performed by D.J. Cram, J.-M. Lehn, and C.J. Pedersen. Their scientific interests were related to host-guest-interactions and molecular recognition in complexes with macrocyclic ligands, such as crown ethers, hemes, and cyclophanes.[10] In 1987 the work of these pioneers was honored with the Nobel Prize, and in the last years, supramolecular chemistry has become a major field of chemistry, penetrating deeply into its neighbor disciplines biology and physics. Host-guest-complexes, where the 'host'-molecules possess defined selectivities for different 'guests', are nowadays widely spread as the base for advanced technologies in many scientific sub-disciplines such as nanotechnology and material science, analytical and medicinal chemistry, or even polymer chemistry and catalysis.

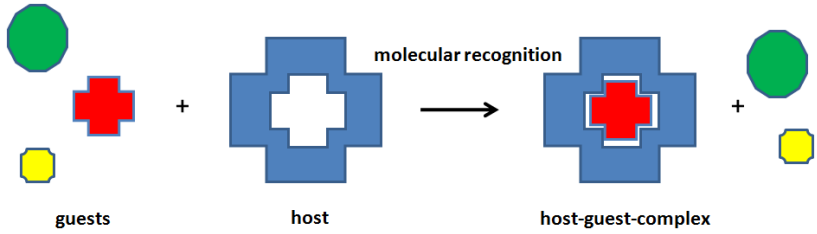

Figure 2.1 *Illustration of the host-guest-complex formation.*

Highly selective host-guest interactions based on molecular recognition can be observed when a substrate binds to an enzyme, a drug sticks to its target, or signals propagate between cells.[9] Therefore it always was considered as highly essential to understand the origins of these interactions. The basic host-guest-concept of supramolecular chemistry is illustrated in *Figure 2.1* on the example of an analytic procedure. In this illustration the differently colored compounds represent a matrix solution with different analytes. The host-molecule is a comparably large molecule (blue) which contains a sizeable hole or cavity with certain convergent binding sites. The guest molecule on the other hand, is a molecular entity which is small enough to fit into the cavity and possesses divergent binding sites (red). The other molecules of the matrix (yellow, green) are either too big, or do not contain the suitable divergent binding sites to form a host-guest-complex, and hence remain during the analytical process in solution. The hosts can be composed of large organic molecules, such as crown ethers, cyclophanes, or even enzymes or antibodies, as well as inorganic systems, such as zeolites or polyoxometalates; whereas the bandwidth of guest molecules ranges from small inorganic cations to more complex systems such as hormones or antigens.[10]

In general, the intermolecular bonding interactions between host and guest systems are of a noncovalent nature.[11] These noncovalent interactions cover a broad variety of attractive and repulsive forces, with different ranges of dissociation energies. The most important interactions are ion-ion-, dipole-dipole-, and ion-dipole-interactions, as well as hydrogen bonds,[12] π-π-stacking,[13] Van-der-Waals forces, and hydrophobic interactions.[14] In *Table 2.1* the energy ranges of these interactions, which vary between 0 and 350 kJ/mol, are summarized. In a supramolecular system of course the interplay of all these interactions, as well as the interplay with the surrounding medium, must be considered; but the contribution of the individual forces can easily be influenced by the design of the molecular structure.[10]

Table 2.1 *Intermolecular interactions and their corresponding dissociation energies.*

Interaction	Energy [kJ/mol]
ion-ion	100 - 350
ion-dipole	50 - 200
dipole-dipole	5 - 50
hydrogen bonding	4 - 120
π-π-stacking	0 - 50
Van-der-Waals forces	<5

It is important to mention, that the idea of supramolecular systems did not arise from chemical laboratories; it was rather first observed in nature and subsequently transferred to the synthetic labs. In living biological systems, self-assembly by molecular recognition is a fundamental principle since the dawn of time. Complex systems, such as nucleic acids assembled by noncovalent interactions, establish the basis of the living biological world.[15] The supramolecular chemistry of life has furthermore developed manifold forms of self-organized systems, which were essential for the development of biological life. Important examples besides nucleic acids are cell membranes built up from phospholipide bilayers with their lipophilic carrier molecules, various porhyrin complexes, which are involved in basic processes like oxygen transport or photosynthesis, and of course a broad variety of tertiary and quaternary structures of enzymes and co-enzymes.

The structurally maybe most impressive example for natural host-guest-assemblies in biological systems, can be found in the world of helical viruses: the Tobacco Mosaic Virus (TMV), which has first been described in the late 19th century.[16-17] Although it is up to date the most investigated and understood viral system, it is still responsible for a severe infect and therefore causes serious decrease in profits of different economically important plants, such as tobacco, tomatoes or pepper. This virus exhibits a tubular structure of approx. 300 nm in length and 20 nm in width (*Figure 2.2 (a)*),[18] and is built up from a single strand of RNA with approx. 6000 nucleobases, which is encased

by more than 2000 hull-proteins (*Figure 2.2 (b)*).[19] Surprisingly, the virus shows the ability to dissociate into its building blocks under slightly alkaline conditions, and reversibly rearranges and recovers its operational capability under physiological conditions. The main driving forces for this reversible supramolecular organization are hydrogen bonds, as well as electrostatic and solvophobic effects.[20] This structural motif inspired many scientists in developing columnar and tubular self-assembled liquid crystals.

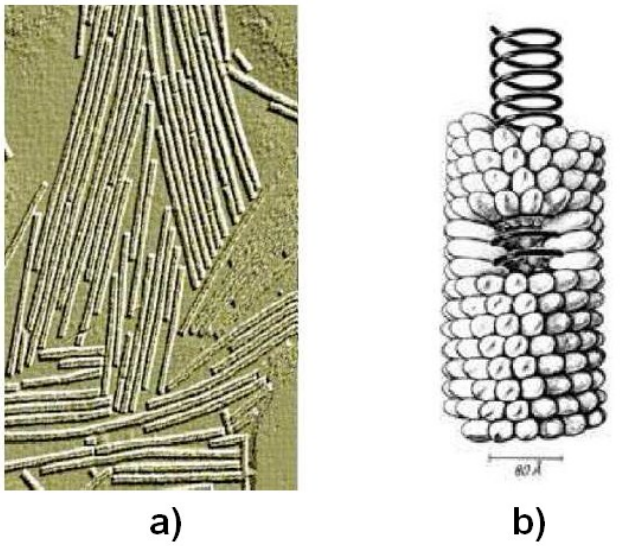

Figure 2.2 *(a) Transmission electron micrograph of the tobacco mosaic virus; (b) schematic drawing of host-guest-interactions forming the inner structure of the tobacco mosaic virus.[18-19]*

Self-assembly by molecular recognition for the formation of systems with high complexity is of course not restricted to bi-molecular host-guest systems. Utilization of molecular design possibilities and therefore harnessing of the previously described intermolecular interactions, allows also the formation of hierarchically structured assemblies, which are built up from only one compound. In the following, different forms of mono-molecular self-assembled systems, which utilize this ‘bottom-up’ principle, are described.

2.1.1 Different Forms of Single Molecule Self-Assembly

At a glance, the formation of mono-molecular self-assembling aggregates requires different polarities or solubilities in one single molecule, which is referred to as amphiphilic molecule (Greek: amphi = between, on both sides; phil = friend) or surfactant. Typical surfactants bear polar non-ionic or even charged an- or cationic head groups in combination with large non-polar organic hydrocarbon based tails. Famous examples for amphiphiles are soap (sodium lauryl sulphate) or phospholipids. Such amphiphiles form numerous supramolecular assemblies, which in turn can serve as host systems or provide organized environments for intermolecular interactions between other molecules.[10-11,21-22] In the following, some selected forms of self-assembled systems (see *Figure 2.3*) are presented.

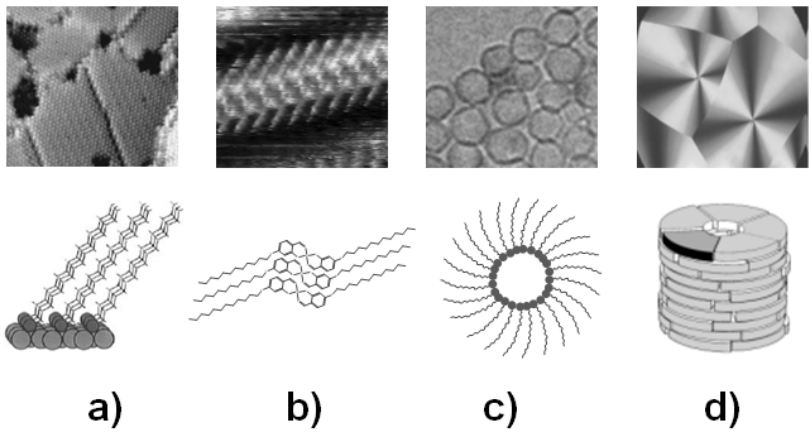

Figure 2.3 *Figures and Schemes describing different self-assembly phenomena: (a) self-assembled monolayers of molecular brushes;[23] (b) two-dimensional crystals of metal organic complex on solid-liquid interface.[24] (c) micellar structures;[25] (d) three-dimensional liquid crystalline assemblies.[26]*

The simplest and best-characterized assembly-forms of surfactants are monolayers, which usually appear at interfaces of liquids of different polarities (oil/water), as well as on liquid-air or liquid-solid interfaces. One prominent example for monolayers in real life is the reduction of surface tension of water by formation of a monolayer of soap-molecules at the air-water interface.[27]

Such liquid-air interface monolayers can be transferred to substrate surfaces using the *Langmuir-Blodgett* (LB) transfer technique; i.e. by slowly raising a solid substrate from the liquid through a monolayer which is spread on the surface of the liquid. During the raising process, the monolayer is transferred to the substrate, depending on the polarities of liquid and substrate surface (*Figure 2.4 (a)*). Using this approach, the polarity of the substrate surface can be inverted, since the differently polarized surfactant molecules orientate themselves according to the polarity of the substrate.[28] One important application of the LB method is the synthesis of solid supported biomimetic membranes (see *Figure 2.4 (b)*).[29] Two major advantages of the LB method are: on the one hand besides monolayers also multilayer can be prepared, and on the other hand also the incorporation of various additives in the self-assembled film is possible. A noteworthy disadvantage is the low stability towards mechanical stress or solvents of the gel-like films.[11]

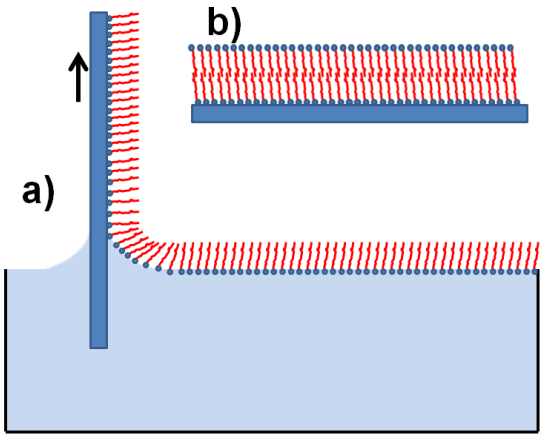

Figure 2.4 *Schematic representation of the LB transfer method (a) and a solid supported biomimetic membrane (b).*

Another way of preparing monolayers on substrate surfaces involves chemisorption (i.e. reactions between the head group of a surfactant molecule and functionalities on the surface of the substrate) of the monolayer film from solution. Using this technique, the so-called self-assembled monolayers (SAMs) or molecular brushes on solid supports are obtained (*Figure 2.3 (a)*).[11,30-31] The most prominent examples are long-chain alkanethiols, which are bound to gold or silver surfaces, as well as long-chain alkyl

functionalized alkoxy- or chlorosilanes chemisorbed on SiO_2 substrates.[23,32-34] In the case of the mercaptane head groups, the interactions with the metal substrates are considered as oxidative addition of the SH functionality to the metal surfaces under H_2 evolution; whereas the alkoxy or chloro functionalized alkylsilanes react with Si-OH functionalities on the SiO_2 surface under formation of Si-O-Si-bonds and subsequent elimination of alcohols or HCl. The alkanethiol and alkylsilane monolayers are mostly used for the fabrication of sensors[35] and in surface hydrophobization reactions,[36] respectively.

Besides brush like assemblies on solid supports, a second possibility for SAMs on surfaces, the formation of so-called two-dimensional (2D) crystals, is known (*Figure 2.3 (b)*). Surface nano patterns, consisting of such 2D crystals can be formed on the interface between a solid substrate and the corresponding solution, and usually are built up from, for instance, organometallic complexes with long-chain alkyl substituents or their respective ligands.[37] Utilization of the 2D crystallization technique allows for fine tuning of sizes and morphologies of the nano patterns by simply changing the ligand design or the coordination metal.[24,38] Furthermore this technique enables the formation of magnetic nano patterned surfaces for emerging applications in molecular electronics.[39]

Formation of mono- and bilayers at interfaces is only one example for the assembly of amphiphiles. Another possible form of surfactant self-organization is the formation of micellar structures (*Figure 2.3 (c)*), which occurs if the concentration of surfactants exceeds the so-called critical micelle concentration (CMC). At that time the air-liquid interface becomes saturated and the surfactant molecules therefore start to find alternative arrangements - the micelles. In an aqueous solution the lipophilic tails of the surfactant molecules are oriented towards the center of the micelles, whereas the hydrophilic head groups arrange themselves to the outside. In an organic solution the situation is of course the other way round. The possible shape of the micelles is not limited to spheres; it can rather change to rod-like cylindrical assemblies or even more complex structures (which then resemble lyotropic liquid crystals), each with own particular CMC.[40]

Of course self-assembly phenomena are not limited to molecules in solution. Already in the late 19th century, Reinitzer *et al*. first described the appearance of distinct color effects in molten compounds of cholesterol derivatives.[41] This optical effects led to conclusions that the molten state consists of superordinate structures of cholesterol molecules.[42] Such formation of discrete structures with long-range order in liquid bulk materials is nowadays referred to as mesomorphic or liquid crystalline behavior.[10]

Typically, liquid crystal phases or mesophases are distinguished between lyotropic and thermotropic (*Figure 2.5*). Lyotropic mesophases are formed in solution by variation of concentration, whereas thermotropic mesophases occur as intermediate steps during the thermal transition from the highly oriented crystalline state to the disordered isotropic melt.[43] Furthermore, thermotropic mesophases can be either enantiotropic or monotropic: enantiotropic mesophases are stable between the crystal melting temperature and the isotropization temperature, whereas monotropic mesophases are only stable below the melting temperature and hence can only be obtained by supercooling of the isotropic melt.[44-45] Thermotropic mesophases can further be classified as nematic, smectic, cholesteric or discotic columnar, which differ in anisotropic orientation (*Figure 2.5*).

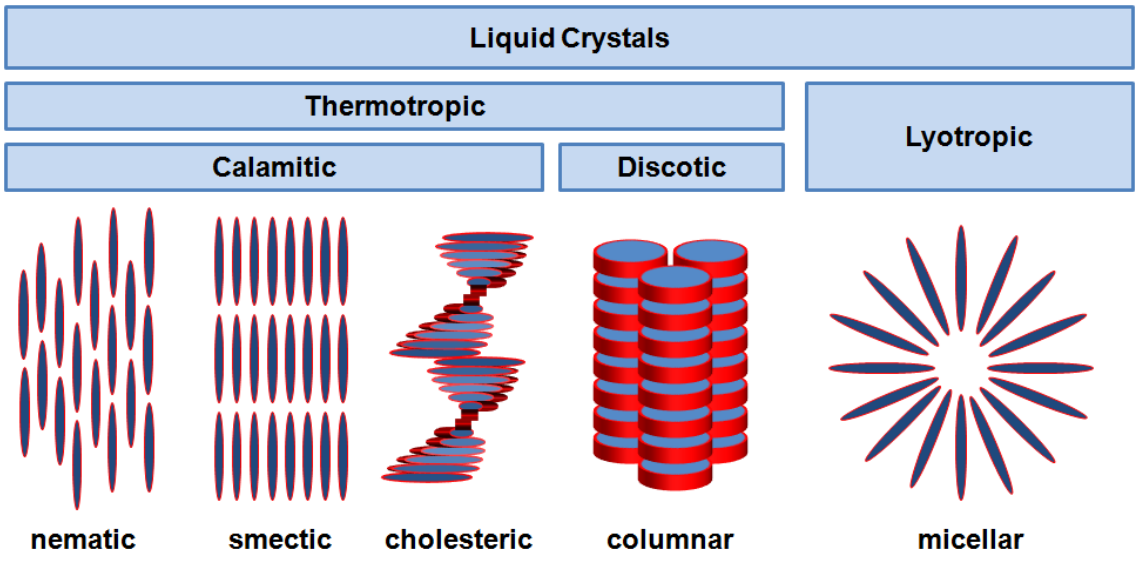

Figure 2.5 *Schematic representation of the classification of liquid crystals.*

2.2 Silicon Containing Oligomers and Polymers

In today's industrial processes, silicon based polymers are the most important polymers with a completely inorganic backbone. Since their discovery in the early 20th century by F.S. Kipping, the interest in silicon containing polymers is continuously growing. The most prominent examples are the manifold polyorganosiloxanes, also known as silicones (*Scheme 2.1 (a)*). Their backbone is composed of alternating silicon and oxygen atoms. Furthermore, they are characterized by chemical and physiological inertness and possess outstanding thermal and mechanical properties.[46-47]

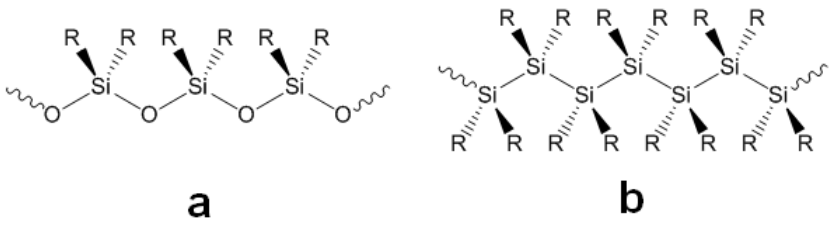

Scheme 2.1 *Sections of the polymeric backbones of (a) polysiloxanes and (b) polysilanes.*

Another important class of Si-polymers are polysilanes, which have a backbone that consists exclusively of catenated Si-atoms (*Scheme 2.1 (b)*).[48-49] This class of materials is very interesting for electronic applications, since it shows certain conductivity due to σ-conjugation along the silicon main chain.[50] Although they have been discovered in the 1920s, synthetic methods for Si-Si bond formation are very rare up to now.

2.2.1 Basic Materials

Production of silicon containing polymers requires as basic material of course metallic silicon. Large-scale synthesis of the metal is performed by electrothermal reduction of SiO_2 with carbon (*Eq. 2.1*).

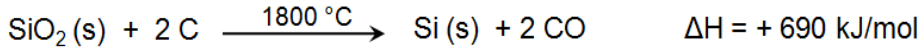

(2.1)

This highly energy consuming process (14 kWh/kg Si) yields every year worldwide more than 6,000,000 t of Si with a purity of up to 99%,[3] which forms the basis for the so-called *Müller-Rochow*-process (MRP). The MRP, which is shown in *Eq. 2.2*, was developed by Müller and Rochow independently during World War II and is nowadays the most important source for chlorosilanes, which are the common monomers for the production of polysiloxanes and polysilanes. Of course dimethyldichlorosilane is only one besides other byproducts with varying substitution motifs (trimethylchlorosilane, methyltrichlorosilane). Differently substituted silanes are technically separated by rectification.

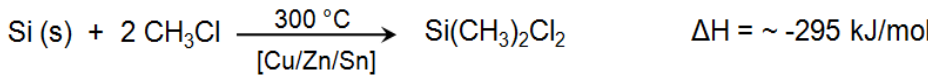

(2.2)

It is well known, that the MRP requires a high purity of Si. With regards to economically efficient production, Si with semiconductor quality cannot be used for the process. Therefore the Si-producing companies have to find appropriate feedstocks to reduce impurities.[47] From *Eq. 2.2* it becomes apparent, that for large scale synthesis of the silane monomers, a large scale source of methylchloride is required. Three different ways are conceivable: chlorination of methane, esterification of methanol with hydrogen chloride, or the methanolysis of chlorosilanes. The first possibility is not effective, and therefore it is not used in industry. The latter two ways are typical industrial strategies, since they are utilizing byproducts of silicone production. A detailed description of the closed production loop is given in the following section.

2.2.2 Polysiloxanes

2.2.2.1 Synthesis

For the synthesis of polysiloxanes many approaches are known. Although many of them are limited to laboratory scale, some found their way into large scale industrial synthesis. Usually the formation of polysiloxanes can be divided in a two step process, first the synthesis of oligomers, and second the chain extension to high molecular weight polymers. All strategies are dealing in the first step with hydrolysis and condensation of silanes, which are substituted with hydrolysable groups, such as chloro or alkoxy functionalities. In the following, three different industrially implemented ways for oligosiloxane synthesis are described:

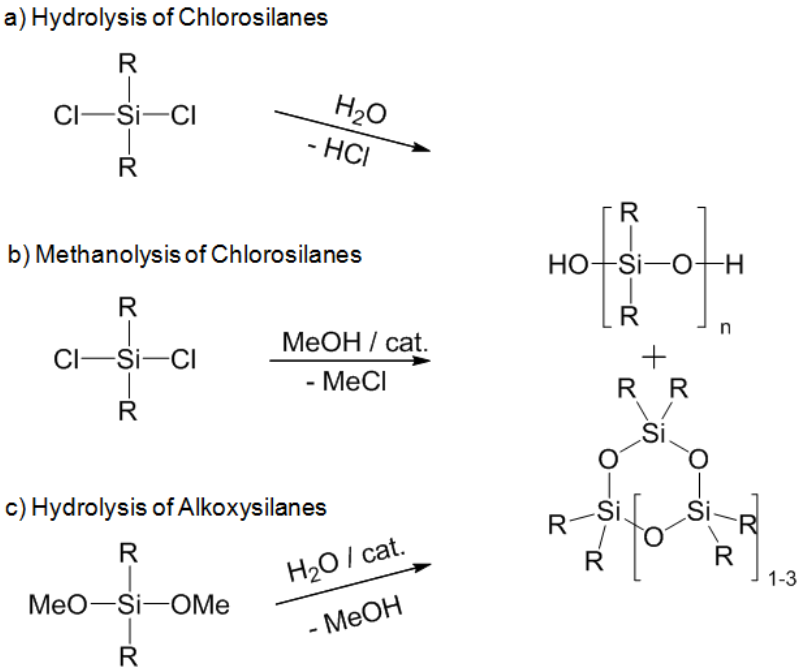

Scheme 2.2 *Schemes describing different industrially implemented synthesis strategies for oligosiloxane prepolymers.*

a) Hydrolysis of chlorosilanes: The hydrolysis and condensation of chlorosilanes is the most important industrial process. As products, linear and cyclic oligosiloxanes are obtained. The molecular masses of both, linear and cyclic compounds are comparably low, i.e. the expected cycles are six to ten membered rings, and the degree of polymerization (DP) of the linear compounds ranges between 30 and 50. The product distribution between linear and cyclic, as well as the molar masses of cyclic compounds can be controlled by different reaction conditions. For instance the addition of silane to water leads to significantly lower molecular masses than the addition of water to silane. Generally a high dilution of the reaction mixture strongly favors cycle formation, whereas fast removal of HCl favors the formation of linear compounds. Hydrolysis of chlorosilanes has the big advantage that HCl, as the only hydrolysis byproduct, can be recycled in a closed loop and reused in the methylchloride production by esterification of methanol (see *Chapter 2.2.1*).[47] A noteworthy disadvantage of this technique is the corrosive nature of HCl; since the industrial reaction vessels usually consist of steel, their lifetime is decreased. The resulting product mixture of linear and cyclic compounds and the low molecular masses require one further production step to obtain high molecular mass siloxanes, which can be one of the chain extension steps in *Scheme 2.3*.

b) Methanolysis of chlorosilanes: Polysiloxane formation by methanolysis and condensation of chlorosilanes is widely known as the *WACKER*- (WP) or the *BAYER*-process (BP). Both processes use chlorosilanes and aqueous methanol but differ strongly in process management. Basically, in the WP a packing material filled counter flow reactor is used, whereas the BP is operated in a column reactor with zinc chloride as catalyst. The WP and the BP lead to linear and cyclic polysiloxanes, respectively. Advantageous in both processes, is the formation of methylchloride as byproduct, which can directly be used in the MRP without an additional esterification step. The amount of methylchloride can even be controlled by addition of HCl during the reaction. Again the formed oligomers require further chain extension steps.[47]

c) Hydrolysis of alkoxysilanes: Hydrolysis and condensation of alkoxysilanes can be run in principle as already described for chlorosilanes. Product distribution and molecular weight can be controlled in the same way. No corrosive intermediates and byproducts occur in this reaction. But since the formation of alkoxysilanes is a complicated step in the process chain, this reaction is of rather low importance in industry.

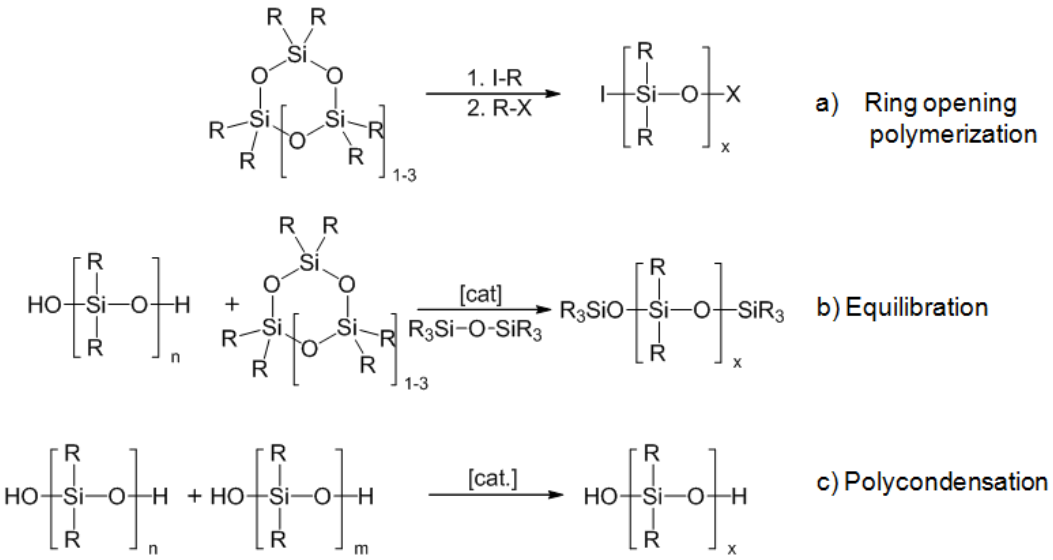

Scheme 2.3 *Schematics describing different techniques for chain extension of oligosiloxanes.*

All techniques, which are described above lead only to the formation of linear and cyclic siloxane oligomers. But for the most technical applications high molecular masses are required. Therefore, different chain extension reactions, which increase the molecular masses drastically, have been developed. In the following the three major techniques, which are depicted in *Scheme 2.3* are described:

a) Ring opening polymerization: The cyclic siloxane oligomers can act as monomers in ionic polymerizations. As initiators in anionic polymerizations nucleophilic bases, such as alkaline silanolates, organolithium compounds, phosphazene bases, or even KOH are used. In cationic polymerization possible initiators are strong *Brønstedt* or *Lewis* acids, such as sulfonic and sulfuric acids, fluorinated acetic acids, or $PNCl_2$. The mechanism of the anionic polymerization, which consists of nucleophilic ring opening, chain

propagation, and determination, is very well understood, whereas the mechanism of the cationic polymerization is still under investigation. The reaction rates are strongly influenced by the ring size; the lowest rates are expected with eight membered rings (D_4). An increase of the reaction rates can be established by polar solvents or addition of promoter substances, such as polyethylene glycol or crown ethers. Bulky or polar substituents dramatically decrease reaction rates and polymer yield.[46]

b) Equilibration: Another possibility to increase molecular masses of oligosiloxanes is the acid or base catalyzed equilibration reaction. Using this reaction type, both linear and cyclic oligomers, and even mixtures of both, can be processed. Reaction rates and resulting chain lengths are influenced by the molar ratio of utilized oligomers and equilibration agent (usually short chain siloxane).[51] Using this technique, organofunctional termini, which are tolerated by the catalyst, can be introduced into the polymer.

c) Polycondensation: Since all three preparation methods for siloxane oligomers, which were described above, can be controlled to yield linear, hydroxy terminated oligomers, the polycondensation reaction becomes very interesting for chain extension. The reaction is performed under elevated temperatures and with acidic catalysts, such as $PNCl_2$. The equilibrium can be displaced to the product side by removal of water. Main advantages of this reaction type are high reaction rates and the possibility to avoid cyclic byproducts. Many different functional groups can be introduced by addition of organofunctional methoxysilanes.

2.2.2.2 Properties and Applications

Silicone polymers are the only commonly used polymers, which are not directly depending on mineral oil production and prices. But this is not their only appeal. Polysiloxanes are clear, color- and odorless, chemically and physiologically inert, thermally stable over a wide temperature range, stable versus UV irradiation, hydrophobic, and vastly soluble in common organic solvents.

Depending on different functional termini and incorporation of functional groups, manifold application possibilities for polysiloxanes can arise. For instance, the most primitive hydroxy terminated polydimethylsiloxanes of variable chain lengths are oils, and can therefore by applied as lubricants in different industrial branches, such as automotive, pharmaceutics, constructions, and even foods. Tailor-made silicones with different organic functionalities e.g. amino, carbinol, or vinyl end groups create more sophisticated application fields. Recent developments showed applications of isocyanate terminated silicones as lightweight and non-flammable foams in the aviation and automotive industry.[52-53] Even thermoplastic elastomers on the basis of silicone copolymers are commercially available.

2.2.3 Three Dimensional Siloxane Structures

2.2.3.1 Crosslinked Polysiloxanes

Crosslinking of polysiloxanes facilitates a broad range of applications, for instance in common technologies, such as coatings, sealants, or adhesives, but also in much more progressive fields, such as life sciences or electronics. Generally, it can be distinguished between chemical and physical crosslinking. While chemical crosslinking is irreversible, and the crosslinked product usually is an elastomer, which cannot be recycled or reshaped, physical crosslinking leads to a thermoplastic and thus reusable product. In the following the different crosslinked systems are presented and discussed.

Chemical crosslinking of silicones can be established using different ways. In *Scheme 2.4* the most important methods, namely condensation of hydrolysable groups (*a*, *b*) and hydrosilylation (*c*), are depicted. For polysiloxane curing by condensation (*a*), the siloxane backbone is equipped with hydrolysable groups, such as chloro, alkoxy or acetyloxy functions, at internal and terminal positions. Moisture induced hydrolysis and condensation of these groups leads to a chemically crosslinked elastomeric siloxane network.

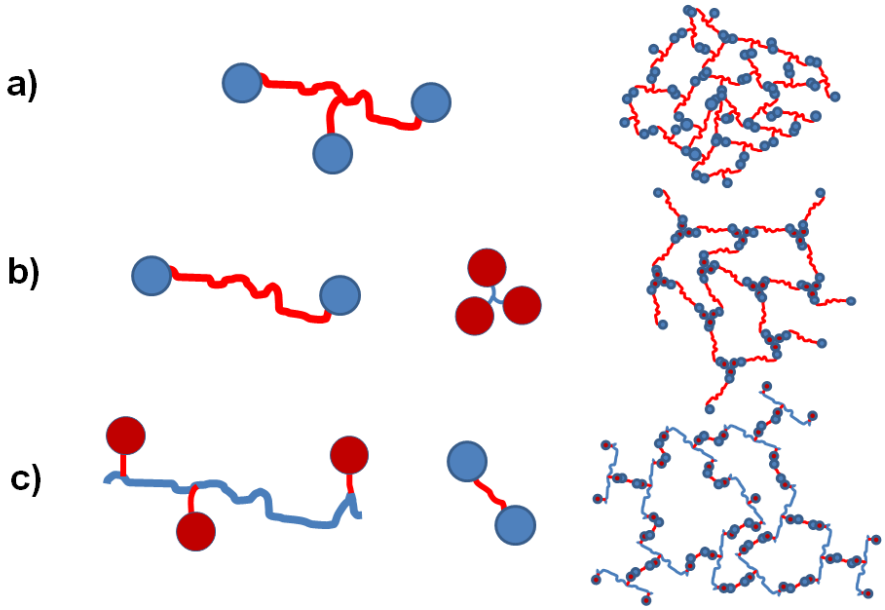

Scheme 2.4 *Different strategies for chemical crosslinking of polysiloxanes.*

For the condensation reaction (*b*) on the other hand, the hydrolysable groups are located only at the terminal positions of the polysiloxane chain. Since condensation of terminal groups is only sufficient for chain extension, for crosslinking a second agent, which bears at least three hydrolysable groups, is needed. In technical products, such as room temperature curable sealants, usually hydroxy-terminated polydimethylsiloxanes and trialkoxy- or triacetyloxysilanes are applied.

The other standard curing method utilizes a hydrosilylation reaction. Usually the required vinylic groups are provided as terminal groups of one component, and the Si-H functionality of the crosslinking agent is located along the polymer backbone of the second silicone component. In industrial applications often short chain polymethylsiloxanes are used as crosslinking agent. These applications can be coating materials for different industrial branches, such as foods, beverages, cosmetics, or pharmaceuticals.

Both curing methods have one important disadvantage: they do not proceed without catalysts. Condensation reactions are typically catalyzed by extremely toxic organo-tin compounds, whereas hydrosilylation reactions require remarkably expensive platinum

catalysts. Although the economical issues are not that important for tin compounds as they are for platinum, the usage of organo-tin compounds is continuously losing public acceptance and therefore will most likely be restricted in the near future. This is the reason for concentrated research on platinum-free hydrosilylation and tin-free silane crosslinking reactions.

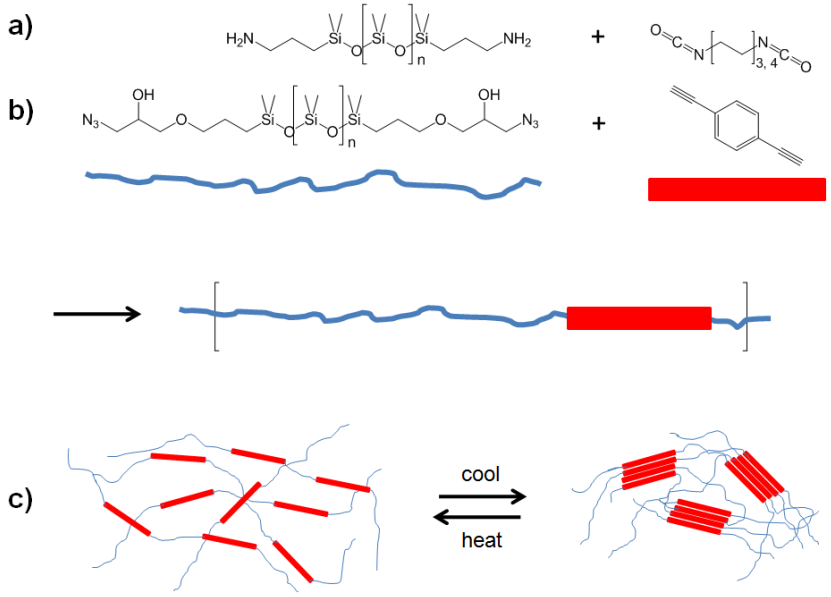

Scheme 2.5 *Synthesis strategies (a, b) and functional principle (c) for physical crosslinking of silicones.*

In *Scheme 2.5*, two selected synthesis strategies for physically crosslinkable polysiloxanes are shown. The combination of alkylamino-terminated polysiloxanes with short-chain spaced diisocyanates *(a)* is a technically implemented process at WACKER, which leads to thermoplastic elastomers of alternating siloxane-urea copolymers (*GENIOMER*®).[54] Whereas, the pathway shown in *(b)* is a modern approach to thermoplastic elastomers, which has recently been reported by our group.[55] This pathway makes use of a modern version of the *Huisgen* 1,3-dipolar cyclo addition, the so called 'click-reaction', which was first described by Sharpless *et al.* in 2001.[56] The thermoplastic properties of the products, obtained by both pathways, are based on the

combination of different chain segments with variable interaction properties. The polysiloxane chains exhibit low intermolecular interactions (soft blocks), whilst the urea and phenyl group linkers, are the ordering moieties (hard blocks) with comparably strong interactions, such as H-bonds or π-π-interactions, respectively. By heating, the hard-block interactions break open, and the material becomes processable, while by cooling these hard-blocks can rearrange, to form the elastomers. This functional principle is shown in *(c)*.

2.2.3.2 Silsesquioxanes

All crosslinked siloxanes, which were described in the last paragraph, are of disordered, random nature. Today, also crosslinked siloxanes with high structural order are known. Silsesquioxanes are such crosslinked siloxanes with the formal molecular formula $[RSiO_{1.5}]_n$. Every Si-atom is tetrahedrally surrounded by three O-atoms and one organic group R. According to that formula different structures are conceivable: disordered random statistic polymers, ladder-like structures with a two-dimensional order, and also three-dimensionally highly ordered cage-like oligomeric structures, the so called POSS-structures (Polyhedral Oligomeric Silsesquioxanes) (*Scheme 2.6*).[57]

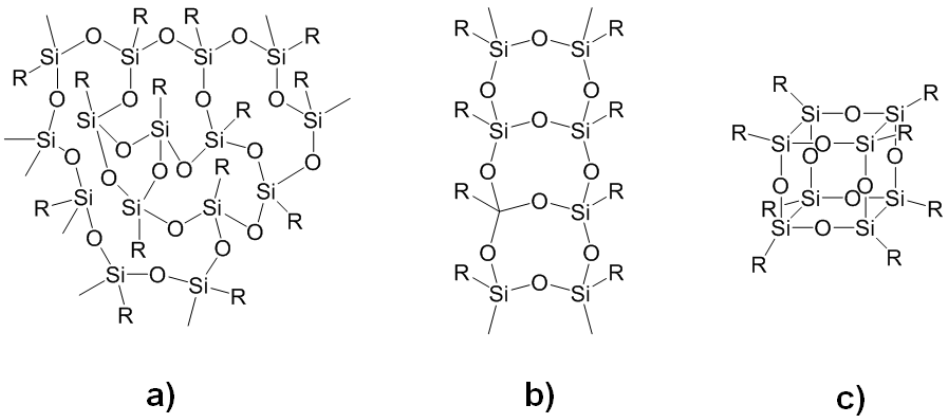

Scheme 2.6 *Different possible structures of silsesquioxanes: (a) random statistical polymer, (b) polymer with ladder structure, (c) polyhedral oligomeric silsesquioxane (POSS).*

The POSS-structures were first synthesized in the 1940s by D. W. Scott, using thermal rearrangement of polydimethylsiloxanes.[58] The common synthesis strategy today is the acid- or base-catalyzed hydrolysis and condensation of trichloro- and trialkoxysilanes. Recently, new methods using tetrabutyl ammoniumflouride (TBAF) catalysis were reported.[59] In the meanwhile, besides the cubic structure with eight Si-atoms manifold different cage structures exist. POSS structures do not have to be perfect, they can even be incomplete; several strategies for opening of one or two corners, and applications of the resulting materials were reported. In such applications, POSS-cages can act as monomeric units in homo- and copolymers.[60] They find applications in hybrid materials, as fillers in plastics industry, or as precursors for ceramics.

2.2.4 Polysilanes

In contrast to countless different synthesis procedures for polysiloxanes, effective processes for industrial polysilane synthesis do not exist up to now. Even though both classes of materials have been discovered in the 1920s, in the following 50 years, no noteworthy progress in the field of polysilanes could be observed. The first synthesis of soluble high molecular weight polysilanes in the 1970 caused a rebirth of interest in this material.[50] Since that time, various synthetical approaches have been investigated, and interesting properties were found.

2.2.4.1 Synthesis

Polysilanes can principally be subdivided in two classes: inorganic and organic. Inorganic polysilanes bear only inorganic substituents, such as H, F, or Cl, whereas organic polysilanes have organic substituents, such as methyl, phenyl, *etc.* (*Scheme 2.1 (b)*). Only a few synthesis routes to inorganic polysilanes have been reported so far. A perchlorinated polysilane could for instance be synthesized by sublimation of a cyclic silane Si_4Cl_8.[61] Also for polyhydrosilanes with the repeating

unit SiH_2, synthesis methods have been reported. One possible method is the decomposition of Mg_2Si with phosphoric acid at elevated temperatures.[62] Another possibility is the plasma assisted synthesis of perchloropolysilanes with subsequent reduction to polyhydrosilanes.[63]

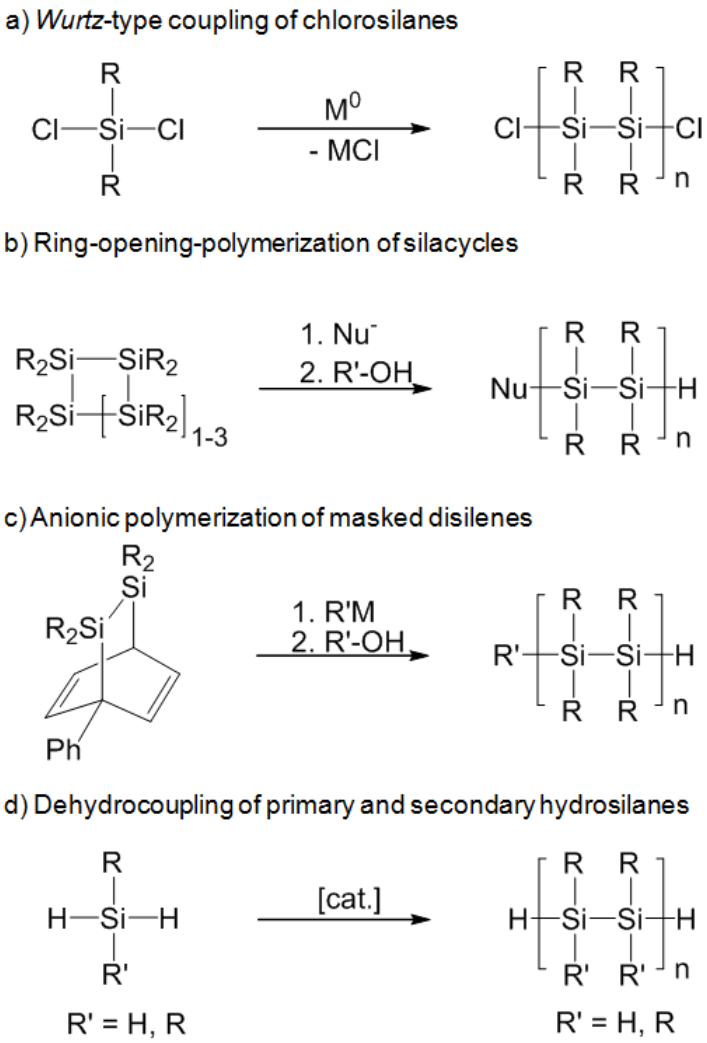

Scheme 2.7 *Schemes showing different synthesis options for polysilanes.*

Unlike the limited number of synthesis methods for inorganic polysilanes, for organic polysilanes a comparably large number is available. In *Scheme 2.7* the different methods for polysilane synthesis are presented. In the following, the presented methods are discussed in detail:

a) Wurtz-type coupling: The reductive coupling of chlorosilanes is the oldest and maybe the most important method for polysilane synthesis. It has been first described by Kipping in the 1920s.[48-49] In this reaction, chlorosilanes are reacted with alkalines to form chains and cycles of catenated silanes and alkaline salt as the only byproduct. The most common alkaline is Na, which is usually molten and suspended in boiling toluene. These harsh reaction conditions limit the introduction possibilities of functionalities on the silane to thermally very stable groups, such as alkyls or aryls. Another disadvantage of this method is the broad and multimodal distribution of molecular masses of the polymers and the formation of low molecular weight cyclic compounds, which presupposes intricate and time-consuming separation and purification of the product.[64] Many attempts to improve mass distribution and versatility of this reaction have been undertaken up to now. Mainly, these attempts dealt with variation of solvent and reaction temperature.[65-67] But also variations of the reducing agent[68-70] (K, Na-K alloy, C_8K, or Na-naphthalide), as well as the implementation of different auxiliary means, such as ultrasound[69,71] or addition of alkaline-ion-sequestering agents,[65,72] have been tested. The major conclusions are: lowering the reaction temperatures leads to higher molecular weights and narrower distributions, but also to much lower reaction rates and yields; thus, an increase of reaction rates and yields can be achieved by applying metals with higher reducing potentials and accelerative techniques such as ultrasonic treatment. Regardless of all advances in the *Wurtz*-type coupling, monomodal distributions are usually not accessible. Hence, there is still a wide scope for improvements left.

b) Ring-opening polymerization (ROP): As already mentioned above, *Wurtz*-type coupling of chlorosilanes can lead to the formation of cyclic oligosilanes under certain conditions.[73] Therefore, a possibility for the conversion of low molecular mass compounds to polymeric systems became eligible. In 1991 an anionic ROP of $(PhMeSi)_4$ was described by Matyjaszewski *et al.* for the first time.[74] Although this technique is limited to strained four- to six-membered rings, and still no monomodal distribution could be achieved, ROP has been shown to be a powerful method for the synthesis of polysilanes with molecular masses up to 100,000 g/mol.

c) Polymerization of masked disilenes: Disilenes can be considered as the analogous Si-compounds to ethylene which has a direct C-C double bond. In comparison to carbon systems, isolated Si-Si double bonds are absolutely unstable, unless they bear substituents, which provide stability by electronic or steric shielding.[75] In *Scheme 2.8* a selection of such stable disilenes is presented. Although these compounds are stable enough to be handled without special precautions, they cannot be used as monomers due to a great sterical hindrance. A different way for the anionic polymerization of disilenes has been chosen by Sakurai *et al*.[76] They made use of a disilene which is masked by an auxiliary group, e.g. biphenyl. This masking of a disilene has been first presented by Roark and Peddle in the early 1970s, utilizing a reaction of dichlorodisilane and a biphenyl anion radical (*Scheme 2.9*).[77]

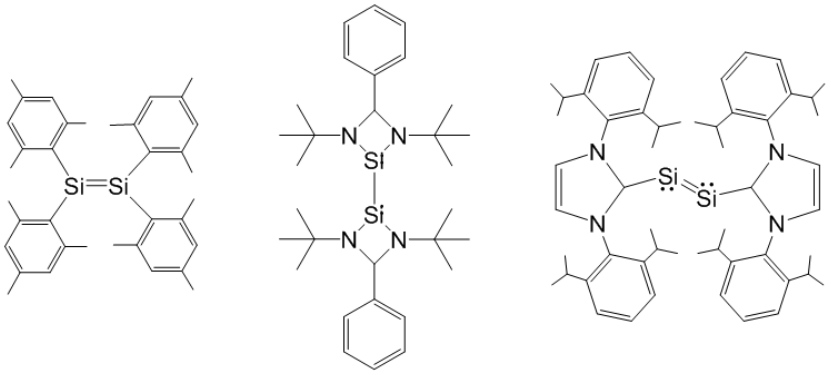

Scheme 2.8 *Differently stabilized disilenes.*[73,78-79]

This strategy made it possible to use disilenes as a monomer, and to synthesize polysilanes by adding a catalytic amount of anionic initiator e.g. an organolithium compound. Due to the anionic nature of the propagating chain, termination of the polymerization can be established by protonation with an alcohol. In this way, monomodal molecular mass distributions with comparably narrow PDIs could be achieved. Furthermore, by adding different masked disilenes or even methylmethacrylate (MMA) prior to the termination step, the living nature of this polymerization type was proven, since blockcopolymers could be obtained.

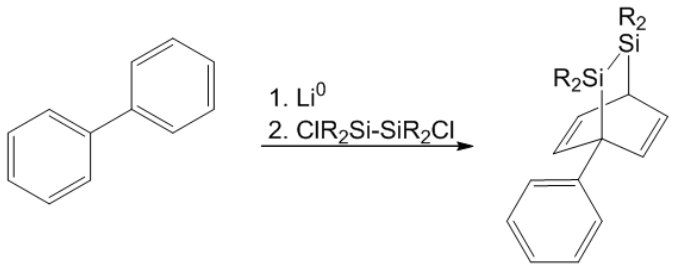

Scheme 2.9 *Synthesis route to a masked disilene.*[77]

d) Dehydrocoupling: The only polymerization type for polysilanes, which is not based on chlorosilanes, is the catalytic dehydrocoupling of primary (*Scheme 2.7 (d)*, R' = H) and secondary (*Scheme 2.7 (d)*, R' = R) hydrosilanes, which was first described by Harrod *et al*. in 1985.[80] This reaction type gives monomodal and comparably narrow distributions. Furthermore, it is the most promising reaction, since the only byproduct is gaseous H_2 and the Si-H termini are more stable than Si-Cl termini, and therefore undesirable side reactions after the polymerization do not occur. If desired, the Si-H termini can even be used for post-functionalization (e.g. hydrosilylation reaction) of the polymer. The catalysts used for dehydropolymerizations are usually metallocenes based on group IV transition metals.

Over the past years, improvements of polysilane chain lengths were achieved by rational ligand design.[81-83] In general, a much broader variety of metals and ligand systems has been reported for primary silanes. Although it has been shown that primary silanes are more reactive than secondary silanes, a few novel catalytic systems exist, which are able to polymerize secondary silanes with acceptable rates.[84]

2.2.4.2 Properties

As mentioned above, polysilanes consist of a backbone of catenated silicon atoms with exclusively σ-σ-bonds. The physical properties are strongly dependent on the substituents attached to the silicon. While the polymers with inorganic or small organic substituents, such as methyl or ethyl, are highly crystalline and thus insoluble in most solvents, longer alkyl chains or other large side groups, such as hexyl or phenyl, lead to decreased crystallinity and thus to good solubility and even elastomeric properties. Their glass transition points can range between -50 °C and +120 °C, depending on molecular masses and the nature of substituents. Furthermore, their thermal stability is remarkably good; most polysilanes do not decompose below 300 °C.[50,73,85]

But it is not the physical properties, which make polysilanes extremely interesting - it is the binding situation and thus the electronic properties. In the 1970s and 1980s remarkable works on the electronic situation in polysilane systems have been published. It has been observed, that with increasing chain length of the polymer, a distinct red shift in absorption spectra and a gradual increase in the molar absorption coefficient can occur. Today we know that this effect is due to the σ-σ-bond-delocalization of the binding electrons. This can be explained with the molecular orbital theory, which tells us, that only a combination of sp^3 hybrid orbitals leads to the formation of delocalized molecular orbitals σ and σ*. An involvement of d-orbitals can be excluded.[50,73]

Besides the number of chain segments, also the nature of the organic substituents plays a crucial role in stabilization of the molecular orbitals. For instance, alkyl substituents stabilize the lowest unoccupied molecular orbital (LUMO) without destabilizing the highest occupied molecular orbital (HOMO), but due to their conjugative effects, aryl groups cause a certain destabilization of the HOMO. Both effects lead to a decrease in HOMO-LUMO band-gap energy (*Scheme 2.10*).[50]

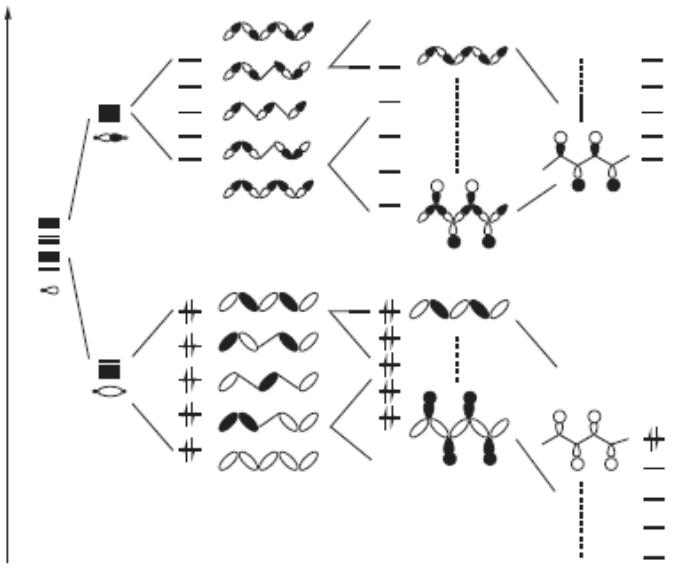

Scheme 2.10 *Contribution of sp3 hybrid atomic orbital to σ and σ* delocalized molecular orbitals.*[50]

Due to the more electropositive nature of the Si-Si-bond compared to the C-C-bond and the low σ-σ*-excitation energy, polysilanes easily can be degraded by UV-light irradiation.[86] On one hand this fact causes big problems in electro-optical device lifetime, but on the other hand it opens application possibilities in the fields of resins and photoresist technology.

2.2.5 Polysilane Networks

As already described in *Section 2.2.3*, the scope of possible applications of linear polymers can be rigorously expanded by conversion of the linear systems into three-dimensional networks. There are different ways to achieve polysilane networks: one possibility is the crosslinking of linear polysilanes by post-synthetical modification procedures; another possibility is the direct synthesis of crosslinked or branched structures. Both possibilities are elucidated in the following.

Crosslinking reactions are very important for the use of polysilanes as precursors for ceramic materials, as well as for the use in photoresist technology. Network polymer formation can be established using chemical and physical methods. Common chemical routes are oxidation and hydrosilylation. By oxidation, Si-O-Si linkages are introduced into the polysilane networks, which sometimes can be undesirable for certain applications. For hydrosilylative crosslinking Si-H groups must be present in the backbone and furthermore a crosslinking agent, which contains vinyl groups, is required. Physical crosslinking can be established by irradiation with light or by thermal treatment. Both treatments lead to scission of the Si-Si bonds and thus to silylradical formation. Also here multiply unsaturated co-agents, which serve as addition points for the silylradicals, are needed. An advantage of the physical over the chemical methods is the absence of catalysts or oxidants; but a big disadvantage is the lack of control of crosslinking degrees.[85]

Polysilane networks with the empiric formula $[R\text{-}Si]_n$ are usually prepared by direct synthesis techniques. They can be considered as intermediates between linear polysilanes and elemental silicon and were first presented by Bianconi *et al.* in the late 1980s.[87-88] In contrast to linear polysilanes, which can be synthesized using different techniques (*Scheme 2.7*), network polysilanes are made by coupling of trifunctional organosilanes, such as alkyl- or aryltrichlorosilanes.[89] Usually they are referred to as ‘polysilynes’ or ‘branched polysilanes’ in the literature. Besides polysilyne homopolymers, also copolymers with different trichlorosilanes, heteroatom substituted trichlorosilanes, or even with dichlorosilanes are known.[90-91] Furthermore, highly defined polysilane dendrimers have been reported.[92] In *Scheme 2.11* the different polysilyne architectures are summarized.

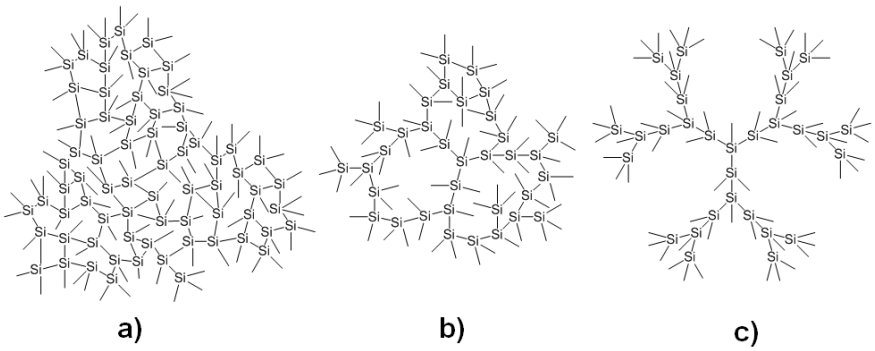

Scheme 2.11 *Different polysilyne systems: randomly branched and crosslinked polysilyne homopolymer (a), polysilyne-polysilane copolymer (b), defined polysilane dendrimer (c).*

Network polysilanes display similar interesting electronic properties as their linear counterparts, since they also consist of catenated silanes with direct Si-Si-σ-bonds. Thus, extensive electron delocalization along the σ-bonds plays a crucial role as well. This makes the networks applicable as photo- and semiconductors or non linear optic materials in many high technology fields, such as displays, organic light emitting diodes (OLEDs), or photovoltaics (PV). Another application possibility arises from good film forming properties. After solution processing and pyrolysis under defined oxidative or inert atmospheres, generation of thin films built up of, silica, silicon carbide or even silicon is possible. Since the soluble polysilynes can be post-synthetically crosslinked, applications in the field of UV-photoresists are conceivable.

2.2.6 Defined Si-based Polyhedra

During the last decades, scientists all around the world were searching for highly sophisticated silicon containing compounds, which mimic prominent carbon compounds, such as benzene or polyhedral prismanes and cubanes. In *Scheme 2.12*, a selection of these compounds is presented. Already in 1975 Dewar *et al*. predicted the existence of cyclic and polyhedral oligosilanes, such as hexasilabenzene or tetrasilatetrahedrane.[93] But it took more than 10 years until the first successful

synthesis of a silicon based polyhedral octasilacubane was presented by Matsumoto *et al*. in 1988.[94] Full characterization of this system, presenting crystal structures, was achieved in 1992 by Sakurai *et al*.[95] One year later, the first synthesis of a silicon based tetrahedrane, which was stable to air, water, and thermal treatment, was presented by Wiberg *et al*.[96] In the same year, Sakurai *et al.* reported also on the synthesis of the first hexasilaprismane.[97] These studies were the advent of manifold studies about silicon based polyhedra, which are summarized in a review article from 1998.[98]

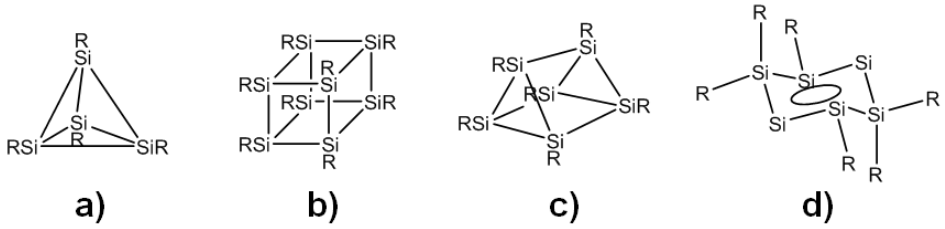

Scheme 2.12 *Silicon based polyhedral compounds: tetrasilatetrahedrane (a), octasilacubane (b), hexasilaprismane (c), and aromatic hexasilabenzene (d).*

Among these polycyclic compounds, hexasilaprismane appears to be the most interesting one, since it is an isomer of a benzene-like structure. The first calculations by Dewar *et al*. in 1975 predicted for hexasilabenzene a planar geometry with sixfold symmetry, which is comparable to that of benzene.[93] More exact calculations led to predictions of a chair-like conformation, which is comparable to that of cyclohexane.[99] In the next decades great synthetical effort has been spent to isolate an aromatic hexasilabenzene. The breakthrough was achieved in 2010 when Scheschkewitz *et al*. presented a synthetic approach and crystal structure analysis of a hexasilabenzene isomer.[100] The crystal structures and calculations using density functional theory (DFT) revealed the chair-like conformation of the compound.

Of course it is worth mentioning, that stability of all aromatic and polycyclic compounds could only be achieved by excessive steric or electronic shielding. Appropriate ligand systems are for instance: mesityl, triisopropylphenyl, or tri-*tert*-butylsilyl groups.

3 Objectives

The use of silicon containing polymers in today's industry is continuously growing in fields where special requirements towards materials arise and therefore carbon based polymers cannot be applied. Polyorganosiloxanes are the most important polymers with a completely inorganic backbone, consisting of alternating silicon and oxygen atoms. Due to their thermal, chemical, and physiological inertness they found use in manifold applications as oils, resins, and elastomers. In contrast, polyorganosilanes, which exclusively consist of silicon backbone-atoms, represent a comparably new class of materials. The unique feature of polysilanes is a significant delocalization of electrons along the backbone. This leads to novel application possibilities in electronic devices, such as OLEDs and OFETs. Problems of polysilanes in industrial processes emerge due to limited stability towards oxidation and irradiation.

As described in the previous chapter, the chemical and physical properties of silicon based oligomers and polymers can be significantly modified by physical and chemical crosslinking to three dimensional networks. Also the generation of self-assembled structures can lead to modification and even enhancement of important physical and chemical properties. In the literature, many different possibilities for inducing self-assembly are described. One prominent way is the combination of oligo- and polymers with mesogenic functionalities in terminal positions and side groups. The interaction of the mesogenic units with each other leads to the formation of discrete and defined structures, which can be layers, spheres, columns and discs. Herein the possible shapes of the assemblies are strongly depending on the shape and functional groups of the

mesogens. Various studies have been performed in the field of siloxanes, where the termination and functionalization of the polymer and oligomer backbones yielded manifold novel self-assembled structures, such as lyotropic and thermotropic liquid crystals.

The present project is dedicated to the investigation of different approaches to novel silicon based structures by molecular recognition and self-assembly. The main objective is the introduction of a 'building block' concept consisting on one hand of polymeric and oligomeric siloxanes and silanes, and on the other hand of carbon based mesogenic molecules, which induce the formation of novel self-assembled structures of the silicon containing compounds. The project is roughly subdivided into two basic parts: a synthetic part, in which possible synthesis strategies for the mesogens as well as the combination of the mesogens with the silicon based mono, oligo, and polymers are investigated; and a second part in which different strategies for characterization of the formed assemblies are described.

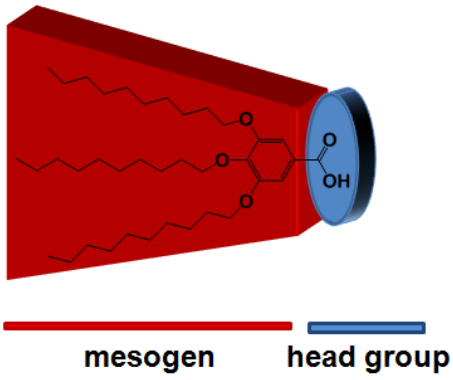

Scheme 3.1 *Gallic acid derivative as model compound for mesogenic systems.*

The first milestone of the synthetic part is the synthesis of appropriate mesogenic building blocks, which bear a certain functional group that can be used for coupling reactions with silicon containing head groups, such as siloxane and silane oligomers, or even polymerizable chlorosilane monomers. In *Scheme 3.1* the mesogenic group, which has been chosen for this project, is depicted. This mesogen is a long chain alkoxy

derivative of gallic acid (3,4,5-trihydroxy benzoic acid) and has been presented for the first time by Percec *et al*. in the early 1990s.[101-102] The arrangement of the alkoxy substituents causes a certain wedge shaped geometry in the molecule (red), which is well known to induce self-assembly of various head groups (blue) in various structures (see *Chapter 2.1*).

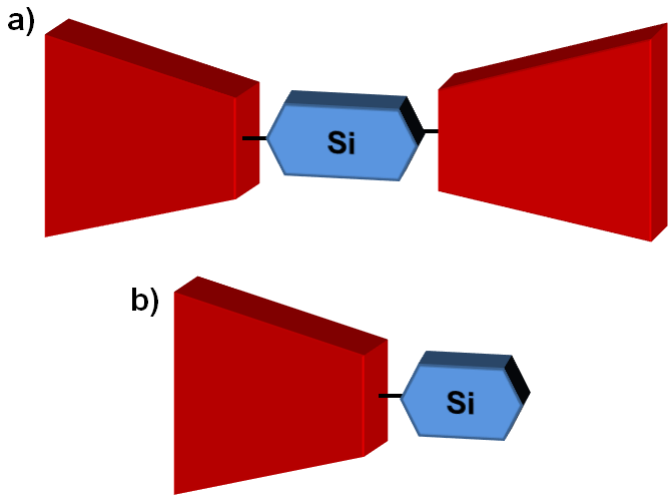

Scheme 3.2 *Schematic of target structures: (a) mesogen-terminated silicon based telechel, (b) mesogen-functionalized silane monomer.*

The second and most important milestone is the combination of the mesogen building blocks with silicon containing head groups. In *Scheme 3.2* selected target structures of this project are shown. By variation of the number of functionalities on the head groups, different arrays of mesogens around the head groups are accessible. On the one hand, a bifunctional head group (*e.g.* α-ω-telechelic oligo silane or siloxane) leads to bimesogens with silicon containing linker, and on the other hand a monofunctional head group results in a silane-functional mesogen, which can be *e.g.* a polymerizable monomer. Furthermore, various reaction mechanisms for the coupling of mesogen and head group, which result in different spacer structures, are conceivable. Different approaches are tested within this study, and the most promising approach is used for further analyses.

The primary intention behind the synthesis of telechelic siloxane bi- and multimesogens is the general investigation of the applicability of gallic acid derivatives as building blocks with the ability to induce self-assembly of silicon based head groups. Moreover, novel self-assembled siloxanes could find new application fields in research and industry. The concept of gallic acid building blocks can subsequently be transferred to the synthesis of polymerizable silane mesogens, which afterwards can be converted to mesogen substituted polysilanes. The introduction of mesogens into polysilanes should lead to novel polymer structures, which can bear physical and chemical properties which have not been observed up to now.

For the synthesis of mesogen decorated polysilanes, different chlorosilanes are tested. In theory, *Wurtz*-type reductive coupling of mesogen monomers with dichloromethylsilane head groups should lead to linear polysilanes, whereas monomers, which are based on mesogens with trichlorosilanes head groups, can serve as source for three dimensional crosslinked polysilane structures. Both concepts are applied and screened within this work.

In the analytical part of this study, different concepts for characterization of the formed structures are presented. These concepts include investigation of the synthesized compounds in various surroundings, *e.g.* in bulk, in thin films, or in solution. Many modern analysis techniques, such as electron and scanning probe microscopy, thermal analyses, or different scattering techniques, are applied. In the further course, the applicability of the self-assembled compounds as templates and precursors for novel nano-structured materials and surfaces is tested. Therefore, the mesoscopic arrays are subjected to pyrolysis and plasma treatment experiments.

4 Mesogen Library

4.1 Introduction

By IUPAC-definition, a mesogen is a part of a molecule or macromolecule, which is endowed with sufficient anisotropy in both attractive and repulsive forces to contribute strongly to mesophase or, in particular, liquid-crystal mesophase formation in low-molar-mass and polymeric substances.[103] In low-molar-mass systems, a typical structural motif for molecules which form mesophases is the combination of at least one rigid and one flexible part. Much more often, mesogenic systems consist of two or more rigid parts with the flexible part acting as a linker or decorating the edges of the rigid parts. The rigid part may be a rod-like or a disc-like organic molecule and the flexible (coil-like) part usually consists of a long alkyl chain.[104] Besides these low-molar-mass systems, mesogens can be bound by a spacer to a polymeric backbone to form mesogenic high-molar-weight polymers.[105-106] For the synthesis of mesogenic polymers two different approaches exist: on one hand the ‘top-down’ strategy deals with the functionalization of existing polymers by mesogens using polymer analogous reactions, and on the other hand the ‘bottom-up’ approach describes the polymerization of pre-functionalized monomers to high-molar-mass systems. Mesophase formation is not only restricted to carbon based systems; numerous studies describe integration of silicon based compounds into the mesogen structures.[107]

In the last decades, the ability for inducing mesophase formation has been tested for many different mesogens. It turned out, that the most promising examples are cyano biphenyl benzoates, phenyl benzoates with long alkyl chains, or cholesteryl benzoates.[107] But in the beginning of the 1990s a novel system, which has been found by Percec *et al*, became popular.[101] This mesogen system combines both, rigid and flexible parts in one molecule. It is based on derivatives of gallic acid (3,4,5-trihydroxy benzoic acid), where the phenyl part is rigid, and the hydroxy functions are etherified with long alkyl chains, and therefore are forming the flexible part. This mesogen represents the fundamental substructure of this work, since it is known to assemble various head groups to different discrete and homogeneous aggregates, and has not been tested yet for the self-assembly of silicon based compounds. Furthermore it has been shown, that small changes in the substitution motif on that mesogen, cause drastic alterations of the structure of the assemblies.[108]

In the following, the elaboration of a feasible synthesis strategy towards alkoxy substituted gallic acid derivatives, as well as a concept, concerning the coupling of the mesogens with silicon based head groups, is described. General problems of different coupling approaches between mesogen and head group are discussed; and as a result thereof, different synthesis strategies towards possible spacer groups are presented.

4.2 Synthesis Strategy

The synthesis strategy for the mesogens is mainly governed by a limitation of possibilities for the coupling of mesogen and head groups. In *Scheme 4.1* the different potential alternatives for coupling reactions are presented. Since each alternative requires a different synthesis route, the different coupling possibilities are discussed first.

In general, for the direct coupling of silicon and carbon atoms two common mechanisms exist. One possibility is a nucleophilic substitution reaction of a halogen, which is bound to the silicon atom, with a carbon nucleophile; and the other common route is a hydrosilylation reaction of unsaturated functional groups on the carbon compound with hydrogen-functionalized silanes. Application of the different routes to the mesogen concept, apparently leads to a broad variation of spacer groups between mesogen and head group

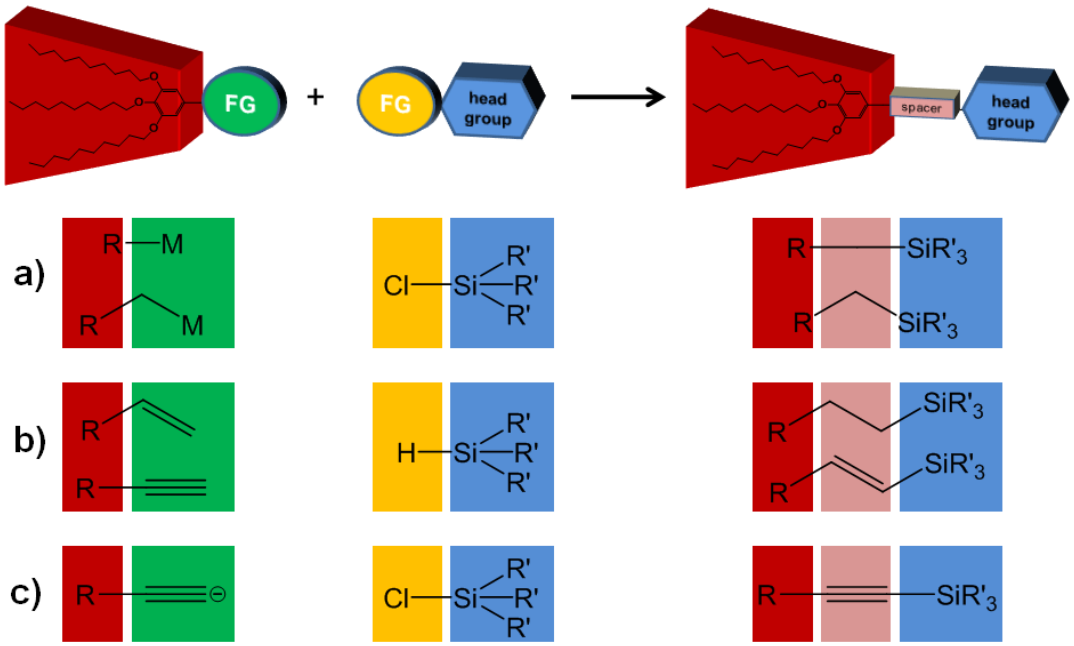

Scheme 4.1 *Schematic representation of different coupling strategies and as result thereof, different possible spacer geometries between mesogen and silicon containing head group (FG = functional group).*

For the nucleophilic substitution reaction on chlorosilanes two different possibilities, which both are based on a halogenated mesogen, are conceivable: on one hand the *Grignard*-reaction, using pre-activated metallic magnesium, and on the other hand a transmetalation, using butyl lithium at low temperatures. Both routes result in an aliphatic spacer or rather no spacer, depending on the position of the halogen prior to the metalation reaction (*Scheme 4.1 a*). The hydrosilylation reaction requires an unsaturated functional group, such as alkene or alkyne on the mesogen and a terminal Si-H functionality on the head group. The resulting spacers can be either an ethylene or an ethenylene group for alkene and alkyne substrates, respectively (*Scheme 4.1 b*). A third possibility, which leads to an ethynylene spacer, is the nucleophilic substitution on a chlorosilane by deprotonation of mesogen substituted acetylenes with strong bases (*Scheme 4.1 c*). As mentioned previously, the different functionalities on the mesogens, which are required for the coupling reactions, are generally accessible *via* different synthesis routes. Within this work these routes were tested and their feasibility is discussed in the following.

4.2.1 Metalated Mesogens for the Nucleophilic Substitution on Chlorosilanes

The synthesis strategy for halogenated mesogens is presented in *Scheme 4.2*. In the upper part a route towards trialkoxy-substituted compounds is shown, whereas the lower part deals with the synthesis of monoalkoxy-substituted mesogens. Since *p*-bromo phenol is commercially available, it directly serves as starting compound for the etherification. 3,4,5-trihydroxy phenyl bromide is accessible in moderate yields (70%) *via* an ether cleavage reaction with BBr_3 from the commercially available 3,4,5-trimethoxy phenyl bromide. This reaction step is rather problematic; since the BBr_3 is highly reactive and corrosive the cleavage can only be performed in argon atmosphere with dry solvents.

The etherification reaction of the mono and trihydroxy phenyl bromides to the target compounds **2** and **1**, respectively, can be performed in decent yields (90-95%, after flash chromatography) without any precautions concerning water content or purity of solvents. Different lengths of alkoxy substituents can be introduced into the mesogens by using alkyl bromides of different lengths.

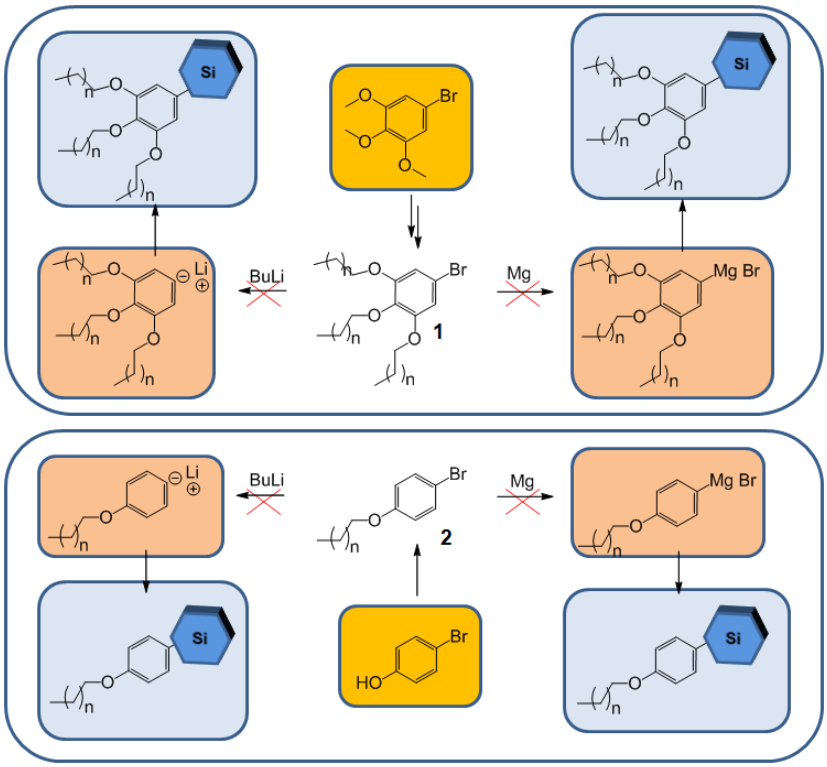

Scheme 4.2 *Reaction scheme for the synthesis route towards metalated mesogens. The color code indicates the commercially available educts (yellow), the target mesogens (red), and the possible coupling products (blue).*

After having obtained the compounds **1** and **2**, both, the *Grignard* and the transmetalation reaction were tested to access the metalated mesogen, which then can be reacted with chlorosilanes in a nucleophilic substitution reaction. For both reactions many parameters exist, which determine the prospect of success. The most important parameters are: solvent, temperature, and surface state of the Mg-metal. Although many attempts were taken to optimize the conditions, none of these two routes succeeded in a

metalation of the mesogen, or the mesogen-silane coupling product. One reason for the disappointing results can be the steric hindrance due to the long alkyl chains. Therefore shorter alkoxy substituents (C_3-C_6) were screened. But also this strategy did not lead to success. Another reason may be the unfavorable electronic conditions on the aromatic ring. To stabilize the negative charge after metalation, electron withdrawing groups on the phenyl ring instead of the electron donating alkyl groups are desirable. Since the problems could not be solved in an appropriate period of time, these reaction pathways were no longer under consideration for coupling of mesogen and head groups, and an alternative strategy, in which hydrosilylation is used, was developed.

4.2.2 Mesogens with Unsaturated Functional Groups

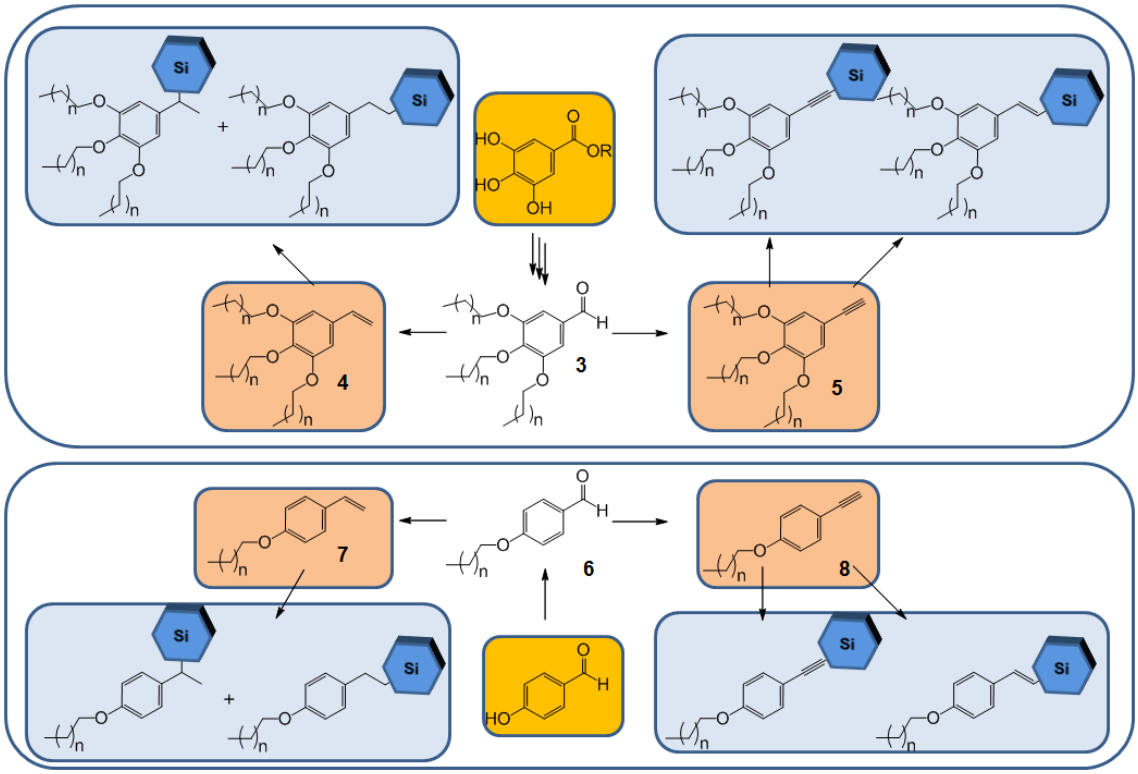

Scheme 4.3 *Reaction scheme for different synthesis strategies towards mesogens with unsaturated functional groups. The color code indicates the commercially available educts (yellow), the target mesogens (red), and the possible coupling products (blue).*

Unsaturated functional groups, such as ethylenes and acetylenes, can be used for hydrosilylation reactions with H-terminated silanes. In the previous paragraph it was shown that nucleophilic substitution reactions are not feasible for coupling of mesogens with silicon based head groups, since the metalation step of halogen substituted mesogens is not working under the tested conditions. Therefore, an alternative coupling route, which uses mesogens with unsaturated groups, was envisioned. In *Scheme 4.3* the new strategy towards the unsaturated mesogens is shown. The key-step is the transformation of alkoxy substituted benzaldehydes (**3**, **6**) to styrene (**4**, **7**) and phenyl acetylene (**5**, **8**) derivatives. For the synthesis of the substituted styrenes a *Wittig*-reaction was used, whereas for the phenyl acetylenes a *Corey-Fuchs*-reaction was applied.

Both, mono- and tri-substituted alkoxy benzaldehydes are easily accessible. The mono-substituted compound **6** is obtained by direct etherification of commercially available *p*-hydroxy benzaldehyde with alkyl bromides in yields of 95-99%. Whereas for the tri-substituted benzaldehyde **3**, a three-step reaction, using gallic acid esters as starting compounds, was performed. This route includes etherification of the hydroxy-groups with alkyl bromides in boiling cyclohexanone, reduction of the ester functionality with $LiAlH_4$, and partial oxidation of the obtained benzyl alcohol with 2-iodoxy benzoic acid (IBX) to the desired benzaldehyde. Since each intermediate step in the three-step route could be performed with yields of 92-99%, the direct etherification of commercial trihydroxy benzaldehyde was abandoned, due to the much lower price of the gallic acid esters.

4.2.2.1 Synthesis of Alkoxy-Substituted Styrene Derivatives

The synthesis of the styrene derivatives **4** and **7** was performed *via* a classical *Wittig* reaction route, using the previously prepared benzaldehydes **3** and **6**. The corresponding reaction mechanism is depicted in *Scheme 4.4*. The first step of the mechanism is the *in situ* formation of a phosphonium-ylide from methyltriphenylphosphonium bromide by deprotonation of an acidic proton on the methyl group with a strong base. In the second

step, a transition state, which is characterized by a four-membered cyclic oxaphosphetane structure, is formed by a [2+2]-cycloaddition of ylide and carbonyl group of the aldehyde. In the last step the styrene is released under formation of triphenylphosphane oxide as byproduct.[109]

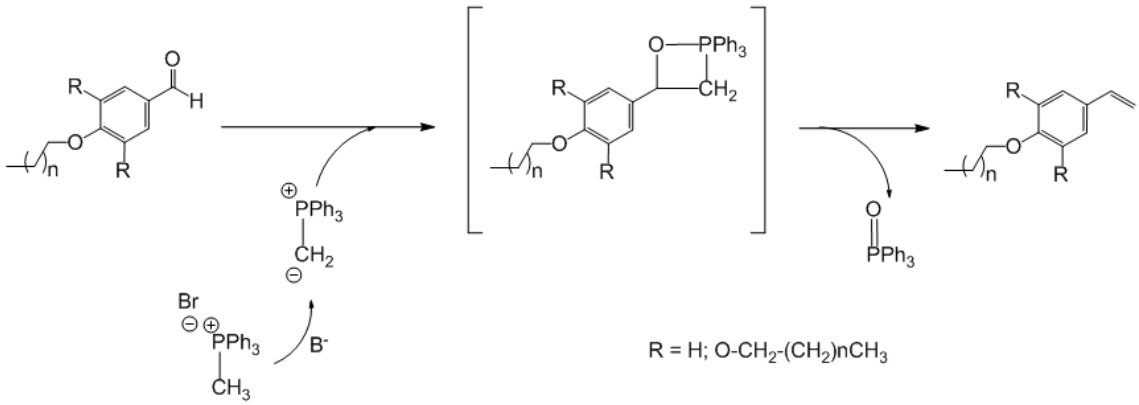

Scheme 4.4 *Schematic representation of the reaction mechanism for the Wittig reaction.*

The yield of the reaction is strongly influenced by the ylide, and its formation by deprotonation is therefore influenced by the base. Two different procedures, which are known in the literature and use different bases, namely butyl lithium (BuLi) and potassium *tert*.-butanolate were tested. Although Napolitano *et al.* reported a quantitative yield of 3,4,5-trimethoxystyrene,[110] our attempts on the deprotonation of the methyl group by butyl lithium led to a yield of 56% and 68%, for mono and tri-substituted alkoxy styrenes, respectively. For the use of KO*t*Bu as base, a procedure, which was reported by Meier *et al.,* was applied.[111] Although once again, the reported yields for mono-substituted alkoxy styrene (92%) could not be reproduced, the procedure allowed the production of mono and tri-substituted styrenes with acceptable yields of 76% and 80%, respectively. Since the procedure by Maier *et al.* led to much higher yields than the *Napolitano*-route, it was used for further syntheses.

4.2.2.2 Synthesis of Alkoxy-Substituted Phenyl Acetylene Derivatives

For the synthesis of the phenyl acetylene mesogens **5** and **8** two different synthesis routes are conceivable: on the one hand a route, which starts from the alkoxyphenyl bromides **1** and **2**, and uses for the introduction of the alkyne function a *Sonogashira-Hagihara* cross coupling reaction of the bromo mesogen with a trimethylsilyl-protected acetylene (TMS-Ac); and on the other hand there is a route via the less popular *Corey-Fuchs* reaction of benzaldehyde mesogens **3** and **6** with a phosphonium-ylide prepared from triphenylphosphine and carbontetrabromide.

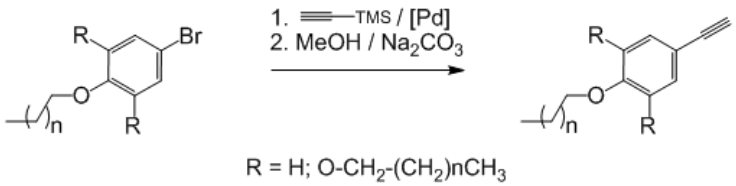

Scheme 4.5 *Schematic representation of the two-step Sonogashira reaction route.*

The *Sonogashira* route basically consists of two reaction steps (*Scheme 4.5*). The first step is the actual coupling reaction between compounds **1** or **2** and a TMS-Ac, whereas the second step is a subsequent deprotection reaction, which forms the phenyl acetylene mesogen. The first step requires as catalysts Pd(0) and Cu(I), and furthermore a base component which can be an amine of primary, secondary, or tertiary nature, and has to be added in large excess. Since Pd(0)-compounds are mostly labile substances, also Pd(II) salts can be added to reaction, which are immediately reduced *in situ* by the base. Different approaches have been tested within this work. For instance, using $PdCl_2(PPh_3)_2$ as catalyst and NEt_3 as base. Also different solvents, such as THF, DMF, or toluene were screened. But the only acceptable results were obtained, with a literature procedure by Müllen *et al.*, using $Pd(PPh_3)_4$ and CuI as catalysts, and piperidine, simultaneously as base and solvent.[112] For compound **3**, the overall yield of the two steps was 86%, which is roughly as good as reported in the named paper (89%), but for compound **6** the reactions with the best results yielded only 38%. Therefore, for further syntheses of phenyl acetylene mesogens, the alternative *Corey-Fuchs* route was used.

The reaction mechanism of the *Corey-Fuchs* reaction is presented in *Scheme 4.6*. Easily, one can recognize the analogies to the previously described *Wittig* reaction. Indeed, the first of the three steps is once again the formation of a phosphonium-ylide, and the subsequent cycloaddition to the oxaphosphetane cycle. But in this case the ylide is formed from carbontetrabromide and triphenylphosphine, because for further steps a geminal dibromide is needed. The ylide can either be previously prepared from an equimolar mixture of CBr_4, PPh_3, and zinc dust, and subsequently added in double excess to the aldehyde; or it is formed *in situ* in a mixture of one equivalent aldehyde, two equivalents CBr_4 and four equivalents PPh_3 in dichloromethane.[113] In a second step, the resulting geminal dibromide can simply be converted into phenyl acetylene, by adding two equivalents of butyl lithium. The complex mechanism of this conversion can briefly be described as halogen-metal-exchange, formation of a carbenoid system, and migration of the hydrogen atom. The so-formed phenyl acetylene is immediately deprotonated by the second equivalent of butyl lithium to a phenyl acetylide. In the third step the acetylide is converted back to the acetylene by acidic work-up.[109]

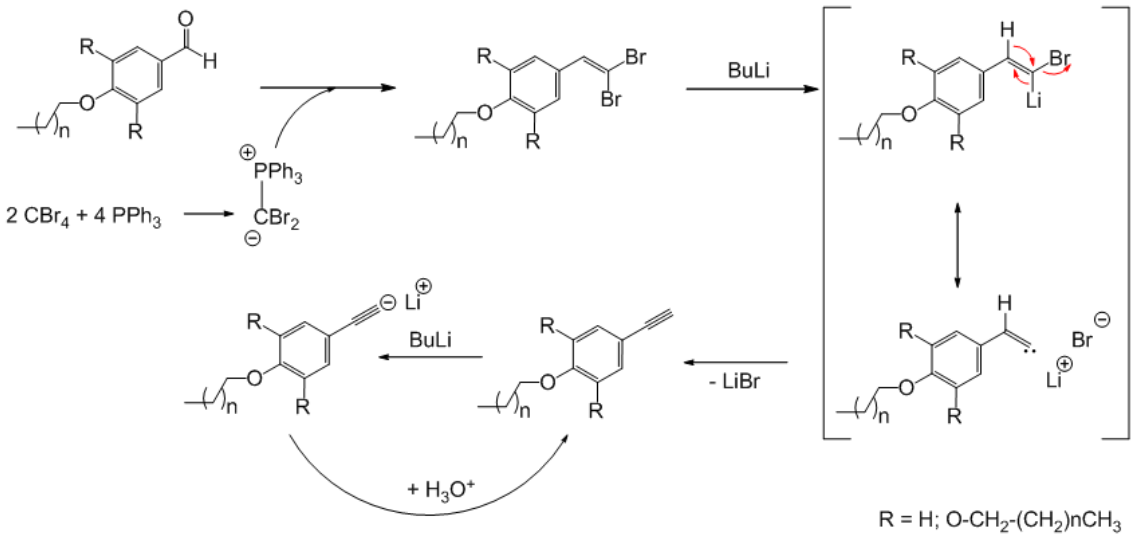

Scheme 4.6 *Schematic representation of the three-step reaction mechanism for the Corey-Fuchs reaction.*[109]

Compared to the *Sonogashira* route, there are three main advantages of the *Corey-Fuchs* route: first of all, the same intermediate products (benzaldehydes **3** and **6**) as for the synthesis of styrene derivatives **4** and **7** *via* the *Wittig* route can be used. Therefore the low-yield reaction steps from the *Sonogashira* route could be omitted just by up-scaling of the benzaldehyde synthesis, and the overall yield of the phenyl acetylene synthesis could be improved to 85% and 74% for mono and trialkoxy substituted phenyl acetylenes, respectively (compared to 35% and 54% from the *Sonogashira* route). Secondly, the use of potentially hazardous chemicals, such as BBr_3, can be avoided. Besides the security aspects, the third and most important advantage is the cost-saving nature of the *Corey-Fuchs* synthesis, since standard reducing and oxidizing agents are used. Therefore, high priced reagents and catalysts, such as BBr_3 and Pd-salts become unnecessary, and thusly, the costs for the synthesis of phenyl acetylene compounds **5** and **8** can be lowered by a factor of ten compared to the *Sonogashira* route.

The fact that the mechanism of the *Corey-Fuchs* reaction proceeds *via* an acetylide intermediate can be harnessed to create a direct coupling strategy to silicon head groups (*Scheme 4.1 c*). As mentioned above, the acetylene, which is obtained after the hydrogen migration step, is directly deprotonated by the second equivalent of BuLi and needs acidic work-up to be reprotonated to the acetylene. If the acidic work-up step is replaced by an addition of chlorosilane, the acetylide mesogen can act as nucleophile, and a substitution of the chlorine-functionality on the silane can occur.[114] In this way, a triple-bonded spacer group can be introduced between mesogen and head group. Besides the hydrosilylation of mesogenic styrenes and phenyl acetylenes, this strategy was utilized for the synthesis of siloxane linked bimesogens and the results are described in the following chapter.

4.3 Summary

In this chapter, various synthesis strategies to build up a library of differently functionalized mesogen building blocks were presented. These routes were chosen with regard to basic coupling methods of the mesogens to differently functionalized silicon-containing head groups. As basic coupling methods, nucleophilic substitution on chlorosilanes by mesogenic nucleophiles and hydrosilylation of unsaturated mesogen functionalities by H-functionalized silane head groups were identified. For the coupling reactions by nucleophilic substitution, two synthesis strategies towards metalated mesogens were developed and investigated. Both transmetalation and *Grignard* synthesis, turned out to be not feasible, since the reaction of halogenated mesogens with magnesium or alkyl lithium reagents did not provide the target structures. Neither variations on the mesogen, nor optimizing of reactions conditions led to the desired metalated mesogens. Therefore, an alternative strategy for mesogen synthesis and coupling to head groups was developed.

Since hydrosilylation of mesogens with unsaturated functionalities was the second promising coupling method, synthesis routes towards mesogenic styrenes and phenylacetylenes were tested. The key steps in these syntheses were *Wittig* and *Corey-Fuchs* reactions for styrene and phenyl acetylene derivatives, respectively. As starting materials for both reactions, mesogenic benzaldehydes with various substitution motifs concerning number and length of alkoxy substituents were prepared. The overall yields of both reaction strategies were augmented by optimization of reaction conditions in the different reaction steps.

The library of mesogens, which is built up by these methods, covers a broad range of possibilities for the coupling of mesogens to silicon based head groups. The different coupling methods allow us the synthesis of silicon containing bi and multimesogens, as well as mesogen substituted chlorosilane monomers with different spacers between mesogen and head group.

5 Bi and Tetramesogens with Silicon Containing Linkers

5.1 Introduction

Since the early 1980s, polysiloxanes with mesogens in the side chain are well known to form self-assembled structures.[115] They attract increasing interest, mainly because of the great flexibility of the siloxane backbone which leads to low viscosities and lower glass transitions compared to other structured polymers, such as polyacrylates or polymethacrylates. Apart from studies about polymeric systems, low molecular weight (LMW) siloxanes combined with mesogens received great attention. The reason for that progression is that the incorporation of Si-atoms into carbon based mesogenic systems, affects in most cases the overall packing of the molecules and alters important features, such as melting points or mesophase morphologies.[107,116] Furthermore low-molecular mass systems are considered to be simple model systems for the much more complicated polymeric systems.[117] Different silicon containing LMW-liquid crystal (LC) systems were synthesized up to now; on one hand oligo(siloxane) and oligo(carbosilane) terminated monomesogens,[118-121] and on the other hand bi, tetra, and oligomesogens with various siloxane, carbosilane, or silsesquioxane linker groups.[122-124]

Most attention has been paid to investigations concerning cyclic and linear oligo(siloxane) linkers. Besides the synthesis of the compounds,[117,125] the different structures and the phase behavior have been studied in experiments[126-127] and in theory by molecular modeling.[128] Furthermore, effects of magnetic and electric fields,[129] as

well as the electrical and electro-optical behavior,[130-131] have been investigated. Various mesogens have been combined with siloxane containing linkers and backbones. The most prominent examples are: cyano biphenyls,[117-118,123,130] biphenyl benzoates,[122,126,129,132] phenyl benzoates with long alkyl chains,[124-125] or cholesteryl benzoates.[125-128] Investigations concerning the gallic acid mesogen, which is described in the previous chapter, have not been performed up to now.

On the basis of the precedent publications it turned out, that the nature of the mesogen has great influence on the structure and phase behavior of the self-assembled systems. Therefore, further advances in the design of mesogens is essential, to get better insights into structure-property-relationships of mesogen and assemblate. One major part of this study, describes possibilities to combine linear and cyclic low molar weight siloxanes with the new mesogen building blocks, using coupling strategies, which were previously described in *Chapter 4*.

In this chapter, different approaches towards bi and tetramesogens, which are linked with linear and cyclic silicon containing head groups, are presented; and strategies for the investigation of the self-assembled structures in bulk and in thin films, which are formed by the synthesized mesogens, are discussed. Moreover, influences on the physical and chemical properties, by variations in different parts of the target molecule are investigated. These variations are established by modifying structural parameters, such as: number and length of alkoxy substituents, nature of the spacer, and composition of the linking head group.

5.2 Synthesis

In the following, the synthesis of mesogen-functionalized low molar weight siloxanes and silanes is reported. As already mentioned, the constitution of the target molecules, is strongly depending on the nature and number of functionalities on the mesogens and head groups which are used for coupling.

The nature of the functional groups on the mesogen leads to different coupling methods (*e.g*. hydrosilylation or nucleophilic substitution), and therefore also to different spacer geometries; while the number of the functionalities on the head group determines the number of mesogens which can be attached to the head group. For instance, a linear siloxane telechel with functionalities in α and Ω position, results in a siloxane-linked bimesogen, whereas a cyclic tetrasiloxane with functionalities on each Si-atom can be used as basis for siloxane-linked tetramesogens. Both principles and their influence on the assemblate formation are investigated within this study.

5.2.1 Bimesogens

A broad variety of bimesogens with different spacers was synthesized, using the two standard reactions mentioned above. As linker groups, oligomeric siloxanes with differrent lengths, as well as dimeric silanes were applied. This strategy allowed numerous structure variations. For further modifications on the target structures, mesogens with different numbers and legths of the alkoxy substituents were used for coupling. This high number of different bimesogens requires a certain systematic nomenclature. In *Scheme 5.1*, the basic structure motifs, and their nomenclature rules are presented.

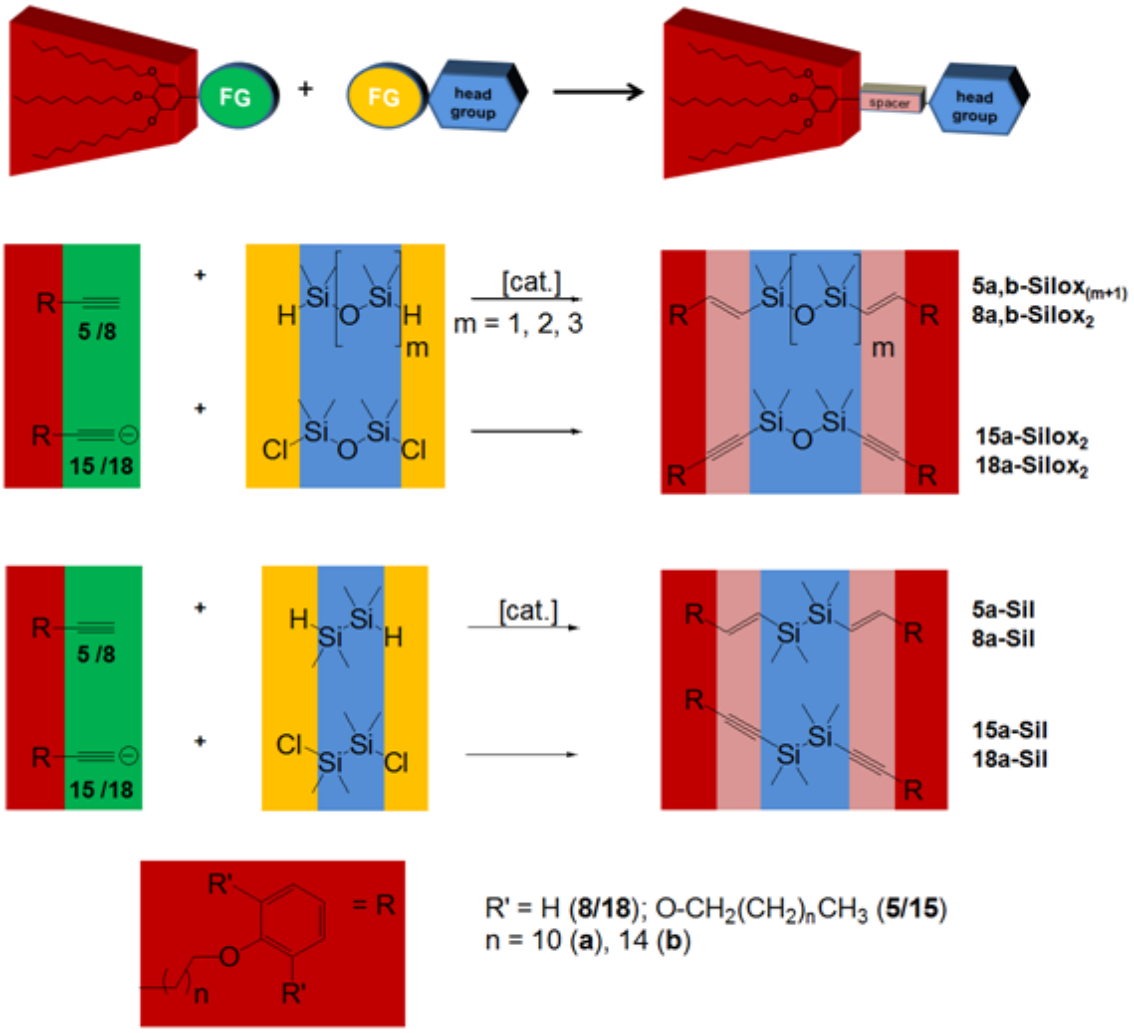

Scheme 5.1 *Formation of siloxane and silane linked bimesogens with different spacers, influenced by different coupling methods. The color code indicates the mesogen (red), the head group or linker (blue), the functional groups for coupling (yellow/green), and the resulting spacer (pink).*

The nomenclature rules are basically subdivided into two parts: the first part is a number, which derives from the utilized mesogen structure and indicates the synthesis method and the number of alkoxy-chains (its small letter index indicates the length); and the second part describes the linking head group (e.g. Silox for siloxane and Sil for silane).

For the synthesis of the bimesogens two different methods, which led to two different spacer geometries, were applied. By hydrosilylation of phenyl acetylene mesogens with H-terminated head groups, bimesogens with double-bonded spacers were obtained; whereas nucleophilic substitution on Cl-terminated head groups with phenyl acetylide mesogens, led to bimesogens with triple-bonded spacer groups.

For bimesogens with double-bonded spacers, a Ru(II) catalyzed (E)-selective hydrosilylation reaction, which was previously reported for small molecules of terminal alkynes by Ozawa *et al.*, was used.[133] The described reaction conditions were simply transferred to mesogenic phenyl acetylene derivatives. This strategy allowed us to synthesize mesogen end capped oligosiloxanes of different lengths (**5a,b-Silox$_{(m+1)}$** and **8a,b-Silox$_2$**), as well as mesogen end capped disilanes (**5a-Sil** and **8a-Sil**) in decent yields (80-95%). The desired products are exclusively obtained as (E)-isomers. The outstanding properties of this reaction concerning regio- and stereoselectivity result from the mechanistic circumstances, when $HCl(CO)(PPh_3)_3Ru$ is used as catalyst. The catalytic cycle is presented in *Scheme 5.2*.

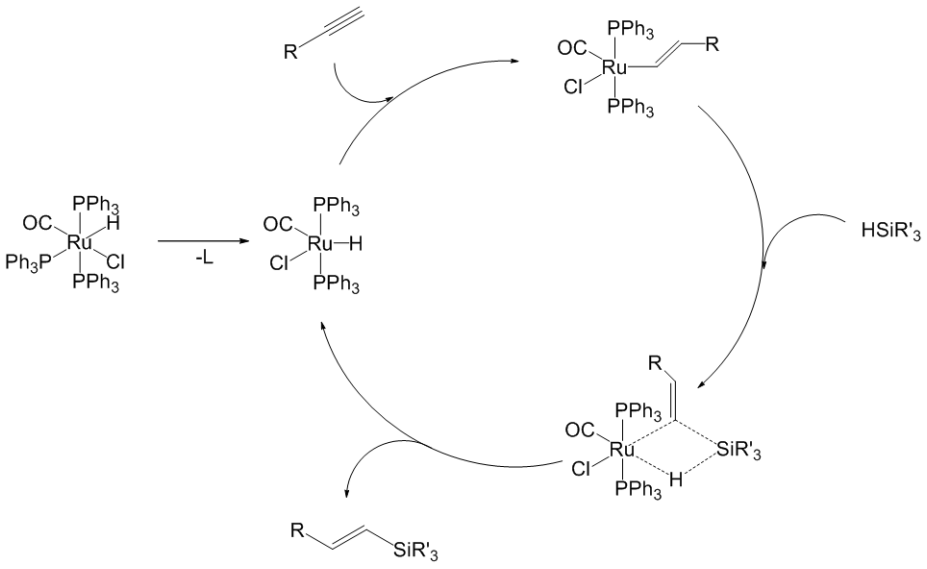

Scheme 5.2 *Catalytic cycle of the Ru(II)-catalyzed (E)-selective hydrosilylation of terminal alkynes, as presented by Ozawa et al.*[133]

In the first step the catalytically active Ru-hydride is obtained by separation of a PPh_3 ligand. In the second step the alkyne can insert into the Ru-H bond, and the 1-alkenyl complex is obtained. This intermediate forms a metalla-cyclobutane transition state with the hydrosilane, from which the thermodynamically favored (E)-olefin is released.

Bimesogens with triple-bonded alkynylene spacers are synthesized by nucleophilic substitution on Cl-terminated siloxanes and silanes. For this reaction, a method was applied, which was previously reported by Wang *et al.*[114] In this report, a *Corey-Fuchs* synthesis was performed without the quenching step (*Scheme 4.6*). Instead of acidic work-up of the intermediate alkynyl anion, an electrophile is added to facilitate a nucleophilic attack. We transferred this methodology to the synthesis of phenyl acetylene mesogens **5** and **8**, and obtained the compounds **15a-Silox2** and **18a-Silox2** as well as **15a-Sil** and **18a-Sil**, in very good yields of 88-92%, just by quenching of the acetylide intermediate with the corresponding α-ω-chlorosilane or siloxane.

5.2.2 Tetramesogens

In *Scheme 5.3* the synthesis route towards siloxane-linked tetramesogens is shown. In contrast to the linear bimesogens, for these tetramesogens only the hydrosilylation route was applied, since the corresponding Cl-functionalized educts were commercially not available.

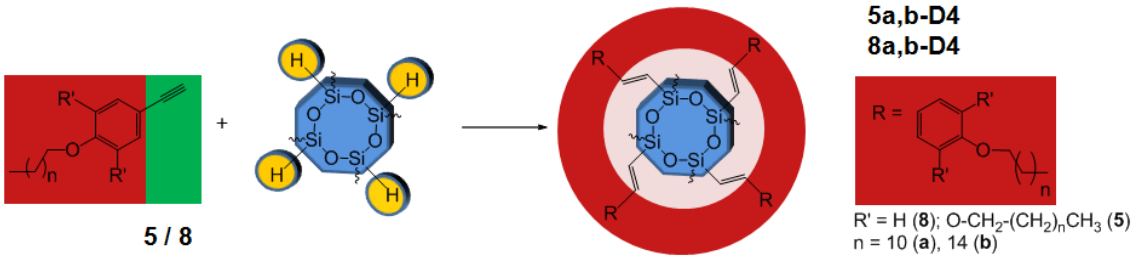

Scheme 5.3 *Formation of cyclotetrasiloxane-linked tetramesogens. The color code indicates the mesogen (red), the head group or linker (blue), the functional groups for coupling (yellow/green), and the resulting spacer (pink).*

As mesogens, both, mono and trialkoxy substituted phenyl acetylenes were tested. However, hydrosilylation with the cyclic siloxane gave isolable products only in combination with the mono-substituted mesogens **8**. Due to sterical issues, using the tri-substituted mesogens **5** for the hydrosilylation reactions to the tetramesogen **5-D4**, leads to product mixtures which contain besides fully functionalized cyclic siloxanes also a big amount of only di- and tri-functionalized cycles. These mixtures could not be separated by the standard purification techniques.

Therefore, we concentrated for further investigations on the siloxane cycles, which were functionalized with monoalkoxy substituted mesogens (**8**). During the hydrosilylation reaction, the formation of a white precipitate was observed. This precipitate was identified as one isomer of compound **8-D4** which could be isolated in comparably low yields of 25-29%. This finding can be explained with the stereochemistry at the Si-atoms in the siloxane cycle, as one takes into account, that the cyclic starting material is commercially available as mixture of stereo-isomers. In *Scheme 5.4*, the possible isomers of compound **8-D4** are depicted. One can easily imagine that only the isomers *a* and *b* possess the ability to form densely packed structures and thus precipitate during the reaction. In *Section 5.3.2* (Structure of Bulk Materials) the results form SAXS analysis are used to discuss, which isomer is obtained most likely. The other isomers could only be isolated as a crude mixture from the residual reaction solution, and were therefore not considered in further analyses.

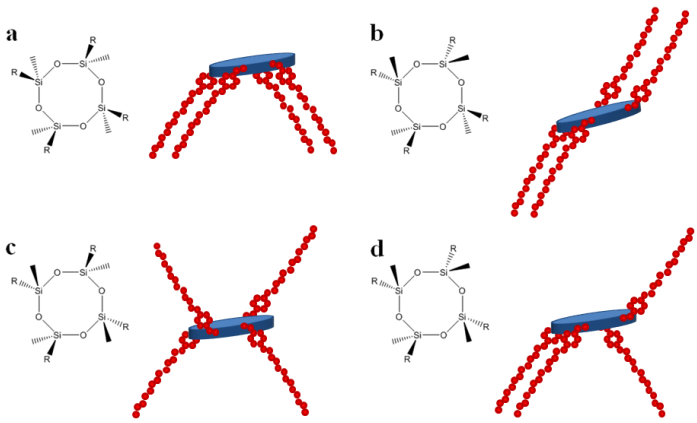

Scheme 5.4 *Possible structures of the different isomers after hydrosilylation of tetramethyl cyclotetrasiloxane.*

5.3 Properties of Bulk Materials

In this section, investigations on the self-assembled structures, which are formed by the synthesized bi- and tetra-mesogens in bulk, are presented. First of all, determination of thermal properties, such as stability and phase transition behavior, using thermal analysis tools, is reported. Subsequently, optical microscopy methods are used to examine first indications for self-assembled structures. Conclusively, structural investigations of the formed assemblies, using X-ray scattering techniques are described.

5.3.1 Thermal Properties and Formation of Mesophases

5.3.1.1 Thermal Stability

In future industrial and scientific applications, thermal stability of the mesogenic systems is a crucial point. One potential weak point in the molecules is the Si-alkene or Si-alkyne bond, since thermal bond scission and rearrangement reaction can occur.[134] Therefore the decomposition points of the synthesized siloxane-mesogens were determined by thermo gravimetrical analysis (TGA).

The different silicon containing mesogens turned out to be remarkably stable towards thermal treatment. For all compounds decomposition occurred between 350 °C and 450 °C when heated under a stream of dry N_2.

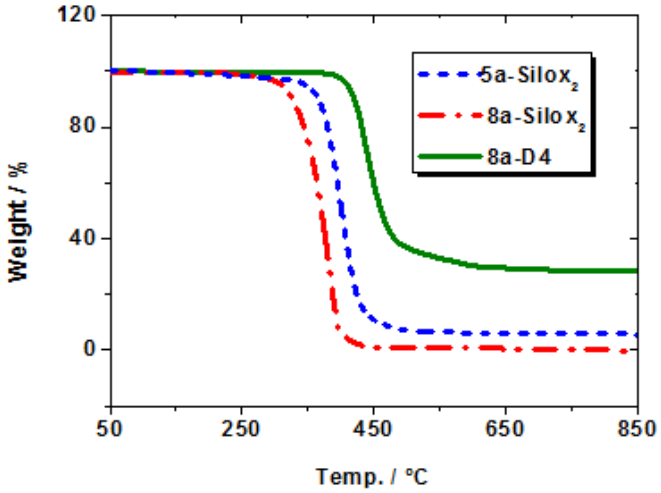

Figure 5.1 *TGA mass loss traces of compounds* ***5a-Silox2****,* ***8a-Silox2****, and* ***8a-D4****. The different compounds are assigned in the inset in the upper right corner.*

Different linker and spacer groups influence strongly the decomposition behavior (temperature and steps) and the residual masses (*Figure* 5.*1*). For instance, the linear compounds with disiloxane or disilane linkers decompose in a single step, whereas the cyclic compounds (**8-D4**) exhibit two-step decomposition. On the other hand, the amount of decomposition steps is not influenced by different number or length of alkyl chains on the mesogens or different spacer geometry (alkene/alkyne).

The residual masses after pyrolysis at 900 °C strongly depend on the nature of the linker or spacer, as well as on the number of alkoxy substituents (*Table 5.1*). For instance, the mesogens with disiloxane linker and one alkoxy substituent (**8-Silox$_2$**) decompose completely, whereas pyrolysis of the compounds with siloxane linkers of different lengths and three alkoxy substituents (**5-Silox$_{2/3/4}$**) leads to a mass residue of 5-6% (*w*/*w*). In the case of a disilane linker, the number of the alkyl chains does not play any role; with both, one and three alkoxy substituents, the mass residue does not exceed 3%. Using the alkyne spacers with any kind of linker, leads to varying mass residues between 1 and 16%, what does not follow any perceptible motif.

Table 5.1 *Phase transitions and decomposition points extracted from DSC and TGA measurements.*

Subst.	T_m1 [a] [°C]	T_m2 [a] [°C]	T_c1 [b] [°C]	T_c2 [b] [°C]	T_d [c] [°C]	m_r [c] [%]
5a-Silox$_2$	36.3	43.6	15.1	0.71	400	5.6
5b-Silox$_2$	34.9	49.4	32.8	13.5	418	5.9
5a-Silox$_3$	1.1	20.7	0.9	-23.7	403	4.6
5a-Silox$_4$	0.7	20.7	-1.55	-14.28	401	4.9
8a-Silox$_2$	69.4	/	52.9	48.4	382	0.0
8b-Silox$_2$	69.4	76.5	60.3	/	389	0.0
15a-Silox$_2$	10.6; 26.7	34.8	10.2	-1.7; -7.6	408	5.1
18a-Silox$_2$	-4.3; 13.6	36.5; 52.4	-0.4	-13.2	372	1.2
5a-Sil	4.21; 22.0	35.4; 41.4	-0.3	-8.5	354	3.6
8a-Sil	47.0	70.4	48.8	-23.7	362	2.3
15a-Sil	2.5	38.2	-1.0	-8.9	406	9.3
18a-Sil	53.9	70.9	42.4	34.7	365	16.4
8a-D4	125.8	/	116.8	115.2	432	27.1
8b-D4	121.5	/	110.3	108.6	436	22.1

[a] from DSC-heating runs; [b] from DSC-cooling runs; [c] from TGA; $T_m1/2$: endothermal phase transitions during heating; $T_c1/2$: exothermal phase transitions during cooling; T_d: decomposition temperature; m_r: residual mass.

The cyclic compounds (**8-D4**) are very much an exception among the different systems, since the residual masses account to 22-27%. In fact these mass losses are much too low to be explained only with the formation of SiO_2, which would give a theoretical residue of 14-16%. Therefore elemental analysis (EA) was performed with the TGA residue. EA showed a composition of 43% C and 26% Si in contrast to 47% Si, which is theoretically expected for SiO_2, i.e. the remaining material consists of a Si-O-C hybrid material. This behavior can be explained with strong interactions between the cyclic tetramesogens and consequential crosslinking of the siloxane cycles during decomposition. The linear mesogen analogues on the other hand, seem to possess less distinctive intermolecular interactions, and thus a crosslinking or the formation of hybrid or silicate structures, which would lead to considerable remaining material, could not be observed. Hence, decomposition of these compounds leads to volatile products and a mass loss of nearly 100%.

5.3.1.2 Phase Transitions and Mesophase Formation

First indications for the presence of self-assembled mesophases, which can occur besides crystalline and liquid phases, can easily be found by temperature controlled optical microscopy with crossed polarization filters, since mesophases possess typical distinctive optical textures, which are caused by birefringent polarization of light.[135-136] Furthermore, thermal analysis techniques, such as DSC can be utilized to monitor phase transitions besides the conventional liquid-crystalline transitions. With a combination of both techniques, one can prove the presence of mesophases with a relatively high certainty.

In *Figure 5.2*, optical textures of different linear bimesogens, obtained with polarized optical microscopy (POM) after instantaneous cooling of the bulk material from the isotropic melt (melting temperatures see *Table 5.1*) to room temperature, are presented. All substances show anisotropic, birefringent behavior, i.e. for all compounds, spherulitic textures which are typical for the formation of thermotropic mesophases are observable.

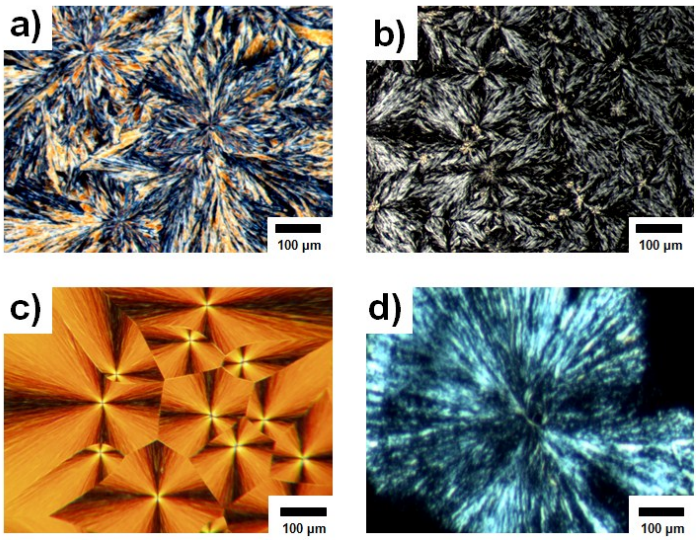

Figure 5.2 *Optical micrographs under crossed polarizer-analyzer geometry of the compounds* ***8a-Silox$_2$*** *(a),* ***8b-Silox$_2$*** *(b),* ***5a-Silox$_2$*** *(c),* ***5a-Silox$_3$*** *(d). Pictures were obtained after instantaneous cooling of the bulk materials from isotropic melt to room temperature.*

The domain sizes and birefringence intensities of the spherulitic textures differ strongly. In general, it is found that increasing alkoxy chain length on the mesogens leads to a decrease in domain size and intensity. This is most probably caused by stronger interactions between the alkyl chains, which consequently induces a higher tendency for interactions of alkoxy substituents from different stacks, and therefore for higher failures in the stacks. This effect is even more pronounced, when mesogens with three alkoxy substituents are used (not illustrated).

Incorporation of longer siloxane linkers affects the mesophase formation much more than variations in alkoxy chain length. The mesophase which is formed by the bimesogen with a trisiloxane linker (**5a-Silox$_3$**) is only observable by cooling of the sample below the melting point over more than 24 h (*Figure 5.2 d)*). Compounds with longer siloxane linkers, e.g. **5a-Silox$_4$**, do not show birefringent textures, not even after cooling to -20 °C over night. The reason for that are higher rotational degrees of freedom in the linker, and therefore a strongly decreased tendency for the formation of stacks or assemblies.

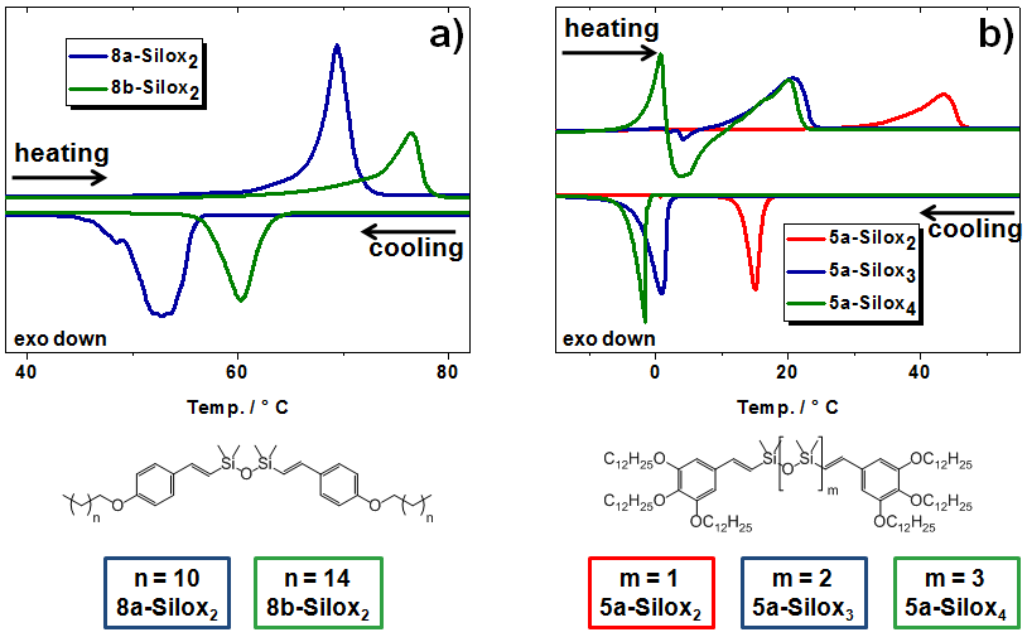

Figure 5.3 *DSC traces obtained during the second heating and cooling runs with heating and cooling rates of 10 K/min. (a) shows a comparison between substances with different alkoxy chain lengths on the mesogens (**8a/b-Silox$_2$**), and (b) a comparison between compounds with different siloxane linker lengths (**5a-Silox$_{2/3/4}$**). The different compounds are assigned in the insets.*

In *Figure 5.3* the results from DSC measurements on the previously discussed compounds are presented. In *a)* the influence of different alkyl chain lengths on the thermal properties is illustrated, whereas in *b)* the comparison between different siloxane linker lengths is shown. Also here a clear trend is observed: although longer siloxane linkers have lower melting points, an increase in alkyl substituent length leads to higher melting points. These findings are in good accordance to the POM results: longer alkyl chains lead to higher intermolecular interactions, but longer siloxane linkers result in higher degrees of freedom and therefore lower melting points. In the DSC-traces for the compounds **5a-Silox$_3$** and **5a-Silox$_4$** a further interesting effect is observable: on heating from low temperatures compound **5a-Silox$_3$** shows first an exothermic peak which is related to a rearrangement of the molecules before the actual melting process starts. In compound **5a-Silox$_4$** this effect is even more pronounced i.e. it possesses a higher enthalpy. Before the same exothermic transition, the system exhibits

even an endothermic transition. Since the exothermic transition and the actual melting points are located for both compounds at the very same temperatures, it seems that the melting process of these two compounds is decoupled into the melting of the siloxane linker and the melting of the alkoxy chains on the mesogen. In general it can be stated, that only the mesogen substitution and not the length of the linker group is responsible for the location of the melting point.

Besides the influence of substituent and linker length variations, also the effects of different linker and spacer types were investigated. As linker type variation, a tetramethyl disilane linker was applied (**5/8a-Sil**), and for an alternative spacer geometry, the alkene spacer was converted to an alkyne spacer and combined with both, disiloxane and disilane linkers (**15/18a-Sil/Silox$_2$**). As expected, all compounds with alternative linker types and spacer geometries show birefringent behavior upon supercooling of the isotropic melt. In *Figure 5.4*, exemplarily optical textures of the compounds **5a-Sil** (*a)*) and **18a-Sil** (*b)*) are presented. Once again, the sizes and intensities of the spherulitic domains vary strongly with varying substitution motifs.

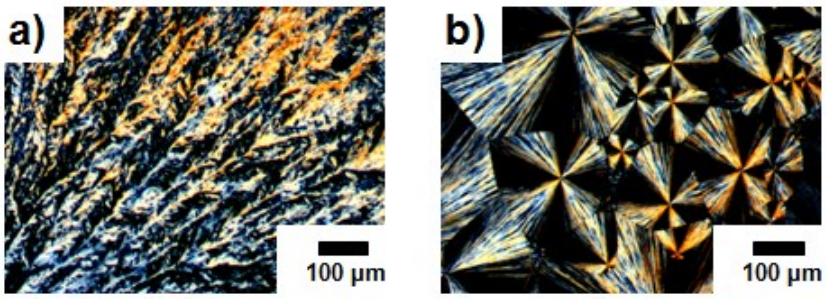

Figure 5.4 *Optical micrographs under crossed polarizer-analyzer geometry of the compounds* ***5a-Sil*** *(a) and* ***18a-Sil*** *(b). Pictures were obtained after instantaneous cooling of the bulk materials from isotropic melt to room temperature.*

For advanced investigations of the influence of alternative spacer and linker groups on the thermal properties, in *Figure 5.5* the data from thermal analysis of these compounds are shown. It can be seen, that the modifications of spacers and linkers do not affect the melting temperatures. Most probably, the reason for that is, as already stated above, that only the mesogen substitution, and not the constitution of the linker or spacer groups, contributes to the location of the melting point.

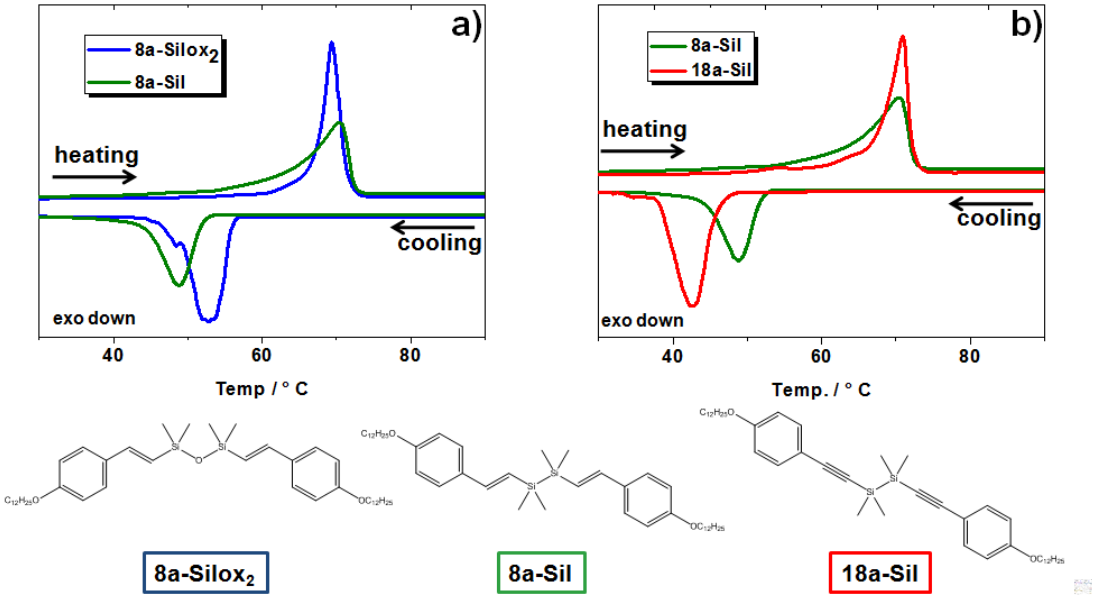

Figure 5.5 *DSC traces obtained during the second heating and cooling runs with heating and cooling rates of 10 K/min. (a) shows a comparison between compounds with different linker types (**8a-Silox$_2$/Sil**), and in (b) a comparison between different spacer types is presented (**8/18a-Sil**). The different compounds are assigned in the insets.*

Additional to the linear bimesogens, also tetramesogens with cyclic tetrasiloxane linkers were studied. As described in *Section 5.2.2* only tetramesogens with monoalkoxy substitution were accessible *via* the standard synthesis route. Therefore the only possible modifications on these molecules were varying lengths of the alkoxy substituents (**8a/b-D4**).

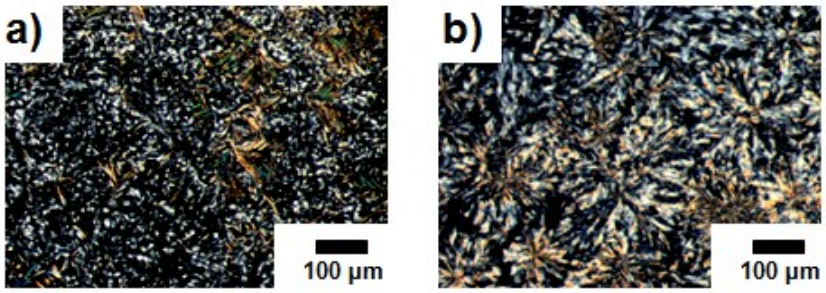

Figure 5.6 *Optical micrographs under crossed polarizer-analyzer geometry of the compounds* ***8a-D4*** *(a) and* ***8b-D4*** *(b). Pictures were obtained after instantaneous cooling of the bulk materials from isotropic melt to room temperature.*

In *Figure 5.6* the optical textures of both tetramesogens are presented. Both compounds show birefringence, but only the compound with longer alkoxy chains on the mesogens (**8b-D4**) exhibits the typical intense spherulitic textures. This is contrary to the linear bimesogens, where increased substituent chain lengths led to decreased size and intensity of the spherulitic textures.

The thermal phase behavior once again differs strongly from the linear bimesogens. With increasing chain length, the melting temperature decreases (*Figure 5.7*). But in general, the melting temperatures of the cyclic systems are twice as high as for the corresponding linear compounds. This can be explained with different strength of interactions between the mesogens. As already observed in TGA analysis, the cyclic compounds seem to possess a much higher tendency to the formation of stacked structures with strong intermolecular interactions. In contrast, the linear compounds have a higher number of degrees of freedom, which leads to lower melting points and a nearly complete decomposition in TGA.

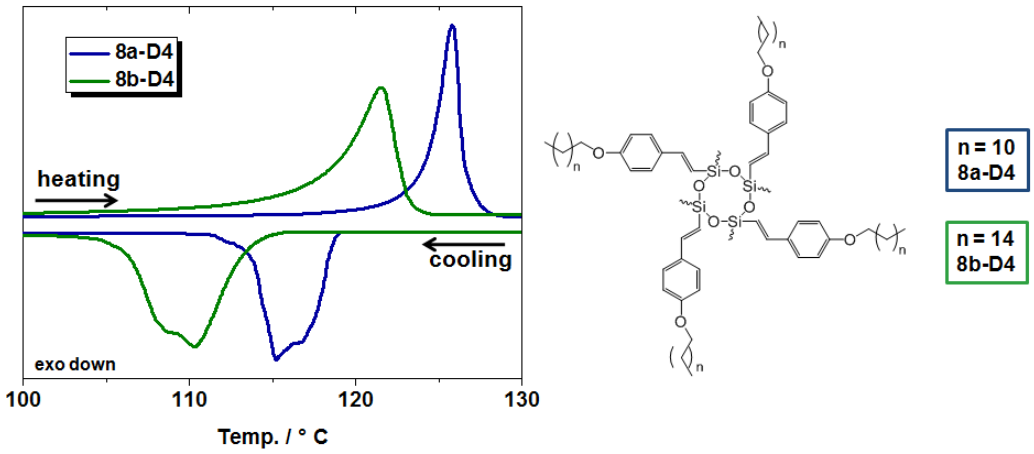

Figure 5.7 *DSC traces of compounds* ***8a-D4*** *and* ***8b-D4****, obtained during the second heating and cooling runs with heating and cooling rates of 10 K/min. The different compounds are assigned in the insets.*

The most important result of thermal analysis is that the mesophase textures of all compounds investigated in this study are only formed during immediate supercooling of the isotropic melts to room temperature. After isothermal crystallization at a temperature of a few K below the crystallization points (*see Table 5.1*), only crystalline textures are formed. Moreover, the crystallization process can be forced into mesophase formation, by abrupt cooling to room temperature during isothermal crystallization. This behavior is illustrated in *Figure 5.8*; when the molten compounds are cooled to a temperature of 2 K below the crystallization point, they start to crystallize. But if the temperature is decreased instantaneously to room temperature during the crystallization process, spontaneous mesophase formation can be observed. This is a strong indication that the mesophases formed by silicon containing bi and tetramesogens are monotropic. Monotropic mesophases are thermodynamically metastable, and can only be obtained on supercooling. They are caused by a kinetic effect, which in turn causes bypassing of the crystallization process.[44-45,137]

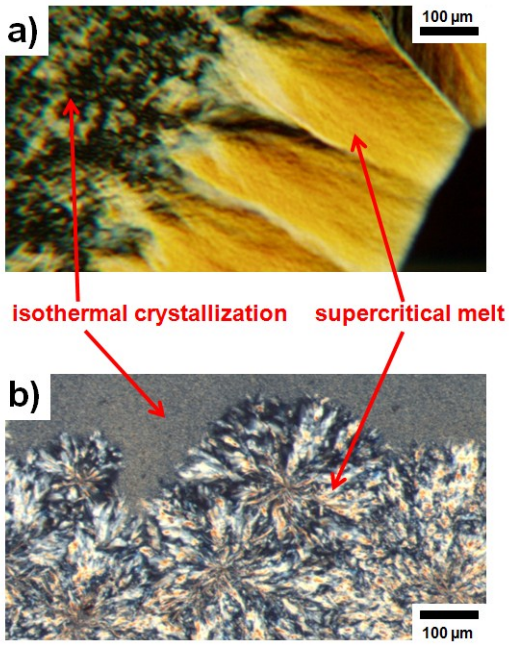

Figure 5.8 *Polarized optical micrographs of compounds* ***5a-Silox₂*** *(a) and* ***8b-D4*** *(b) taken after isothermal crystallization at 2 K below the crystallization temperature (see Table 5.1) and subsequent instantaneous cooling to room temperature.*

These results are strongly supported by thermal analysis using DSC. In the DSC diagrams all heating traces show only one peak for phase transition during melting (*Figures 5.3, 5.5, 5.7*); the presence of the monotropic mesophase is only indicated by small shoulders in the melting peaks. On the other hand, in the cooling traces, mostly two phase transition peaks are observed. But their overlapping indicates that the temperature ranges of the mesophases are very narrow (*Figures 5.3 a), 5.7*). Improvement in resolution of the multiple peaks in the heating and cooling traces could not be achieved; neither by heating of previously quenched isotropic melts, nor by applying different cooling rates, respectively.

In summary, we consider the phases which exhibit spherulitic textures in POM images as ‘frozen’ states of the mesophases or even as non-crystalline self-assembled solids. The structures of the frozen mesophases of some selected compounds were analyzed in bulk and thin films using different scattering techniques; this is reported in the next section.

5.3.2 Structures of Bulk Materials

To assess the inner structures of the 'frozen' mesophases in bulk, structure analysis was performed using synchrotron irradiation small-angle X-ray scattering (SAXS). From the scattering data, packing structures and domain sizes can be obtained. As synchrotron radiation source, beamline A2 at HASYLAB at DESY in Hamburg (Germany) was utilized. Several samples with different substitution motifs were analyzed. For linear bimesogens, besides the influence of different alkoxy chain lengths and numbers, also the influence of different linker types was investigated; whereas for cyclic tetramesogens, only different substituent lengths were assessed.

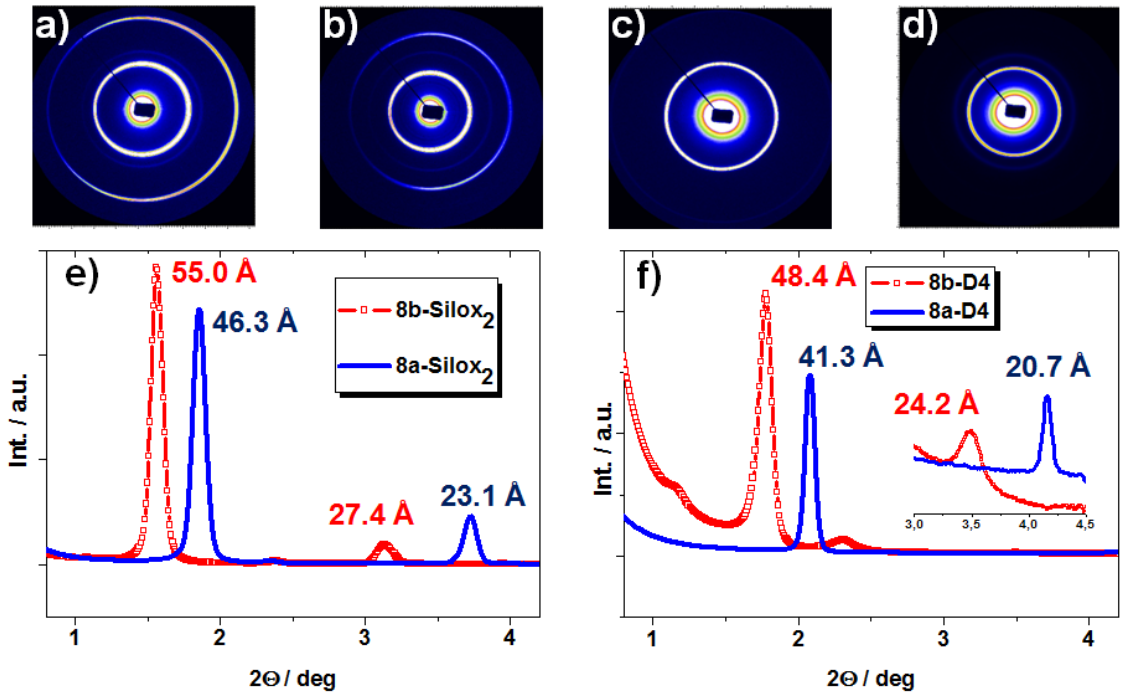

Figure 5.9 *2D scattering images of the compounds* ***8a-Silox₂*** *(a),* ***8b-Silox₂*** *(b),* ***8a-D4*** *(c),* ***8b-D4*** *(d) and SAXS traces (e, f) (derived from azimuthal averaging of the 2D data) of the same compounds (inset in (f) is the magnified area between 2Θ = 3.0 and 2Θ = 4.5).*

First the influence of different lengths of alkoxy substituents on the mesogens is discussed. In *Figure 5.9 a) - d)* typical 2D SAXS-profiles, which were observed for the compounds **8a/b-Silox$_2$** and **8a/b-D4** are shown; whereas in *e)* and *f)*, the corresponding azimuthally averaged and background-corrected curves are presented. The scattering angles (2Θ) as well as the layer distances, calculated using the *Bragg*-equation, are summarized in *Table 5.2*. The scattering data were acquired with samples which were heated above the melting point and subsequently cooled to room temperature. Therefore, the samples are in the previously mentioned state of a frozen mesophase.

Table 5.2 *Bragg peaks, and corresponding layer spacings obtained from SAXS.*

Subst.	2Θ [deg.]		D[a] [Å]		$2\Theta_1$:$2\Theta_2$
	1	2	1	2	
8a-Silox$_2$	1.85	3.72	46.3	23.1	1:2
8b-Silox$_2$	1.56	3.13	55.0	27.4	1:2
8a-D4	2.08	4.16	41.3	20.7	1:2
8b-D4	1.78	3.49	48.4	24.2	1:2
5a-Silox$_2$	2.60	-	33.1	-	-
5a-Sil	2.80	-	30.7	-	-

[a]: obtained by insertion of 2Θ values in *Bragg*-equation.

The monoalkoxy-substituted compounds show at least two strong diffraction peaks. These peaks can be attributed to spacings of layers, which are formed by the bi- and tetramesogens. Furthermore, the relations between the first and the second *Bragg*-peaks are 1:2. This ratio indicates the presence of a lamellar structure[138] which is typical for a smectic-type arrangement of the mesogens. For all compounds, we found strongly pronounced diffraction peaks between 2Θ = 1.5 ° and 2Θ = 2.3 °, and less pronounced peaks between 2Θ = 3.1 ° and 2Θ = 4.2 °. The corresponding layer spacings amount to 46 Å and 55 Å for compounds **8a-Silox$_2$** and **8b-Silox$_2$**, and 41 Å and 48 Å for compounds **8a-D4** and **8b-D4**, respectively. In the case of the linear compounds, the

observed spacings, as well as the difference in spacings of C_{12} and C_{16} substituents, correspond very well with the theoretically calculated values of 45 Å (**8a-Silox$_2$**) and 54 Å (**8b-Silox$_2$**) for completely stretched molecules (theoretical values were extracted from molecular models using previously published bond lengths and bond angles[139]). As result thereof, we propose densely packed and stacked domain structures of fully stretched bimesogens (*Scheme 5.5 a)*).

Since the observed spacing values for the cyclic compounds **8a-D4** and **8b-D4** are significantly smaller, the proposed structure for the linear systems is not appropriate for the cyclic mesogens, and the packing of the tetramesogens in the bulk is different (*Scheme 5.5 b)*). One possible reason for lower spacing values than in the case of the linear compounds with the same substitution is the angulated core of the tetramesogens. Another reason may be the stacked arrangement, which leads to a tilting of the mesogens in the stacks and thus to a lower spacing compared to the non-tilted arrangement. As already discussed in the 'synthesis' section (*Section 5.2.2*), hydrosilylation of phenyl acetylenes with tetramethyl cyclotetrasiloxane leads to four different stereoisomers (*Scheme 5.4*). Only two of these possible isomers are assumed to be able to form densely packed assemblies. Using the spacing values of 41 Å and 48 Å, one may conclude that only the stretched isomer with *anti*-conformation (*Scheme 5.4 b)*) was obtained.

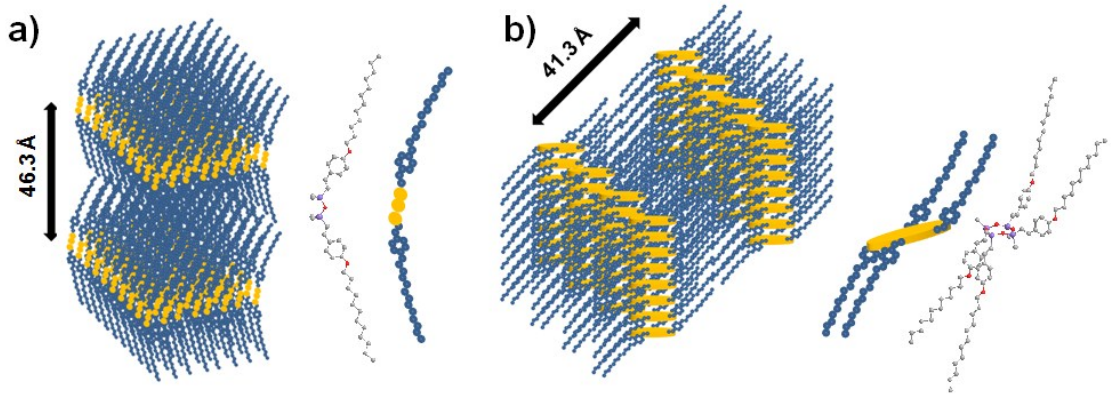

Scheme 5.5 *Schematic drawing of the mesogen packing in the self-assembled structures of linear bimesogens* ***8-Silox$_2$*** *(a) and cyclic tetramesogens* ***8-D4*** *(b).*

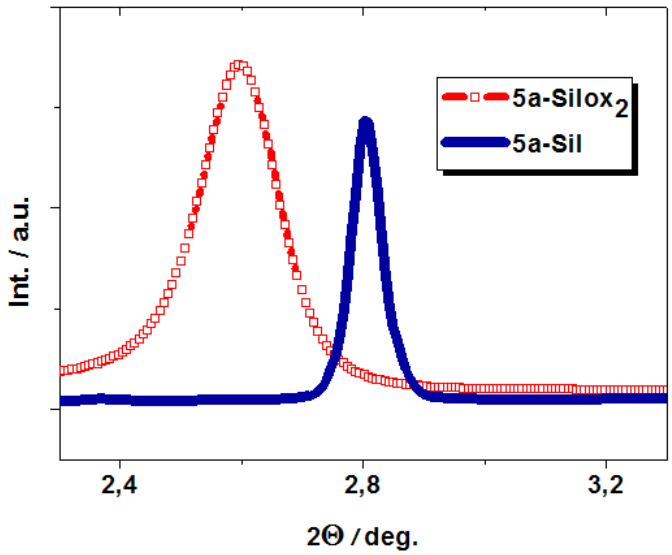

Figure 5.10 *SAXS traces derived from azimuthal averaging of 2D scattering images of the compounds* ***5a-Silox₂*** *and* ***5a-Sil****.*

In contrast to the monoalkoxy-substituted bimesogens, the SAXS traces of the compounds with three alkoxy substituents show only one distinct diffraction peak within the detection range, regardless of the linker type (*Figure 5.10*). The peaks of the compounds **5a-Silox₂** and **5a-Sil** are found at 2Θ = 2.60 ° and 2Θ = 2.80 °, respectively. The corresponding layer spacings therefore amount to 33.1 Å and 30.7 Å. These values are 10 - 15 Å smaller than in the mono-substituted systems, what indicates that the packing structure is similar, but shows, due to an increased amount of alkyl substituents, a higher degree of overlapping or interlocking between the individual stacks (*Scheme 5.6*). Also the difference in spacing (2.4 Å) between the siloxane and silane linked substances is reasonable, if one takes into account that the siloxane linked compound bears an additional O-atom. Furthermore the missing O-atom of the disilane linked compound **5a-Sil** results in a different configuration, and therefore in a denser packing of the bimesogens.

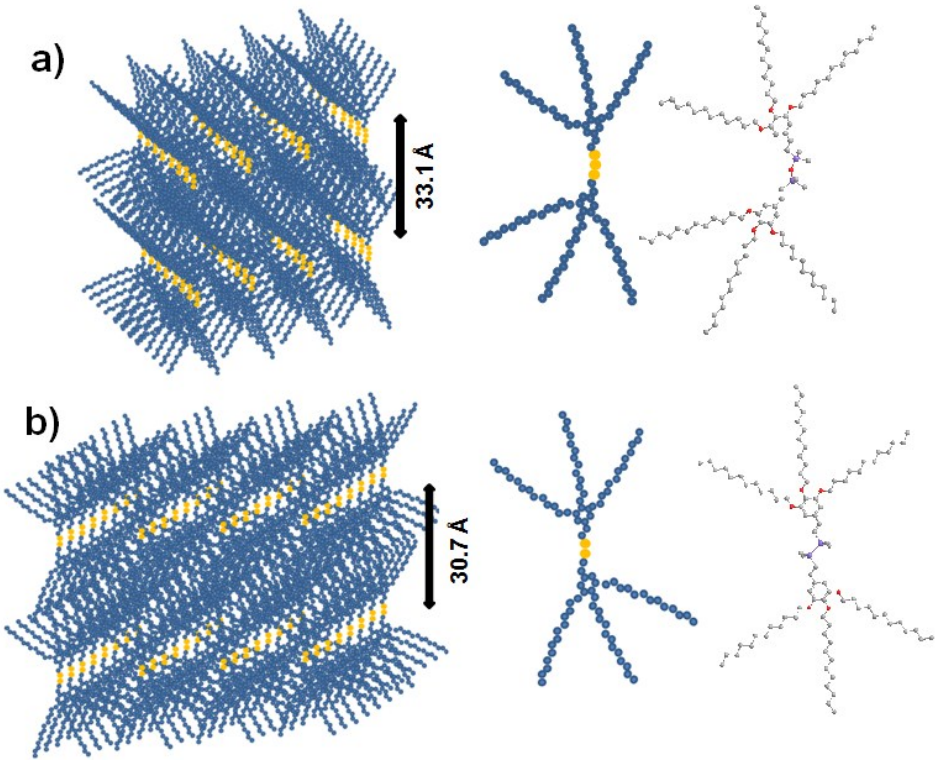

Scheme 5.6 *Schematic drawing of the mesogen packing in the self-assembled structures of tri-alkoxy substituted linear bimesogens* ***5a-Silox₂*** *(a) and* ***5a-Sil*** *(b).*

In this section it has been shown that different substitution motifs of the multimesogens with silicon containing linkers, cause considerable effects on the structures of the assemblies, and therefore on thermal stability and phase behavior. All multimesogenic systems with different substitution variations formed monotropic mesophases, which could be transferred into non-crystalline assemblies with defined layered smectic-type structures. Tetramesogens with cyclic oligo(siloxane) linkers showed the highest decomposition points and phase transition temperatures, but could only be synthesized with mono-alkoxy substitution on the mesogen. Linear bimesogens on the other hand, were accessible in high structural variations, since mono- and trialkoxy substituted mesogens could be utilized for coupling. This led to a high controllability of layer spacings and phase transition points. In the next section, the most promising multimesogens are used for structural investigations in thin films.

5.4 Morphologies and Structures of Thin Films

The ability of silicon containing multimesogens to form self-assembled thermotropic mesophase structures in bulk materials has been pointed out in the previous sections. As a corollary of these results, in this section, two different multimesogens are used to study the formation of self-assembled surface nano structures in thin films. The films were prepared by spin casting of $CHCl_3$-solutions of the compounds to Si-wafers, and the film characteristics, such as thickness and roughness, were assessed by white-light interferometry (WLI). For structure visualization on the surface of the thin films, atomic force microscopy (AFM) was used, whereas for the investigation of inner film structures grazing incidence small angle X-ray scattering (GISAXS) was employed. Furthermore the influence of thermal treatment on the surface structures is investigated.

5.4.1 Surface Structures Visualized by AFM

The surface morphologies of two films, which were prepared from the compounds **8a-Silox$_2$** and **8a-D4**, were studied using AFM. In *Figure 5.11*, 3D topographies of both samples are presented. Even though the stacking in the films is not perfect, it is seen that both compounds form layered domain structures. Furthermore, the domains, which are formed by the linear compound **8a-Silox$_2$** are more extended and much better defined than the ones, which are formed by the cyclic compound **8a-D4**. The local root mean square (rms) roughness acquired on images with a size of 10 x 10 μm^2 amounts to 124 and 20 nm for the samples **8a-Silox$_2$** and **8a-D4**, respectively. This result confirms the visual impression of a high orientational inhomogeneity of the smectic domains in sample **8a-Silox$_2$**. The domains in sample **8a-D4** are more homogenous, both in size and orientation.

From high resolution images (*Figure 5.12 (a)*), the layer distances are obtained (*Table 5.3*). For sample **8a-Silox$_2$** the smallest identifiable distances are 46 Å, whereas they are 44 Å for **8a-D4** (not illustrated). These values correspond very well with spacing values which were obtained from SAXS on bulk samples. Hence, for both bulk and thin films, a similar (smectic-type) mesogen packing inside the layered domains can be anticipated.

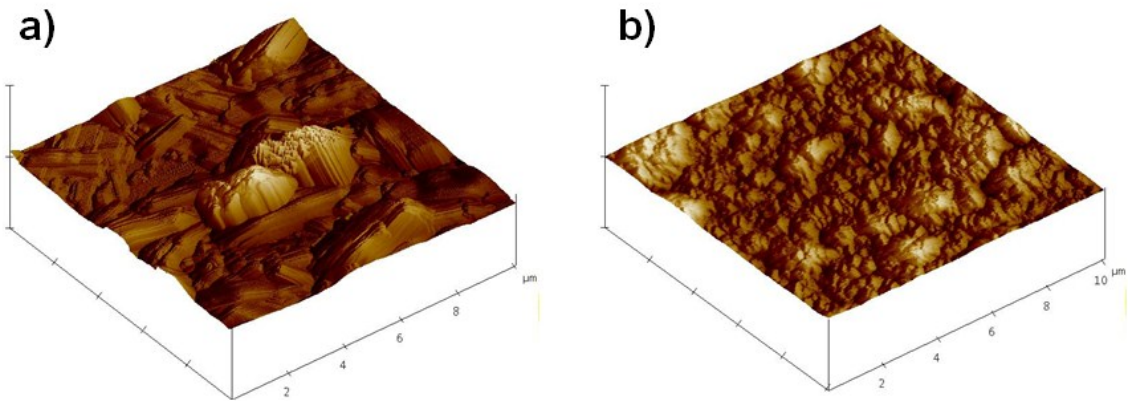

Figure 5.11 *3D AFM height contrast images of the layered surface structures of compounds* ***8a-Silox$_2$*** *(a) and* ***8a-D4*** *(b) (x, y, and z-scales are 2 µm/div).*

Table 5.3 *Results from AFM, white-light interferometry and GISAXS.*

Subst.	D_{film} [a] [Å]	r [a] [Å]	D [b] [Å]	D [c] [Å]	r [c] [Å]	ρ [b] [Å^{-3}]	D_{domain} [b] [Å]	Λ [b] [Å]
8a-Silox$_2$	822	8	48	46	16.1	0.28	300	1085
8a-D4	328	19	43	44	14.6	0.34	400	270

[a] from white-light interferometry (WLI), [b] from GISAXS, [c] from AFM. D_{film}: film thickness, r: roughness (WLI: 1 x 1 mm^2, AFM: 1 x 1 µm^2). D: layer thickness, ρ: electron density, D_{domain}: domain size along film normal, Λ: cut-off length of lateral correlations (see *Scheme 5.7*).

In *Figure 5.12 (b)*, an AFM height contrast image of sample **8a-Silox$_2$** after annealing above the melting point and subsequent cooling to room temperature is presented. Wide areas of flat, sheet-like arrangements are perceptible. Although these mesogen sheets are comparably large, their inner structure seems to be not completely dense, since a certain porosity can be observed. The same procedure which leads to the formation of monotropic mesophases in the bulk induces an increase in the lateral order of the layered structures in thin films. Conclusively, this technique allows us to form comparably large, non-covalent siloxane sheet structures with a lateral expansion of several micrometers. This procedure is restricted to linear bimesogens, since this behavior was not observed when cyclic systems were used.

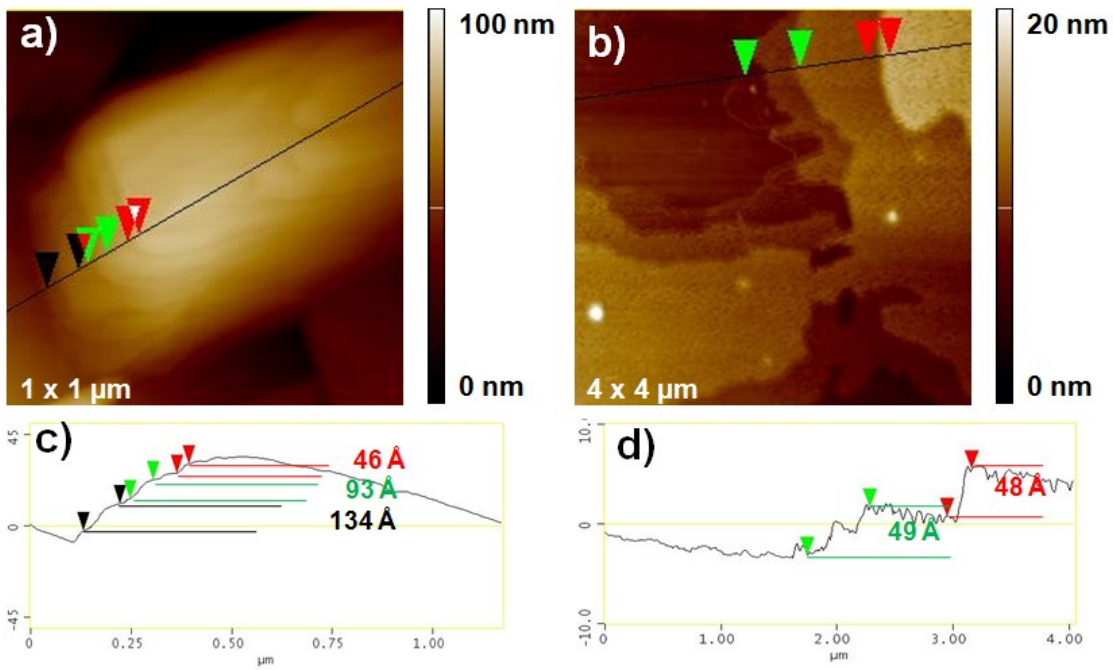

Figure 5.12 *AFM height contrast images (a, b), and corresponding z profiles (c, d) (black line in the AFM image). (a) and (c) show the structure formed by compound* ***8a-Silox$_2$*** *after spin casting; (b) and (d) show the analysis of the same sample after annealing at 80 °C and subsequent cooling to room temperature.*

5.4.2 Determination of Thin Film Characteristics

For determination of thin film characteristics such as thickness, roughness, and inner structures, the identical films as investigated using AFM were studied using WLI and GISAXS. WLI showed that, even though prepared from the same concentration and under the same conditions, the film from **8a-Silox$_2$** was thicker than the one from **8a-D4** (*Table 5.3*), indicating different solution viscosities. The thicknesses (822 Å and 328 Å) are much higher than the layer spacings, i.e. a large number of layers are stacked in the film (~18 for **8a-Silox$_2$** and ~8 for **8a-D4**). Also the surface roughnesses, measured using WLI, differ by more than a factor of two with the film from **8a-Silox$_2$** being much smoother (*Table 5.3*). These roughness values are averaged over the spot size of the light beam on the film and thus differ from local observations made by AFM. Since a larger area is averaged over, the WLI values are statistically more relevant than the ones from AFM.

The 2D GISAXS images from the film of **8a-Silox$_2$** (*Figure 5.13*) show – apart from strong diffuse scattering around the specularly reflected beam – two diffuse *Bragg* sheets (DBS) at q_z values between ~0.13 and 0.18 Å^{-1}. They can be attributed to first-order reflections of a layered and lamellar structure. Upon variation of the incident angle, the lower DBS stays at the same q_z position and thus corresponds to the scattering of the direct beam (*M1*). In contrast, the upper one moves upwards and becomes weaker as k_{iz} is increased; it is thus due to scattering from the specularly reflected beam (*P1*). For this film, the DBSs are relatively broad in q_z direction. The reason may be that the layer thickness is not well defined or that the film consists of domains in which only a few layers are stacked. Moreover, the DBSs do not extend far along q_y. The cut-off length of lateral correlations between different interfaces (Λ) is thus relatively high, i.e. the layer thickness remains correlated over a larger distance Λ (*Scheme 5.7*).

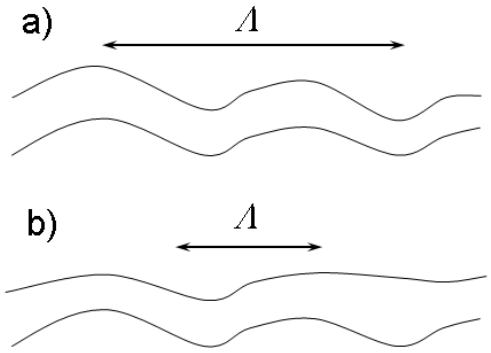

Scheme 5.7 *Meaning of the cut-off length Λ. (a) High value of Λ: long-range lateral correlation of different interfaces, (b): low value of Λ: short-range lateral correlation of different interfaces. For simplicity, only two interfaces are shown.*

These qualitative observations are analyzed in detail in the following. Fitting *Equation 2* (for equations see experimental section) to the intensity profiles $I(q_z)$ results in the q_z positions of the DBSs given in *Figure 5.14 (a)* as a function of the *z*-component of the incident wave vector, k_{iz}. Fitting *Equation 1* to the q_z positions results in the critical wave vector of the film $k_c = 0.010$ Å^{-1} and the layer thickness $D = 48$ Å (*Figure 5.14*, *Table 5.3*). This layer thickness is consistent with values, which were obtained for the same compound using SAXS and AFM. Furthermore, from k_c, an electron density of the film of $\rho = 0.28$ Å^{-3} can be calculated. The widths of the first-order DBS (*M1*) along the film normal q_z, are independent of k_{iz}, as expected, and scatter around a value $w_{z,M1} = (0.0167 \pm 0.0003)$ Å^{-1}. This width results in $D_{domain} \cong 300$ Å, i.e. each domain consists of ~6 layers (fluctuations of the layer thickness *D* are neglected). Note that the film on average consists of ~18 layers, as estimated from the ratio of D_{film} and *D*. Consistent with AFM observations (*Figure 5.12 (a)*), the stacking of the layers is thus not perfect; rather, domains are present within the film. The width of the first-order DBS *M1* along q_y amounts to $w_{y,M1} = (5.79 \pm 0.06)\ 10^{-3}$ Å^{-1}. The cut-off length *Λ* of lateral correlations is 1085 Å, thus the correlations between different layers extend very far in the film plane.

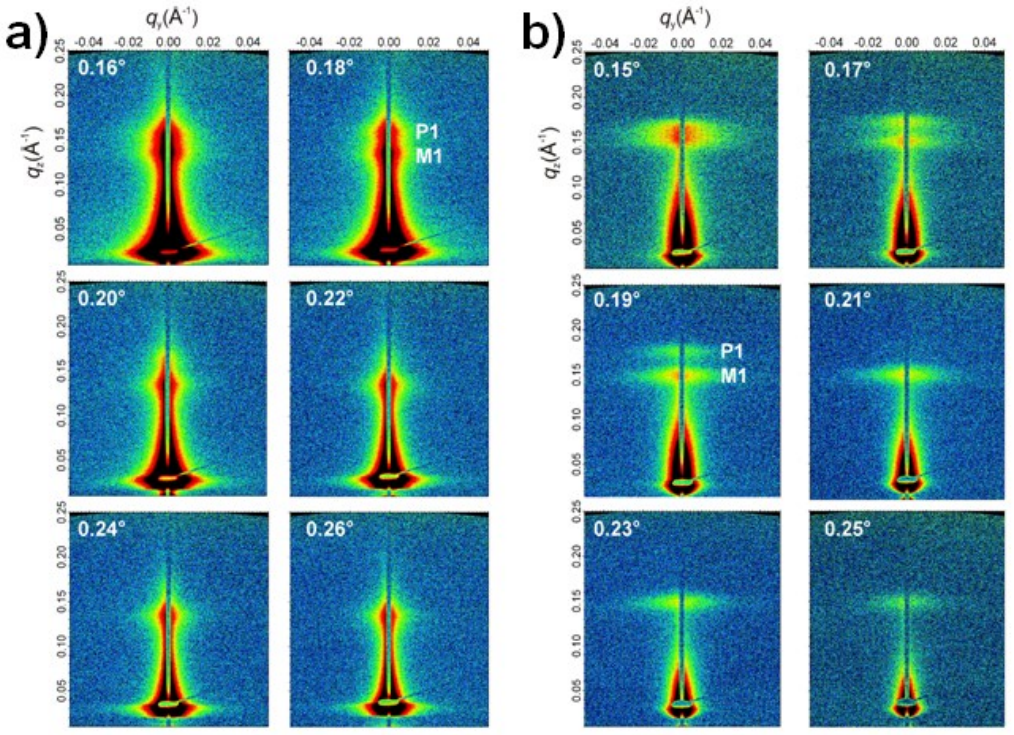

Figure 5.13 *2D GISAXS images from a thin film of* ***8a-Silox$_2$*** *(a) and* ***8a-D4*** *(b) taken at the incident angles indicated in the images. The logarithmic intensity scale runs from 9 cts (blue) to 50 cts (red). Shadows from the vertically mounted, rod-like beamstop as well as from the round beamstop covering the specularly reflected beam are observed. P1 and M1 are indicated in the images taken at 0.18 ° (a) and 0.19 ° (b).*

The GISAXS images from **8a-D4** are given in *Figure 5.13 (b)*. They also display DBSs, which, however, are located at higher q_z positions. Moreover, they are much wider along q_y and much narrower along q_z than the ones of **8a-Silox$_2$**. The film thus has a layer structure as well, however, with different characteristics: The layers are thinner, the domains are larger along the film normal (or the layer thickness is better defined), and the lateral correlation is less extended than in **8a-Silox$_2$**. The analysis of the DBSs' positions and widths confirms this hypothesis (*Figure 5.14 (c)*). From the fit of Eq. 1 to the peak positions, we obtain $k_c = 0.011$ Å^{-1} and $D = 43$ Å (*Figure 5.14*, *Table 5.3*). The higher k_c value of this sample results in a higher electron density, $\rho = 0.34$ Å^{-3}. This is consistent with our model for the packing of the different mesogens, which predicts denser packing structures for cyclic tetramesogens compared to the linear bimesogens

(*Section 5.3.2*). The average width of the DBS along q_z is $w_{z,M1}$ = (0.0125 ± 0.001) Å^{-1}, thus significantly smaller than for **8a-Silox2**. The resulting domain size is $D_{domain} \cong 400$ Å, i.e. more than 9 layers are correlated. This value is comparable to the number of layers contained in the film (~8); we conclude that the layer stacking is close to perfect. In contrast, the average width along q_y of **8a-D4** is $w_{y,M1}$ = (0.0231 ± 0.0005) Å^{-1}, i.e. significantly higher than for **8a-Silox2**. The cut-off length of lateral correlations is thus Λ = 270 Å. The correlations between different layers thus extend less far in the film plane than for **8a-Silox2**.

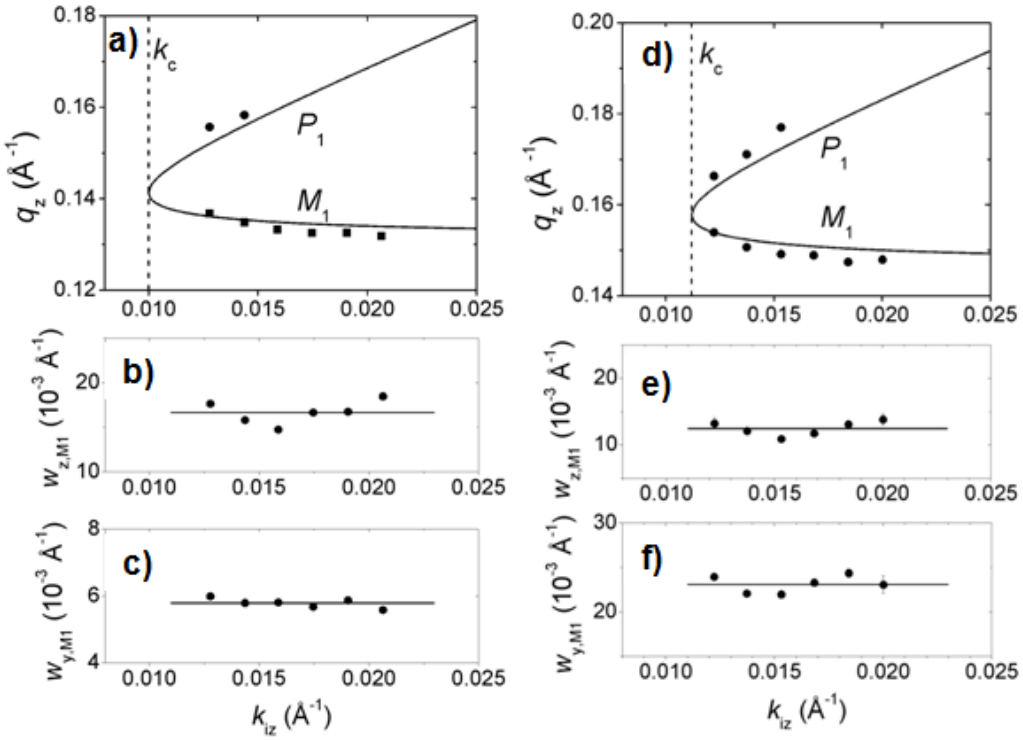

Figure 5.14 *Positions of the DBSs from Figure 5.13 a and b (a, d) and widths of the M1 DBS along q_z (b, e) and q_y (c, f) as a function of the z-component of the incident wave vector. The full lines in (a) and (b) are fits of Eq. 1 (see experimental section) to the experimental data (full circles). The dashed line marks the critical wave vector k_c. The full lines in (b), (c), (e), and (f) indicate the average values.*

5.5 Summary

In this chapter, the usage of various compounds from the mesogen library (see *Chapter 4*) for the synthesis of linear and cyclic bi and tetramesogens with silicon containing linker groups, as well as the self-assembly behavior of the target multimesogens, is described.

For the synthesis of the multimesogens, Ru-catalyzed hydrosilylation reactions of the unsaturated functional groups on the mesogens with H-functionalized linear and cyclic oligomeric silanes and siloxanes were utilized. This reaction route led to linear silane and siloxane linked bimesogens in exceptionally high yields of up to 99%, whereas the cyclic siloxane linked tetramesogens on the other hand, were only accessible with a yield of around 25%, which was shown to be due to the formation of different stereoisomers, of which only one could be isolated. Another possibility to synthesize bimesogens was shown, using an approach *via* a modified *Corey-Fuchs* reaction, which led to bimesogens with triple-bonded acetylene spacers between mesogen and silicon containing linker. All multimesogens were found to be extraordinary stable towards air, moisture, and also thermal treatment, which is important for later applications.

Investigations of the self-assembly behavior showed that all synthesized multimesogens possess the ability to form bulk mesophases, which were then analyzed using POM and DSC. The most important result was that the mesophases, which exhibit spherulitic textures in POM, were found to be monotropic and therefore only occur during supercooling of isotropic melts to room temperature. Furthermore, this result led to the assumption, that the spherulitic textures are a special form of frozen mesophases.

Different structural parameters of the multimesogens, such as linker type, linker length, or different alkoxy substitution motifs on the mesogens were systematically varied, and the influence of the structural changes on the mesophase formation was investigated. It turned out that among the linear bimesogens the most influential parameter on the

properties of the mesophases was the length of the siloxane linker, followed by the number of alkoxy groups on the mesogen. The type of the linker (silane/siloxane), as well as the type of the spacer (ethylene/acetylene) was found to be of secondary importance for mesophase formation.

The inner structures of the self-assembled ‘frozen’ bulk mesophases were assessed using small angle X-ray scattering with synchrotron irradiation. For SAXS analysis, linear silane and siloxane linked bimesogens with differently substituted mesogens, as well as cyclic siloxane linked tetramesogens were used. It was shown that the mesophases of all investigated compounds form smectic type layered structures with different layer thicknesses, which mainly depend on the mesogen’s alkoxy chain lengths. Furthermore it was observed that different linker types and different alkoxy chain numbers lead to noticeable variations in stacking structures. Therefore different packing models were developed according to the scattering data.

In the last part, different linear and cyclic mesogens were used for the formation of solution processed thin films on substrate surfaces. These thin films allowed the visualization of the layered structures by AFM; using this technique it has been found that the smectic type layered structures appear in domains. Furthermore thermal annealing of the thin films allowed the formation of non-covalent siloxane sheet structures with a lateral expansion of several micrometers. Additional properties of the films, such as the sizes of the domains, cut-off lengths, or even electron densities were assessed by grazing incidence small angle X-ray scattering.

In summary, it has been shown that the combination of the compounds from the mesogen library with silicon based linker groups offers a powerful tool to form layered structures in bulk and thin films; and by slight variations of the chemical structure of the mesogens, full control over the dimensions and structures of the layers can be obtained.

6 Silicon Based Polymers

6.1 Introduction

In the 1970s, the first synthesis procedures for soluble high molecular weight polysilanes appeared in literature. Although this class of materials was known since the 1920s, in the next 50 years no viable synthesis methods were found. Therefore, these publications caused worldwide unprecedented attention in formation and application of polysilanes.[50] The high interest is justified by their outstanding electronic properties, which are based on the σ-σ-bond delocalization of the binding electrons along the backbone, consisting of catenated Si atoms. Although in the last 20 years the common interest on polysilanes strongly declined due to lacking stability of the Si-Si bonds, growing demand for new materials for OLED and OFET devices, as well as new precursors for high performance ceramics, led to recent developments of new synthesis strategies.[140]

Furthermore, recent developments in supramolecular chemistry and catalysis, as well as groundbreaking innovations in analysis techniques, such as electron and scanning probe microscopy, facilitated discoveries of novel structural motifs in carbon based chemistry and the accompanying industrial fabrication methods of carbon allotropes, such as carbon nanotubes or graphenes.[141] Hence, our motivation for combining a supramolecular approach with the use of modern analysis tools to find new synthesis and characterization methods for novel silicon polymer structures, is based upon the described progress.

Although in *Chapter 2* numerous modern procedures for polysilane synthesis were described, we only focus in this work on the well established *Wurtz*-type reductive polymerizations. For this reason the synthesis of various monomer structures, which combine polymerizable di- and trifunctional chlorosilanes with different mesogens from the mesogen library (*Chapter 4*), is described. For the polymerization of these monomers, the effectiveness of different reducing agents and reaction conditions is screened.

The obtained polymers are investigated towards their chemical and physical properties, as well as the formation of self assembled structures. Furthermore the polymers are used as precursors for the synthesis of nanostructured silica and silicon based ceramics by pyrolysis.

6.2 Synthesis of Monomers

In this section, the synthesis strategy to mesogen-substituted chlorosilane monomers, which are later used for reductive *Wurtz*-type polymerizations, is reported. *Scheme 6.1* shows the different synthesis routes, based on hydrosilylation reactions of mesogen building blocks with H-functional chlorosilanes. As already described for oligo-mesogens in the previous chapter, the properties of the target polymers strongly depend on number and length of alkoxy substituents as well as the constitution of the spacer group between head group and mesogen. Therefore differently substituted styrene (**4**/**7**) and phenyl acetylene (**5**/**8**) based mesogens from the mesogen library in *Section 4.2.2* are used as substrates for hydrosilylation reactions.

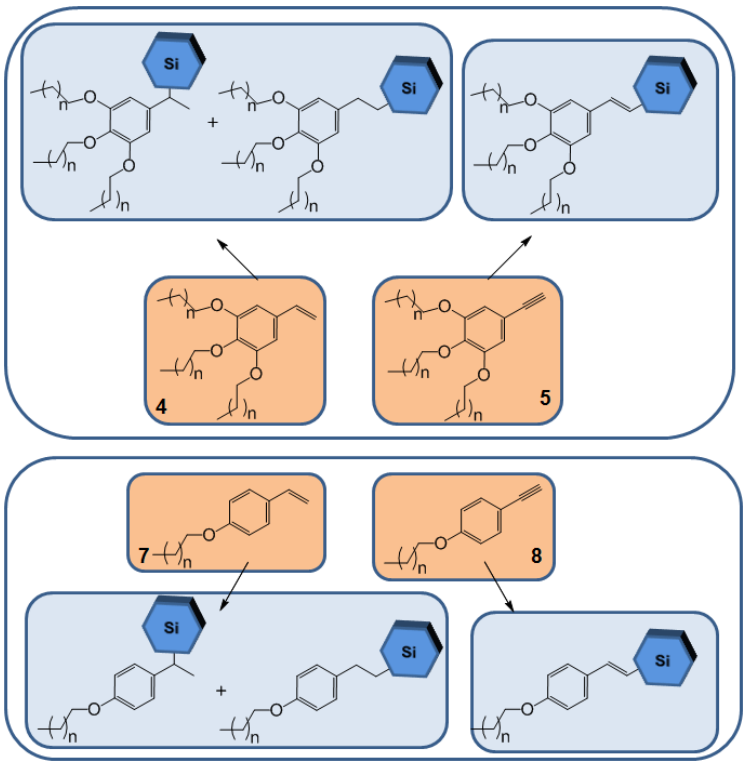

Scheme 6.1 *Synthesis strategy towards mesogen substituted chlorosilane monomers by hydrosilylation of different mesogen building blocks.*

As can be concluded from *Scheme 6.1*, each hydrosilylation reaction of styrene mesogens **4** and **7** can lead to two different regio-isomers with different saturated spacer groups due to *Markovnikov's* rule.[142] Whereas hydrosilylation of phenylacetylenes **5** and **8** with a Ru-based catalyst, which was presented in *Section 5.2.2*, yields exclusively one unsaturated regio- and stereoisomer. In the following, different synthetic approaches, leading to different variations of mesogenic chlorosilane monomers are presented and discussed.

6.2.1 Phenylacetylene-Based Monomers

The synthesis route to phenylacetylene-based chlorosilane monomers with unsaturated spacer groups is shown in *Scheme 6.2*. This route consists of a Ru-catalyzed hydrosilylation reaction, which is well known to produce the monomers with high regio- and stereo-selectivity. The catalyst in this reaction was discovered by Ozawa *et al.*[133] and was already used in this work for the synthesis of siloxane-linked oligomesogens (see *Section 5.2.2*).

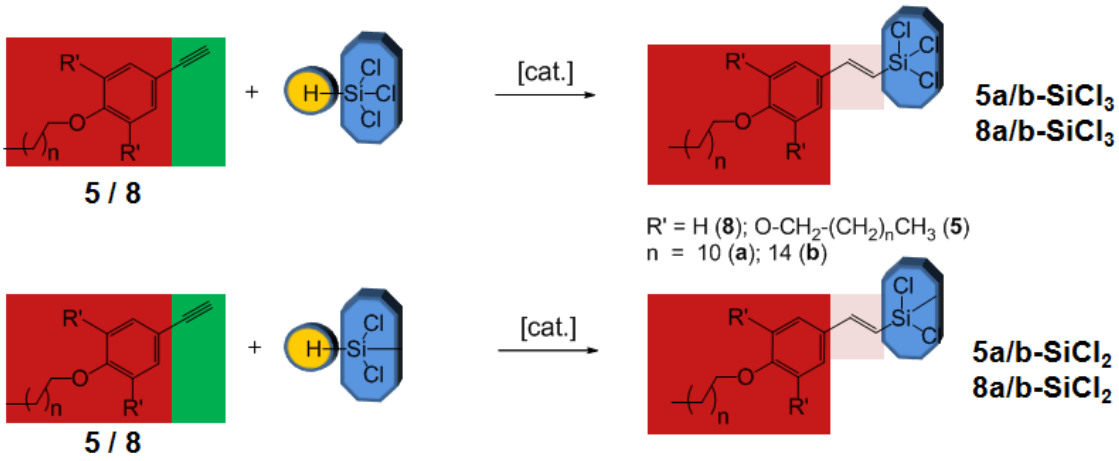

Scheme 6.2 *Synthesis schemes towards di and trifunctional silane monomers by hydrosilylation of phenylacetylene mesogens.*

Besides different mesogenic phenylacetylene building blocks, two different chlorosilanes were utilized for hydrosilylation: on the one hand dichloro methylsilane leading to difunctional monomers (**α/β-5/8-SiCl$_3$**), which serve as educts for linear polysilanes; and on the other hand trichloro silane, which gives trifunctional monomers (**α/β-5/8-SiCl$_3$**) for the synthesis of network polysilanes.

The reactions were performed using the same procedure as already described for siloxane-linked oligomesogens. An excess of chlorosilane was added to a mixture of phenylacetylene mesogen and 2-5% (n/n) of catalyst in DCM. Reaction control was performed by monitoring the disappearance of the acetylene signal (δ = 2.99 ppm) in proton NMR.

Also here, all Ru-catalyzed hydrosilylations were extremely effective; the monomers with different functionalities were obtained exclusively as (E)-isomers in quantitative yields. This is essential for later polymerizations, since the chlorosilane monomers cannot be isolated with standard purification techniques due to high sensitivity towards hydrolysis.

6.2.2 Styrene-Based Monomers

In the synthetic approach towards mesogenic chlorosilane monomers with saturated spacer groups, homogeneously catalyzed hydrosilylation of styrene based mesogen building blocks with H-functionalized chlorosilanes is used. In *Scheme 6.3* the reaction schemes, leading to different monomers are presented. Also here two different chlorosilanes were utilized: dichloro methylsilane leading to difunctional monomers (**α/β-4/7-SiCl$_2$**), and trichloro silane, which gives trifunctional monomers (**α/β-4/7-SiCl$_3$**).

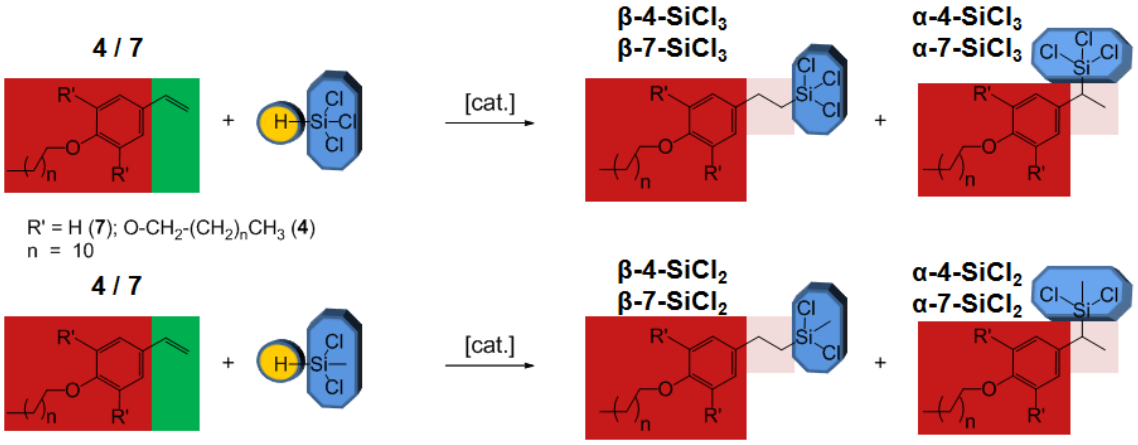

Scheme 6.3 *Synthesis schemes towards di and trifunctional silane monomers by hydrosilylation of styrene mesogens.*

All hydrosilylation reactions of styrene derivatives **4** and **7** were performed under homogeneous catalysis, using transition metal based catalysts such as e.g. *Karstedt's* catalyst (*Scheme 6.4 (a)*). *Karstedt's* catalyst is the standard, most used catalytic system in scientific and industrial hydrosilylation syntheses. But throughout this work, it showed considerable differences in activity between differently substituted styrene mesogens. For instance the quantitative hydrosilylation of monoalkoxy substituted styrene **7** could be performed with *Karstedt's* catalyst at room temperature over night, whereas the quantitative hydrosilylation of trialkoxy styrene **4** in the same period of time required elevated temperature (80 °C) and double the amount of catalyst. In *Table 6.1* the results on hydrosilylation reaction using *Karstedt's* catalyst are summarized.

Besides the problems concerning activity, also the regio-selectivity is an issue. Apparently, using *Karstedt's* catalyst, leads in certain cases to mixtures of the two different regio isomers. As it can be seen from *Table 6.1*, the selectivity is strongly depending on different factors, such as the substitution motifs on the styrene derivative or the silane. For instance the reaction between dichloro dimethylsilane with styrene **7** leads to a product distribution of 1:1 between α- and β-adduct, whereas the same conditions in the reaction with styrene **4** yields exclusively the β-adduct.

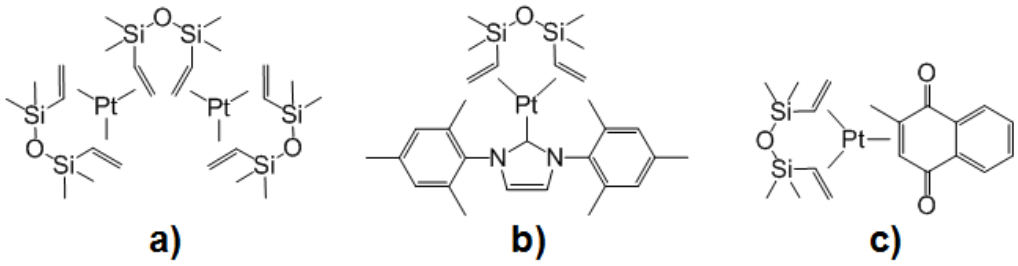

Scheme 6.4 *Chemical structures of selected Pt based catalysts for homogeneously catalyzed hydrosilylation reactions (Karstedt's catalyst (a), Markó's catalyst (b), Dötz's catalyst (c)).*

The formation of the different regio-isomers (α/β) can easily be explained by the reaction mechanism of the hydrosilylation reaction. In *Scheme 6.5*, the mechanistic cycle of hydrosilylation reactions, which has been postulated by *Chalk* and *Harrod* in the 1960s, is shown.[143-144] This mechanism consists exclusively of steps, which are well known in transition metal catalysis. The first two are coordination of the olefin to the metal center (Pt^0) (**a**) and subsequent oxidative addition of the silane and formation of Pt^{II}-species (**b**). The following olefin insertion is the decisive step for the formation of the different regio-isomers. In this step, the hydride originating from the silane can be transferred either to the internal (**c**) or to the terminal (**d**) C atom of the olefin. In the last step, which is a reductive elimination, the α- or the β-product is released (**e**/**f**) and the Pt^0 center is regenerated. The decision which route is the most probable is basically depending on steric and electronic issues. This can be essentially affected, besides by the reactants, by the type of the ligands on the catalytic species. Furthermore it is influenced by solvent and reaction temperature.

The results of the coupling reactions using *Karstedt's* system forced us to screen other, more recent catalysts, such as *Markó's*[145] or *Dötz's*[146] systems (see *Scheme 6.4 (b/c)*), to identify the best conditions for high activity and high regio-selectivity at the same time. In the following section the approaches towards regio-selective hydrosilylations are presented and discussed.

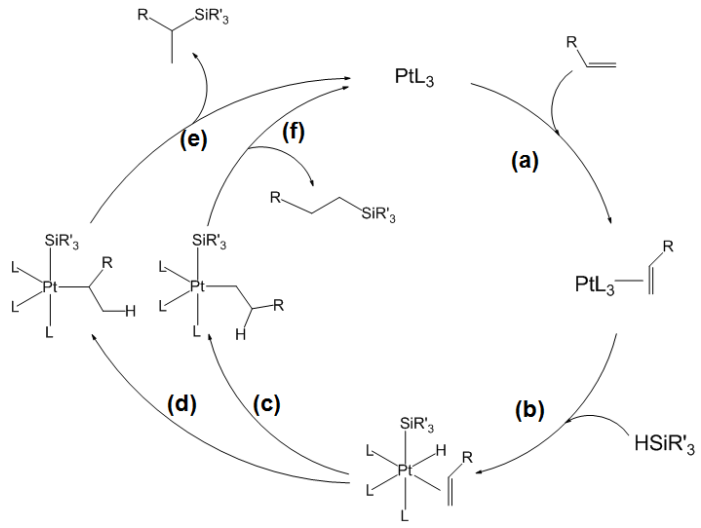

Scheme 6.5 *Catalytic cycle of the Chalk-Harrod-mechanism for homogeneous catalysis of hydrosilylation reactions on substituted olefins.*[143-144]

Table 6.1 *Results on selected hydrosilylation reactions of mesogenic styrene derivatives with differently substituted silanes.*

Subst.	silane	catalyst	conversion [%]	α [%]	β [%]
7	$HSiCH_3Cl_2$	*Karstedt*	100 [a]	55	45
4	$HSiCH_3Cl_2$	*Karstedt*	85 [b]	0	100
4	$HSiCl_3$	*Karstedt*	100 [b]	30	70
7	$HSiCH_3Cl_2$	*Markó*	30 [c]	0	100
7	$HSiCl_3$	*Markó*	10 [d]	50	50
4	$HSiCl_3$	*Markó*	100 [b]	30	70
4/7	$HSiCl_3$	*Dötz*	0 [e]	0	0
4/7	$HSiCl_3$	*Pd-P1*	100 [a]	100	0
4/7	$HSiCl_3$	*Pd-P2*	100 [a]	100	0
4/7	$HSiCl_3$	*Pd-P3*	100 [f]	100	0

[a] after 16 h at RT; [b] after 72 h at 80°C; [c]after 120 h at RT; [d] after 96 h at RT;[e] after 16 h at RT formation of huge amount of colloid; [f]after 4h at RT

6.2.2.1 Regio-Selective Hydrosilylations of Mesogenic Styrenes

For the interpretation of the results of later studies on self-assembly, the mesogen-decorated polymers should consist of regio-isomer-pure monomers. Since the hydrosilylation of styrenes using *Karstedt's* catalyst showed different issues concerning regio-selectivity and also activity, other catalytic systems were tested to achieve isolation of the two different regio-isomers. In the literature many Pt-based derivatives of *Karstedt's* complex are known.[142] Two of them are the previously mentioned *Markó's*[145] and *Dötz's*[146] catalysts (*Scheme 6.4 (b/c)*). *Markó's* system is based on N-heterocyclic carbene (NHC) ligands and was first presented in early 2000's. These ligand systems are well known to tolerate a wide range of functional groups and to produce a low amount of colloids. Furthermore they are known for regio-selective conversions of substituted styrenes. *Dötz's* system, which was presented in 2000 is based on quinone (Vitamin K) and can easily be synthesized from *Karstedt's* system. Although *Dötz's* catalyst is also known for regio-selective conversions, prevention of colloid formation has not been described.

Besides the Pt-based systems (*Scheme 6.4*), also recently discovered Pd-based systems, were used. These systems are shown in *Scheme 6.6*: As catalyst precursor serves the dimer of palladium allylchloride (*(a)*) to which different phosphorous containing ligands can be attached (*(b)-(d)*). These catalysts are referred to as *Pd-P1/2/3*. Although Pd-based system are not generally regarded as good hydrosilylation catalysts because of the ease of their reduction to the metal by silicon hydrides, a considerable amount of reports suggest the effectiveness of Pd^0-phosphine complexes.[142]

In *Table 6.1* the results of the hydrosilylation reactions with alternative Pt- and Pd-based catalysts are summarized. Indeed with these systems enhanced regio-selectivity and in one case even strongly improved activity was achieved. In the following the reactions are discussed in detail:

Markó: The NHC-based systems show enhanced regio-selectivity only in the case of styrene **7** and dichloro dimethylsilane. In all other cases the selectivity is comparable to *Karstedt's* catalyst. But the activity seems to be much lower.

Dötz: The quinone based catalyst is the only system, which is regio-selective towards the β-adduct. Unfortunately, a considerable amount of colloidal side-product, which cannot be separated with standard purification techniques due to high affinity towards hydrolysis, is formed.

Pd-P1/P2: Both Pd-based catalysts with triphenylphosphine- and binaphthyl diphenylphosphine-ligands yield exclusively the α-isomer with a conversion of 100% after 72 h at room temperature.

Pd-P3: Although the sulfoxide bridged phenylphosphine ligand also yields 100% of α-isomer, the activity of the catalyst is considerably higher: full conversion is achieved already after 4 h at room temperature.

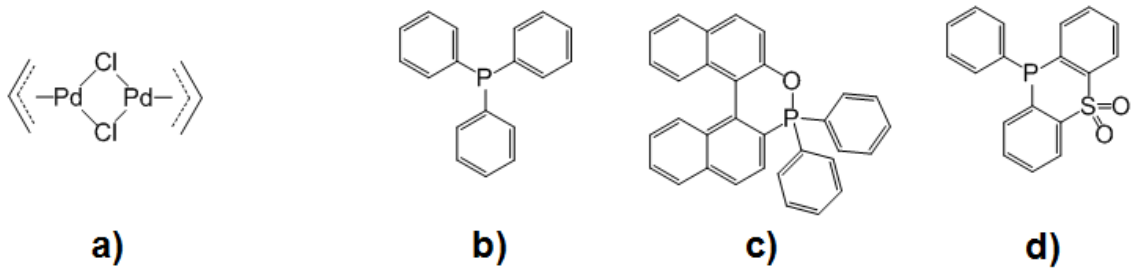

Scheme 6.6 *Chemical structures of Pd based catalysts for homogeneously catalyzed hydrosilylation reactions (Palladium allylchloride dimer precursor (a), phosphorous based ligands P1 (b), P2 (c), and P3 (d)).*

In summary, with the alternative catalysts regio-selective hydrosilylation reactions on mesogenic styrenes were possible. Furthermore the activities could be significantly improved. Unfortunately with these catalysts only the α-adduct was accessible. Although one system showed good regio-selectivity towards the β-isomer, the formation

of colloids made isolation and following polymerization reactions impossible. To obtain the monomers as β-adducts, different synthesis strategies were developed. These approaches are presented in the following section.

6.2.2.2 Alternative Synthesis Routes to the β-Isomer

The crucial step to analyze and understand the self-assembly patterns of polysilanes is to obtain polymers, which are built up from isomerically pure monomers. The α-isomer was effectively synthesized by choosing the proper catalyst system, whereas no catalytic route was found, to form the β-adduct. Therefore other synthetic strategies were needed. Numerous different strategies were identified, and two potentially feasible routes are presented in *Scheme 6.7*.

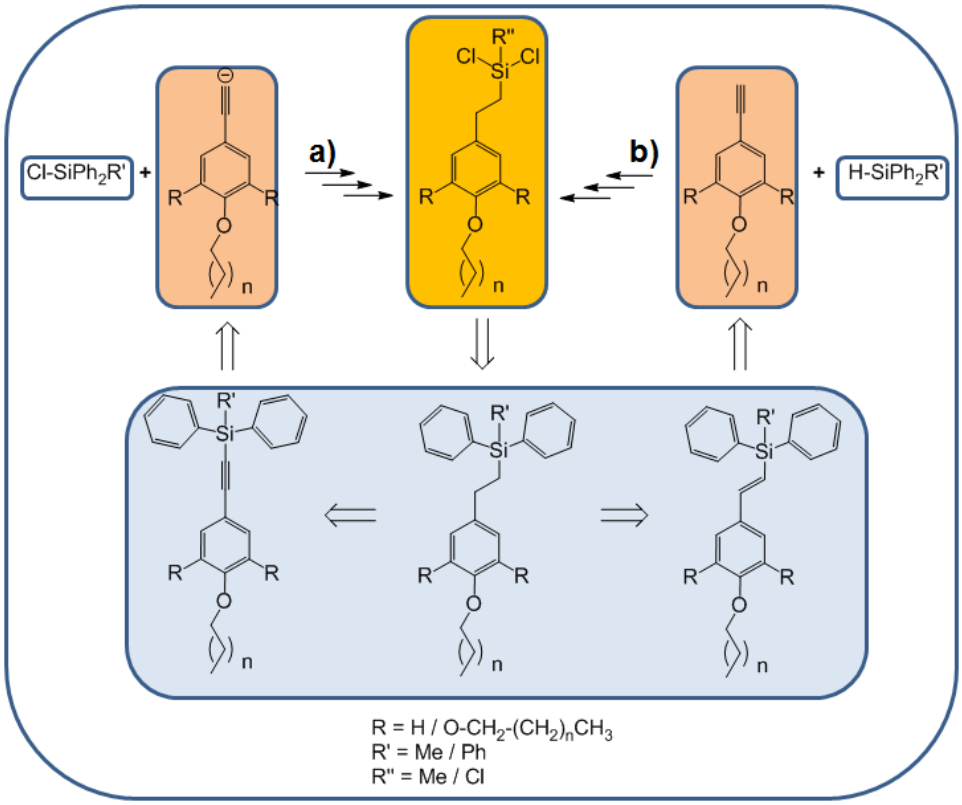

Scheme 6.7 *Alternative synthesis routes to the β-isomer of chlorosilane monomers, which cannot be synthesized via hydrosilylation (Corey-Fuchs-route (a), hydrosilylation route (b)).*

Both routes to mesogenic chlorosilane monomers with saturated spacer groups consist of three steps, which are based on reductive hydration of phenylsilane mesogens with unsaturated spacers, after formation of these mesogens *via* previously described hydrosilylation (*Scheme 6.7 (b)*) or *Corey-Fuchs* (*Scheme 6.7 (a)*) syntheses, and successive chlorination of the phenylsilanes.

The synthesis routes *via* stable mesogenic phenylsilanes were chosen, after previously performed tests on hydration of chlorosilane mesogens with unsaturated spacers turned out to be unsuccessful. In the proton NMR spectrum of the product two different sets of signals were found, of which one is undoubtedly originating from a styrene functionality. In *Scheme 6.8* a hypothetic reaction pathway due to reductive scission of Si-C-bonds is shown. After the separation of the head group, the chlorosilane is reduced and HCl, which is formed as side-product can react with the styrene functionality. In the following, the Corey-Fuchs route was developed, after it turned out, that hydrosilylation of phenylacetylene mesogens with triphenylsilane was impossible, most probably due to sterical issues.

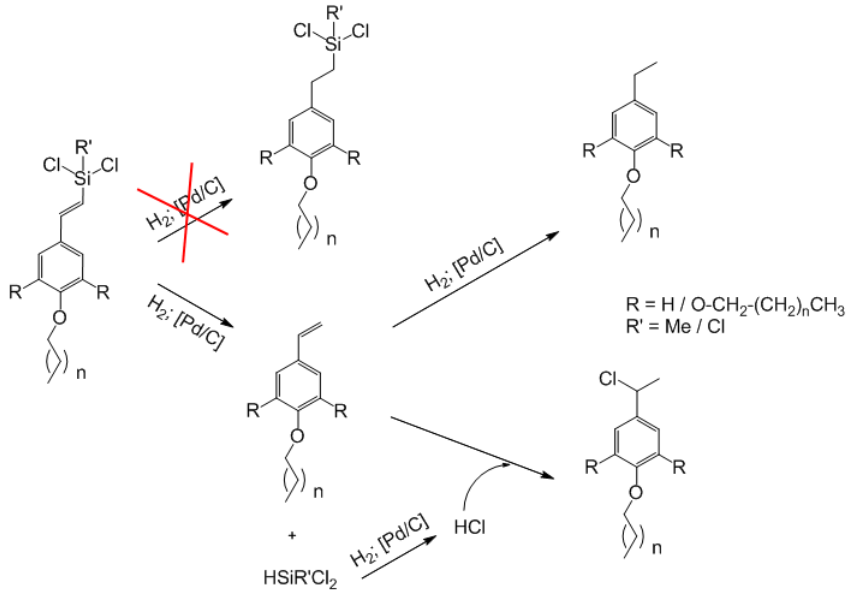

Scheme 6.8 *Schematic drawing of different routes to β-adduct of mesogenic chlorosilane monomers.*

Hydration of di- and triphenylsilane mesogens with double and triple bond spacers, respectively, was performed under heterogeneous catalysis with Pd on activated carbon as catalyst. Both reaction pathways yielded the desired mesogens with saturated spacers quantitatively. As expected from the results of previous reactions, also the hydrosilylation and *Corey-Fuchs* reactions with methyldiphenylsilane and triphenylsilane, respectively, yielded quantitative amounts of unsaturated phenylsilane mesogens.

Regardless of the effectiveness of the first two steps, the most challenging step is the chlorination of phenylsilane functionalities on the saturated mesogens. In the literature numerous ways for the conversion of phenylsilanes to chlorosilanes are described. The most promising strategies were presented by Frohn in 1998.[147] In the named paper, chlorination of methyl(pentafluorophenyl)diphenylsilane with gaseous HCl and catalytic amounts of $AlCl_3$ in hexane, as well as chlorination with stoichiometric amount of $AlCl_3$ in DCM, is presented. Both procedures were applied to different phenylsilane mesogens. Furthermore also alternative chlorination agents, such as $HCl/InCl_3$, thionylchloride, or oxalylchloride were tested. But the results on each chlorination reaction were deflating. None of the named pathways resulted in the desired mesogenic chlorosilane monomers. In all cases, where metal chlorides were used as reactant or catalyst, as dominating side reaction scission of the ether bonds on the alkoxy groups on the mesogen was identified. In all other cases, where alternative chlorination agents were tested, no reaction occurred at all.

In summary it was not possible to synthesize exclusively the β-isomer, neither by finding the proper catalyst, nor by applying alternative reaction routes. Despite the fact, that this isomer would be important for studies of self-assembly, further polymerization reactions and the following structure determinations were performed with the α-adduct or with mixtures of both isomers.

6.3 *Wurtz*-Type Reductive Polymerizations

In the previous section the synthesis of the different mesogenic chlorosilane monomers was discussed. After having obtained the monomers, the next step was to use these monomers for the synthesis of various silane based polymers in a *Wurtz*-type reductive polymerization. In this polymerization type typically chlorosilanes are reductively coupled by a stoichiometric amount of a strong reducing agent, such as a neat alkaline metal. Therefore one can easily influence the microstructure of the polymer by the monomer design e.g. the number of the chloro substituents. In this study di- and trifunctional silane monomers were synthesized to obtain linear or crosslinked polymers, respectively.

The effectiveness of the *Wurtz* reaction is influenced by various factors. On the one hand there are the reactivities of the chlorosilanes and the reduction potentials of the reducing agents, and on the other hand there are reaction temperatures, solvent polarities and the quality of the metal dispersion. Regarding these facts, polymer synthesis was performed with differently substituted chlorosilanes to test the reactivities of the monomers. In the monomer structure, three parameters were systematically modified: different saturated and unsaturated linker groups between silane head group and mesogen, as well as different numbers and lengths of alkoxy substituents on the mesogens. Furthermore three different reducing agents accompanied by different reaction conditions were screened.

Different reaction conditions resulted from different melting points of the metals, since their dispersion could only be achieved in the molten state by vigorous stirring. For coupling reactions with neat sodium, harsh reaction conditions were required. Due to its comparably high melting point of 98 °C, a high boiling solvent was needed. In this case boiling toluene (b.p. = 110 °C) was used for dispersion. Potassium on the other hand could already be dispersed in boiling THF (b.p. = 66 °C), since its melting point is at

63 °C. As the third reducing agent, potassium graphite intercalate (C_8K) was applied. This intercalate does not need to be molten, since is well dispersable in THF at room temperature. Besides different dispersion and reaction conditions, the three reducing agents featured varying reducing potentials. Na is the metal with the lowest reducing power, followed by K with slightly increased reducing potential. Although the graphite intercalate C_8K bears the highest reducing power, it has got one undoubtedly serious, yet readily controllable disadvantage: difficult handling due to its highly pyrophoric character.[148]

The pyrophoricity of the intercalate compound, required its synthesis in controlled glove box atmosphere. Graphite powder was dried at elevated temperatures in vacuum over night, before potassium, which was previously cut into pieces, was added. The mixture was heated to 150 °C and stirred mechanically, until the black color of the graphite turned into a bronze color, indicating the formation of K-C intercalate (see *Figure 6.1*). The compound was synthesized in bigger amounts (up to 30 g) and stored in the glove box until further use.

The optimal polymerization conditions were determined by screening of coupling reactions of selected monomers, using different reducing agents under the previously described reaction conditions. In *Figure 6.1* the results of a representative screening is shown. In this screening, the trifunctional monomer **8a-SiCl$_3$** was polymerized using Na in boiling toluene, K in boiling THF, or C_8K in THF at RT. After standard workup, molecular masses and polydispersity indices (PDIs) were determined using gel permeation chromatography (GPC) with refractive index (RI) detection in THF. Although the RI detector was calibrated to polystyrene (PS) standards, and thus the molecular masses cannot be regarded as absolute values, a comparison between polymers, which are built up of the same monomer but under different synthesis conditions, can nevertheless be legitimate.

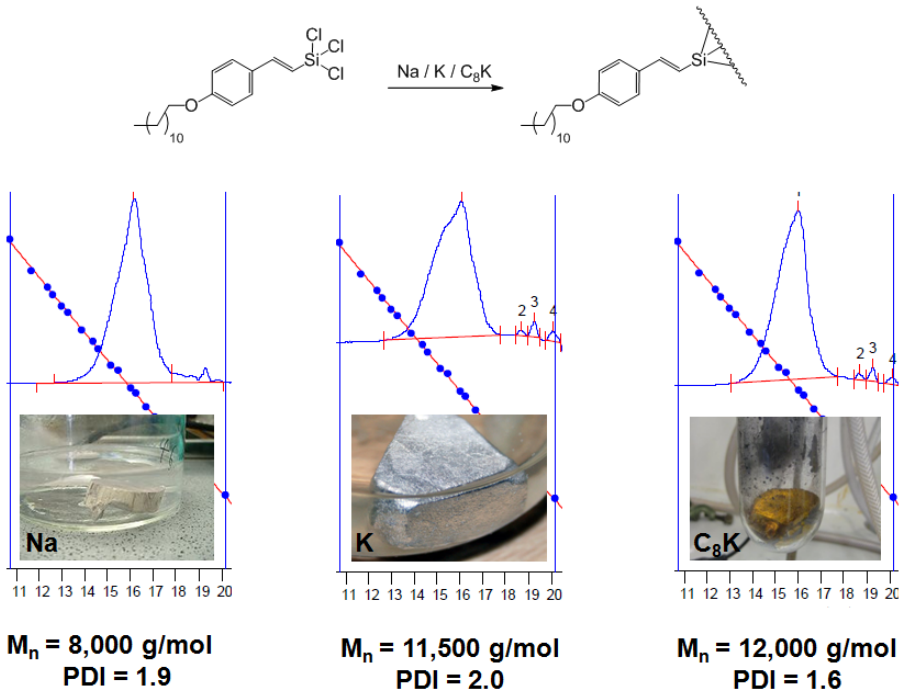

Figure 6.1 *GPC traces (IR detection) of resulting polymers from coupling of monomer* ***8a-SiCl$_3$****, using different reducing agents. The insets show photographs of the reducing agents. (Source for Na and K photographs: Wikipedia).*

The GPC results show, that polymerization with Na leads to a polymer with the lowest molar mass (M_n = 8,000 g/mol) and high polydispersity (PDI = 1.9). It seems that the reducing power of Na is not sufficient for polymerizations of such sterically demanding monomers. Another reason can be thermally induced depolymerization due to the high reaction temperature in boiling toluene.[149] Polymerization with K yields a polymer with increased molar mass (M_n = 11,500), but also with slightly increased polydispersity (PDI = 2.0). This result is also consistent with theoretical considerations; increased reduction potential of K compared to Na leads to higher molecular masses, but the temperature seems to be still too high for increased uniformity in the polymer. Using C_8K as coupling agent combines both requirements - it bears the highest reducing potential among the three coupling agents, and furthermore it can be used in dispersion already at room temperature. According to the theory, the resulting polymers show the best properties of all tested systems. The molar mass is relatively high (M_n = 12,000) and the polydispersity in turn relatively low (PDI = 1.6).

Since investigations on different linear and crosslinked systems showed similar trends, these conditions turned out to be the optimal conditions for reductive polymerizations of mesogen substituted chlorosilanes. Therefore, further syntheses of all other polymers were performed using C_8K in THF at RT.

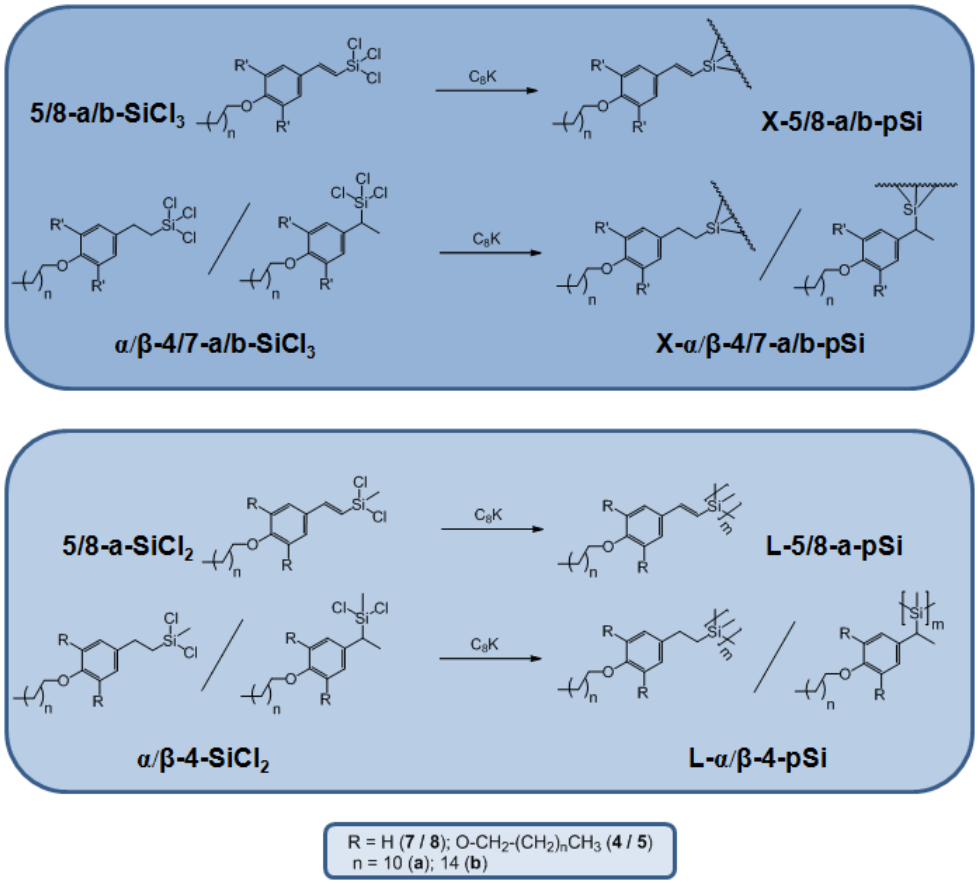

Scheme 6.9 *Reaction schemes for Wurtz-type polymerizations of di- and trifunctional monomers to differently substituted, linear (**L-pSi**) and crosslinked polysilanes (**X-pSi**).*

After having demonstrated the best polymerization conditions, all polymerization reaction towards linear and network polymers **L-pSi** and **X-pSi** (*see Scheme 6.9*) were performed using 1 eq. of potassium-graphite intercalate (C_8K) per each chlorine atom in dry THF at room temperature. The reactions provided the different polymers as yellow to dark brown oils, viscous pastes, or solids in varying yields of 60-95%. The work-up was performed by repeated precipitation in MeOH.

Appropriate reaction times for network polymers were determined by elemental analysis (EA) prior to the work-up procedure and after separation of solid graphite and alkaline salts, which were formed during the coupling reaction, by centrifugation. Analysis of the chlorine content is an appropriate method to determine the grades of conversion and crosslinking, since it is assumed to drop with the formation of Si-Si-bonds. The best case scenario for considering the reactions as completed was obtained when the remaining chlorine content in the polymer was below the detection limit of EA. This means, that no reactive groups are left, and the polymer network cannot grow anymore. The worst case on the other hand was fulfilled when the chlorine content did not show any change. In this case the reactivity of the chlorine groups is too low, and thus the coupling reaction is stopped. Too low reactivity can be due to steric or electronic reasons. Complete removal of chlorine atoms before quenching is essential to avoid the addition of methoxy groups to the polymer. Therefore, in the worst case scenario, the polymers could not be worked-up using the standard conditions, and thus, the analysis had to be performed under glove-box conditions.

The differences in reaction times between monomers with different substitution motifs were peculiar. First the sterical influence was investigated; therefore unsaturated monomers with different lengths and numbers of alkoxy substituents (**5/8-a/b-SiCl$_3$**) were polymerized. The reaction rates of the polymerization reactions did not differ much; after two hours of polymerization, in both mono- and trialkoxy substituted monomers with C_{12} or C_{16} alkyl chains no remaining chlorine content could be detected. In the following, the influence of the electronic surrounding of the silane group was tested. Polymerization of saturated monomers **α/β-4/7-SiCl$_3$** was found to be significantly slower. After 24 h of polymerization, still a significant chlorine content was detected in polymers made from mono- and trialkoxy substituted monomers. Detailed analysis of the obtained oligomers is presented in the following section. From these results it can be concluded, that for polymerization rates, the electronic influence is much more important than the influence of sterical factors.

To estimate the influence of the alkoxy substituents on the polymer characteristics of the crosslinked systems, two different control monomers without alkoxy groups were synthesized (see *Scheme 6.10*). The control compounds for both systems with saturated and unsaturated spacers were polymerized using the same polymerization conditions.

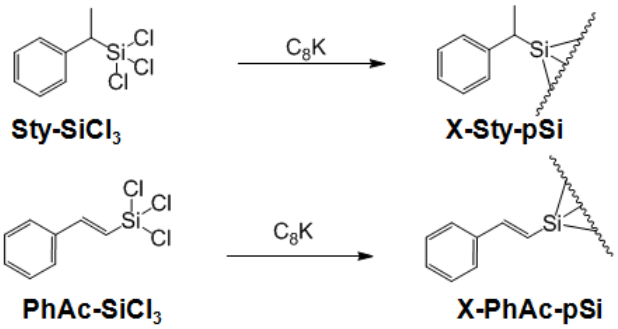

Scheme 6.10 *Chemical structures of the saturated and unsaturated control monomers without alkoxy functionalities, and their resulting polymers.*

In both cases the reductive coupling reaction led to polymers, which were highly crosslinked. Therefore, these polymers were insoluble and precipitated during the reaction. Conclusively, it was impossible to separate the polymers from other reaction media such as graphite or potassium salts. The only difference was the reaction time; although the reaction of saturated monomer **Sty-SiCl3** needed 24 h to form a crosslinked insoluble polymer, the monomer with the unsaturated spacer **PhAc-SiCl3** precipitated already after 4 h of polymerization.

Since both products were insoluble, no standard analysis technique could be applied to assess molecular masses or chemical compositions of the polymers. But the most important result of the reactions with the control monomers is that the alkoxy substituents on the mesogens are essential in formation of uniform polymer particles with a high degree of crosslinking, since they provide solubility. And solubility is not only important for characterization of the polymers, but also for subsequent formation of self-assembled structures.

6.4 Determination of Polymer Characteristics

After the optimization of polymerization conditions, various polymers using the differently substituted monomers were synthesized. Prior to investigations of self-assembly behavior, complete characterization of the resulting polymers is indispensable. Therefore, in this section the results from different approaches to explore the chemical and structural properties of the synthesized polymers are presented and discussed. For the analysis of molecular masses, GPC measurements using different detection modes were performed; for selected systems also the particle dimensions were determined by dynamic light scattering (DLS). Furthermore, determination of the chemical compositions of the polymers was performed using NMR spectroscopy and elemental analysis. At last, the results of thermal property analysis are discussed.

6.4.1 Polymers from Saturated Monomers

In the following, characterization of chemical and structural properties of polymerization products from *Wurtz*-type reductive coupling of dichloro- and trichlorosilane functionalized mesogenic monomers with saturated spacers is presented. Linear polymers were only synthesized from one dichloro substituted monomer (**L-α/β-4-pSi**), whereas for the synthesis of network polymers, five differently substituted trichlorosilane monomer variations were used. On the one hand the coupling product of an α-β-isomer mixture of tridodecyloxy substituted trichlorosilane monomer (**X-α/β-4a-pSi**) was analyzed, and on the other hand, pure α-isomers of mono- and tridodecyloxy and hexadecyloxy substituted monomers were investigated. The molecular masses were analyzed using GPC with refractive index (RI) detection. In *Table 6.2* the results of GPC analysis are summarized. Although the RI detector is only calibrated to polystyrene standards, previous results of GPC investigations on defined siloxane-linked bi and tetramesogens, which are described in *Chapter 5*, showed that the obtained molecular masses for oligomers are in a realistic value range. Since it turned

out, that the molecular masses of the reductively coupled chlorosilane monomers with saturated spacers are located in the lower oligomer range, this type of analysis was considered as reliable, and no further analysis techniques were implemented.

Table 6.2 *Results from GPC analysis of oligomesogens with saturated spacers.*

Subst.	M_n [a] [g/mol]	DP [a]	PDI [a]
L-α/β-4-pSi	5,500	8	1.51
X-α/β-4-pSi	4,000	6	1.58
X-α-4a-pSi	1,500	2	1.37
X-α-4b-pSi	1,300	2	1.39
X-α-7a-pSi	1,400	5	1.26
X-α-7b-pSi	1,700	5	1.30

[a] from conventional GPC with RI detection (standard: polystyrene) after 24 h of polymerization.

In the previous section it was already mentioned that, due to the electronic surrounding of the silane head group, the reactivities of the saturated monomers are comparably low. This was concluded from high remaining chlorine contents after 24 h of polymerization and before work-up of the products. In *Table 6.3* the elemental compositions (from EA) of two selected coupling products are presented and compared to the theoretical composition of their monomers. One can identify that in both cases less than 50% of the monomer chlorine groups are converted. Since no K-content was detected, the whole chlorine content obviously originates from the coupling product and not from potentially formed potassium chloride. In the case of **X-α-4a-pSi** the EA results indicate, that only one of the three chlorine groups was converted, whereas in the case of **X-α-7a-pSi** every second chlorine group is still present after coupling. Hence only low molecular weight oligomeric compounds can be obtained. The contents of carbon, silicon and hydrogen in the coupling products are slightly higher than the calculated

values from the monomer. This is most probably due to the formation of Si-Si-bonds and thus accompanies the reduction of chlorine content.

Table 6.3 *Results from elemental analysis of oligomesogens with saturated spacers.*

Subst.	C		H		Si		Cl		K	
	calc.[a]	det.	calc.[a]	det.	calc.[a]	det.	calc.[a]	det.	calc.[a]	det.
X-α-4a-pSi	66.68	73.02	10.30	11.01	3.54	4.32	13.42	9.80	0	0
X-α-7a-pSi	56.66	70.66	7.85	10.02	6.63	7.30	25.09	14.20	0	0

[a] calculated from the composition of the monomer.

As it could be expected from the remaining chlorine contents, the resulting molecular masses obtained by GPC are remarkably low. The calculated degrees of polymerization (DPs) are located between dimers and hexamers. The lowest DPs were obtained for α-isomers of trialkoxy substituted monomers with trichloro functionality. The formation of di- or trimeric compounds is consistent with the results from EA-analysis. Monoalkoxy substituted monomers have slightly higher DPs, here the formation of pentamers is observed. Surprisingly, the highest DPs are found for the coupling products of α-β-isomer mixtures of trialkoxy substituted monomers (**X-α/β-4a-pSi**). These results indicate that the sterical influence of the α-isomer's methyl group in direct proximity to the Si-center is much more decisive than the sterical influence of the higher number of alkoxy substituents. Unfortunately, in this work no feasible route towards the synthesis of monomers consisting of pure β-isomer was found. Therefore, this statement concerning the sterical influence remains an assumption. But since in previous section it was shown that polymerization of a monomer without alkoxy substituents leads to insoluble and highly crosslinked material, it can be concluded that also the long alkoxy chains of the mesogens are strongly influencing the reactivities of the monomers in reductive coupling reactions.

To obtain information about the chemical composition of the oligomers after quenching of the reaction, proton NMR spectra were recorded. In *Figure 6.2* a representative spectrum of **X-α-4a-pSi** after 24 h of polymerization is presented. All signals which were present in the monomer spectrum are still present in the spectrum of the oligomer. As it is expected for spectra of oligomers the signal peaks are broadened. Furthermore it is perceptible, that although the oligomer was reprecipitated in methanol, no methoxy signals are observed, which would indicate methanolysis of the chlorine groups. These signals should be present at approximately δ = 3.5 ppm. Unfortunately on the Si-atom no functional group, which can serve as proton NMR active probe, is present; hence no information about the bonding situation between the single monomers could be obtained. Also ^{29}Si-NMR did not provide additional information. Besides the signal of the internal standard tetramethyl silane (TMS) no further signals are present. This is most probably caused by a low concentration of Si atoms in the oligomers, and furthermore by a high variety of magnetically inequivalent nuclei due to different linking possibilities between the trichlorosilane monomers.

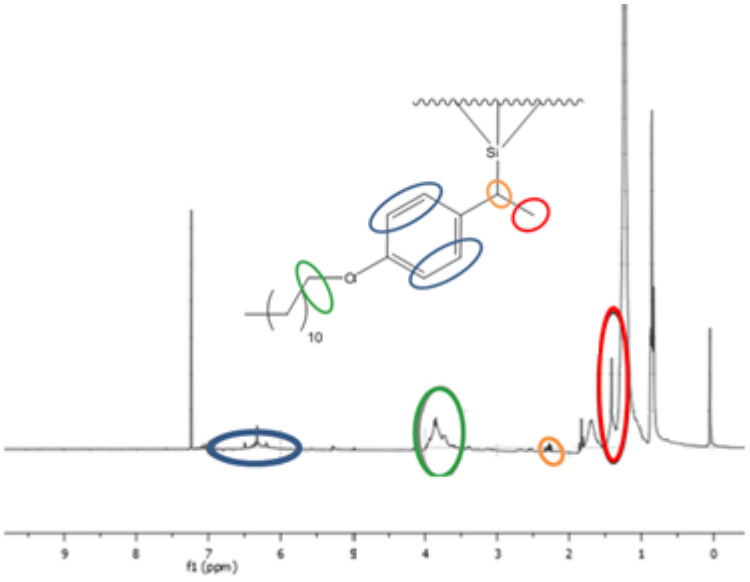

Figure 6.2 *Proton NMR spectrum of the coupling product* ***X-α-4a-pSi****.*

In summary, polymerization of chlorosilane monomers with saturated spacers between mesogen and head group, does not provide a feasible route to polysilanes with high molecular weights and DPs. Previously mentioned sterical hindrance of the methyl group in direct vicinity to the Si center, as well as of the alkoxy substituents of the mesogens, is one possible reason. But another reason can also be the electronic surrounding of the Si-center. In the present monomers the chlorosilane group does not benefit from the conjugation of the phenyl group, since it is decoupled from the conjugation by the saturated spacers. Hence its reactivity is too low to form polymers with higher DPs. As a result thereof, in the next section the influence of an unsaturated spacer on the reactivity of the monomers is investigated.

6.4.2 Polymers from Unsaturated Monomers

In this section, the chemical and structural properties of the coupling products from *Wurtz*-type coupling reaction of mesogen substituted chlorosilane monomers with unsaturated spacers are investigated. These monomers differ from the monomers with saturated spacers in their electronic properties. In contrast to the saturated monomers, here the chlorosilane group is part of the conjugation of the mesogen, since it is directly coupled to a double-bonded C atom. Accordingly the Si-center bears higher electron density, and therefore is expected to show higher reaction rates and to yield higher molecular masses and DPs than the saturated monomers.

6.4.2.1 Molecular Masses and Particle Sizes

The resulting linear (**L-5/8-a-pSi**) and crosslinked (**X-5/8-a/b-pSi**) polymers, which were synthesized from di- and trichloro functionalized monomers, are investigated using various analysis techniques. For determination of molecular masses and PDIs, two different GPC-techniques were utilized. On one hand a conventional GPC setup with refractive index (RI) detection (versus polystyrene standards) was used, and on the other

hand a modern GPC setup with combined RI and static light scattering (SLS) detection was implemented. Additionally the particle sizes of the crosslinked polymers were determined using dynamic light scattering analysis.

In *Table 6.4* the results of the different analytical approaches are summarized. Compared to the results of the coupling products from saturated monomers, which are described in the previous section, the unsaturated polymers show in general significantly higher molecular masses and DPs obtained by conventional GPC analysis with RI detection. For instance the trialkoxy substituted monomers yield crosslinked polymers (**X-5-a/b-pSi**) with M_n between 4,000 and 6,000 which is in average three times higher than the M_n of saturated oligomers with the same side chain substitution. In the case of monoalkoxy substituted polymers (**X-8-a/b-pSi**) the differences in DPs are even more tremendous; the unsaturated monomers lead to polymers with molar masses between 12,000 and 16,000, which exceed the M_n of the saturated oligomers by a factor of ten.

These results are a striking evidence for the hypothesis of increased reactivity due to the influence of electronic effects and decreased sterical hindrance by lacking of the methyl group in direct vicinity. It seems that including the chlorosilane group into the extended conjugation of the mesogen, influences the reaction rates of the *Wurtz*-type coupling enormously. From the remarkable difference between the molecular masses of the polymers with mono and trialkoxy substituted mesogens, one can furthermore conclude, that the polymerization reaction is much more affected by the sterical influence of the mesogen side chains when the reactivity is increased. During the coupling reaction the monomers with only one alkoxy group, can reach the reaction center more easily, and therefore generate a higher DP and a higher crosslinking, than in the case of the trialkoxy substituted monomers.

Variations in alkyl chain length do not affect the DP to the same extent as the number of alkyl chains. Generally it is found, that the DPs of the trialkoxy substituted polymers (**X-5-a/b-pSi**) decrease with increasing alkyl chain length. On the other hand the effect is the other way round, when monoalkoxy substituted polymers are observed. This is

most probably due to a highly sensitive equilibrium, in which the effects of sterical hindrance and templating are balanced.

Furthermore, the uniformity of the formed crosslinked polysilanes is remarkably good; the mass-distribution is monomodal and the polydispersity indices (PDI) range between 1.2 for monoalkoxy substituted and 1.9 for trialkoxy substituted polymers. Usually, the mass distributions for polysilanes from *Wurtz*-type coupling are bi- or multimodal with comparably high PDI values ranging between 3 and 10.[150]

Table 6.4 *Results from GPC and DLS analysis of linear and crosslinked mesogenic polymers with unsaturated spacers.*

Subst.	M_n (RI) [g/mol] [a]	*DP* (RI) [a]	*PDI* (RI) [a]	M_n (SLS) [g/mol] [b]	*DP* (SLS) [b]	*PDI* (SLS) [b]	*d* (DLS) [nm] [c]
L-5a-pSi	5,000	8	1.4	n/a	n/a	n/a	n/a
X-5a-pSi	6,000	9	1.3	13,200	19	1.2	7.14
X-5b-pSi	4,000	5	1.2	7,400	9	1.2	5.70
X-8a-pSi	12,000	38	1.6	13,400	42	1.5	8.13
X-8b-pSi	16,000	43	1.9	17,400	47	1.7	8.41

[a] from conventional GPC with RI detection (standard: polystyrene); [b] from modern GPC setup with combined RI and SLS detection; [c] diameters from DLS; n/a: not acquired.

Surprisingly, the linear polysilanes (**L-4/5-pSi**) do not show any influence of the spacer group if the DPs of coupling products from saturated and unsaturated monomers are compared. Coupling reactions with trialkoxy substituted monomers result in exactly the same DP of 8 no matter which monomer is used.

The same samples of crosslinked polysilanes, which have been analyzed with conventional GPC, were subsequently investigated using a modern GPC setup, which combines RI and SLS detection. SLS-detection in GPC analysis can be considered as the much more precise method, since no calibration with external standards, such as polystyrene, is required. In the case of mesogen substituted crosslinked polysilanes the chemical structure of the polymers is not comparable to polystyrene, which is used for calibration of the conventional GPC setup. Therefore, the real conditions should be much better reflected by SLS-detection, than by the conventional RI-method.

In this study, the molecular masses which were obtained with SLS-GPC are significantly higher than the ones from the conventional method. The common trend shows that the M_n values of trialkoxy substituted polymers **X-5-a/b-pSi** are twice as high as the values found with RI-detection, whereas for monoalkoxy substituted polymers **X-8a/b-pSi** the M_n from SLS-GPC is only increased by 10%, which most probably means that this kind of polymer is more similar to the polystyrene standard. Although there are considerable differences in M_n between the different analysis methods, the PDIs determined with both methods are comparable for all investigated systems.

Particularly with regard to later investigation on self-assembly of the polymers and determination of the structures of the assemblies, information on the size of the polymer particles is invaluable. Therefore, the particle sizes of the polysilanes, derived from hydrodynamic radii, were acquired using dynamic light scattering (DLS). In *Figure 6.3* a representative size distribution profile of compound **X-α-5a-pSi** is shown and in *Table 6.4* the results of the particle sizes of the other polymers are summarized. The hydrodynamic diameters of the polymer particles range between 6 and 9 nm, whereas the light scattering results can be very well correlated to the DPs obtained by GPC; as expected, increasing DPs lead to an almost linear increase of the particle sizes.

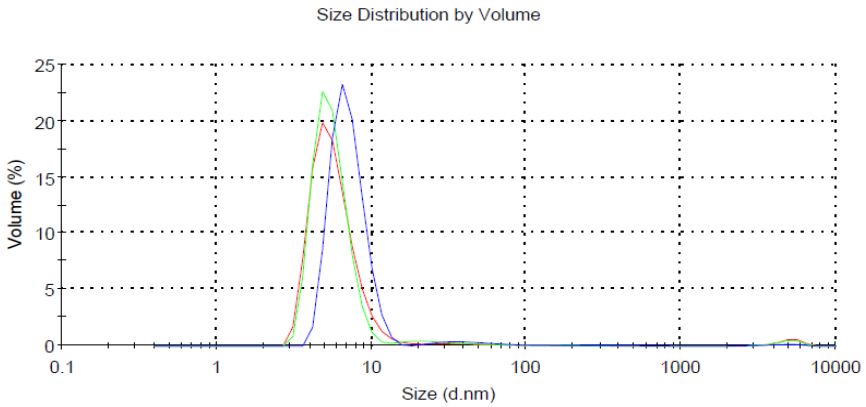

Figure 6.3 *Particle size distribution profile of compound* ***X-α-5a-pSi*** *obtained by DLS.*

In *Chapter 5* the dimensions of disiloxane-linked bimesogens were calculated and determined using SAXS. The results showed that the length of a bimesogen molecule in a stretched conformation amounts to 4.5 and 5.4 nm for C_{12} and C_{16} alkoxy-substitution, respectively. A comparison of these results with the hydrodynamic diameters of the polysilanes with the same substitution shows on the one hand, that the DLS results are situated in a realistic region, and on the other hand allows the proposal of a structure model which shows that the polysilane particles most probably are arranged in a spherical form, consisting of a crosslinked polysilane core and a mesogen shell. In *Scheme 6.11* this model is depicted. As mentioned above, this model will be important for later discussion of the results on self-assembled structures.

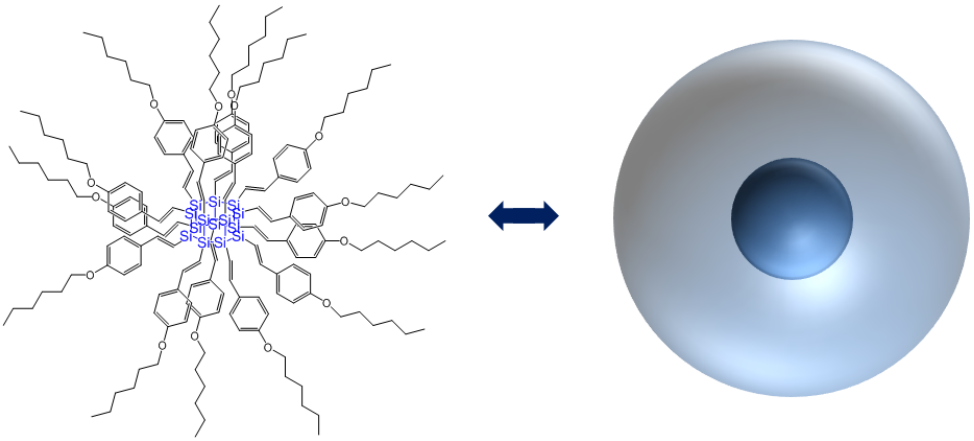

Scheme 6.11 *Schematic model of the assumed spherical structure of a polysilane particle.*

6.4.2.2 Chemical Properties

The chemical composition of the polymers was determined using different qualitative and quantitative analysis methods. The quantitative approach included elemental analysis (EA) and NMR spectroscopy, whereas as additional qualitative methods XPS spectroscopy and metal-nanoparticle formation by reduction of dissolved metal salts with Si-Si-bond containing compounds were tested.

Table 6.5 *Results from elemental analysis of polysilanes with unsaturated spacers.*

Substance	C		H		Si	
	calc.[a]	det.	calc.[a]	det.	calc.[a]	det.
L-5a-pSi	77.3	77.8	11.8	11.2	4.0	3.7
X-5a-pSi	77.2	73.2	11.6	10.8	4.1	3.8
X-5b-pSi	78.9	75.1	12.2	10.5	3.2	2.9
X-8a-pSi	76.1	72.7	9.9	9.5	8.9	7.3
X-8b-pSi	77.6	73.8	10.6	10.2	7.6	6.3

[a] calculated from the composition of the corresponding monomer without chlorine atoms.

Elemental analysis of the polymers was performed before quenching of the coupling reaction with MeOH. Prior to the analysis, the insoluble materials, such as graphite or potassium salt, were separated by centrifugation followed by evaporation of the solvent. Since neither a content of Cl nor a content of K was detected, the reaction was considered as completed. In *Table 6.5* the results of EA for different polymers are summarized. The calculated elemental compositions were obtained from the molecular masses of the corresponding monomers after omitting of the chlorine atoms. It is perceptible, that the composition of the linear polymer is equivalent to the composition of the corresponding monomer, which indicates a regular structure. On the other hand, the compositions of the crosslinked polymers deviate slightly from the expected values.

The biggest differences between obtained and calculated values are found in the carbon and hydrogen contents, whereas the silicon contents are situated in the expected range. This is assumed to be due to the separation of one or more mesogen groups during the polymerization or also to the content of remaining catalyst from the previous hydrosilylation reaction.

In *Figure 6.4* two representative proton NMR spectra of the compounds **X-8a-pSi** and **X-5a-pSi** are shown. For all polymers, proton NMR spectra show again peaks which have chemical shifts, which are comparable to the peaks in the monomer spectra. The relations between the integrals in aliphatic and aromatic regions have values which are expected from theoretical calculations, and show for polymers typical peak broadening.

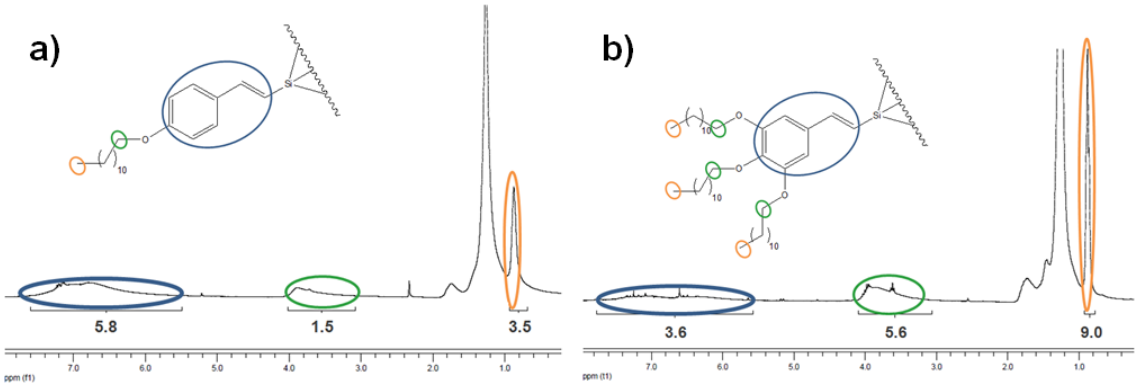

Figure 6.4 *Proton NMR spectra of the polymers* ***X-8a-pSi*** *(a) and* ***X-5a-pSi*** *(b).*

As expected, ^{29}Si spectra of the trichloro substituted monomers show one peak at -1.7 to -1.9 ppm. During the polymerization process, the peak for the monomer silicon atom disappears, but no formation of other peaks can be detected. As already discussed for the saturated systems, this is most probably due to a low percentage and a concurrently broad variety of magnetically nonequivalent Si-nuclei in the polymers.

Although with NMR analysis no doubtless confirmation of the presence of Si-Si-bonds was obtained, a combination of the results of elemental analysis and the certainty that all reactions were performed in controlled self drying conditions with C_8K in glove box atmosphere, leads to the conclusion that all Si-Cl bonds must have been converted to Si-Si-bonds. Nevertheless, different analysis techniques had to be found to ascertain the presence of these bonds.

One possibility was found in the literature: Tamai *et al* were previously using polysilanes to reduce Au and Pd salts to metal nanoparticles.[151] This technique has been adapted, and different crosslinked polysilanes were stirred in solutions of $Pd(OAc)_2$ during 24 h. The resulting solution was subsequently analyzed using transmission electron microscopy (TEM). In *Figure 6.5*, a representative TEM-image is shown. One clearly can identify metal nanoparticles with homogeneously distributed particle sizes. This is a clear evidence for the presence of Si-Si-bonds in the crosslinked polymers.

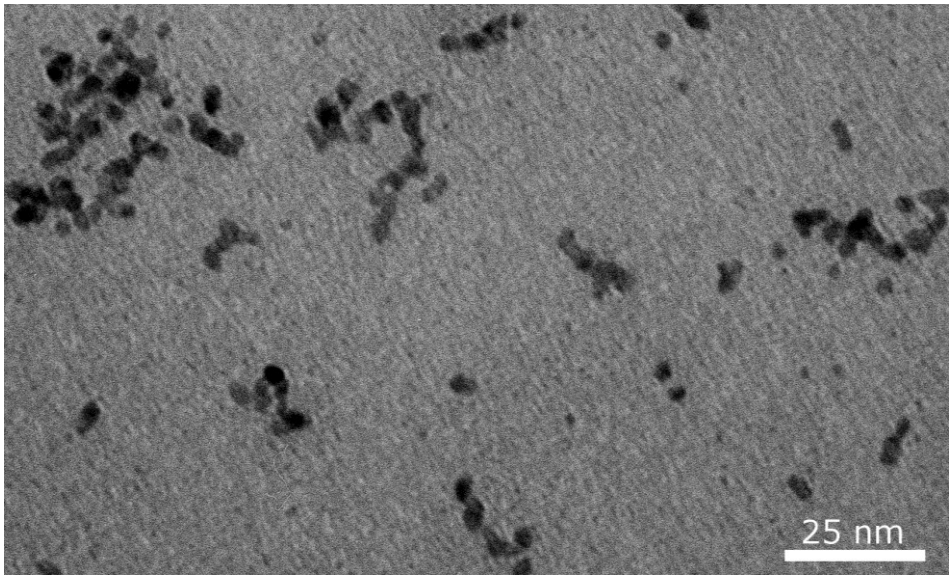

Figure 6.5 *Transmission electron micrograph of Pd nanoparticles after reduction of $Pd(OAc)_2$ with solution of crosslinked polysilane.*

To diminish last possible doubts, also XPS spectroscopy of polysilane films, which were deposited by spin casting to a substrate surface made of highly oriented pyrolytic graphite (HOPG), was performed. Since no comparable systems were previously analyzed, no XPS data which could serve as orientation existed. Therefore, a crosslinked polyphenylsilane which was synthesized in our group by a homogeneous catalysis route[152] was analyzed as reference.

In *Figure 6.6*, the obtained spectra of **X-8a-pSi** and the mentioned reference polysilane are presented. The spectra could be fitted with each four peaks based on *Gaussian-Lorentzian*-functions. The blue peak on the right can be attributed to Si cores, which are surrounded by three other Si atoms (100.0 eV for **X-8a-pSi** and 99.0 eV for control polysilane), whereas the green peak on the left is originating from a Si core surrounded by three oxygen atoms (103.2 eV for **X-8a-pSi** and 102.9 eV for control polysilane). The middle peaks in red and orange originate from Si cores with two Si cores and one O core, or one Si core and two O cores, respectively. This means that both polymers were partly oxidized at the time as the analysis has been performed. For both polymers quantitative analysis of compositions could not be performed, since the thicknesses and integrities of the films were very low. Nevertheless, the qualitative presence of the blue peaks at low eV values shows that the synthesized polymers consist of crosslinked polysilane cores.

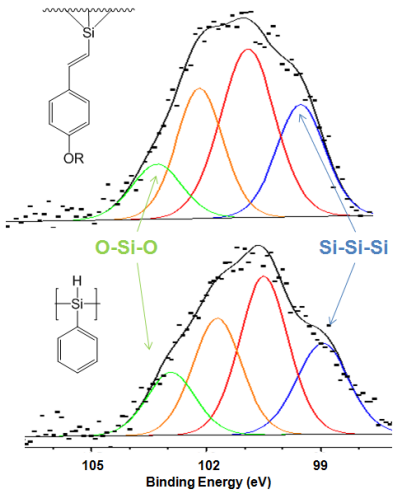

Figure 6.6 *Si_{2p} high resolution core level spectra obtained by XPS analysis of spin casted thin films of the corresponding polymers on HOPG surfaces.*

6.4.2.3 Thermal Properties

With thermal analysis techniques, such as differential scanning calorimetry (DSC) and thermo-gravimetrical analysis (TGA), thermal properties of crosslinked polysilanes with unsaturated spacers were determined. Interesting properties are e.g. resistances of the polymers versus thermal treatment, masses of remaining materials after pyrolysis, as well as the phase transition characteristics.

The resulting plots of thermal weight loss from pyrolysis in TGA as well as heat flow traces from DSC are presented in *Figure 6.7 a/b* and *c*, respectively. Furthermore, in *Table 6.6* the numerical data of decomposition temperatures or phase transition points are summarized. Thermal stabilities were determined in TGA under inert N_2 environment, as well as under a stream of dry synthetic air. In general, thermal stability of the polymers turned out to be exceptionally good, but also to strongly depend on the substitution motif on the mesogen. For monoalkoxy substituted polymers with long alkoxy chains, decomposition starts above 400 °C in both, inert N_2 or synthetic air environments, whereas for trialkoxy substituted polymers with the same length of alkoxy chains the decomposition temperature is found to be about 35 K lower (see *Table 6.6*).

For all compounds the decomposition in air proceeds in two steps. The mass loss of the first step decreases with decreasing amount and length of alkyl chains, whereas the second step is almost constant for all compounds. Therefore, these steps can be attributed to the degradation of the alkoxy groups at lower temperatures, and the decomposition of the phenyl groups at higher temperatures. The values for mass residue of the fully pyrolyzed compounds are in the expected range and moreover of good consistency with theoretical values for the formation of silica structures, which means that only the mesogens decompose and the crosslinked polysilane core is being oxidized to SiO_2.

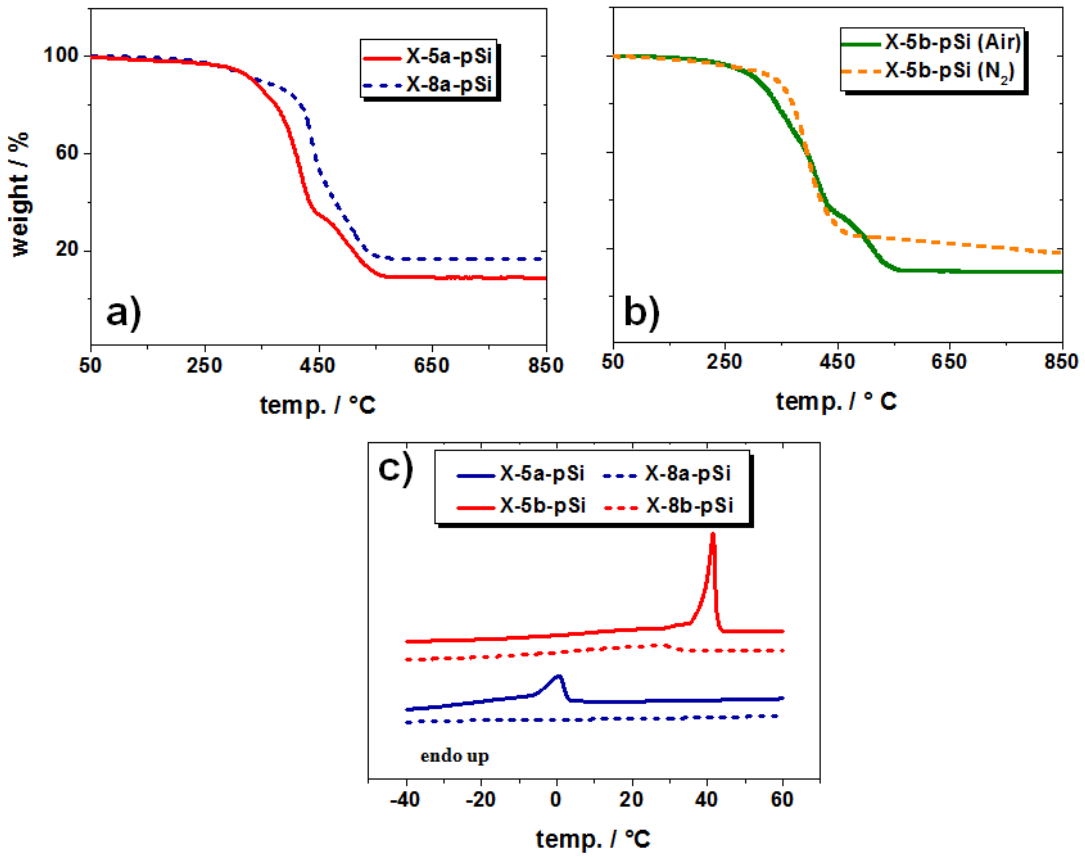

Figure 6.7 *TGA mass (a, b) and DSC heat flow (c) traces of differently substituted polymers (for clarity, the DSC heat flow diagrams are presented with a certain offset on the y-axis). In the insets, the plots are assigned to the corresponding compounds.*

The plots of TGA measurements under inert N_2 conditions show in all cases only one single decomposition step. Here the decomposition procedures start at temperatures, which are 20 to 40 K higher than the decomposition points of the corresponding compounds in air. After the main degradation step, which has its bottom point approximately at the starting point of the second decomposition step in the case of pyrolysis in air (see *Figure 6.7 b*), the mass loss curves do not immediately reach a plateau, but the mass values decrease until a temperature of 850 °C is reached. In this period, instead of the oxidation of the phenyl groups, primarily carbonization occurs. This is concluded from the fact, that the masses of the residues are two times higher than the residual masses of the corresponding polymers after pyrolysis in air. As already observed for siloxane linked cyclic tetramesogens in *Chapter 5*, also here the residual

material is a certain Si-O-C hybrid material, which is indicated by the obtained chemical compositions from elemental analysis. These results will become important in *Section 6.6*, when the retention of nanostructures upon pyrolysis is discussed.

Table 6.6 *Results from thermal analysis of polysilanes with unsaturated spacers.*

	T_m[a]	T_d (air)[b]	$T_d(N_2)$[c]	m_r[b](air)	m_r[c](N_2)
		[°C]		[%]	
X-5a-pSi	0.8	370	414	8.9	18.3
X-5b-pSi	41.4	380	418	8.5	17.2
X-8a-pSi	/	405	438	16.4	29.0
X-8b-pSi	28.0	415	428	15.6	27.7

[a] from DSC; [b] from TGA in air; [c] from TGA in N_2 atmosphere.

As well as the decomposition behavior, the phase transition properties are strongly dependent on the mesogen substitution. At room temperature the appearances of the polymers differ strongly. The compounds with shorter alkoxy chains (**X-5/8-a-pSi**) are viscous liquids, whereas the compounds with longer alkoxy chains (**X-5/8-b-pSi**) are solids with varying crystallinity. In *Figure 6.7 c*, DSC heat flow traces of all polymers with unsaturated linkers, which were recorded during the first heating run between -40 and 60 °C, are shown. The behavior of the polymers with the dodecyloxy substituents (**X-5/8-a-pSi**) differs between mono and trialkoxy substituted ones: the polymer with monoalkoxy substitution does not show any phase transitions, but the trisubstituted crosslinked polysilane has a melting point with comparably low enthalpy at around 0 °C. The compounds with the longer hexadecyloxy substituents (**X-5/8-b-pSi**) have both melting points between 28 and 42 °C with a strong difference in enthalpy. Since the melting enthalpy is directly connected to the degree of crystallinity, it can be conclusively said, that increasing length or number of alkyl substituents leads to an increase in crystallinity of the polymer bulk. A reason for that are stronger interactions between the alkyl side chains with increasing length.

6.5 Self-Assembly on Surfaces

After discussion of synthesis procedures and characterization of chemical and thermal properties of various crosslinked and linear polysilanes in the previous section, the polymers with unsaturated spacer groups were chosen as the most promising systems for further investigations towards the formation of self-assembled nano-structures. Nevertheless, in this section the self-assembly behavior of the named polymers are compared with the behavior of linear polysilanes, and silane oligomers with saturated spacers. The characterization of self-assembly phenomena of the polysilane networks was performed using different imaging techniques, such as atomic force microscopy (AFM), transmission electron microscopy (TEM), and scanning electron microscopy (SEM).

For AFM and SEM analysis the polymers were deposited on polished Si wafers by spin casting of highly diluted $CHCl_3$-solutions, whereas for TEM analysis drop casting onto a carbon-coated Cu grid was utilized. Different coverage densities of the coatings were achieved using different polymer concentrations for spin casting. In the following, surface coverage densities obtained by casting of two different concentrations are compared.

In *Figure 6.8*, AFM height and phase contrast images, as well as the corresponding z-profiles of selected, representative regions, of the polysilane samples **X-5a-pSi** and **X-8a-pSi**, are presented. The spin casting procedure with a polymer concentration of 0.01 mg/mL in $CHCl_3$ led to a surface coverage density on sub-monolayer scale. In both, height and phase images, one can easily identify homogeneously distributed particles with varying heights and diameters for the differently substituted polymers. The trialkoxy substituted polymer **X-5a-pSi** assembles to particles of around 50 nm in diameter and 3 nm in height, whereas the assemblies of the monoalkoxy substituted polymer **X-8a-pSi** are around 75 nm wide and 2.5 nm high.

The difference in the dimensions can be explained on one hand with the different dimensions of the primary particles, which were detected by DLS (see *Table 6.4*), and on the other hand by differences in the intermolecular interactions between polymer molecules with mono- and trialkoxy substitution motifs. In principal, bigger primary particles lead to bigger assemblies; but the size difference of the primary particles is not sufficient to explain the size difference of the assemblies.

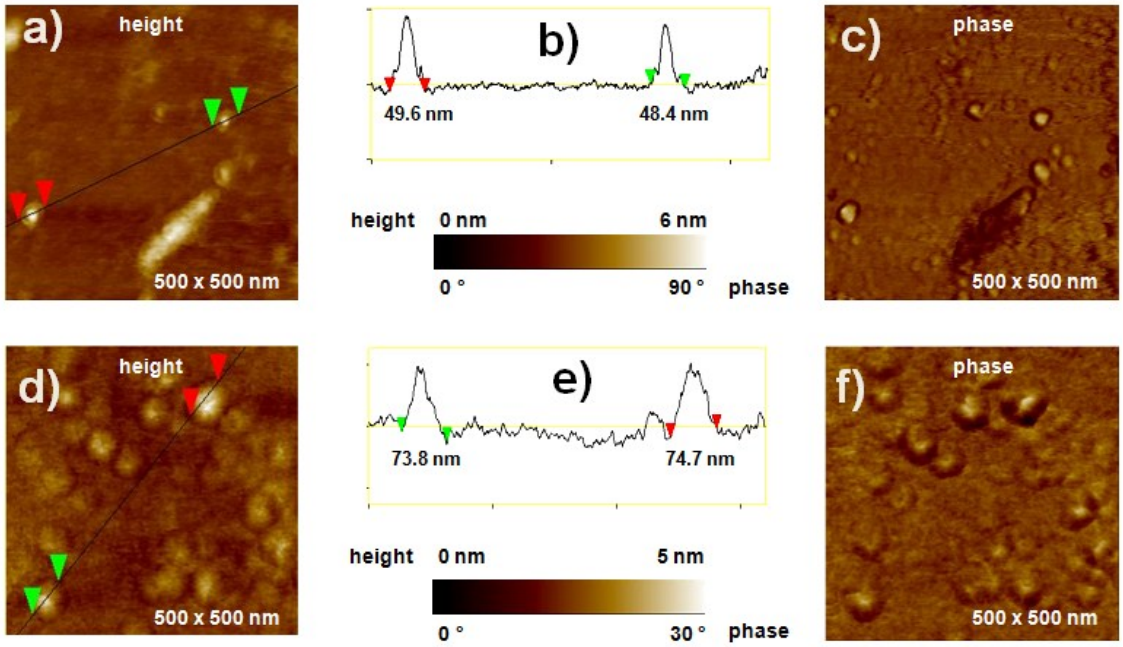

Figure 6.8 *AFM topography (a/d) and phase contrast (c/f) images of self-assembled particles prepared by spin casting of 0.01 mg/mL $CHCl_3$ solutions of crosslinked polysilanes* ***X-5a-pSi*** *(a-c) and* ***X-8a-pSi*** *(d-f) on polished Si wafer substrates. In (b) and (e), z-profiles along the corresponding black lines in the topography images are presented.*

The diameter relations between assemblies and primary particles are for **X-5a-pSi** and **X-8a-pSi** approximately 7 and 9, respectively. This means that the monoalkoxy substituted polymers tend to assemble more primary particles. The reason can be found in the higher sterical demand of the trialkoxy substituted polymers; the polymers, which have only one alkoxy chain per monomer, show less repulsion between the alkyl chains, and can therefore set up larger assemblies. Also the difference in height can be

explained with repulsive forces between the alkyl chains. In the case of **X-5a-pSi** the increased repulsive forces between the three alkyl chains, lead to constraint stretching of these chains, and thus to increased height of the assemblies. On the other hand, decreased repulsion between the single chain substituted polymer (**X-8a-pSi**), leads to a more collapsed state of the alkyl chains, and thus to lower height of the assemblies.

Corroborating arguments for this assumption can be found in the phase contrast images (*Figure 6.8 (c)* and *(f)*). Larger phase contrast means larger difference in materials elasticity. In this case, the elasticity of stretched alkoxy chains is much higher than the elasticity of particles with collapsed alkoxy chains. This issue is expressed in the different phase scales (0 - 90° for **X-5a-pSi** and 0 - 30° for **X-8a-pSi**).

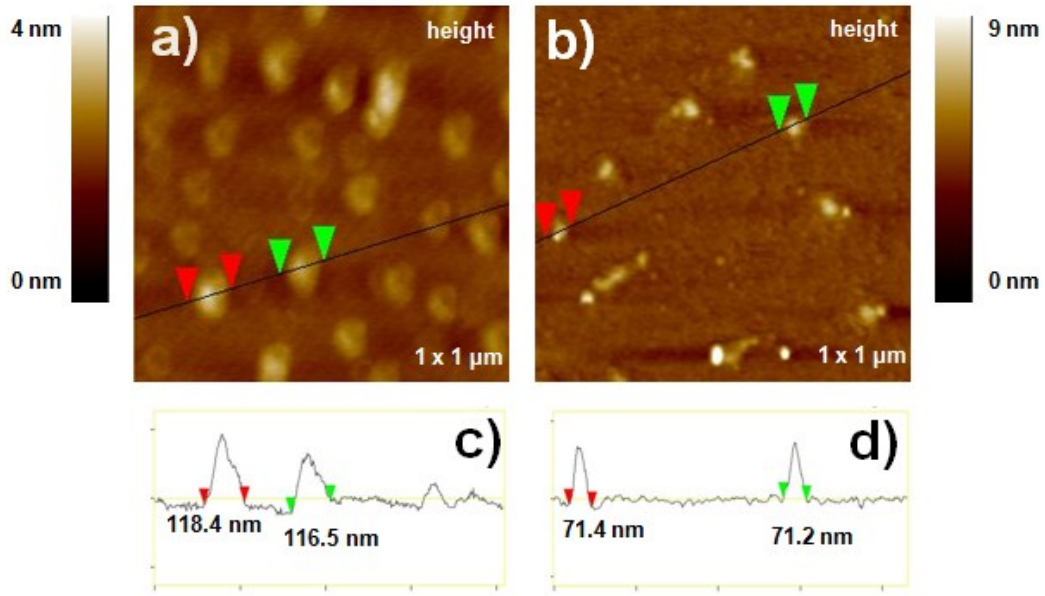

Figure 6.9 *AFM topographies (a/b) and corresponding z-profiles (c/d) along the black lines in the images of self-assembled particles of compounds* ***X-8b-pSi*** *(a/c) and* ***X-5b-pSi*** *(b/d) after spin casting of 0.01 mg/mL $CHCl_3$ solutions.*

Similar trends for diameters and heights are found for the hexadecyloxy substituted polymers **X-5b-pSi** and **X-8b-pSi** (see *Figure 6.9*). In this case, the longer substituents on the mesogens lead to bigger assemblies and therefore to bigger ratios between the diameters of secondary and primary particles (12 for **X-5b-pSi** and 14 for **X-8b-pSi**).

The assembly of a higher number of primary particles compared to the polymers with shorter side chains can be explained with a better interaction between the longer side chains, which also leads to a higher crystallinity, as explained in the previous section on thermal analysis.

Of course, the comparison of AFM and DLS data can be afflicted with a certain inaccuracy, because by DLS, hydrodynamic radii, which include solvent interactions, are obtained, and the AFM measurements on the other hand are performed in dry state. Conclusively, these results allow us to state a theoretical model for the self-assembly behavior of differently substituted crosslinked polysilanes. In *Scheme 6.12* this model is illustrated. We suppose that the flat, disc-like structures on the surface arise from a side by side assembly of primary particles, which can of course only be considered as spherical when they are solvated, but collapse to flat discs when deposited on a substrate. Therefore, the resulting dimensions of the assemblies are strongly dependent on diameter and number of the corresponding primary particles.

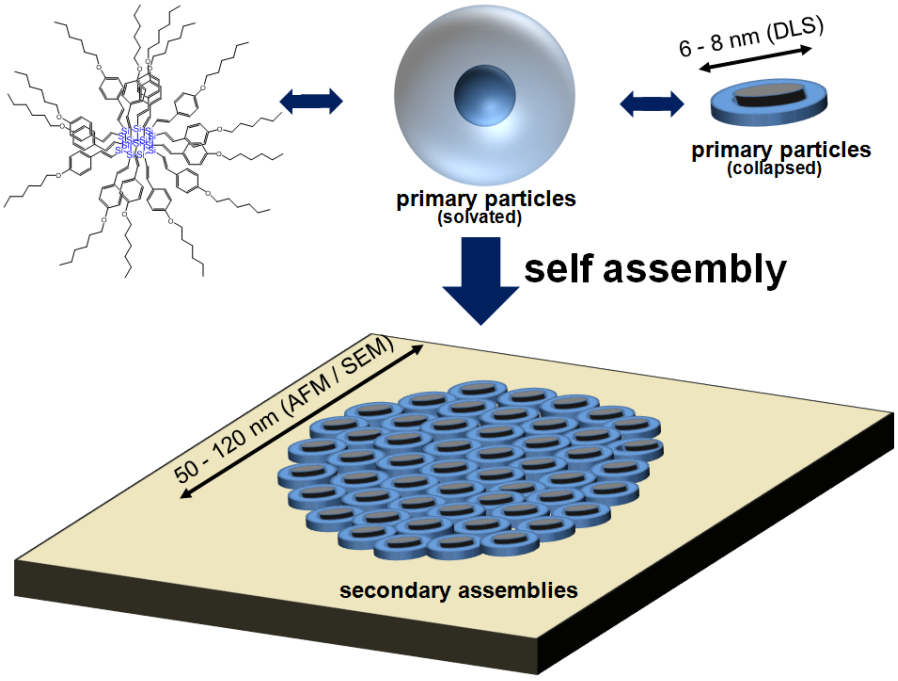

Scheme 6.12 *Schematic illustration of the hypothetical model for the self-assembly of crosslinked polysilanes on substrates.*

Besides the structural parameters of the polymers, also the influence of the polymer concentration on the particle dimensions was studied. For that reason, differently concentrated solutions were used for spin casting. In *Figure 6.10 (a)* an AFM height contrast image of a substrate, which was coated with a 0.1 mg/mL solution of compound **X-5a-pSi**, is shown. One easily can observe that in this case the surface coverage density is much higher than on samples, which were coated with polymer solutions with concentrations that are lower by one order of magnitude. Instead of isolated particles a closed polymer film is found on the surface. This film is internally structured with discotic features, which are similar to the isolated particles. The dimensions of the discotic features are approximately 200 nm, and hence much bigger than the secondary particles which were obtained by casting of higher diluted solutions. This finding once again shows that the nanostructures, which are formed during spin casting of polysilanes, are assemblies of primary polymer particles. Furthermore it shows that the dimensions of the self-assembled particles can be controlled by both, polymer structure and solution concentration.

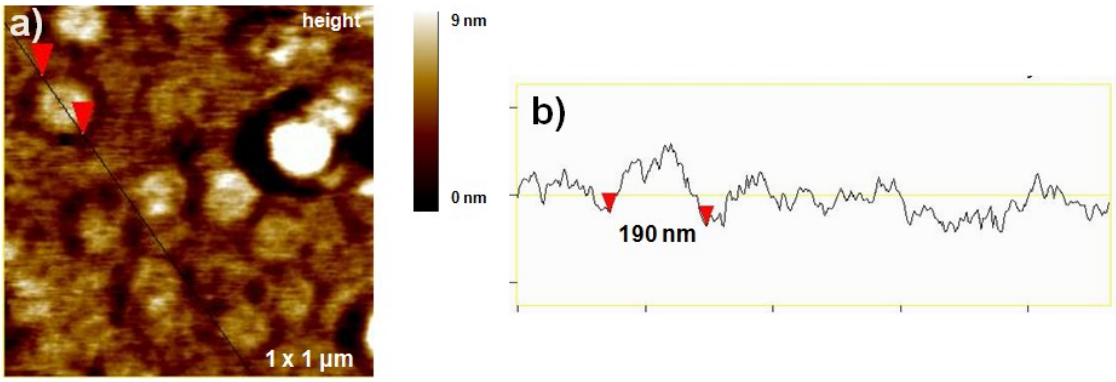

Figure 6.10 *AFM height contrast image (a) and corresponding z-profile along the black line (b) of compound* ***X-5a-pSi*** *after spin casting of a 0.1 mg/mL $CHCl_3$ solution.*

Complementary information about the polymer assemblies was obtained using electron microscopy techniques. In *Figure 6.11* an image from HR-SEM investigation is shown. In *Figure 6.12* on the other hand, a representative high resolution (HR) TEM image of compound **X-8a-pSi**, as well as chemical mappings from the corresponding area in the TEM image using energy dispersive X-ray spectroscopy (EDX), are presented. With

both microscopy techniques resolution of self-assembled secondary particles could be achieved, but only by TEM, resolution of primary polymer particles was successful. The particle sizes for primary and secondary particles obtained by electron microscopy are very well consistent with the sizes, which were determined by DLS and AFM, respectively.

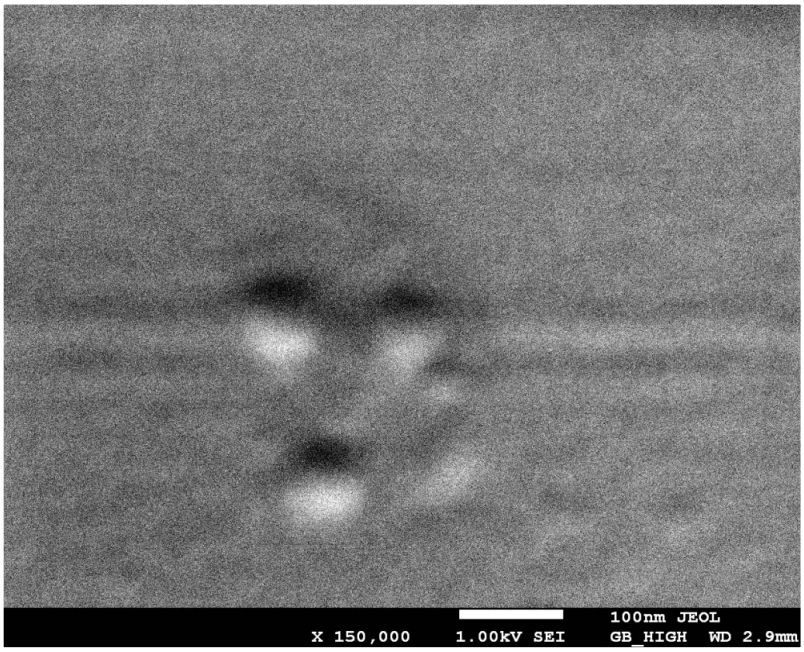

Figure 6.11 *HR-SEM micrograph of polysilane* ***X-5a-pSi****, prepared by spin casting of a* $CHCl_3$ *solution (0.01 mg/mL) to a polished Si wafer. The scale bar accounts to 100 nm.*

In addition to the size information, TEM with EDX chemical mapping provides spatial resolution of the elemental composition of the sample. One easily can see that the major part of the signals from silicon and oxygen atoms arises from the area of the assemblate, what means, that the particle consists of the present polymer. Moreover, one can distinguish, that the bright spot on the lower edge of the particle is not a feature of the polymer, but rather an insignificant contamination of potassium chloride, which was formed as byproduct of the polymerization process.

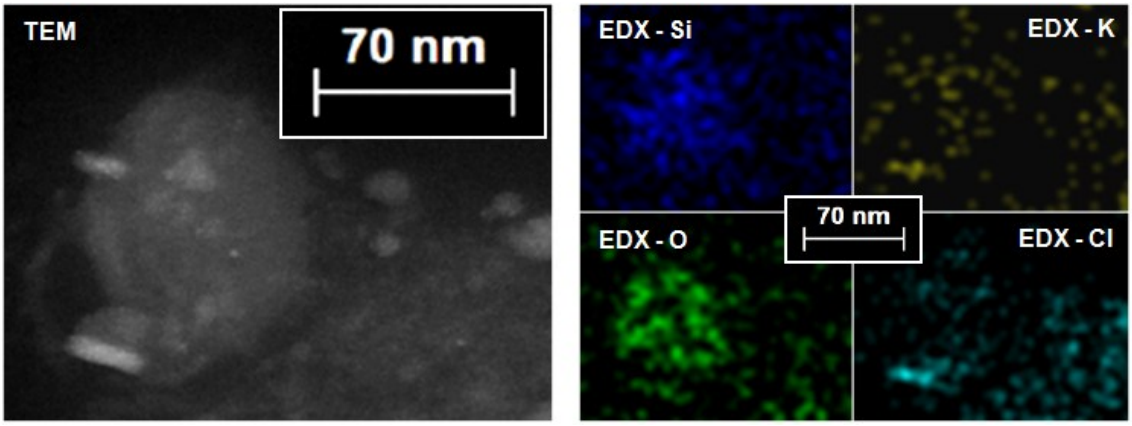

Figure 6.12 *HR-TEM micrograph and chemical mappings from EDX analysis (middle) of the corresponding area of the TEM image of polysilane* ***X-8a-pSi****, prepared by drop casting of a diluted* $CHCl_3$ *solution to a Cu grid. EDX colors are blue (Si), green (O) and yellow (K) and light blue (Cl).*

Conclusively, the combination of three independent microscopy techniques gives a sound overview of the self-assembled structures of the mono- and trialkoxy substituted crosslinked polymers with unsaturated spacers. Furthermore the combination of microscopy based data with light scattering analysis allows speculations about the self-assembly behavior and even the development of a detailed model for the formation of self-assembled secondary structures.

Although crosslinked polysilanes with saturated spacers show similar self-assembled disc like aggregates when deposited on substrates, one polymer system with saturated spacers was found to behave exceptionally. In *Figure 6.13* the AFM height contrast image of compound **X-α/β-4a-pSi** is presented: In contrast to the standard discotic features, much more complicated helical structures are perceptible. These helical assemblies are not an individual case, but spread all over the investigated substrate. Furthermore, from the magnified inset one can recognize that the helices are consisting of smaller features, which are similar to all other discs. This leads to the assumption that the helices are superlattices or tertiary structures.

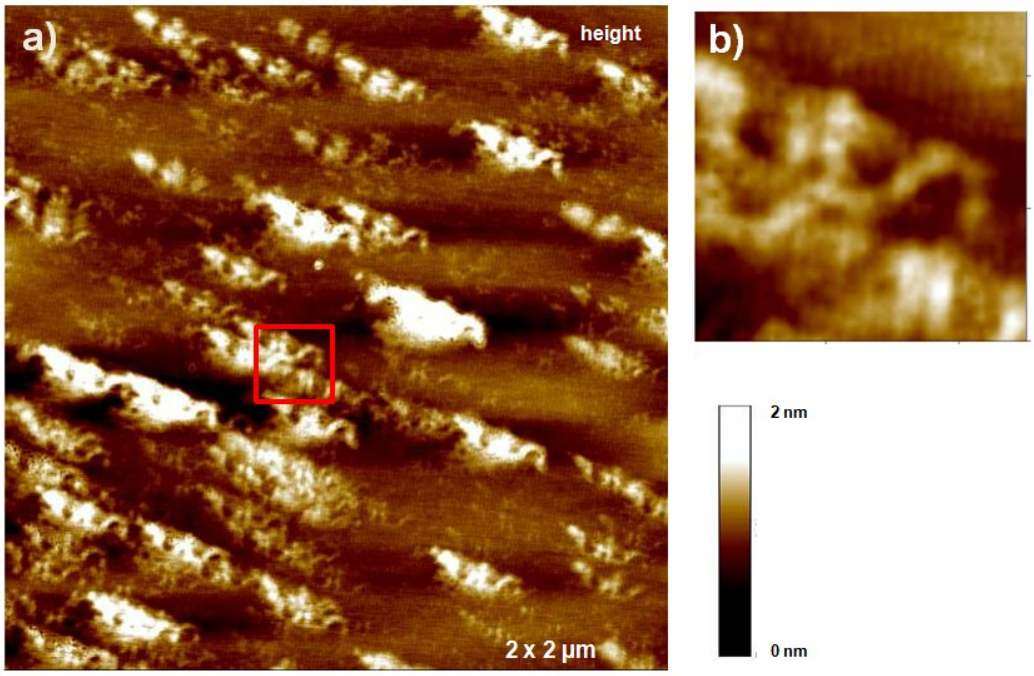

Figure 6.13 *AFM height contrast image of compound* ***X-α/β-4a-pSi*** *(a) and magnified area in the red square (b).*

Regarding the fact that the helices were only found with this particular polymer system, consisting of a mesogen mixture of saturated α- and β-isomers, one can hypothesize that the structural feature, which is responsible for the helices, must be the β-isomer. This assumption is also supported by the finding that the other saturated coupling products, consisting of only α-isomers, tend to assemble to disc like structures. Unfortunately, during this work no possibility to synthesize a polysilane built up exclusively of β-isomers was found. Therefore no evidence for this hypothesis could be supplied.

For a comparison of crosslinked polymers with linear coupling products, further samples, which were coated with solutions of linear polymers (**L-4/5-pSi**) were analyzed by AFM. From *Figure 6.14* it is perceptible that the linear polymers do not assemble to regular structures, but rather agglomerate to irregular forms (the optical impression of orientation along one axis derives from the spin casting process). This finding was a further reason to cease further investigations on linear polymers.

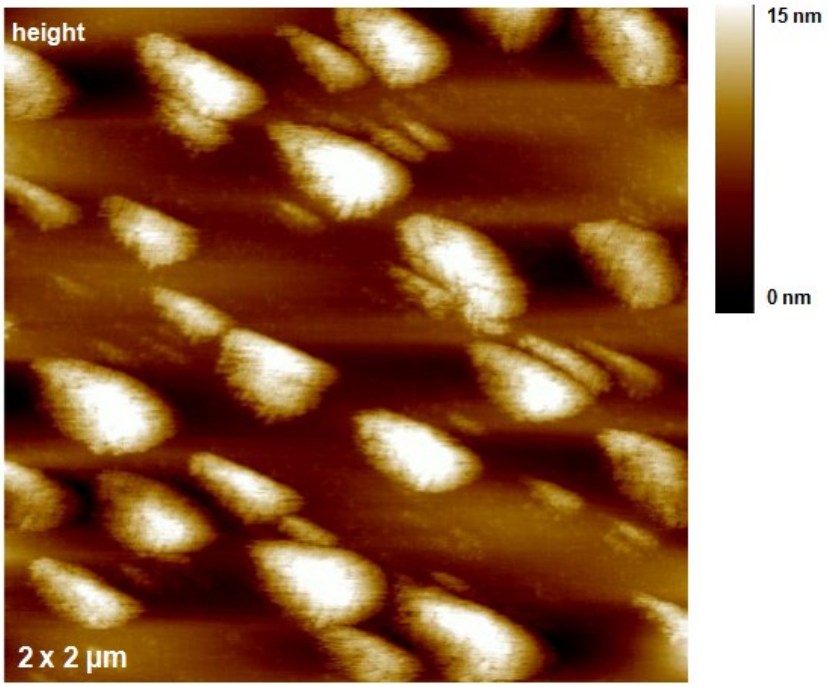

Figure 6.14 *AFM height contrast image of compound* ***L-5a-pSi****.*

In this section, characterization of self-assembled structures using different optical methods was discussed. In general, it was found that the crosslinked polymers show the ability to form disc like aggregates of primary polymer particles, by collapsing of alkoxy chains due to interactions with the substrate. The dimensions of these aggregates are substantially depending on two factors: mesogen substitution and polymer concentration during the casting process. Therefore, by variation of these two parameters certain particle size control is obtained.

6.6 Effect of Pyrolysis on Nanostructures

Nanostructured silicon based surfaces is a widely investigated scientific field. Silica nanostructures are of high interest in, for instance, biochemical and biomedical applications, whereas nanostructures of silicon carbide and other ceramic materials can imply many improvements in the field of nanoelectronics. Therefore, in this work the applicability of self-assembled crosslinked polysilane nanoparticles as pyrolyzable precursors for different kinds of silicon based surface nanostructures was investigated. It was found, that pyrolysis of polysilane assemblies under various conditions, proceeds under structure retention, and therefore surfaces, which are structured with well defined and homogeneously distributed nanoparticles, can be obtained.

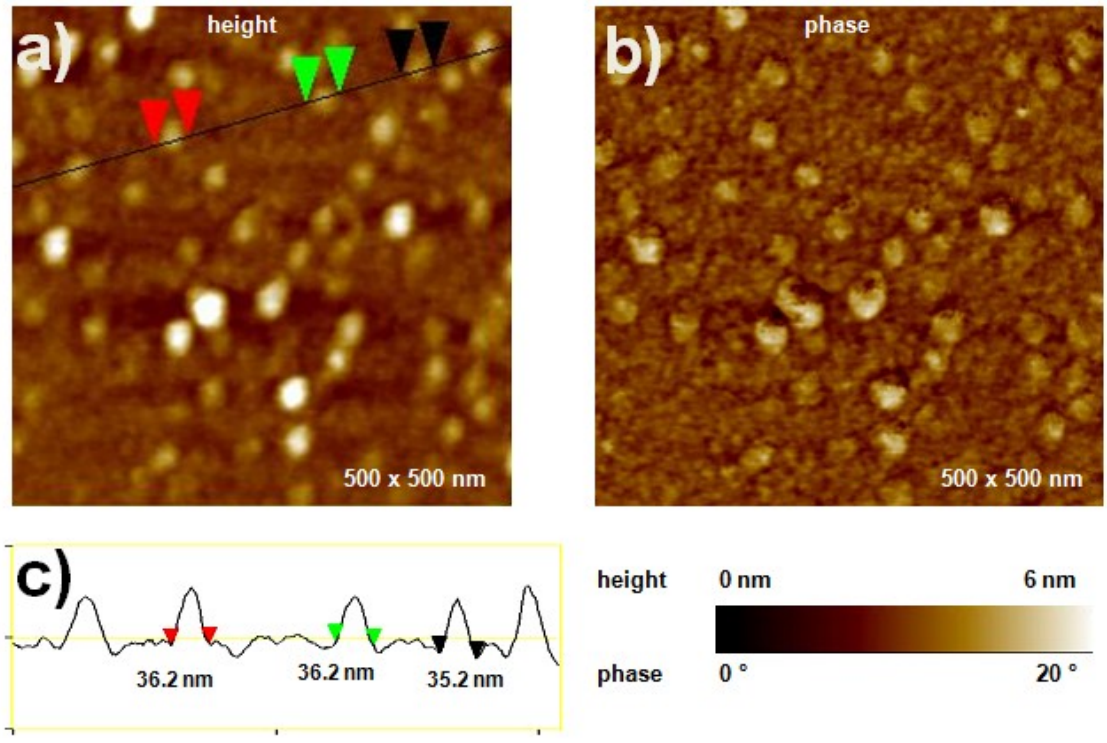

Figure 6.15 *AFM topography (a) and phase contrast (b) images of pyrolyzed sample of crosslinked polysilane* ***X-5a-pSi*** *on polished Si wafer substrates. In (c) the z-profile along the corresponding black line in the topography image is shown.*

In *Figure 6.15* and *Figure 6.16* this statement is exemplified by results of the analysis of a pyrolyzed sample using different microscopy techniques. *Figure 6.15 (a)* and *(b)* show AFM height and phase contrast images of polymer **X-5a-pSi** (same sample as in *Figure 6.8 (a) - (c)*) after being pyrolyzed in TGA under a stream of synthetic air, whereas in *Figure 6.16*, a micrograph from HR-SEM analysis of the very same sample is presented. Both analysis techniques show, that during the pyrolysis of crosslinked polysilane particles, no significant structure alteration occurs, and although the resulting particles are significantly smaller than the previously detected assemblies, their shape and homogeneity is preserved. The shrinkage in diameter and height accounts to approximately 30% (from AFM), what implies, that a loose, amorphous and porous silica material is formed. Also from the low contrast in the phase contrast image in *Figure 6.15 (b)* one can conclude that a material, which bears mechanical properties that are similar to the surrounding substrate, is formed.

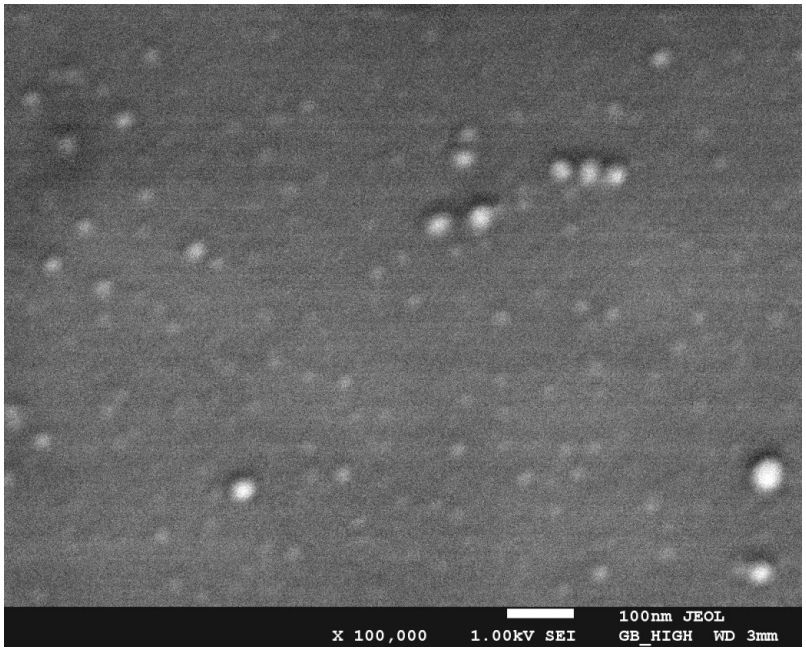

Figure 6.16 *HR-SEM micrograph of a pyrolyzed sample of compound* ***X-5a-pSi*** *casted to a Si wafer surface. The scale bar accounts to 100 nm.*

The presence of SiO_2 after pyrolysis of the polymers was previously proven by TGA analysis (described in *Section 6.4.2.3*). For additional reassurance, the residual product from pyrolysis of bulk polymer material was analyzed by SEM. In *Figure 6.17 (a)* a SEM micrograph and EDX chemical mapping images of the residuals from pyrolysis in air are shown. The EDX images clearly show that the particle is only emitting signals from silicon and oxygen. Hence the residual material from spin casted samples must exclusively be composed of silica.

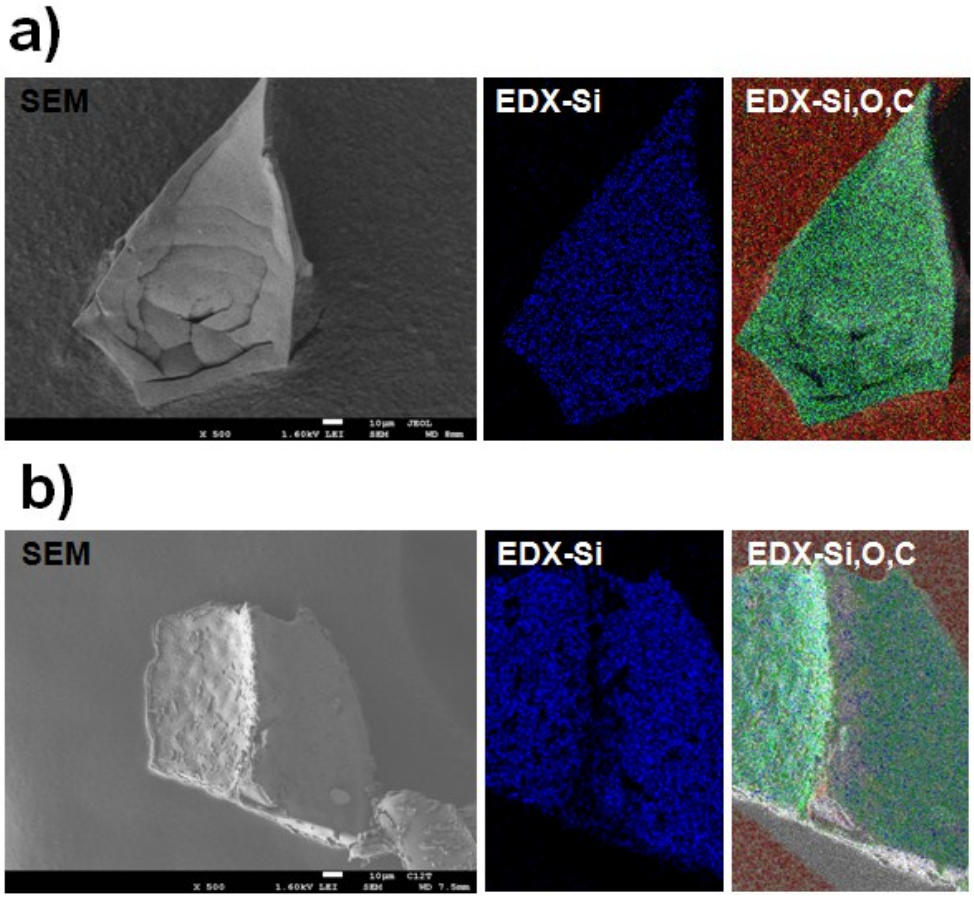

Figure 6.17 *SEM micrographs and chemical mapping of the corresponding areas using EDX on bulk materials of compound* ***X-5a-pSi*** *pyrolyzed under a stream of synthetic air (a) and dry nitrogen (b). The scale bar accounts to 10 µm. EDX colors are blue (Si), green (O) and red (C).*

Alternatively to the pyrolysis in air, the same polymers were pyrolyzed in nitrogen atmosphere. This procedure led with spin casted samples to the same particle structures and shrinkage values as obtained after pyrolysis in air (not shown). Once again, for chemical characterization the bulk residuals from pyrolysis were used. EDX analysis revealed besides the expected silicon and oxygen content also the presence of considerable amounts of carbon. This means that a ceramic SiC / SiOC hybrid material is obtained, which was already predicted from TGA analysis (see *Section 6.4.2.3*), and furthermore expected from its black color (compared to the white color of the air pyrolysis product). In *Figure 6.17 (b)* the resulting chemical mapping from EDX is shown. The main part of the carbon signal originates from the areas near to the sharp edge in the middle of the sample, which gives the impression that the planar areas are oxidized after the pyrolysis procedure.

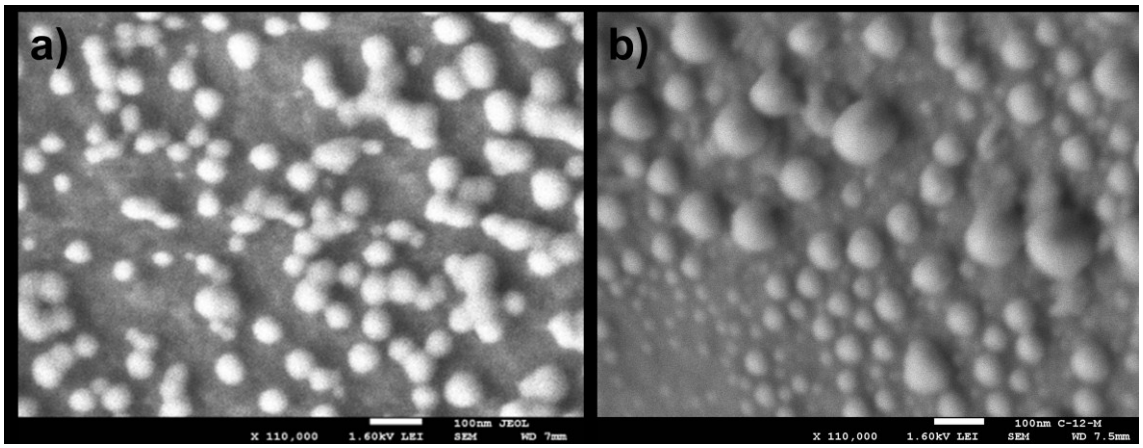

Figure 6.18 *HR-SEM micrographs of bulk samples of compound* ***X-5a-pSi****, which were pyrolyzed in air (a) and* N_2 *(b). The scale bar accounts to 100 nm.*

Besides the consolidated findings from chemical analysis, analysis of the bulk residue materials in SEM led to a surprising result concerning the structure of the materials. In *Figure 6.18* this structures are illustrated, since these micrographs show high resolution images of the surfaces of pyrolyzed bulk materials in air *(a)* and nitrogen *(b)*. It is perceptible that the surfaces of the bulk residues are composed of nanoparticles. Compared to the dimensions of single particle assemblies of sub-monolayer films, the dimensions of the bulk particles are slightly larger. They are furthermore dependent on

the pyrolysis conditions; if the pyrolysis proceeds in air, the obtained particles are smaller than the ones after pyrolysis in inert nitrogen atmosphere. An explanation for this result can be found in the pyrolysis conditions. During the pyrolysis in air, the mesogen substituents are removed by combustion and therefore do not influence the crosslinking of the silane-based cores to silica material – hence the primary structures are more or less preserved. During the pyrolysis in N_2 on the other hand, carbon atoms are included into the primary structures, which leads to SiOC hybrid material and is assumed to be decisive for the enlarged particles of the pyrolysis product.

Although the nanoscaled particle structures were found on the surfaces of the pyrolyzed bulk materials, transformation of these pyrolysis conditions to spin casted thicker continuous films on surfaces of substrates could not be achieved. Pyrolysis of thicker films of crosslinked polysilanes could find interesting application possibilities as nanoporous substrates in for instance electrode technology. Unfortunately, the pyrolysis of thicker films always resulted in discontinuous surface layers with irregular particle agglomeration. This is supposed to depend on the higher mobility of the molten polymer particles at high temperatures in the TGA. Therefore an alternative route to silicon based nanostructured surfaces was searched. One possible attempt is described in the next section.

In conclusion it was shown that pyrolysis of self-assembled polymer particles is a feasible route to fabricate silicon based surface nanostructures by removal of the mesogen substituents after the self-assembly process. This can be regarded as an effective templating technique. Using this technique, two different particle compositions were obtained by applying two different atmospheres during thermal treatment. Furthermore the dimension of silica and hybrid carbon-silicon based ceramic nanoparticles could be controlled by the substitution motif on the polymer. Although both, sub-monolayers and bulk materials could be used to form nano-structured surfaces upon pyrolysis, the formation of nano scaled structures in thicker surface films was not achieved due to agglomeration of the polymer precursors to inhomogeneous structures.

6.7 Homogeneously Nanostructured Films by Plasma Treatment

In the previous section it was described, that although isolated self-assembled nanoparticles of crosslinked polysilanes could be pyrolyzed under structure retention, pyrolysis of homogeneous thicker polymer layers did not lead to nanostructured surface coatings, because the coatings tended to agglomerate during thermal treatment due to an elevated mobility of the polymer particles in the films. Therefore a different technique was required, which does not create high temperatures. Here an alternative possibility to create nanostructured surface layers is presented. The method of choice comprises spin casting of continuous layers of crosslinked polysilanes and subsequent treatment with radio frequency based inductively coupled plasma (RF-ICP), composed of a mixture of hydrogen and argon.

Once again, for investigation of plasma treatment, polymer coatings from coupling products of mono and trialkoxy substituted mesogenic chlorosilane monomers (**X-8a-pSi** and **X-5a-pSi**) were utilized. As comparative control system, also coatings from crosslinked polyphenylsilane (**pPhS**), which was synthesized via a catalytic route with transition metal based catalysts[152] were investigated.

The samples were prepared by spin casting of $CHCl_3$-solutions of the polymers with variable concentrations to different substrates. Regarding the subsequently applied analysis techniques, Si or Ge wafers as well as freshly cleaved HOPG surfaces were used as substrates. The properties (thickness/integrity) of the resulting films were investigated using ellipsometry before and after plasma treatment. The ellipsometry results are summarized in *Table 6.7*. Plasma treatment was performed in a custom built cylindrically shaped reactor, using a controlled low pressure atmosphere consisting of Ar and H_2. The optimum in plasma treatment time was found to be 5 min at a plasma power of 600 W concerning the integrity of the resulting layer surfaces.

Prior to the investigation of thicker films, also samples with isolated self-assembled nanoparticles were treated with plasma. The same results as already observed after thermal pyrolysis were obtained with plasma treatment. As expected, after 5 min of treatment in the plasma reactor, again nanoparticles with comparable size shrinkage were found.

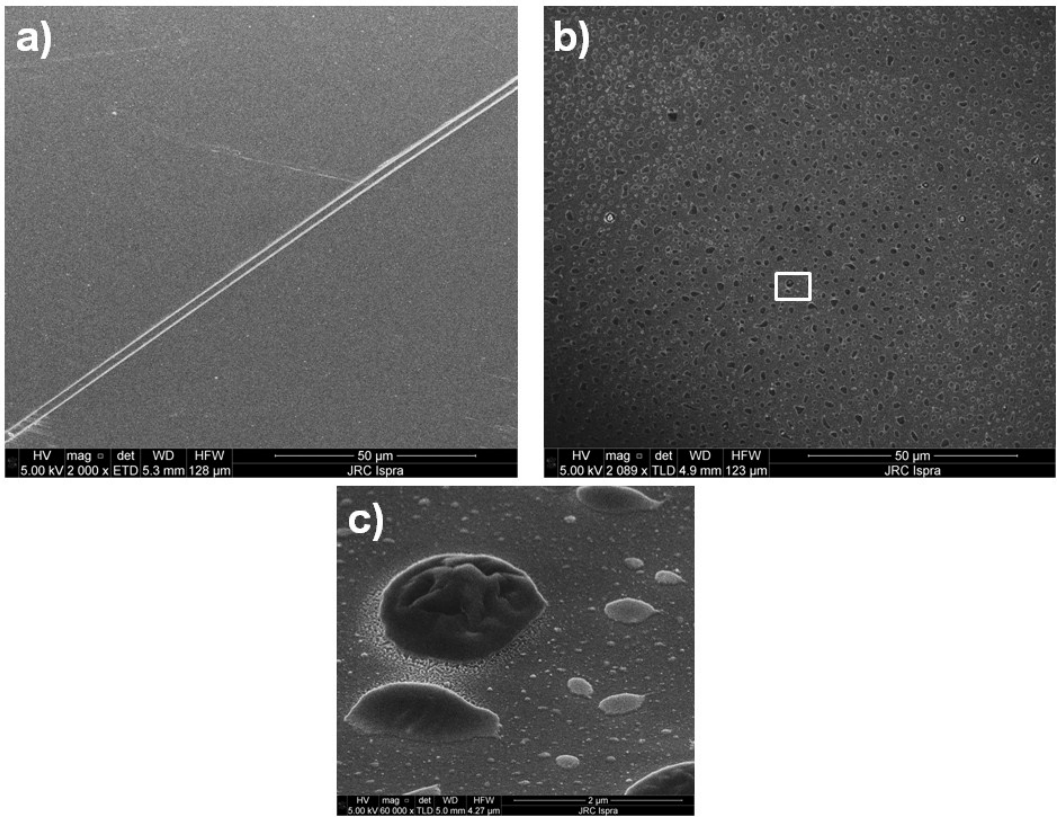

Figure 6.19 *SEM micrographs of compounds* ***X-5a-pSi*** *(a) and* ***pPhS*** *(b), which were plasma treated in a mixture of Ar and H_2. In (c) the magnified area in the white square of (b) with an image tilting of 45 ° is shown. The scale bars account to 50 µm (a, b) and 2 µm (c).*

But the much more interesting results were obtained, when the plasma treatment was applied to polymer films with an average thickness of 10 nm (see *Table 6.7*). In *Figure 6.19*, representative SEM micrographs of plasma treated films from compound **X-5a-pSi** (*a*) and the previously mentioned control polymer **pPhS** (*b, c*) on Si wafer substrates are presented. One clearly can see that in the case of the coating with

crosslinked polysilane **X-5a-pSi**, the plasma treatment yields homogeneous surfaces at a scale of tens of micrometers. This effect can be seen at the white lines in the image. These lines are due to a scratch through the surface coating, which was applied mechanically with a blade to show that there is still a remaining film on the substrate surface. Treatment of the linear control polymer **pPhS** on the other hand, led to discontinuous agglomerates with sizes of a few micrometers (*Figure 6.19 b, c*), which are comparable to the agglomerates after pyrolysis of thick layers of crosslinked polysilane systems. This issue also can clearly be seen in the data from ellipsometry (see *Table 6.7*), since after plasma treatment, due to a lacking in integrity of the film, no mathematic model for fitting of the film thickness could be found. From these results one can conclude that the mesogen substitution is absolutely essential to obtain homogeneously coated substrates after plasma treatment. These results are not restricted to tests on silicon wafer substrates - the same results were also obtained when different substrates, such as Ge or HOPG were used.

Table 6.7 *Results of film thicknesses from ellipsometry.*

	film thickness[a]	
Subst.	before plasma [nm]	after plasma [nm]
X-5a-pSi	10.2	2.3
X-8a-pSi	11.8	2.5
pPhS	10.6	/

[a]: obtained from polymer samples on Ge substrates after applying a three layer model (Ge substrate, GeO layer, polymer film).

In the next step, the structures of the homogeneous films were assessed on the nano scale. In *Figure 6.20*, representative AFM height contrast images of plasma treated films of compounds **X-5a-pSi** and **X-8a-pSi** are presented. It is perceptible that the homogeneity of the surface continues even on the nano scale. The particle sizes as well as the dimensions of the pores in between are of remarkable uniform distribution. The sizes of the particles from the monoalkoxy substituted compound **X-8a-pSi** account to approximately 70 nm and therefore are consistent with the particle sizes of the same compound after thermal pyrolysis of bulk materials. On the other hand, the particles of

the trialkoxy substituted compound **X-5a-pSi** seem to possess a bimodal particle size distribution. The bigger particles account to approximately 120 nm, which fits quite good to the dimensions of the particles of thermally pyrolyzed bulk in inert atmosphere. But besides these bigger particles also smaller ones with dimensions of approximately 40 nm are present. This dimensions fit very well to the obtained particles from pyrolysis in air. The size difference indicates again a higher extent of crosslinking of the polysilane cores during plasma modification due to an inclusion of carbon atoms. Another possibility for interpretation is that the bigger particles are secondary structures, which are constructed from smaller primary units.

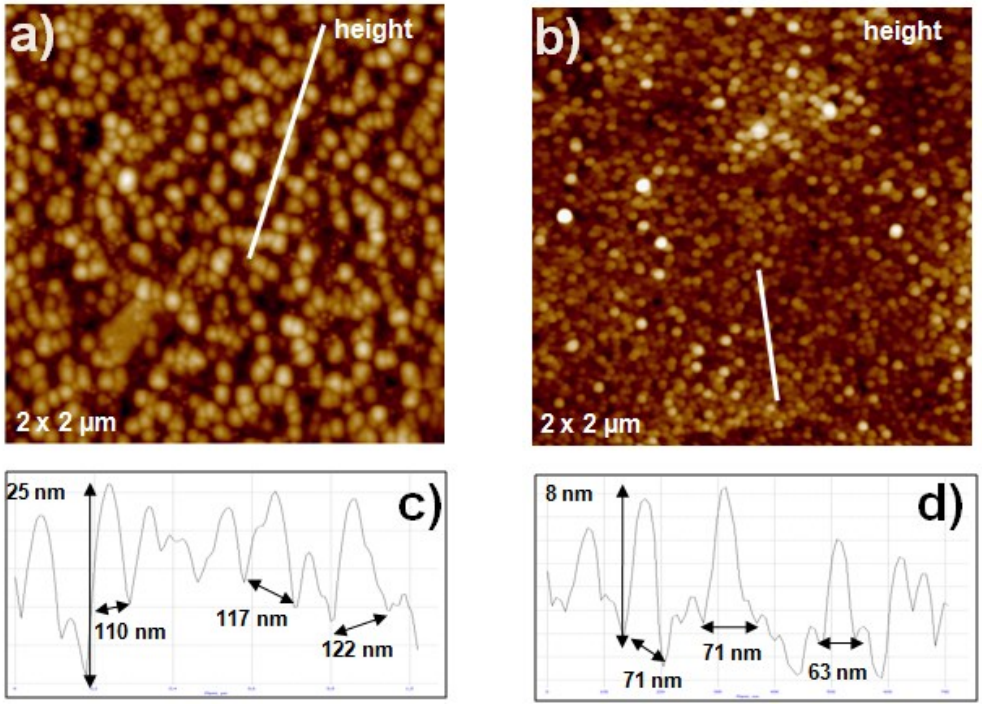

Figure 6.20 *AFM height contrast images of crosslinked polysilanes* ***X-5a-pSi*** *(a) and* ***X-8a-pSi*** *(b) on polished Si wafer substrates after 5 min of plasma treatment. In (c) and (d) the z-profiles along the corresponding white lines in the topography images are shown.*

To assess this issue, once again HR-SEM analysis was utilized. In *Figure 6.21* the obtained micrographs of compound **X-5a-pSi** are shown. In part *a)* of the figure one clearly can observe a homogeneous distribution of the bigger particles, whereas a

zoomed area in part *b)* shows that these particles consist of smaller subunits with dimensions of approximately 20 nm. A similar result is obtained, when compound **X-8a-pSi** is investigated, which means that in both cases the particles, which result from plasma treatment of thicker films are assembled from smaller primary subunits with particle sizes of around 20 nm.

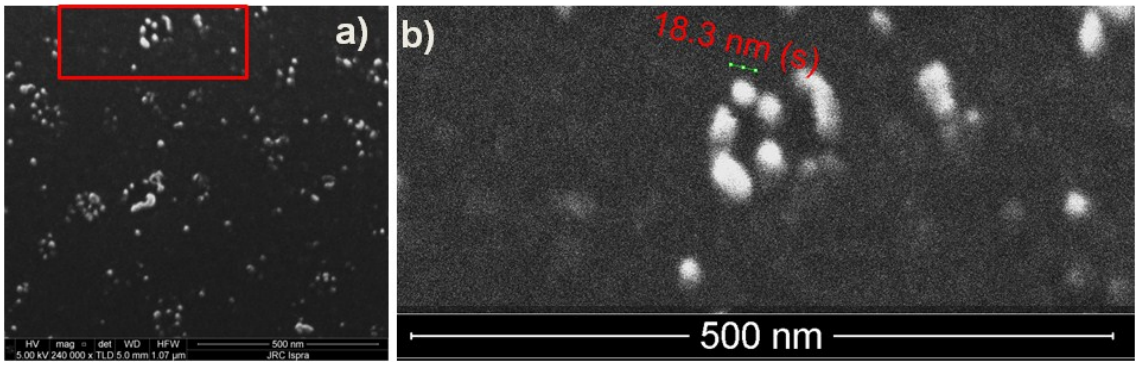

Figure 6.21 *HR-SEM micrographs of thick films of compound* ***X-5a-pSi*** *after plasma treatment. The scale bar accounts to 500 nm.*

Since the thicknesses of the films after plasma treatment were extremely low (*Table 6.7*), the only viable possibility to perform chemical analysis of the surface structures was found in XPS spectroscopy. Although this technique usually leads to absolutely reliable quantitative analysis results, we faced in this case several problems, which made only a qualitative analysis of the surface films accessible. Regardless the nature of the substrates, the plasma treated polymer films were too thin to obtain a XPS signal exclusive from the coatings; in all cases, a not negligible part of the signal was also originating from the substrates. Since this problem could not be solved by angle resolved analysis, the porosity of the treated films must also be taken into account. Therefore the obtained atomic concentrations from survey spectra were not helpful. Hence only the high resolution core level spectra could be evaluated.

In *Section 6.4.2.2* the analysis results of XPS spectroscopy on polysilane films prior to plasma treatment were reported. Already there, the quantitative analysis was not possible due to a low film thickness. But a combination of core level spectra evaluation with other analysis techniques, revealed the presence of Si-Si-bonds in the polymer. In *Figure 6.22* the Si_{2p} core level spectrum of plasma treated compound **X-8a-pSi** is compared to the untreated polymer spectrum from *Figure 6.6* in *Section 6.4.2.2*. After plasma treatment the core level spectrum still can be fitted with four peaks, what indicates that the chemical composition of the crosslinked silane cores in the film did not change much. But a close look to the fitted peaks shows that all four peaks underwent a change in intensities and furthermore are slightly shifted to higher binding energies. The low binding energy peaks decreased in intensity, whereas the peaks at high binding energies increased. This means that the content of Si atoms which are surrounded by other Si atoms decrease and the O-Si-O functions increase. Most probably the plasma treatment leads to etching of the polymers and results in reactive groups on the particle surfaces, which are then oxidized upon contact to the environment.

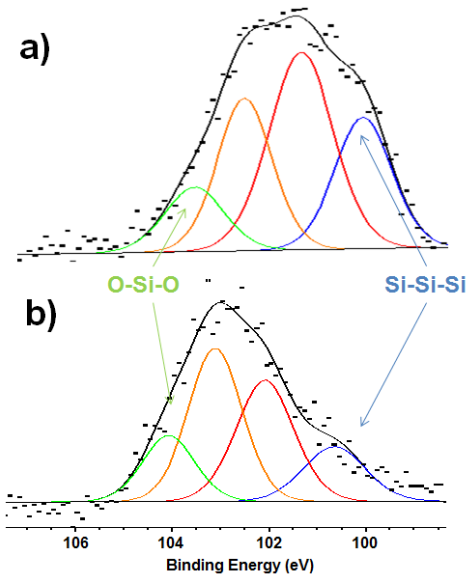

Figure 6.22 *Si_{2p} high resolution core level spectra obtained by XPS analysis of spin casted thin film of compound **X-8a-pSi** on HOPG substrate before (a) and after plasma treatment (b).*

Conclusively it can be stated, that plasma treatment of solution processed polysilane films is a feasible and relatively simple method to obtain nanostructured silicon based surface coatings. Compared to other methods, which use polysilanes as precursors for silicon based coatings, this route provides absolutely homogeneous nanostructures without cracks or agglomerates, and furthermore offers the possibility to control the dimensions of the structures. Therefore, for certain applications in the field of e.g. nanoelectronics, defined silicon based surface structures can be tailored.

6.8 Summary

In this chapter, the use of the mesogenic building blocks from the mesogen library in *Chapter 4* for the synthesis of chlorosilane based monomers, as well as their subsequent *Wurtz*-type reductive polymerization to crosslinked polysilanes is described.

Two different types of alkoxy-functionalized mesogens with unsaturated functional groups (styrene and phenyl acetylene) were used as substrates for hydrosilylation reactions with H-functionalized chlorosilanes under homogeneous catalysis with transition metal catalysts. For the phenyl acetylene based monomers, the same reaction conditions as already presented in *Chapter 5* for the synthesis of multimesogens with silicon based linkers were applied. Again fully regio- and stereoselective products were obtained. On the other hand, when styrene based mesogens were used as substrates for hydrosilylation, regio- and stereoselectivity was a huge issue, since two different regioisomers (*Markovnikoff* and anti-*Markovnikoff*) are theoretically possible. Dealing with this issue involved screening of various catalyst-systems, as well as different solvents and reaction conditions. Despite all efforts, besides mixtures of both isomers, only the α-isomer could be obtained isomerically pure. Although various alternative routes to obtain the β-isomer were tested, none of these routes was successful.

From the obtained monomers, different polysilanes were synthesized using the *Wurtz*-type reductive coupling reaction, which involves strong reduction agents, such as neat alkaline metals or graphite-alkaline-intercalates. Screening of various reaction conditions led to optimized effectiveness of this reaction. The necessity of the alkoxy substitution motif on the mesogens towards the solubility of the resulting crosslinked polymers was demonstrated by comparison with polymers from unsubstituted styrene and phenyl acetylene based chlorosilane monomers. These unsubstituted control polymers appeared to be absolutely insoluble in standard solvents, and therefore could not be used for studies of self-assembly.

The chemical compositions of the obtained polymers were investigated using different qualitative and quantitative analytical approaches. A combination of the results clearly showed the presence of Si-Si-bonds. Further characteristics of the polymers, such as molecular masses or particle sizes, were assessed by various polymer analysis techniques. The results led to the development of a simplified spherical structural model of the crosslinked polysilanes, which served as basis for subsequent understanding of self-assembly patterns in bulk materials and on surfaces.

These self-assembly phenomena were investigated using different optical and scanning surface analysis tools, such as TEM, SEM, or AFM. For that reason the polymers were deposited on substrate surfaces by spin or dip coating from highly diluted solutions. This approach led to isolated structures in sub-monolayers and closed continuous thin films with a thickness of approximately 10 nm.

The isolated sub-monolayer particles were identified as flat, disc like structures, with varying but homogeneous dimensions between 50 and 120 nm depending on the structural features of the mesogenic monomers. Combination of results from AFM and DLS, led to the assumption, that the disc like structures are secondary assemblies of collapsed spherical primary particles. Complementary indications of the secondary structures were provided by SEM and TEM analysis. In contrast to the isolated sub-monolayer particles, the continuous films did not show the presence of any structural features.

In the further progress of the study, the applicability of the polysilane nanostructures as precursors for homogeneously structured silica and silicon ceramic surfaces was evaluated. It was found that pyrolysis of the isolated disc like structures in air or under inert N_2 atmosphere at 900 °C, results in retention of the discs with certain shrinkage of the particles. Although also pyrolyzed bulk materials exhibited particular nanostructures on the surface, the conversion of continuous thin films to structured surface coatings was not successful, due to agglomeration of the particles.

To avoid particle agglomeration and finally obtain continuous and homogeneously structured silicon based surface coatings, etching of continuous polysilane films with inductively coupled low pressure Ar-H_2-plasma was performed. This plasma etching approach finally led to the desired nanostructured coatings with controllable particle sizes and porosities.

In conclusion, combination of the mesogen building blocks with polymerizable chlorosilane functionalities is a feasible approach to obtain polysilane nanostructures by mesogen induced self-assembly. These structures can be used as precursors for different homogeneous silicon based nanostructures by pyrolysis and plasma treatment which are necessary for emerging technologies in the fields of electronics or nano-biotechnology.

7 Summary

Although silicon can be found in the periodic table in the same main group as carbon, the structural variety of silicon based compounds is very low compared to their carbon based neighbors. Therefore, in this study a novel approach towards the synthesis of defined three-dimensional silicon based structures is described. This approach comprises the design of a construction kit of carbon based mesogenic building blocks, which are known to form defined structures by molecular self assembly, and furthermore can be used for coupling with silicon containing molecules, such as siloxane oligomers or polymerizable chlorosilanes. The combination of the carbon mesogens with silicon-based head groups enabled the formation of three-dimensional assemblies of the obtained silicon mesogens.

In the first part of this study different multi-step synthesis routes to form a library of carbon mesogens are described. As adequate mesogen systems, derivatives of the so-called *Percec*-mesogens were identified. These mesogens are long-chain alkoxy substituted derivatives of gallic acid, and therefore enabled us to combine rigid phenyl-groups with flexible alkyl chains, which is one important requirement for molecular self-assembly. Furthermore, the mesogens were equipped with different functional groups, such as unsaturated double- or triple-bonded groups or nucleophilic functions, which served as anchoring points for H- or Cl-terminated oligo-siloxanes and polymerizable silanes. This mesogen library covers a broad range of possibilities for the coupling of silicon based head groups and also for the alteration of physical and chemical properties of the target molecules, by variation of numbers and lengths of the alkoxy substituents on the mesogens.

The second part of the study deals with the utilization of different mesogens from the previously established library for coupling with linear and cyclic silane and siloxane oligomers. The coupling reactions proceeded *via* Ru-catalyzed hydrosilylations of unsaturated mesogens with H-terminated Si-oligomers or nucleophilic substitutions of Cl-terminated siloxanes and silanes with charged mesogens. The obtained silicon based multimesogens were investigated in terms of structure formation by self-assembly, using different analysis techniques, such as DSC, POM, and SAXS. It was found that all multimesogens possess the ability to form mesophases in bulk materials. The most important outcome was that the mesophases are monotropic and therefore occur only upon supercooling isotropic melts, which is unusual for this class of materials. This led to the assumption that the investigated structures were a special form of frozen mesophases. Structure analysis of the frozen mesophases by SAXS revealed the presence of layered smectic type structures and the dependence of their dimensions from the lengths of the alkoxy substituents on the mesogens. These results could be verified by analysis of the structures in thin films, which were made by spin casting of the multimesogens to substrate surfaces. Using AFM the layered domains could be visualized and by GISAXS the domain sizes and even electron densities could be assessed.

In the third and last part of the study, the synthesis of polymerizable mesogen monomers by coupling of the mesogens from the library with chlorosilane monomers, as well as their subsequent polymerization to linear and crosslinked polysilanes is described. Utilization of styrene and phenylacetylene based mesogens led to mesogen monomers with different spacer groups between mesogens and polymerizable head groups, which were found to be strongly influential towards the molecular masses of the resulting polymers from *Wurtz*-type reductive coupling reactions with alkaline metal based reduction agents. The polymerization reactions were performed with di- and trichlorosilane mesogens and yielded soluble polymers even in the case of crosslinked polysilanes, which is remarkable, since polymerization of trichlorosilanes without mesogenic substituents, led to insoluble crosslinked solids.

After performing investigations of standard polymer properties, such as chemical compositions and molecular masses, the polymers were investigated in terms of self-assembly. For this reason, the polymers were deposited by spin casting to substrate surfaces. In the case of crosslinked polysilanes homogeneously distributed disc like nanoparticles were found using visualization techniques, such as AFM, SEM, or TEM; whereas the linear polysilanes did not show any features of self-assembly. The sizes of the polysilane nanoparticles were between 50 and 120 nm, depending on the substitution motif on the mesogens. The results from imaging techniques were combined with standard polymers analytics, such as DLS, what led to an advanced model of self-assembly, which showed that the nanoparticles are secondary assemblies of primary polymer particles. In the further progress of the study, the self-assembled particle systems were used to synthesize homogeneous silica and silicon ceramic particles, as well as homogeneously nanostructured porous coatings of silicon ceramic materials, by pyrolysis in different atmospheres and plasma etching, respectively.

Conclusively it has been shown that combining mesogenic building blocks with silicon based head groups can easily be applied to induce self-assembly in siloxane and silane linked multimesogens, as well as in mesogen functionalized crosslinked polysilanes. Although this approach did not lead to the discovery of new modifications of silicon, novel layered smectic siloxane structures and homogeneously distributed polysilane nanoparticles, as well as a new route to tightly bound silicon based nanoporous surface coatings was found. Future investigations should concentrate on the assessment of electrochemical properties of the obtained porous coatings, for emerging applications in electronics or energy storage materials. Furthermore the simplification of the synthesis route should be envisioned, since the described route will not lead to commercially viable applications due to extraordinary high costs.

8 Zusammenfassung

Obwohl Silicium im Periodensystem der Elemente in derselben Hauptgruppe steht wie Kohlenstoff, ist die strukturelle Vielfalt an siliciumbasierten Komponenten deutlich niedriger, als die der auf dem benachbarten Kohlenstoff basierenden Verbindungen. Aus diesem Grund wurde im Rahmen dieser Arbeit ein neuer Ansatz zur Synthese von definierten, dreidimensionalen siliciumbasierten Strukturen verfolgt. Das zugrundeliegende Konzept beruht auf dem Aufbau eines Baukastensystems aus kohlenstoffbasierten Verbindungen, welche dafür bekannt sind, durch molekulare Selbstorganisation definierte Strukturen zu bilden, und darüber hinaus auch mit siliciumbasierten Molekülen, wie zum Beispiel Siloxanoligomeren oder polymerisierbaren Chlorsilanen, gekoppelt werden können. Diese Kombination von Kohlenstoffmesogenen mit siliciumbasierten Kopfgruppen sollte dann die molekulare Selbstorganisation der synthetisierten Siliciummesogene zu dreidimensionalen Strukturen ermöglichen.

Im ersten Teil dieser Arbeit werden verschiedene mehrstufige Synthesen beschrieben, die die Grundlage für einen Baukasten von Kohlenstoffmesogenen bilden. Als dafür am besten geeignete Systeme, konnten Derivate der sogenannten *Percec*-Mesogene identifiziert werden, bei welchen es sich um langkettige, alkoxysubstituierte Derivate der Gallussäure handelt. Dieses Substitutionsmuster ermöglichte die Kombination von starren Phenylgruppen mit flexiblen Alkylketten, welche generell eine wichtige Voraussetzung für molekulare Selbstorganisation darstellt. Darüber hinaus wurden die

Mesogene mit verschiedenen funktionellen Gruppen, wie zum Beispiel ungesättigten Doppel- oder Dreifachbindungen oder nucleophilen Funktionen, ausgestattet, die als Anknüpfungspunkte für H- oder Cl-terminierte Oligosiloxane oder polymerisierbare Chlorsilane dienten. Diese so erhaltene Mesogenbibliothek deckt sowohl ein breites Spektrum an Kopplungsmöglichkeiten von siliciumbasierten Kopfgruppen, als auch die Variation der physikalischen und chemischen Eigenschaften der Zielmoleküle, durch Veränderung der Anzahl und Länge der Alkoxysubstituenten an den Mesogenen, ab.

Der zweite Teil dieser Arbeit beschreibt den Einsatz verschiedener Mesogene aus der Mesogenbibliothek für Kopplungen mit linearen und zyklischen Silan- und Siloxanoligomeren. Hierfür wurden ungesättigte Mesogene mit H-terminierten Si-Oligomeren in Ruthenium katalysierten Hydrosilylierungsreaktionen umgesetzt, oder in nucleophilen Substitutionsreaktionen Cl-terminierte Siloxane und Silane mit geladenen Mesogenen gekoppelt. Die auf diese Art synthetisierten siliciumbasierten Multimesogene wurden mit verschiedenen Analysemethoden, wie zum Beispiel DSC, POM und SAXS, auf Strukturbildung durch Selbstorganisation untersucht. Dabei konnte beobachtet werden, dass alle Multimesogene im Bulkmaterial Mesophasen ausbilden. Auffällig war hier vor allem die monotrope Natur dieser Mesophasen, welche für diese Molekülklasse außerordentlich untypisch ist und sich dadurch auszeichnet, dass die Mesophasen nur beim Unterkühlen isotroper Schmelzen auftreten. Diese Beobachtungen führten zu der Annahme, dass es sich bei den untersuchten Strukturen um eine spezielle Form von erstarrten Mesophasen handelt. Im Rahmen der weiterführenden Strukturanalyse dieser erstarrten Mesophasen mittels SAXS, zeigten sich smektische Schichtstrukturen, deren Schichtdicken stark von der Länge der Alkoxysubstituenten der Mesogene abhängen. Diese Ergebnisse konnten durch Untersuchungen an Multimesogendünnfilmen, welche durch Spincoating auf Substratoberflächen erzeugt wurden, bestätigt werden. Außerdem konnten die schichtförmigen Domänen mittels AFM visualisiert, und durch GISAXS deren Größe und sogar Elektronendichte bestimmt werden.

Im dritten und letzten Teil dieser Arbeit wird die Synthese von polymerisierbaren Mesogenmonomeren, durch die Kopplung von Mesogenen aus der Mesogenbibliothek mit verschiedenen Chlorsilanen und deren anschließende Polymerisation zu linearen und vernetzten Polysilanen, beschrieben. Die Verwendung von styrol- und phenylacetylenbasierten Mesogenen ermöglichte die Synthese von Mesogenmonomeren mit verschiedenen Spacergruppen zwischen den Mesogenen und den polymerisierbaren Kopfgruppen. Die unterschiedlichen Spacer zeigten einen starken Einfluss auf die Molmassen, der durch reduktive *Wurtz*-Kupplung mit alkalimetallbasierten Reduktionsmitteln, erhaltenen Polymere. Die Polymerisationen wurden mit Di- und Trichlorsilanmesogenen durchgeführt und es entstanden immer, sogar im Fall der vernetzen Polysilane, lösliche Polymere. Dies ist vor allem deshalb bemerkenswert, da die Polymerisation von Trichlorsilanen ohne mesogene Substituenten üblicherweise zu unlöslichen, vernetzten Feststoffen führt.

Im Anschluss an die Standarduntersuchungen der Polymereigenschaften, wie Molmassen, chemische Zusammensetzungen und thermische Eigenschaften, wurden die erhaltenen Makromoleküle mittels Spincoating auf unterschiedlichste Substrate aufgebracht, und anschließend auf Selbstorganisation hin untersucht. Im Falle der vernetzten Polysilane wurden, mittels verschiedener bildgebender Verfahren wie AFM, SEM oder TEM, homogen verteilte scheibenartige Partikel gefunden, deren Größe abhängig vom Substitutionsmuster der Mesogene, zwischen 50 und 120 nm liegt. Die Ergebnisse der bildgebenden Analysenmethoden wurden durch die Standardpolymeranalytik, wie z.B. DLS, unterstützt. Aus diesen Ergebnissen konnte ein Modell für die Selbstorganisation erstellt werden, welches zeigt, dass die ‚Nanodisks' sekundäre Assemblate von kleineren Polymerprimärpartikeln sind. Im weiteren Verlauf dieser Arbeit wurden diese selbstorganisierten Systeme zur Synthese von homogenen Silica- und siliciumkeramischen Partikeln mittels Pyrolyse verwendet. Darüber hinaus konnten daraus auch homogen nanostrukturierte poröse Beschichtungen aus einem siliciumkeramischen Material mittels Plasmaätzen hergestellt werden.

Zusammenfassend wurde in dieser Arbeit gezeigt, dass die Kombination von mesogenen Bausteinen mit siliciumbasierten Kopfgruppen, ein relativ einfaches aber wirkungsvolles Mittel zur Selbstorganisation von verschiedenen siliciumbasierten Systemen darstellt. Obwohl dieser Ansatz nicht zu der Entdeckung von bisher unbekannten Siliciummodifikationen geführt hat, konnten neue Wege, sowohl zu definierten Schichtstrukturen aus Siloxanen, als auch zu homogenen Nanopartikeln aus Polysilanen gefunden werden. Desweiteren wurde eine völlig neue Möglichkeit aufgezeigt, fest adhärierte siliciumbasierte nanoporöse Oberflächenbeschichtungen herzustellen.

Bei zukünftigen Untersuchungen sollte die Aufklärung der elektrochemischen Eigenschaften der erzeugten porösen Beschichtungen, im Hinblick auf Anwendungsmöglichkeiten sowohl in der Nanoelektronik, als auch als neuartige Energiespeichermaterialien, im Vordergrund stehen. Darüber hinaus sollte eine Vereinfachung der Syntheseroute angestrebt werden, da der hier beschriebene Syntheseweg, auf Grund des extrem hohen finanziellen und personellen Aufwandes, nicht zu kommerziell anwendbaren Materialen führen kann.

9 Experimental Part

9.1 Methods

9.1.1 Thin Film Preparation

Thin films were prepared by spin casting of the compounds from $CHCl_3$ solutions with varying concentrations (0.01 mg/mL to 5 mg/mL) to Si wafer substrates (0.5 x 0.5 cm^2 to 5 x 5 cm^2, Siltronic AG) which were previously cleaned by sequential sonication in trichloro benzene, hexane, ethanol and millipore water; as well as HOPG substrates (Momentive Performance Materials). Spin coating was performed utilizing a KARL SUSS RC8 spin coater. The parameters were: t=2 min, v=1800 rpm, a=200 rpm/s. After spin coating, the resulting films were dried in vacuum. Selected films were annealed for 10 min above the corresponding melting temperatures using the microscope heating stage, which was described above.

9.1.2 Plasma Treatment of Polymer Thin Films

Plasma treatment of the polysilane films was performed in a homemade cylindrically shaped low pressure plasma reactor, designed for basic studies in plasma processing and previously described in detail.[153-154] The reactor setup is illustrated in *Figure 9.1*. The vacuum chamber has an internal volume of 5 L and the discharge is generated using a

radio frequency - inductively coupled plasma (RF-ICP) configuration. The plasma treatments were performed in a gas-mixture, which consisted of Ar and H_2. The Ar/H_2 plasma was generated by means of an external double-spiral planar-coil inductive antenna (external diameter: 220 mm; the advantage of this configuration is that the efficiency, in terms of plasma density, is a factor of two higher than for a standard one-turn coil[155]). The antenna was powered by a RF generator (AE-Cesar 1310-01E operating at 13.56 MHz) and positioned above a 20 mm thick quartz glass window (diameter: 300 mm). The pressure in the reaction chamber was monitored with an MKS Baratron pressure transducer and maintained through a computer-controlled butterfly valve using a turbomolecular pump (Edwards EXT70) backed by rotary pump (Edwards 28), base pressure obtained before treatments was $1 \cdot 10^{-2}$ Pa. The flow rates of the working gases were regulated using a set of mass flow controllers (MKS Mass-Flo). The reactor was equipped with a vacuum load-lock transfer chamber, through which the samples were inserted and placed 55 mm above the quartz window (the samples facing the antenna side of the vacuum chamber) using a steel lance. Plasma treatment time was 5 min., operating with an input power of 0.12 $W \cdot cm^{-3}$. The gas flow rates were 11 sccm (standard cubic centimeters) for Ar and 11 sccm for H_2 at a working pressure of 5 Pa.

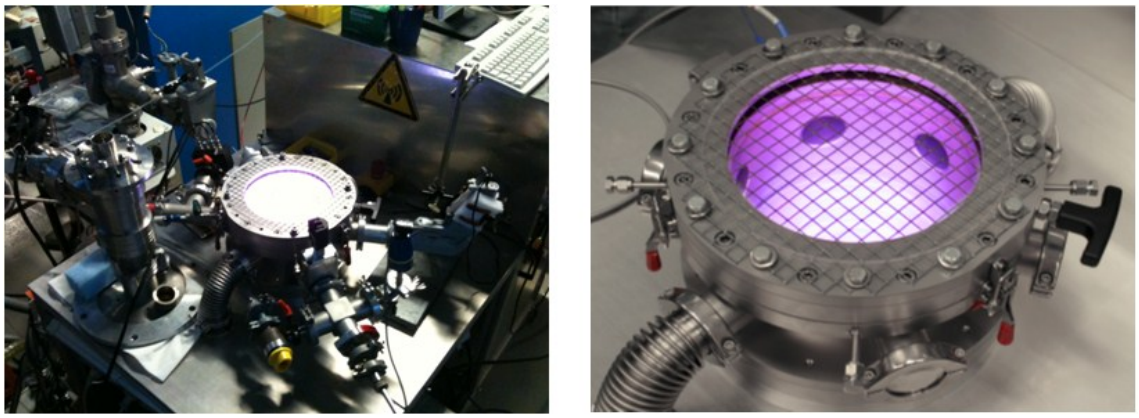

Figure 9.1 *Photographs of the plasma reactor setup.*

9.1.3 Polymer Analysis

9.1.3.1 Gel Permeation Chromatography

Conventional GPC analysis was performed with a PolymerLaboratories GPC50 Plus chromatograph running with HPLC-grade THF at a flow rate of 1 mL/min. Retention times and molecular masses were obtained using the integrated RI detector. For calibration polystyrene standards were used.

GPC analysis with SLS detection was carried out on a Varian LC-920 equipped with two PL Polargel columns, running with HPLC-grade THF at a flow rate of 1 mL/min. Retention times and molecular masses were obtained using a combination of a WTC Dawn Heleos II MALS detector and the integrated RI detector (356-LC).

9.1.3.2 Dynamic Light Scattering (DLS)

The average size and the size distribution of the polymer particles were determined by DLS in HPLS-grade THF, using a Zeta Nanosizer (Malvern Instruments), equipped with a detector to measure the intensity of the scattered light at 173 ° to the incident beam.

9.1.3.3 Thermal Analysis (DSC/TGA)

TA Instruments (Waters) DSC Q2000 and TGA Q5000 were utilized. The DSC was operated with helium at heating and cooling rates of 10 K/min. Only the second heating and cooling runs are plotted. TGA analysis was performed under N_2 or synthetic air with a flow rate of 10 ml/min and a heating rate of 10 K/min.

9.1.4 Imaging Techniques

9.1.4.1 Polarized Optical Microscopy (POM)

POM was performed using a Leica MZ8 optical microscope equipped with a Leica KL1500 light source, polarization filters and a Mettler Toledo FP52 microscope heating stage. Micrographs were obtained at 50 fold magnification using a QImaging micropublisher 5.0 RTV CCD camera and QCapture Pro 6.0 imaging software. Samples were prepared by placing the material between two glass plates, annealing above the corresponding melting temperature for 10 min and instantaneously cooling the isotropic melt to room temperature.

9.1.4.2 Scanning Electron Microscopy (SEM)

SEM was performed using two different microscopes. The as-deposited and heat-treated samples were investigated using a JSM-7500F microscope (JEOL Ltd.) with imaging EDX from Oxford, whereas the plasma treated samples were analyzed using a Quanta 3D FIB SEM (FEI Comp.).

9.1.4.3 Transmission Electron Microscopy (TEM)

TEM was performed using two different microscopes. The Pd-nanoparticles from qualitative analysis of polysilanes were investigated using a JEM-100CX microscope (JEOL Ltd.) with W-cathode and 100 kV acceleration voltage, whereas the crosslinked polysilane particles were analyzed with a JEM-2200FS microscope (JEOL Ltd.) equipped with a FE Schottky cathode with 200 kV acceleration voltage and imaging EDX from Oxford.

9.1.4.4 Atomic Force Microscopy (AFM)

AFM experiments on most samples were carried out on a commercial atomic force microscope (Nanoscope IIIa from Veeco Instruments) using Veeco RTESP tips (p-doped Si; spring constant, 20-80 N/m; radius of curvature, 10 nm) The topography images were acquired using a 50×50 μm^2 scanner in tapping mode under ambient conditions.

AFM experiments on plasma treated samples were carried out on a commercial atomic force microscope (NT-MDT, Smena head; Solver Instruments, Moscow, Russia). P-doped Si AFM cantilevers (radius of curvature, 30 nm; spring constant, 0.58 Nm) were provided by NanoAndMore (Lady's Island, SC). The topography images were acquired using a 50×50 μm^2 scanner in tapping mode under ambient conditions.

9.1.5 Structure Analysis

9.1.5.1 Ellipsometry

The film thicknesses of polysilane films before and after plasma treatment were measured using a variable angle, single-wave imaging ellipsometer (EP^3; Nanofilm Surface Analysis GmbH; Germany). The measurements were performed in air at room temperature for different angles of incidence (80 measurements between 40 and 80 °). The light source was a low-capacity laser with a wavelength of 532 nm. A conventional PCSA (polarizer-compensator-sample-analyzer) null-ellipsometric procedure was used to obtain the Δ and Ψ angles. The thickness and the refractive index were calculated with the help of a mathematical model, which is included in the analytical software EP^3 View (provided with the instrument), from the acquired values for Δ and Ψ. For modelling of the polysilane layer thicknesses a three-layer system consisting of Ge, GeO and polysilane was assumed.

9.1.5.2 White-Light Interferometry

The film thicknesses and roughnesses of siloxane multimesogens were measured using a white-light interferometer F20 (Filmetrics Inc. San Diego). A single-layer model including a surface roughness was used to fit the reflectivity curves and thus to determine the film thickness and the surface roughness. The values are given in *table 2*. The roughness value is averaged over the size of the beam spot (of the order of 1 mm^2).

9.1.5.3 Small-Angle X-Ray Scattering (SAXS)

SAXS experiments were carried out at beamline A2 at HASYLAB at DESY in Hamburg, Germany. An X-ray beam with a wavelength λ = 1.50 Å was used. A MarCCD camera with a pixel size of 158 µm × 158 µm was mounted in 1.04 m or 1.32 m distance from the sample as a detector. A piece of lead was used as a beamstop. The samples were mounted in glass capillaries of diameter 2 mm. Measuring times were between 20 and 600 s. Measurements were carried out at room temperature. The 2D data were azimuthally averaged. The transmission-corrected scattering of the capillary was subtracted from the data. The calibration of the detector and the determination of the position of the direct beam were carried out using silver behenate.

9.1.5.4 Grazing Incidence Small-Angle Scattering (GISAXS)

GISAXS experiments were carried out at beamline BW4 at HASYLAB/DESY.[156] The wavelength λ was 1.381 Å. The beam was ~20 µm high and 40 µm wide; the projection on the sample under the grazing angle is thus shorter than 1 cm. A MarCCD camera with a pixel size of 79.5 µm × 79.5 µm was used as a detector with a sample-detector distance of 1.9 m. $q_{||} = \sqrt{q_x^2 + q_y^2}$ and q_z are the in-plane and the normal components of the scattering vector, $\vec{q}$, respectively. For small incidence and scattering angles, the coordinates of the 2D detector correspond approximately to q_y and to q_z, and we use this

notation in the remainder of the paper. A tantalum rod (diameter 1 mm) was placed vertically in front of the CCD camera to screen it from the reflected beam as well as the intense diffuse scattering at small q_y. The specularly reflected beam was additionally masked by a round beamstop.

In the GISAXS geometry, kinetic scattering effects have to be taken into account which is done here in the framework of the distorted-wave Born approximation (DWBA). For a layered structure, DWBA predicts diffuse Bragg sheets (DBSs) at q_z values[157]

$$q_z = k_{iz} + \sqrt{k_c^2 + \left[\frac{2\pi m}{D} \pm \sqrt{k_{iz}^2 - k_c^2}\right]^2} \qquad (1)$$

where $k_{iz}=k_0\sin\alpha_i$ and $k_c= k_0\sin\alpha_c$ with $k_0=2\pi/\lambda$. α_i is the incidence angle of the X-ray beam with respect to the film surface. α_c is the critical angle of total external reflection of the thin film, which is related to the electron density by $\alpha_c = \lambda\sqrt{r_e\rho/\pi}$ where ρ is the electron density of the thin film and $r_e = 2.814\times10^{-5}$ Å the Thomson electron radius. D is the layer thickness and m the order of the reflection. For each value of m, two DBSs denoted 'minus branch (M)' and 'plus branch (P)', are expected, which correspond to scattering of the direct beam (M) and of the beam reflected from the substrate (P), respectively.[157] For a precise determination of the layer thickness, we carried out GISAXS measurements at several incidence angles α_i between 0.13 and 0.26°, thus allowing fitting of Eq. 1 in a range of k_{iz} values. To determine the q_z positions and the widths of the peaks of the DBSs along q_z, intensity profiles along q_z were created by averaging over the range -0.005 Å^{-1} < q_y < 0.005 Å^{-1}. These profiles were found to be fitted well by the following function:

$$I(q_z) = I_0 + c\times q_z + \frac{A_{M1}}{w_{z,M1}\sqrt{\pi/2}}\times\exp\left[-2\frac{(q_z - q^*_{z,M1})^2}{w^2_{z,M1}}\right] + \frac{A_{P1}}{w_{z,P1}\sqrt{\pi/2}}\times\exp\left[-2\frac{(q_z - q^*_{z,P1})^2}{w^2_{z,P1}}\right] \qquad (2)$$

where I_0 is the background, c the slope of the background in the peak region, A_{M1}, A_{P1}, $w_{z,M1}$, $w_{z,P1}$, $q_{z,M1}$ and $q_{z,P1}$ the areas, the widths along q_z and the q_z positions of the two

DBSs (*M1* and *P1*). The domain size along the film normal, D_{domain}, was estimated from $w_{z,M1}$ using the Scherrer formula

$$D_{domain} = \frac{2\pi K}{w_{z,M1}\sqrt{2\ln(2)}} \quad (3)$$

with K = 0.93. Resolution effects[158] can be neglected compared to the peak widths because of the small bandwidth of the beam, its low divergence and the small beam footprint.

Intensity profiles along q_y were created by averaging over a q_z range 0.14 Å^{-1} < q_z < 0.16 Å^{-1} for **28 b** and 0.125 Å^{-1} < q_z < 0.145 Å^{-1} for **18 b**, i.e. around the DBS *M1*. These profiles could be fitted with a Lorentzian:

$$I(q_y) = I_0 + \frac{2A}{\pi} \times \frac{w_{y,M1}}{4q_y^2 + w_{y,M1}^2} \quad (4)$$

where I_0 is the background, A the area and $w_{y,M1}$ the width along q_y. From $w_{y,M1}$, the lateral cut-off length of correlations of the layer interfaces, Λ, was estimated using the relation $\Lambda = 2\pi/w_{y,M1}$.[159] The cut-off length is the lateral distance over which the correlation between interfaces is lost. Thus, the wider the DBS along q_y, the lower is the cut-off length, i.e. the smaller the distance over which correlation is lost.

9.1.5.5 X-Ray Photoelectron Spectroscopy (XPS)

For XPS analysis, samples were mounted on a stainless steel bar sample holder using ultrahigh-vacuum- (UHV-) compatible, Si-free carbon double-side adhesive tape. The measurements in this study were performed on an AXISULTRA spectrometer (Kratos Analytical, Manchester, U.K.) equipped with a monochromatic Al Kα (*hv*=1486.6 eV) X-ray source. Measurements were carried out at a takeoff angle (TOA) of 90° with

respect to the sample surface, and the area of analysis was 400×700 μm^2. The base pressure of the instrument was less than 8×10^{-10} Torr, and the operating pressure was below 3×10^{-9} Torr. For each sample, a survey spectrum (0-1150 eV), from which the surface chemical compositions (at. %) were determined, was recorded at a pass energy (PE) of 160 eV. In addition, high-resolution detail spectra (PE=20 eV) were also recorded on each sample. A magnetic immersion lens system (I_{fil}=1.9 A, balance=3.6 V, bias=1.3V) was used for charge neutralization, and all spectra were corrected by setting the C 1s peak of hydrocarbon to 285.00 eV. The total acquisition time was kept below 20 min to avoid any possible contamination and/or X-ray-induced damage. To ensure the reproducibility of the measurements, spectra were obtained from at least two different positions on each sample. The data were processed using Vision2 software (Kratos Analytical, Manchester, U.K.) and CasaXPS v2.3.10 (Casa Software, Cheshire, U.K.). After linear background subtraction, sample compositions were obtained from the survey spectra using the relative sensitivity factors (RSFs) included in the software, which were derived from Scofield cross sections. This method is estimated to give an accuracy of 10% in the measurement of elemental compositions. Curve fitting of Si_{2p} peaks was carried out using the same initial parameters and interpeak constraints to reduce scattering. The Si_{2p} envelope was fitted with Gaussian-Lorentzian functions (G/L=30) and a variable full width at half-maximum (fwhm).

9.2 Syntheses

9.2.1 Reagents and Methods

All reactions were performed under an atmosphere of argon using either standard *Schlenk* techniques, or a glovebox from MBraun operating at 1ppm oxygen and water. All chemicals were purchased from Sigma-Aldrich, ABCR, or Acros Organics and used as received unless differently noted. Dry solvents were obtained by filtering with a solvent purification system (MB SPS-800, MBraun). All glassware was heat dried under vacuum prior to use. Unless described differently, the workup was performed as follows; aqueous phases were extracted with suitable organic solvents (ethyl acetate, DCM or diethyl ether) and the organic phases were subsequently washed with water and dried using anhydrous Na_2SO_4 prior to evaporation using a rotatory evaporator or the ultra high vacuum line.

Flash chromatography was performed using an Analogix Flash Chromatography System from Varian equipped with silica gel columns with a particle size of 0.035-0.050 mm under variable wavelength UV-detection and application of appropriate solvent gradients. ^{1}H, ^{13}C and ^{29}Si NMR spectra were recorded on a Bruker ARX 300 spectrometer at ambient temperature. The spectra (^{1}H and ^{13}C) were referenced to the residual solvent signals of the deuterated solvents (Deutero); chemical shifts are reported in δ (ppm). Elemental analysis (EA) was performed at the Microanalytic Laboratory, Institute of Inorganic Chemistry, Technsche Universität München.

9.2.2 Compounds of the Mesogen Library

9.2.2.1 Sonogashira Route to Mono- and Trialkoxy Substituted Phenylacetylene Mesogens

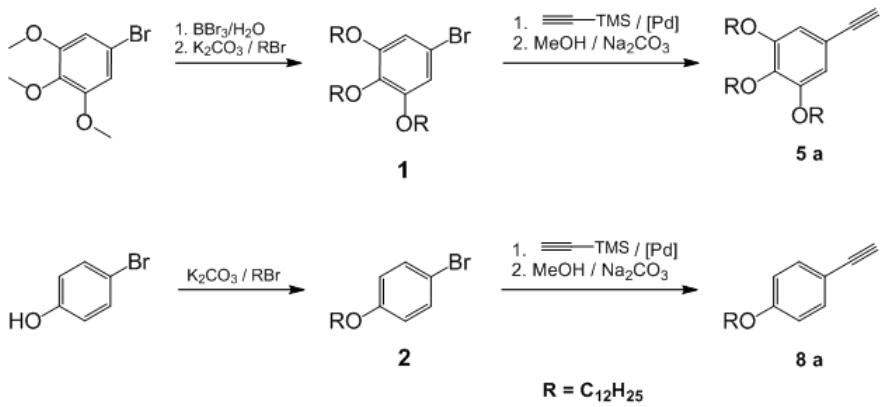

Scheme 9.1 *Synthesis scheme of the Sonogashira route.*

Synthesis of 3,4,5-Tridodecyloxy Phenylbromide 1:

Compound **1** was synthesized in a two-step reaction starting from 3,4,5-trimethoxy phenylbromide and consisting of methyl ether cleavage followed by a reetherification with a long chain alkylbromide. In the first step 50 mmol of (3,4,5)trimethoxy phenyl bromide were reacted with 150 mL of a 1M solution of BBr_3 in dry DCM at -78 °C. After 72 h the reaction was quenched with ice-water and the product was obtained by evaporating the solvent from the separated organic phase (yield: 8.1 g (78%), no analytics). The second step was a *Williams* etherification of 40 mmol of crude 3,4,5-trihydroxy phenylbromide with each 3.2 eq. dodecylbromide and K_2CO_3 in boiling cyclohexanone. The crude product was obtained after quenching with water and evaporation of the solvent from the separated organic phase. The crude product was purified by flash chromatography.

Yield: 21.8 g (77%); after flash chromatography (hexane/DCM, gradient).

^{1}H NMR ($CDCl_3$, 300.13 MHz): δ = 0.88 (t, 9H, 3J = 6.75 Hz, CH_2-**CH_3**), 1.20 – 1.60 (m, 54H, CH_3-**CH_2-CH_2**), 1.60-1.90 (m, 6H, O-CH_2-**CH_2**), 3.92 (m, 6H, O-**CH_2**), 6.67 (s, 2H, **Ph-H**).

^{13}C NMR ($CDCl_3$, 75.47 MHz): δ = 14.1, 22.7, 26.0, 26.1, 29.2, 29.4, 29.6, 29.7, 30.2, 31.9, 69.2, 73.4, 110.0, 115.5, 137.3, 153.8.

Synthesis of Dodecyloxy Phenylbromide 2:

Compound **2** was synthesized in a *Williams* etherification of 50 mmol of commercially available 4-bromophenol with 1.2 eq. dodecylbromide and 1.5 eq. K_2CO_3 in boiling ethanol. The crude product was obtained after quenching with water, extracting with ethyl acetate and evaporation of the organic phase. Purification was performed by recrystallization from ethanol.

Yield: 15.8 g (93%); after recrystallization from EtOH.

^{1}H NMR ($CDCl_3$, 300.13 MHz): δ = 0.88 (t, 3H, 3J = 6.75 Hz, CH_2-**CH_3**), 1.20 – 1.50 (m, 18H, CH_3-**CH_2-CH_2**), 1.76 (m, 2H, O-CH_2-**CH_2**), 3.91 (t, 2H, 3J = 6.60 Hz, O-**CH_2**), 6.77 (d, 2H, 3J = 9.00 Hz, **Ph-H**), 7.36 (d, 2H, 3J = 9,00 Hz, **Ph-H**).

Sonogashira Cross Coupling Reaction to 3,4,5-Tridodecyloxy Phenylacetylene 5 a:

Compound **5 a** was synthesized using a *Sonogashira* cross coupling reaction of 17 mmol of the trialkoxy substituted phenylbromide **1** and 1.1 eq. of trimethylsilyl-protected acetylene in 60 mL piperidine as solvent and base component. Furthermore 0.02 eq. of tetrakis triphenylphosphane palladium (I) and 0.05 eq. of CuI were used as catalyst and cocatalyst, respectively. The reaction proceeded after mixing of the

reactants and catalysts under *Schlenk* and reflux conditions over night and was subsequently quenched with aqueous NH_4Cl solution. The product was extracted with diethylether and used after evaporation of the solvent without further purification. In a second step the protected acetylene was deprotected by stirring it with a suspension of K_2CO_3 and methanol in DCM for 16 h.

Yield: 9.4 g (86%); after flash chromatography (hexane/DCM, gradient).

^{1}H NMR ($CDCl_3$, 300.13 MHz): δ = 0.88 (t, 9H, 3J = 6.75 Hz, CH_2-**CH_3**), 1.20 - 1.60 (m, 54H, CH_3-**CH_2-CH_2**), 1.60 - 1.90 (m, 6H, O-CH_2-**CH_2**), 2.99 (s, 1H, C**C-H**), 3.94 (m, 6H, O-**CH_2**), 6.69 (s, 2H, **Ph-H**).

^{13}C NMR ($CDCl_3$, 75.47 MHz): δ = 14.1, 22.7, 26.0, 26.1, 29.3, 29.4, 29.6, 29.7, 29.8, 30.3, 31.9, 69.1, 73.5, 75.7, 84.0, 110.5, 116.3, 139.4, 152.9.

Sonogashira Cross Coupling Reaction to 4-Dodecyloxy Phenylacetylene 8 a:

Synthesis of compound **8 a** was performed according to the synthesis procedure of compound **5 a**, which is described above.

Yield: 2.32 g (38%); after flash chromatography (hexane/DCM, gradient).

^{1}H NMR ($CDCl_3$, 300.13 MHz): δ = 0.88 (t, 3 H, 3J = 6.75 Hz, CH_2-**CH_3**), 1.20 – 1.50 (m, 18 H, CH_3-**CH_2-**CH_2), 1.70 – 1.83 (m, 2 H, O-CH_2-**CH_2**), 2.99 (s, 1 H, C**C-H**), 3.95 (t, 2 H, 3J = 6.60 Hz, O-**CH_2**), 6.83 (d, 2 H, 3J = 8.90 Hz, **Ph-H**), 7.41 (d, 2 H, 3J = 8,90 Hz, **Ph-H**).

^{13}C NMR ($CDCl_3$, 75.47 MHz): δ = 14.1, 22.7, 26.0, 29.1, 29.3, 29.4, 29.5, 29.6, 29.7, 31.9, 68.0, 75.6, 83.8, 113.8, 114.4, 133.5, 159.5.

9.2.2.2 Wittig and Corey-Fuchs Route to Trialkoxy-Substituted Styrene and Phenylacetylene Mesogens

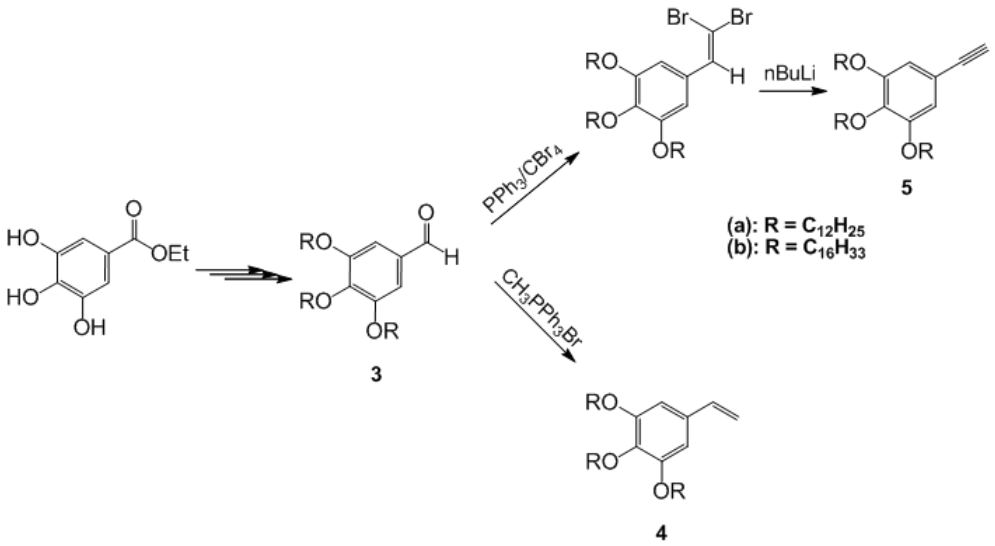

Scheme 9.2 *Synthesis scheme of the Corey-Fuchs route.*

Synthesis of Benzaldehydes 3 (a, b):

The compounds **3** were synthesized in three-step reactions starting from commercially available gallic acid ethyl ester. The first step was a *Williams* etherification of 50 mmol of gallic acid ethyl ester, using 3.2 eq K_2CO_3 and 3.1 eq of the corresponding bromo alkane and refluxing the mixture in cyclohexanone over night to give the trialkoxy-substituted compounds. The second step was a reduction of 20 mmol ethyl trialkoxy benzoate, to the corresponding benzyl alcohols with 0.75 eq $LiAlH_4$ in dry THF. The third step was a selective oxidation of 15 mmol of the alcohols to the corresponding benzaldehydes **3** with 2 eq 2-iodoxy benzoic acid (IBX) (which was freshly prepared from 2-iodo benzoic acid and $KHSO_5$*$KHSO_4$*K_2SO_4 (Oxone®)) in THF. Each reaction gave yields between 89 and 96% and the products could be isolated in good purities after recrystallization from appropriate solvents.

Ethyl-3,4,5-tridodecyloxy benzoate:

Yield: 34.5 g (96%); after recrystallization from EtOH.

^{1}H NMR ($CDCl_3$, 300.13 MHz): δ = 0.88 (t, 9 H, 3J = 6.60 Hz, CH_2-**CH_3**), 1.20 – 1.50 (m, 54 H, CH_3-**CH_2-CH_2**), 1.38 (t, 3 H, 3J = 7.13, COO-CH_2-**CH_3**), 1.60-1.90 (m, 6 H, O-CH_2-**CH_2**), 4.07 (t, 6 H, 3J = 6.53, O-**CH_2**), 4.35 (q, 2 H, 3J = 7.13, COO-**CH_2**-CH_3), 7.25 (s, 2 H, **Ph-H**).

^{13}C NMR ($CDCl_3$, 75.47 MHz): δ = 10.5, 14.1, 22.7, 26.1, 29.3, 29.5, 29.6, 29.7, 29.8, 31.9, 66.5, 69.1, 73.4, 107.9, 125.0, 142.2, 152.7, 166.5.

Ethyl-3,4,5-trihexadecyloxy benzoate:

Yield: 38.8 g (89%); after recrystallization from EtOH.

^{1}H NMR ($CDCl_3$, 300.13 MHz): δ = 0.88 (t, 9 H, 3J = 6.60 Hz, CH_2-**CH_3**), 1.20 – 1.50 (m, 78 H, CH_3-**CH_2-CH_2**), 1.38 (t, 3 H, 3J = 7.13, COO-CH_2-**CH_3**), 1.60-1.90 (m, 6 H, O-CH_2-**CH_2**), 4.07 (t, 6 H, 3J = 6.53, O-**CH_2**), 4.35 (q, 2 H, 3J = 7.13, COO-**CH_2**-CH_3), 7.25 (s, 2 H, **Ph-H**).

^{13}C NMR ($CDCl_3$, 75.47 MHz): δ = 10.5, 14.1, 22.7, 26.1, 29.2, 29.3, 29.4, 29.5, 29.6, 29.7, 29.8, 30.1, 30.2, 31.9, 66.5, 69.1, 73.4, 107.9, 125.0, 142.2, 152.7, 166.5.

3,4,5-Tridodecyloxy benzyl alcohol:

Yield: 12.9 g (98%); after recrystallization from EtOAc.

^{1}H NMR ($CDCl_3$, 300.13 MHz): δ = 0.88 (t, 9 H, 3J = 6.60 Hz, CH_2-**CH_3**), 1.20 – 1.50 (m, 54 H, CH_3-**CH_2-CH_2**), 1.60-1.90 (m, 6 H, O-CH_2-**CH_2**), 3.97 (t, 6 H, 3J = 6.53, O-**CH_2**), 4.59 (s, 2 H, **CH_2**-OH), 6.56 (s, 2 H, **Ph-H**).

^{13}C NMR ($CDCl_3$, 75.47 MHz): δ = 14.1, 22.7, 26.1, 29.3, 29.5, 29.6, 29.7, 29.8, 31.9, 65.7, 69.1, 73.4, 105.2, 135.9, 137.5, 153.2.

3,4,5-Trihexadecyloxy benzyl alcohol:

Yield: 16.0 g (96%); after recrystallization from EtOAc.

^{1}H NMR ($CDCl_3$, 300.13 MHz): δ = 0.88 (t, 9 H, 3J = 6.60 Hz, CH_2-**CH_3**), 1.20 – 1.50 (m, 78 H, CH_3-**CH_2-CH_2**), 1.60-1.90 (m, 6 H, O-CH_2-**CH_2**), 3.97 (t, 6 H, 3J = 6.53, O-**CH_2**), 4.59 (s, 2 H, **CH_2**-OH), 6.56 (s, 2 H, **Ph-H**).
^{13}C NMR ($CDCl_3$, 75.47 MHz): δ = 14.1, 22.7, 26.1, 29.2, 29.3, 29.4, 29.5, 29.6, 29.7, 29.8, 30.1, 30.2, 31.9, 65.7, 69.1, 73.4, 105.2, 135.9, 137.5, 153.2.

3,4,5-Tridodecyloxy benzaldehyde (3 a):

Yield: 9.3 g (94%); without purification.

^{1}H NMR ($CDCl_3$, 300.13 MHz): δ = 0.88 (t, 9 H, 3J = 6.60 Hz, CH_2-**CH_3**), 1.20 – 1.50 (m, 54 H, CH_3-**CH_2-CH_2**), 1.60-1.90 (m, 6 H, O-CH_2-**CH_2**), 4.03 (t, 6 H, 3J = 6.53, O-**CH_2**), 7.08 (s, 2 H, **Ph-H**), 9.83 (s, 1 H, O=C-**H**).

^{13}C NMR ($CDCl_3$, 75.47 MHz): δ = 14.1, 22.7, 26.1, 28.9, 29.5, 29.6, 29.7, 29.8, 32.1, 69.3, 73.4, 107.9, 131.5, 143.9, 153.6, 191.5.

3,4,5-Trihexadecyloxy benzaldehyde (3 b):

Yield: 11.2 g (90%); without purification.

^{1}H NMR ($CDCl_3$, 300.13 MHz): δ = 0.88 (t, 9 H, 3J = 6.60 Hz, CH_2-**CH_3**), 1.20 – 1.50 (m, 78 H, CH_3-**CH_2-CH_2**), 1.60-1.90 (m, 6 H, O-CH_2-**CH_2**), 4.03 (t, 6 H, 3J = 6.53, O-**CH_2**), 7.08 (s, 2 H, **Ph-H**), 9.83 (s, 1 H, O=C-**H**).

^{13}C NMR ($CDCl_3$, 75.47 MHz): δ = 14.1, 22.7, 26.1, 28.3, 28.9, 29.3, 29.4, 29.5, 29.6, 29.7, 29.8, 31.9, 32.1, 69.3, 73.4, 107.9, 131.5, 143.9, 153.6, 191.5.

Wittig Reaction to Styrene Mesogens 4 (a, b):

The styrene derivatives **4** were synthesized in a *Wittig* reaction from the trialkoxy substituted benzaldehydes **3**. Each 21.3 mmol methyl triphenyl phosphonium bromide and K*t*BuOH were dissolved in THF, before a solution of 15.2 mmol **3** in THF was added. The reactions were quenched with methanol and the solvents were evaporated after 16 h. Subsequently the products were extracted from the residual with diethylether. After evaporation of the ether, the crude products were purified using flash chromatography.

3,4,5-Tridodecyloxy Styrene (4a):

Yield: 8.02 g (80%); after flash chromatography (hexane/DCM, gradient).

^{1}H NMR ($CDCl_3$, 300.13 MHz): δ = 0.88 (t, 9H, 3J = 6.60 Hz, CH_2-**CH_3**), 1.20 - 1.50 (m, 54H, CH_3-**CH_2-CH_2**), 1.60-1.90 (m, 6H, O-CH_2-**CH_2**), 3.95-4.20 (m, 6H, O-**CH_2**), 5.17 (dd, 1H, 2J = 0,80 Hz, 3J = 10.8 Hz, CH=C**H_2**), 5.62 (dd, 1H, 2J = 0,80 Hz, 3J = 17.5 Hz, CH=C**H_2**), 6.60 (m, 3H, **Ph-H**, C**H**=CH_2).

^{13}C NMR ($CDCl_3$, 75.47 MHz): δ = 14.1, 22.7, 26.1, 29.4, 29.6, 29.7, 29.8, 30.3, 31.9, 69.1, 73.5, 104.8, 112.7, 132.7, 136.9, 138.3, 153.2.

3,4,5-Trihexadecyloxy Styrene (4b):

Yield: 7,5 g (70%); after flash chromatography (hexane/DCM, gradient).

^{1}H NMR ($CDCl_3$, 300.13 MHz): δ = 0.88 (t, 9H, 3J = 6.6 Hz, CH_2-**CH_3**), 1.20 - 1,50 (m, 78H, CH_3-**CH_2-CH_2**), 1.60 - 1.90 (m, 6H, O-CH_2-**CH_2**), 3.9 - 4.0 (m, 6H, O-**CH_2**), 5.15 (d, 2H, 3J = 11,3 Hz, CH=C**H_2**), 5.60 (dd, 1H, 3J = 17,5 Hz, 2J = 0,6 Hz, CH=C**H_2**), 6.58 (s, 2H, **Ph-H**)

Corey-Fuchs Reaction to Phenylacetylenes 5 (a, b):

The phenylacetylene-mesogens **5** were synthesized according to a modified *Corey-Fuchs*-reaction.[160] This reaction consisted of two steps. In the first step 10 mmol CBr_4 were dissolved in a *Schlenk* flask in 50 ml dry DCM and cooled to 0 °C on an ice bath. 20 mmol of PPh_3 in 100 ml DCM were added dropwise during 20 min. To the resulting yellow solution, 5 mmol of the corresponding benzaldehyde **3** dissolved in 50 ml DCM were added dropwise during 5 min. The resulting mixture was stirred for 3 h at 0 °C and for another 3 h at room temperature. To precipitate the formed phospine oxide, 250 ml of pentane were added and the resulting suspension was filtered through a pad of celite. The solvent of the filtrate was removed by vacuum distillation and the crude intermediate products were purified by flash chromatography with a gradient of DCM in hexane.

The phenylacetylenes were synthesized in a second step. Solutions of 3 mmol of the intermediate products in 20 ml dry THF were cooled to -78 °C with a mixture of dry ice in acetone. Subsequently, 7 mmol n-butyl lithium (1.6 M in hexane) were added dropwise and the reaction mixture was stirred for 1 h at -78 °C. The reaction was

warmed to room temperature and subsequently quenched with 50 ml of 2M aqueous NH_4Cl solution. The organic layer was separated, washed with water and concentrated in vacuum. The products were used for further reactions without purification.

1-(2,2 Dibromo vinyl)-3,4,5-tridodecyloxy benzene:

Yield: 3.5 g; (86%); after flash chromatography (hexane/DCM gradient)

^{1}H NMR ($CDCl_3$, 300.13 MHz): δ = 0.88 (t, 9 H, 3J = 6.60 Hz, CH_2-**CH_3**), 1.20 – 1.50 (m, 54 H, CH_3-**CH_2**-CH_2), 1.60-1.90 (m, 6 H, O-CH_2-**CH_2**), 3.96 (m, 6 H, O-**CH_2**), 6.77 (s, 2 H, **Ph-H**), 7.37 (s, 1 H, CBr_2=**CH**);

^{13}C NMR ($CDCl_3$, 75.47 MHz): δ = 14.1, 22.7, 26.1, 29.3, 29.4, 29.6, 29.7, 29.8, 30.3, 31.9, 69.1, 73.4, 88.0, 107.1, 130.0, 136.8, 138.6, 152.8.

1-(2,2 Dibromo vinyl)-3,4,5-trihexadecyloxy benzene:

Yield: 3.9 g (79%); after flash chromatography (Hexane/DCM gradient).

^{1}H NMR ($CDCl_3$, 300.13 MHz): δ = 0.88 (t, 9 H, 3J = 6.60 Hz, CH_2-**CH_3**), 1.20 – 1.50 (m, 78 H, CH_3-**CH_2**-CH_2), 1.60-1.90 (m, 6 H, O-CH_2-**CH_2**), 3.96 (m, 6 H, O-**CH_2**), 6.77 (s, 2 H, **Ph-H**), 7.37 (s, 1 H, CBr_2=**CH**);

^{13}C NMR ($CDCl_3$, 75.47 MHz): δ = 14.1, 22.7, 26.1, 28.3, 28.9, 29.3, 29.4, 29.5, 29.6, 29.7, 29.8, 31.9, 32.1, 69.1, 73.4, 88.0, 107.1, 130.0, 136.8, 138.6, 152.8.

3,4,5-Tridodecyloxy phenyl acetylene (5 a):

Yield: 1.92 g (98%); without purification.

^{1}H NMR ($CDCl_3$, 300.13 MHz): δ = 0.88 (t, 9 H, 3J = 6.75 Hz, CH_2-**CH_3**), 1.20 – 1.60 (m, 54 H, CH_3-**CH_2**-CH_2), 1.60-1.90 (m, 6 H, O-CH_2-**CH_2**), 2.99 (s, 1 H, C**C-H**), 3.94 (m, 6 H, O-**CH_2**), 6.69 (s, 2 H, **Ph-H**);

^{13}C NMR ($CDCl_3$, 75.47 MHz): δ = 14.1, 22.7, 26.0, 26.1, 29.3, 29.4, 29.6, 29.7, 29.8, 30.3, 31.9, 69.1, 73.5, 75.7, 84.0, 110.5, 116.3, 139.4, 152.9.

3,4,5-Trihexadecyloxy phenyl acetylene (5 b):

Yield: 2.45 g (99%); without purification

^{1}H NMR ($CDCl_3$, 300.13 MHz); δ = 0.88 (t, 9 H, 3J = 6.75 Hz, CH_2-**CH_3**), 1.20 – 1.60 (m, 78 H, CH_3-**CH_2**-CH_2), 1.60-1.90 (m, 6 H, O-CH_2-**CH_2**), 2.99 (s, 1 H, C**C-H**), 3.94 (m, 6 H, O-**CH_2**), 6.69 (s, 2 H, **Ph-H**);

^{13}C NMR ($CDCl_3$, 75.47 MHz): δ = 14.1, 22.7, 26.1, 28.3, 28.9, 29.3, 29.4, 29.5, 29.6, 29.7, 29.8, 31.9, 32.1, 69.1, 73.5, 75.7, 84.0, 110.5, 116.3, 139.4, 152.9.

9.2.2.3 Wittig and Corey-Fuchs Route to Monoalkoxy-Substituted Styrene and Phenylacetylene Mesogens

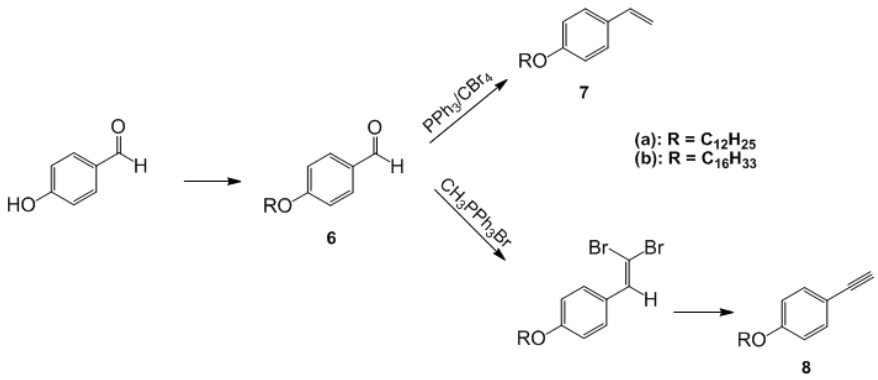

Scheme 9.3 *Synthesis scheme of the Corey-Fuchs route.*

Synthesis of Benzaldehydes 6 (a, b):

50 mmol of 4-hydroxy benzaldehyde were converted in a *Williams* etherification with each 1.1 eq of K_2CO_3 and the corresponding bromo alkanes to get compound **6**. The reaction was performed in boiling ethanol over night. The crude product was purified by recrystallization from ethanol.

4-Dodecyloxy benzaldehyde (6 a):

Yield: 14.92 g (97%); after recrystallization from ethanol.

^{1}H NMR ($CDCl_3$, 300.13 MHz): δ = 0.88 (t, 3 H, 3J = 6.60 Hz, CH_2-**CH_3**), 1.20-1.50 (m, 18 H, CH_3-**CH_2-CH_2**), 1.60-1.90 (m, 2 H, O-CH_2-**CH_2**), 4.03 (t, 2 H, 3J = 6.53, O-**CH_2**), 6.99 (d, 2 H, 3J = 8.70 Hz, **Ph-H**), 7.82 (d, 2 H, 3J = 8.70 Hz, **Ph-H**), 9.88 (s, 1 H, O=C-**H**).

^{13}C NMR ($CDCl_3$, 75.47 MHz): δ = 14.1, 22.7, 26.1, 28.9, 29.5, 29.6, 29.7, 29.8, 32.1, 68.4, 114.7, 129.7, 132.0, 164.3, 190.9.

4-Hexadecyloxy benzaldehyde (6 b):

Yield: 16.87 g (97%); after recrystallization from ethanol.

^{1}H NMR ($CDCl_3$, 300.13 MHz): δ = 0.88 (t, 3 H, 3J = 6.60 Hz, CH_2-**CH_3**), 1.20 – 1.50 (m, 26 H, CH_3-**CH_2-CH_2**), 1.60-1.90 (m, 2 H, O-CH_2-**CH_2**), 4.03 (t, 2 H, 3J = 6.53, O-**CH_2**), 6.99 (d, 2 H, 3J = 8.70 Hz, **Ph-H**), 7.82 (d, 2 H, 3J = 8.70 Hz, **Ph-H**), 9.88 (s, 1 H, O=C-**H**).

^{13}C NMR ($CDCl_3$, 75.47 MHz): δ = 14.1, 22.7, 26.1, 28.9, 29.3, 29.4, 29.5, 29.6, 29.7, 29.8, 30.2, 31.1, 32.1, 68.4, 114.7, 129.7, 132.0, 164.3, 190.9.

Wittig Reaction to Styrene Mesogens 7 (a, b):

The styrene derivatives **7** were synthesized from the benzaldehydes **6** according to the synthesis procedure for styrene derivatives **4**, which is described above.

4-Dodecyloxy Styrene (7 a):

Yield: 2.38 g (56%); after flash chromatography (hexane/DCM, gradient).

^{1}H NMR ($CDCl_3$, 300.13 MHz): δ = 0.88 (t, 3H, 3J = 6.60 Hz, CH_2-**CH_3**), 1.20 - 1.50 (m, 18H, CH_3-**CH_2-CH_2**), 1.60-1.90 (m, 2H, O-CH_2-**CH_2**), 3.95 (t, 2H, 3J = 6.60 Hz, O-**CH_2**), 5.11 (dd, 1H, 2J = 0.90 Hz, 3J = 10.90 Hz, CH=**CH_2**), 5.60 (dd, 1H, 2J = 0.90 Hz, 3J = 17.60 Hz, CH=**CH_2**), 6.66 (dd, 1H, 3J = 10.90 Hz, 3J = 17.60 Hz, **CH**=CH_2), 6.85 (d, 2H, 3J = 8.70 Hz, **Ph-H**), 7.34 (d, 2H, 3J = 8.70 Hz, **Ph-H**).

^{13}C NMR ($CDCl_3$, 75.47 MHz): δ = 14.1, 22.7, 26.0, 29.3, 29.4, 29.6, 29.7, 31.9, 68.0, 111.4, 114.4, 127.3, 130.2, 136.2, 158.9.

4-Hexadecyloxy Styrene (7 b):

Yield: 12,3 g (99%); after flash chromatography (hexane/DCM, gradient).

^{1}H NMR ($CDCl_3$, 300.13 MHz): δ = 0.88 (t, 3H, 3J = 6.60 Hz, CH_2-**CH_3**), 1.20 - 1.50 (m, 26H, CH_3-**CH_2-CH_2**), 1.78 (m, 2H, O-CH_2-**CH_2**), 3.95 (t, 2H, 3J = 6.60 Hz, O-**CH_2**), 5.11 (dd, 1H, 2J = 0.90 Hz, 3J = 10.90 Hz, CH=**CH_2**), 5.60 (dd, 1H, 2J = 0.90 Hz, 3J = 17.60 Hz, CH=**CH_2**), 6.66 (dd, 1H, 3J = 10.90 Hz, 3J = 17.60 Hz, , **CH**=CH_2), 6.85 (d, 2H, 3J = 8.70 Hz, **Ph-H**), 7.34 (d, 2H, 3J = 8.70 Hz, **Ph-H**).

Corey-Fuchs Reaction to Phenylacetylenes 8 (a, b):

The phenylacetylene derivatives **8** were synthesized according to the procedure for phenylacetylene derivatives **5**, which is described above.

1-(2,2 Dibromo vinyl)-4-dodecyloxy benzene:

Yield: 1.98 g (89%); after flash chromatography (hexane/DCM, gradient)

^{1}H NMR ($CDCl_3$, 300.13 MHz): δ = 0.88 (t, 3 H, 3J = 6.60 Hz, CH_2-**CH_3**), 1.20 - 1.50 (m, 18 H, CH_3-**CH_2**-CH_2), 1.60 - 1.90 (m, 2 H, O-CH_2-**CH_2**), 3.96 (m, 2 H, O-**CH_2**), 6.88 (d, 2 H, 3J = 8.75 Hz, **Ph-H**), 7.40 (s, 1 H, CBr_2=**CH**), 7.50 (d, 2 H, 3J = 8.75 Hz, **Ph-H**).

^{13}C NMR ($CDCl_3$, 75.47 MHz): δ = 14.1, 22.7, 26.1, 29.1, 29.3, 29.4, 29.5, 29.6, 29.7, 31.9, 68.0, 87.0, 114.3, 127.5, 129.8, 136.3, 159.2.

1-(2,2 Dibromo vinyl)-4-hexadecyloxy benzene:

Yield: 2.16 g (86%); after flash chromatography (hexane/DCM, gradient)

^{1}H NMR ($CDCl_3$, 300.13 MHz): δ = 0.88 (t, 3 H, 3J = 6.60 Hz, CH_2-**CH_3**), 1.20 - 1.50 (m, 26 H, CH_3-**CH_2**-CH_2), 1.60 - 1.90 (m, 2 H, O-CH_2-**CH_2**), 3.96 (m, 2 H, O-**CH_2**), 6.88 (d, 2 H, 3J = 8.75 Hz, **Ph-H**), 7.40 (s, 1 H, CBr_2=**CH**), 7.50 (d, 2 H, 3J = 8.75 Hz, **Ph-H**).

^{13}C NMR ($CDCl_3$, 75.47 MHz): δ = 14.1, 22.7, 26.1, 29.1, 29.3, 29.4, 29.5, 29.6, 29.7, 30.2, 30.4, 30.6, 31.9, 68.0, 87.0, 114.3, 127.5, 129.8, 136.3, 159.2.

4-Dodecyloxy phenyl acetylene (8 a):

Yield: 1.13 g (98%); without purification

^{1}H NMR ($CDCl_3$, 300.13 MHz): δ= 0.88 (t, 3 H, 3J = 6.75 Hz, CH_2-**CH_3**), 1.20 - 1.50 (m, 18 H, CH_3-**CH_2**-CH_2), 1.70 - 1.83 (m, 2 H, O-CH_2-**CH_2**), 2.99 (s, 1 H, C**C-H**), 3.95 (t, 2 H, 3J = 6.60 Hz, O-**CH_2**), 6.83 (d, 2 H, 3J = 8.90 Hz, **Ph-H**), 7.41 (d, 2 H, 3J = 8,90 Hz, **Ph-H**).

^{13}C NMR ($CDCl_3$, 75.47 MHz): δ = 14.1, 22.7, 26.0, 29.1, 29.3, 29.4, 29.5, 29.6, 29.7, 31.9, 68.0, 75.6, 83.8, 113.8, 114.4, 133.5, 159.5.

4-Hexadecyloxy phenyl acetylene (8 b):

Yield: 1.33 g (97%); without purification

^{1}H NMR ($CDCl_3$, 300.13 MHz) *δ* = 0.88 (t, 3 H, 3J = 6.75 Hz, CH_2-**CH_3**), 1.20 - 1.50 (m, 26 H, CH_3-**CH_2**-CH_2), 1.70 - 1.83 (m, 2 H, O-CH_2-**CH_2**), 2.99 (s, 1 H, C**C-H**), 3.95 (t, 2 H, 3J = 6.60 Hz, O-**CH_2**), 6.83(d, 2 H, 3J = 8.90 Hz, **Ph-H**), 7.41 (d, 2 H, 3J = 8.90 Hz, **Ph-H**).

^{13}C NMR ($CDCl_3$, 75.47 MHz): δ = 14.1, 22.7, 26.0, 29.1, 29.4, 29.6, 29.7, 31.9, 68.0, 75.6, 83.8, 113.8, 114.4, 133.5, 159.5.

9.2.3 Bi and Tetramesogens with Silicon Containing Linkers

9.2.3.1 Bimesogens with Linear Siloxane Linkers

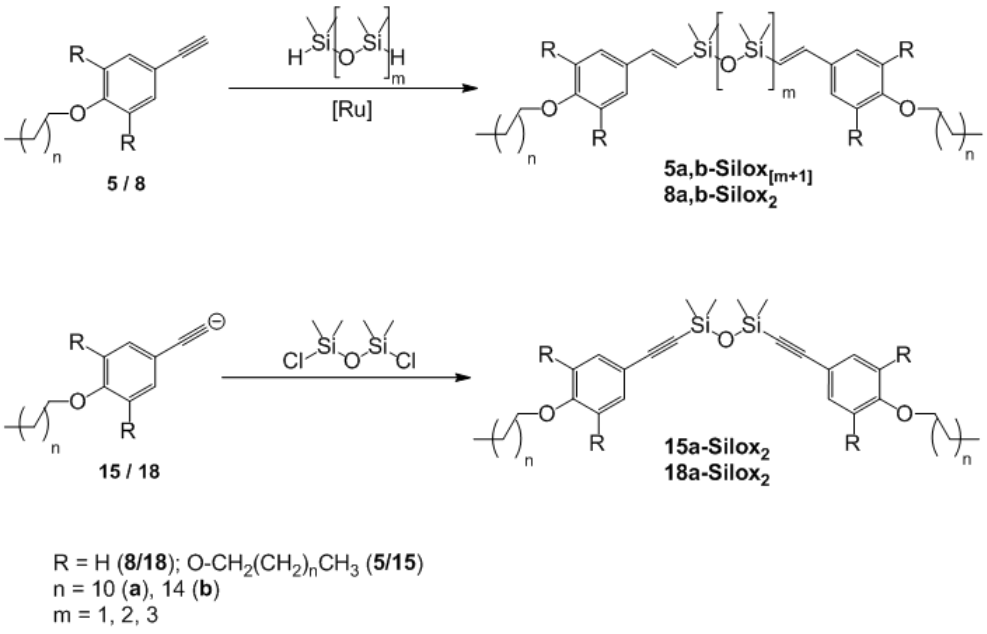

Scheme 9.4 *Synthesis scheme for linear siloxane bimesogens.*

Hydrosilylations of Phenylacetylenes with H-terminated Oligosiloxanes

Hydrosilylation of phenyl acetylenes **5** and **8** with H-terminated oligosiloxanes was performed according to a modified literature procedure.[133] To solutions of 2.5 mmol of the phenylacetylene compounds **5a, 5b, 8a, 8b** in 40 ml of dry DCM were added 0.03 eq of the catalyst $HCl(CO)(PPh_3)_3Ru$. Subsequently 1.25 mmol of the corresponding siloxane were added with a syringe. The reaction mixture was stirred overnight. After the solvent was evaporated, the crude products were purified by flash chromatography using appropriate gradients of hexane and DCM.

1,3-Di-((E)-3',4',5'-tridodecyloxystyryl)-1,1,3,3-tetramethyl disiloxane (5a-Silox$_2$):

Yield: 1.45 g (80%); after flash chromatography (hexane/DCM, gradient).

^{1}H NMR ($CDCl_3$, 300.13 MHz) δ = 0.25 (s, 12 H, Si-**CH_3**), 0.88 (t, 18 H, 3J = 6.5 Hz, CH_2-**CH_3**), 1.20 - 1.50 (m, 108 H, CH_3-**CH_2**-CH_2), 1.70 - 1.83 (m, 12 H, O-CH_2-**CH_2**), 3.95 (t, 12 H, 3J = 6.60 Hz, O-**CH_2**), 6.3 (d, 2 H, 3J = 19.2, CH=**CH**), 6.8 (d, 2 H, 3J = 19.2, CH=**CH**), 6.6 (s, 4 H, **Ph-H**).

^{13}C NMR ($CDCl_3$, 75.47 MHz) δ = 0.96, 14.1, 22.7, 26.0, 26.1, 29.3, 29.4, 29.6, 29.7, 29.8, 30.3, 31.9, 69.0, 73.5, 105.0, 127.0, 133.3, 138.6, 144.3, 153.2.

^{29}Si NMR ($CDCl_3$, 59.63 MHz) δ = 6.6.

Elemental Analysis: Calcd. for $C_{92}H_{170}O_7Si_2$: C, 76.50; H, 11.86; O, 7.75 Si, 3.89. Found: C, 76.49; H, 12.05; Si, 3.90.

1,3-Di-((E)-3',4',5'-trihexadecyloxystyryl)-1,1,3,3-tetramethyl disiloxane (5b-Silox$_2$):

Yield: 1.84 g (83%); after flash chromatography (hexane/DCM, gradient).

^{1}H NMR ($CDCl_3$, 300.13 MHz) δ = 0.25 (s, 12 H, Si-**CH$_3$**), 0.88 (t, 18 H, 3J = 6.5 Hz, CH_2-**CH$_3$**), 1.20 - 1.50 (m, 172 H, CH_3-**CH$_2$**-CH_2), 1.70 - 1.83 (m, 12 H, O-CH_2-**CH$_2$**), 3.95 (t, 12 H, 3J = 6.60 Hz, O-**CH$_2$**), 6.3 (d, 2 H, 3J = 19.2, CH=**CH**), 6.8 (d, 2 H, 3J = 19.2, CH=**CH**), 6.6 (s, 4 H, **Ph-H**).

^{13}C NMR ($CDCl_3$, 75.47 MHz) δ = 0.96, 14.1, 22.7, 26.1, 28.3, 28.9, 29.3, 29.4, 29.5, 29.6, 29.7, 29.8, 31.9, 32.1, 69.0, 73.5, 105.0, 127.0, 133.3, 138.6, 144.3, 153.2.

^{29}Si NMR ($CDCl_3$, 59.63 MHz) δ = -1.84.

Elemental Analysis: Calcd. for $C_{160}H_{218}O_7Si_2$: C, 78.22; H, 12.34; O, 6.29 Si, 3.15. Found: C, 78.13; H, 12.64; Si, 3.07.

1,3-Di-((E)-4-dodecyloxystyryl)-1,1,3,3-tetramethyl disiloxane (8a-Silox$_2$):

Yield: 0.72 g (81%); after flash chromatography (hexane/DCM, gradient).

^{1}H NMR ($CDCl_3$, 300.13 MHz) δ = 0.23 (s, 12 H, Si-**CH$_3$**), 0.88 (t, 6 H, 3J = 6.5 Hz, CH_2-**CH$_3$**), 1.20 - 1.50 (m, 36 H, CH_3-**CH$_2$**-CH_2), 1.70 - 1.83 (m, 4H, O-CH_2-**CH$_2$**), 3.95 (t, 4H, 3J = 6.60 Hz, O-**CH$_2$**), 6.2 (d, 2H, 3J = 19.2, CH=**CH**), 6.8 (d, 4H, 3J = 8.6, **Ph-H**), 6.9 (d, 2H, 3J = 19.8, CH=**CH**), 7.4 (d, 4H, 3J = 8.7, **Ph-H**).

^{13}C NMR ($CDCl_3$, 75.47 MHz) δ = 0.9, 14.1, 22.7, 26.0, 29.2, 29.3, 29.4, 29.5, 29.6, 29.7, 31.9, 68.0, 114.4, 125.6, 127.7, 130.8, 143.7, 159.2.

^{29}Si NMR ($CDCl_3$, 59.63 MHz) δ = -1.9.

Elemental Analysis: Calcd. for $C_{44}H_{74}O_3Si_2$: C, 74.72; H, 10.55; O, 6.79; Si, 7.94. Found: C, 74.72; H, 10.93; Si, 7.60.

1,3-Di-((E)-4-hexadecyloxystyryl)-1,1,3,3-tetramethyl disiloxane (8b-Silox$_2$):

Yield: 0.82 g (80%); after flash chromatography (hexane/DCM, gradient).

^{1}H NMR ($CDCl_3$, 300.13 MHz) δ = 0.23 (s, 12 H, Si-**CH$_3$**), 0.88 (t, 6 H, 3J = 6.5 Hz, CH_2-**CH$_3$**), 1.20 - 1.50 (m, 52 H, CH_3-**CH$_2$**-CH_2), 1.70 - 1.83 (m, 4H, O-CH_2-**CH$_2$**), 3.95 (t, 4H, 3J = 6.60 Hz, O-**CH$_2$**), 6.2 (d, 2H, 3J = 19.2, CH=**CH**), 6.8 (d, 4H, 3J = 8.6, **Ph-H**), 6.9 (d, 2H, 3J = 19.8, CH=**CH**), 7.4 (d, 4H, 3J = 8.7, **Ph-H**).

^{13}C NMR ($CDCl_3$, 75.47 MHz) δ = 0.9, 14.1, 22.7, 26.0, 29.2, 29.3, 29.4, 29.5, 29.6, 29.7, 31.9, 68.0, 114.4, 125.6, 127.7, 130.8, 143.7, 159.2.

^{29}Si NMR ($CDCl_3$, 59.63 MHz) δ = -3.56.

Elemental Analysis: Calcd for $C_{52}H_{90}O_3Si_2$: C, 76.22; H, 11.07; O, 5.86; Si, 6.85. Found: C, 76.37; H, 11.15; Si, 7.02.

1,3-bis-((E)-3',4',5'-tridodecyloxystyryl)-1,1,3,3-tetramethyl trisiloxane (5a-Silox$_3$):

Yield: 1.36 g (72%); after flash chromatography (hexane/DCM, gradient).

^{1}H NMR ($CDCl_3$, 300.13 MHz) δ = 0.10 (s, 6 H, Si-**CH$_3$**), 0.24 (s, 12 H, Si-**CH$_3$**), 0.88 (t, 18 H, 3J = 6.5 Hz, CH_2-**CH$_3$**), 1.20 - 1.50 (m, 108 H, CH_3-**CH$_2$**-CH_2), 1.70 - 1.83 (m, 12 H, O-CH_2-**CH$_2$**), 3.95 (t, 12 H, 3J = 6.60 Hz, O-**CH$_2$**), 6.25 (d, 2 H, 3J = 19.2, CH=**CH**), 6.63 (s, 4 H, **Ph-H**), 6.82 (d, 2 H, 3J = 19.2, CH=**CH**).

^{13}C NMR ($CDCl_3$, 75.47 MHz) δ = -0.32, 0.81, 14.1, 22.7, 26.0, 26.1, 29.3, 29.4, 29.6, 29.7, 29.8, 30.3, 31.9, 69.0, 73.5, 105.0, 127.0, 133.3, 138.6, 144.3, 153.2.

^{29}Si NMR ($CDCl_3$, 59.63 MHz) δ = -19.3, -2.9.

1,3-bis-((E)-3',4',5'-tridodecyloxystyryl)-1,1,3,3-tetramethyl tetrasiloxane (5a-Silox$_4$):

Yield: 1.48 g (74%); after flash chromatography (hexane/DCM, gradient).

^{1}H NMR ($CDCl_3$, 300.13 MHz) δ = 0.10 (s, 12 H, Si-**C**$\mathbf{H_3}$), 0.24 (s, 12 H, Si-**C**$\mathbf{H_3}$), 0.88 (t, 18 H, 3J = 6.5 Hz, CH_2-**C**$\mathbf{H_3}$), 1.20 - 1.50 (m, 108 H, CH_3-**C**$\mathbf{H_2}$-CH_2), 1.70 - 1.83 (m, 12 H, O-CH_2-**C**$\mathbf{H_2}$), 3.95 (t, 12 H, 3J = 6.60 Hz, O-**C**$\mathbf{H_2}$), 6.25 (d, 2 H, 3J = 19.2, CH=**C**$\mathbf{H}$), 6.63 (s, 4 H, **Ph-H**), 6.82 (d, 2 H, 3J = 19.2, CH=**C**$\mathbf{H}$).

^{13}C NMR ($CDCl_3$, 75.47 MHz) δ = -0.43, 0.76, 14.1, 22.7, 26.0, 26.1, 29.3, 29.4, 29.6, 29.7, 29.8, 30.3, 31.9, 69.0, 73.5, 105.0, 127.0, 133.3, 138.6, 144.3, 153.2.

^{29}Si NMR ($CDCl_3$, 59.63 MHz) δ = -20.5, -2.9.

Nucleophilic Substitution on Cl-terminated Siloxanes

For the nucleophilic substitution reaction the acetylide intermediate from the *Corey-Fuchs* route (mechanism see *Chapter 4.2.2.2*), which was obtained by BuLi-treatment of the geminal dibromide, as well as Cl-terminated siloxanes are used. 2.5 mmol of the geminal dibromide component were reacted during 1 h with 2 eq. of n-BuLi (2.5 M in hexane) at -78 °C and warmed to room temperature. Subsequently the mixture was once again cooled to -78 °C and 0.45 eq. of dichloro tetramethyl disiloxane were added under *Schlenk* conditions. The reaction mixture was stirred for 16 h at room temperature and quenched with aqueous NH_4Cl solution. After removal of the solvent by evaporation, the crude products were purified by flash chromatography.

1,3-bis((3,4,5-tris(dodecyloxy)phenyl)ethynyl)-1,1,2,2-tetramethyldisiloxane (15a-Silox$_2$):

Yield: 1.67 g (93%); after flash chromatography (hexane/DCM, gradient).

^{1}H NMR ($CDCl_3$, 300.13 MHz) δ = 0.29 (s, 12 H, Si-**CH_3**), 0.88 (t, 18 H, 3J = 6.5 Hz, CH_2-**CH_3**), 1.20 - 1.50 (m, 108 H, CH_3-**CH_2-**CH_2), 1.70 - 1.83 (m, 12 H, O-CH_2-**CH_2**), 3.95 (t, 12 H, 3J = 6.60 Hz, O-**CH_2**), 6.65 (s, 4 H, **Ph-H**).

1,3-bis((4-(dodecyloxy)phenyl)ethynyl)-1,1,2,2-tetramethyl disiloxane (18a-Silox$_2$):

Yield: 0.76 g (86%); after flash chromatography (hexane/DCM, gradient).

^{1}H NMR ($CDCl_3$, 300.13 MHz) δ = 0.27 (s, 12 H, Si-**CH_3**), 0.88 (t, 6 H, 3J = 6.5 Hz, CH_2-**CH_3**), 1.20 - 1.50 (m, 36 H, CH_3-**CH_2-**CH_2), 1.70 - 1.83 (m, 4 H, O-CH_2-**CH_2**), 3.95 (t, 4 H, 3J = 6.60 Hz, O-**CH_2**), 6.78 (d, 4H, 3J = 8.6, **Ph-H**), 7.47 (d, 4H, 3J = 8.7, **Ph-H**).

9.2.3.2 Bimesogens with Linear Disilane Linkers

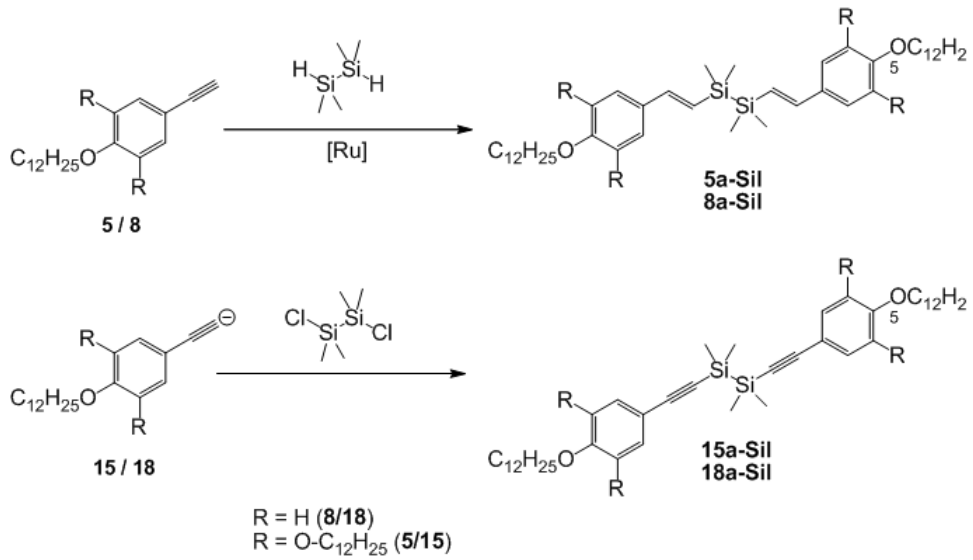

Scheme 9.5 *Synthesis scheme for linear disilane bimesogens.*

Hydrosilylations of Phenylacetylenes with H-terminated Oligosiloxanes

Hydrosilylation of phenyl acetylenes **5** and **8** with H-terminated tetramethyl disilanes to **5a/8a-Sil** was performed according to the procedure for hydrosilylation with H-terminated oligosiloxanes (to **5/8-Silox**), which was described above.

1,3-Di-((E)-3',4',5'-tridodecyloxystyryl)-1,1,3,3-tetramethyl disilane (5a-Sil):

Yield: 1.58 g (88%); after flash chromatography (hexane/DCM, gradient).

^{1}H NMR ($CDCl_3$, 300.13 MHz) δ = 0.24 (s, 12 H, Si-**CH_3**), 0.88 (t, 18 H, 3J = 6.5 Hz, CH_2-**CH_3**), 1.20 - 1.50 (m, 108 H, CH_3-**CH_2**-CH_2), 1.70 - 1.83 (m, 12 H, O-CH_2-**CH_2**), 3.95 (t, 12 H, 3J = 6.60 Hz, O-**CH_2**), 6.35 (d, 2 H, 3J = 19.2, CH=**CH**), 6.61 (s, 4 H, **Ph-H**), 6.73 (d, 2 H, 3J = 19.2, CH=**CH**).

^{13}C NMR ($CDCl_3$, 75.47 MHz) δ = -2.9, 14.1, 22.7, 26.0, 26.1, 29.3, 29.4, 29.6, 29.7, 29.8, 30.3, 31.9, 69.0, 73.5, 105.0, 127.0, 133.3, 138.6, 144.3, 153.2.

^{29}Si NMR ($CDCl_3$, 59.63 MHz) δ = -23.8.

1,3-Di-((E)-4-dodecyloxystyryl)-1,1,3,3-tetramethyl disilane (8a-Sil):

Yield: 0.82 g (80%); after flash chromatography (hexane/DCM, gradient).

^{1}H NMR ($CDCl_3$, 300.13 MHz) δ = 0.22 (s, 12 H, Si-**CH$_3$**), 0.88 (t, 6 H, 3J = 6.5 Hz, CH_2-**CH$_3$**), 1.20 - 1.50 (m, 52 H, CH_3-**CH$_2$**-CH_2), 1.70 - 1.83 (m, 4H, O-CH_2-**CH$_2$**), 3.95 (t, 4H, 3J = 6.60 Hz, O-**CH$_2$**), 6.32 (d, 2H, 3J = 19.2, CH=**CH**), 6.77 (d, 2H, 3J = 19.8, CH=**CH**), 6.83 (d, 4H, 3J = 8.6, **Ph-H**), 7.33 (d, 4H, 3J = 8.7, **Ph-H**).

^{13}C NMR ($CDCl_3$, 75.47 MHz) δ = -3.9, 14.1, 22.7, 26.0, 29.2, 29.3, 29.4, 29.5, 29.6, 29.7, 31.9, 68.0, 114.4, 125.6, 127.7, 130.8, 143.7, 159.2.

^{29}Si NMR ($CDCl_3$, 59.63 MHz) δ = -6.8.

Nucleophilic Substitution on Cl-terminated Silanes

The nucleophilic substitution reactions on Cl-terminated disilanes to the compounds **15a/18a-Sil** were performed according to the synthesis procedures for the compounds **15a/18a-Silox$_2$**, which were described above.

1,2-bis((3,4,5-tris(dodecyloxy)phenyl)ethynyl)-1,1,2,2-tetramethyldisilane (15a-Sil):

Yield: 1.45 g (81%); after flash chromatography (hexane/DCM, gradient).

^{1}H NMR ($CDCl_3$, 300.13 MHz) δ = 0.29 (s, 12 H, Si-**CH_3**), 0.88 (t, 18 H, 3J = 6.5 Hz, CH_2-**CH_3**), 1.20 - 1.50 (m, 108 H, CH_3-**CH_2-**CH_2), 1.70 - 1.83 (m, 12 H, O-CH_2-**CH_2**), 3.95 (t, 12 H, 3J = 6.60 Hz, O-**CH_2**), 6.65 (s, 4 H, **Ph-H**).

1,2-bis((4-(dodecyloxy)phenyl)ethynyl)-1,1,2,2-tetramethyl disilane (18a-Sil):

Yield: 0.67 g (87%); after flash chromatography (hexane/DCM, gradient).

^{1}H NMR ($CDCl_3$, 300.13 MHz) δ = 0.37 (s, 12H, Si-**CH_3**), 0.88 (t, 3H, 3J = 6.60 Hz, CH_2-**CH_3**), 1.20 - 1.60 (m, 36H, CH_3-**CH_2-**CH_2), 1.77 - 1.83 (m, 4H, O-CH_2-**CH_2**), 3.94 (t, 4H, 3J = 6.60 Hz, O-**CH_2**), 6.79 (d, 4H, 3J = 8.85 Hz, **Ph-H**), 7.38 (d, 4H, 3J = 8,85 Hz, **Ph-H**).

^{13}C NMR ($CDCl_3$, 75.47 MHz) δ = -2.8, 14.1, 22.7, 26.0, 29.2, 29.3, 29.4, 29.5, 29.6, 29.7, 31.9, 68.0, 90.3, 107.9, 114.3, 115.1, 133.4, 159.3.

9.2.3.3 Tetramesogens with Cyclic Tetrasiloxane Linkers

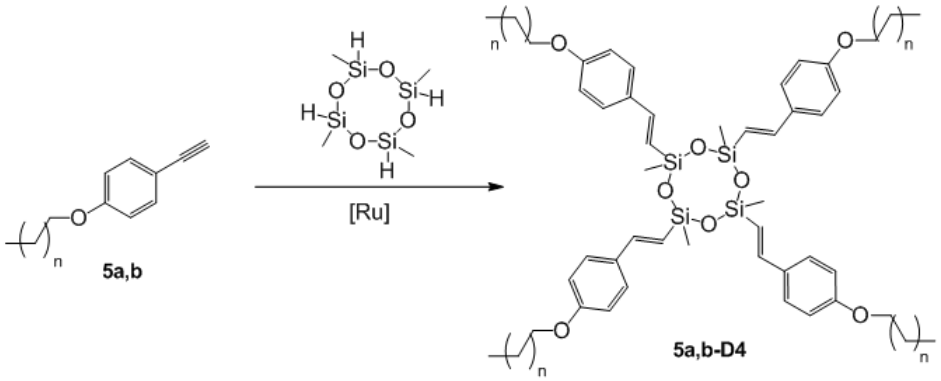

Scheme 9.6 *Synthesis scheme for cyclic tetramesogens.*

Synthesis of Compounds 5a,b-D4:

Hydrosilylation of phenyl acetylenes **5a,b** with tetramethyl cyclotetrasiloxanes was performed according to a modified literature procedure.[133] To solutions of 2.5 mmol of the phenyl acetylene compounds in 40 ml of dry DCM were added 0.03 eq of the catalyst $HCl(CO)(PPh_3)_3Ru$. Subsequently 0.625 mmol of tetramethyl cyclotetrasiloxane were added with a syringe. The reaction mixture was stirred overnight. One fraction of the product precipitated during the reaction. The precipitated fraction was separated using a centrifuge at 9000 rpm and subsequently washed with pentane. The remaining solution was concentrated in vacuum, dissolved once again in 5 ml DCM and added dropwise to 200 ml of cold methanol. Precipitation in methanol gave another fraction of the product. Only the fraction which precipitated during the synthesis was used for further analyses.

Tetra-(E)-(4-dodecyloxystyryl)-tetramethyl cyclotetrasiloxane (5a-D4):

Yield: 0.25 g (29%); precipitated fraction.

^{1}H NMR ($CDCl_3$, 300.13 MHz) δ = 0.29 (s, 12 H, Si-**CH_3**), 0.88 (t, 12 H, 3J = 6.5 Hz, CH_2-**CH_3**), 1.20 - 1.50 (m, 72 H, CH_3-**CH_2**-CH_2), 1.70 - 1.83 (m, 8H, O-CH_2-**CH_2**), 3.95 (t, 8H, 3J = 6.60 Hz, O-**CH_2**), 6.2 (d, 4H, 3J = 19.2, CH=**CH**), 6.8 (d, 8H, 3J = 8.7, **Ph-H**), 7.0 (d, 4H, 3J = 19.2, CH=**CH**), 7.3 (d, 8H, 3J = 8.7, **Ph-H**).

^{13}C NMR ($CDCl_3$, 75.47 MHz) δ = -0.9, 14.1, 22.7, 26.0, 29.2, 29.3, 29.4, 29.5, 29.6, 29.7, 31.9, 68.0, 114.4, 122.6, 127.7, 130.8, 145.7, 159.2.

^{29}Si NMR ($CDCl_3$, 59.63 MHz) δ = -30.0.

Elemental Analysis: Calcd for $C_{84}H_{136}O_8Si_4$: C, 72.78; H, 9.89; O, 9.23; Si, 8.10. Found: C, 72.28; H, 9.85; Si, 7.85.

Tetra-(E)-(4-Hexadecyloxystyryl)-tetramethyl cyclotetrasiloxane (5b-D4):

Yield: 0.27 g (27%); precipitated fraction.

^{1}H NMR ($CDCl_3$, 300.13 MHz) δ = 0.29 (s, 12 H, Si-**CH_3**), 0.88 (t, 12 H, 3J = 6.5 Hz, CH_2-**CH_3**), 1.20 - 1.50 (m, 104 H, CH_3-**CH_2**-CH_2), 1.70 - 1.83 (m, 8H, O-CH_2-**CH_2**), 3.95 (t, 8H, 3J = 6.60 Hz, O-**CH_2**), 6.2 (d, 4H, 3J = 19.2, CH=**CH**), 6.8 (d, 8H, 3J = 8.6, **Ph-H**), 6.9 (d, 4H, 3J = 19.2, CH=**CH**), 7.4 (d, 4H, 3J = 8.7, **Ph-H**).

^{13}C NMR ($CDCl_3$, 75.47 MHz) δ = -0.1, 14.1, 22.7, 26.0, 29.2, 29.3, 29.4, 29.5, 29.6, 29.7, 31.9, 68.0, 114.4, 122.6, 127.7, 130.8, 145.7, 159.2.

^{29}Si NMR ($CDCl_3$, 59.63 MHz) δ = -31.8.

Elemental Analysis: Calcd for $C_{100}H_{168}O_8Si_4$: C, 74.57; H, 10.51; O, 7.95; Si, 6.97. Found: C, 74.34; H, 10.02; Si, 6.85.

9.2.4 Chlorosilane-based Monomers

9.2.4.1 Phenylacetylene Monomers

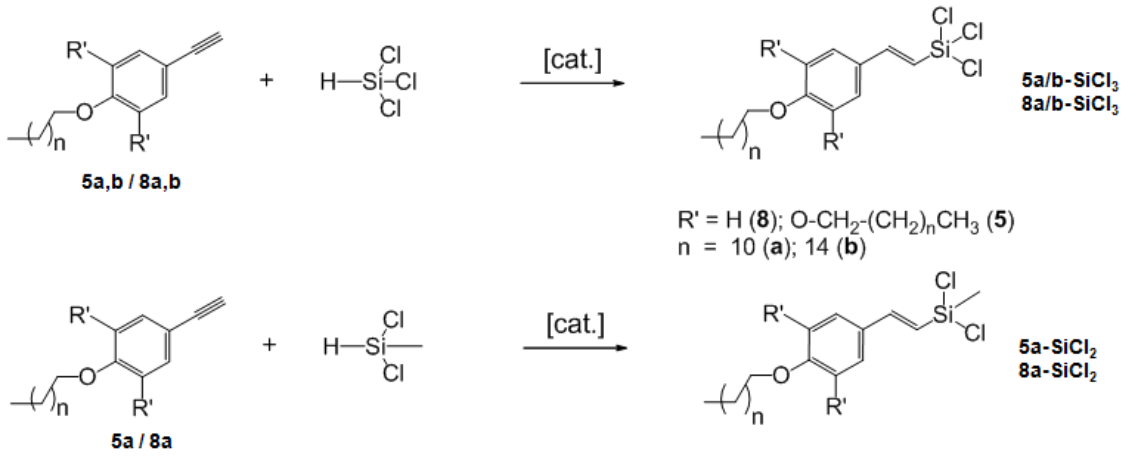

Scheme 9.7 *Synthesis scheme for phenylacetylene based chlorosilane monomers.*

The synthesis of the unsaturated monomers proceeded according to the previously described Ru-catalyzed hydrosilylations with H-terminated siloxanes. 1 mmol of the acetylenes **5/8** and 0.03 mmol of the catalyst $HCl(CO)(PPh_3)_3Ru$ were dissolved in 10 mL of dry DCM in a Schlenk tube. Subsequently 1.5 mmol of the corresponding chlorosilane, (freshly distillated) were added with a syringe. After 16 h the solvent was evaporated in vacuum and the monomers were used without further purification for the following polymerization reactions.

(E)-Trichloro(3,4,5-tris(dodecyloxy)styryl)silane (5a-$SiCl_3$):

^{1}H NMR ($CDCl_3$, 300.13 MHz) δ = 0.88 (t, 9H, 3J = 6.75 Hz, CH_2-**CH_3**), 1.20 - 1.60 (m, 54H, CH_3-**CH_2**-CH_2), 1.60 - 1.90 (m, 6H, O-CH_2-**CH_2**), 4.00 (m, 6H, O-**CH_2**), 6.28 (d, 1H, 3J = 18.60 Hz, CH=**CH**), 6.71 (s, 2H, **Ph-H**), 7,26 (d, 1H, 3J = 18.60 Hz, CH=**CH**).

^{13}C NMR ($CDCl_3$, 75.47 MHz) δ = 14.1, 22.7, 26.0, 29.4, 29.6, 29.7, 29.8, 30.3, 31.9, 31.0, 69.2, 73.6, 106.2, 117.2, 130.4, 140.5, 151.6, 153.4.

^{29}Si NMR ($CDCl_3$, 59.63 MHz) δ = -1.9.

(E)-Trichloro(3,4,5-tris(hexadecyloxy)styryl)silane (5b-$SiCl_3$):

^{1}H NMR ($CDCl_3$, 300.13 MHz) δ = 0.88 (t, 9H, 3J = 6.75 Hz, CH_2-**CH_3**), 1.20 - 1.60 (m, 78, CH_3-**CH_2**-CH_2), 1.60 - 1.90 (m, 6H, O-CH_2-**CH_2**), 4.00 (m, 6H, O-**CH_2**), 6.28 (d, 1H, 3J = 18.60 Hz, CH=**CH**), 6.71 (s, 2H, **Ph-H**), 7,26 (d, 1H, 3J = 18.60 Hz, CH=**CH**).

^{13}C NMR ($CDCl_3$, 75.47 MHz) δ = 14.1, 22.7, 26.0, 29.3, 29.4, 29.5, 29.6, 29.7, 29.8, 30.3, 31.9, 31.0, 69.2, 73.6, 106.2, 117.2, 130.4, 140.5, 151.6, 153.4.

^{29}Si NMR ($CDCl_3$, 59.63 MHz) δ = -1.8.

(E)-Trichloro(4-dodecyloxystyryl)silane (8a-$SiCl_3$):

^{1}H NMR ($CDCl_3$, 300.13 MHz) δ = 0.88 (t, 3H, 3J = 6.60 Hz, CH_2-**CH_3**), 1.20 - 1.50 (m, 18H, CH_3-**CH_2**-CH_2), 1.65 - 1.96 (m, 2H, O-CH_2-**CH_2**), 3.98 (t, 2H, 3J = 6.60 Hz, O-**CH_2**), 6.24(d, 1H, 3J = 18.60 Hz, CH=**CH**), 6.89 (d, 2H, 3J = 8.80 Hz, **Ph-H**), 7.31 (d, 1H, 3J = 18.60 Hz, CH=**CH**), 7.45 (d, 2H, 3J = 8.80 Hz, **Ph-H**).

^{13}C NMR ($CDCl_3$, 75.47 MHz) δ = 14.1, 22.7, 26.0, 29.1, 29.3, 29.6, 29.7, 31.9, 68.2, 114.7, 115.5, 127.9, 129.3, 151.1, 161.1.

^{29}Si NMR ($CDCl_3$, 59.63 MHz) δ = -1.7.

(E)-Trichloro(4-hexadecyloxystyryl)silane (8b-$SiCl_3$):

^{1}H NMR ($CDCl_3$, 300.13 MHz) δ = 0.88 (t, 3H, 3J = 6.60 Hz, CH_2-**CH_3**), 1.20 - 1.50 (m, 26H, CH_3-**CH_2**-CH_2), 1.65 - 1.96 (m, 2H, O-CH_2-**CH_2**), 3.98 (t, 2H, 3J = 6.60 Hz, O-**CH_2**), 6.24(d, 1H, 3J = 18.60 Hz, CH=**CH**), 6.89 (d, 2H, 3J = 8.80 Hz, **Ph-H**), 7.31 (d, 1H, 3J = 18.60 Hz, CH=**CH**), 7.45 (d, 2H, 3J = 8.80 Hz, **Ph-H**).

^{13}C NMR ($CDCl_3$, 75.47 MHz) δ = 14.1, 22.7, 26.0, 29.1, 29.3, 29.4, 29.5, 29.6, 29.7, 31.9, 68.2, 114.7, 115.5, 127.9, 129.3, 151.1, 161.1.

^{29}Si NMR ($CDCl_3$, 59.63 MHz) δ = -1.7.

(E)-Dichloro(methyl)(3,4,5-tris(dodecyloxy)styryl)silane (5a-$SiCl_2$):

^{1}H NMR ($CDCl_3$, 300.13 MHz) δ = 0.80 - 0.95 (m, 12H, Si-**CH_3**/CH_2-**CH_3**), 1.20 - 1.60 (m, 54H, CH_3-**CH_2**-CH_2), 1.60 - 1.90 (m, 6H, O-CH_2-**CH_2**), 3.99 (m, 6H, O-**CH_2**), 6.28 (d, 1H, 3J = 18.60 Hz, CH=**CH**), 6.70 (s, 2H, **Ph-H**), 7,12 (d, 1H, 3J = 18.60 Hz, CH=**CH**).

^{13}C NMR ($CDCl_3$, 75.47 MHz) δ = 5.9, 14.1, 22.7, 26.1, 29.4, 29.7, 29.8, 30.3, 31.9, 69.1, 73.5, 105.8, 119.7, 131.3, 139.9, 149.3, 153.3.

^{29}Si NMR ($CDCl_3$, 59.63 MHz) δ = -8.7.

(E)-Dichloro(4-dodecyloxystyryl)methylsilane (8a-$SiCl_2$):

^{1}H NMR ($CDCl_3$, 300.13 MHz) δ = 0.88 (t, 3H, 3J = 6.75 Hz, CH_2-**CH_3**), 0.92 (s, 3H, Si-**CH_3**), 1.20 - 1.60 (m, 18H, CH_3-**CH_2**-CH_2), 1.79 (m, 2H, O-CH_2-**CH_2**), 3.97 (t, 2H, 3J = 6.60 Hz, O-**CH_2**), 6.25 (d, 1H, 3J = 18.90 Hz, CH=**CH**), 6.88 (d, 2H, 3J = 8.80 Hz, **Ph-H**), 7.17 (d, 1H, 3J = 18,90 Hz, CH=**CH**), 7.43 (d, 2H, 3J = 8.80 Hz, **Ph-H**).

^{13}C NMR ($CDCl_3$, 75.47 MHz) δ = 5.7, 14.1, 22.7, 26.0, 29.2, 29.4, 29.6, 29.7, 31.9, 68.1, 114.6, 118.0, 127.7, 128.7, 148.7, 160.5.

^{29}Si NMR ($CDCl_3$, 59.63 MHz) δ = -8.9

9.2.4.2 Styrene Monomers

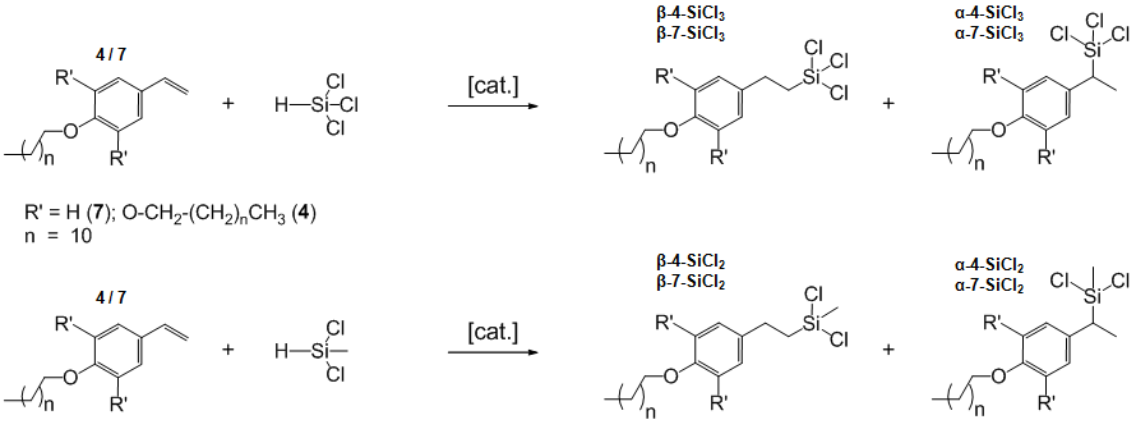

Scheme 9.8 *Synthesis scheme for styrene based chlorosilane monomers.*

The synthesis of the saturated monomers was performed using different combinations of educts, silanes, catalysts and reaction times. The styrene mesogens were lyophilized from benzene based solutions prior to the conversions. 1 mmol of the styrenes **4/7** and certain amounts of the catalysts were dissolved in 10 mL of dry toluene in a *Schlenk* tube. Subsequently 1.5 mmol of the corresponding chlorosilane, (freshly distillated) were added with a syringe. After different reaction times the solvent was evaporated in vacuum and the monomers were used without further purification for the following polymerization reactions. In *Table 9.1* the combinations are summarized, whereas in *Scheme 9.9* and *9.10* the different catalysts are presented. Yields and isomer distributions were calculated from appropriate relations of integrals in ^1H-NMR spectra.

Table 9.1 *Different combinations of reactants and catalysts for hydrosilylation reactions of styrene mesogens.*

entry	Subst.	silane	catalyst	amount [mmol]	temp. [°C]	reaction time [h]	yield. [%]	α [%]	β [%]
1	**7**	$HSiCH_3Cl_2$	*Karstedt*	[a]	RT	16	100	55	45
2	**4**	$HSiCH_3Cl_2$	*Karstedt*	[b]	80	72	85	0	100
3	**4**	$HSiCl_3$	*Karstedt*	[b]	80	72	100	30	70
4	**7**	$HSiCH_3Cl_2$	*Markó*	0.0015	RT	120	30	0	100
5	**7**	$HSiCH_3Cl_2$	*Markó*	0.0015	RT	96	16	0	100
6	**7**	$HSiCH_3Cl_2$	*Markó*	0.0015	RT	24	0	0	0
7	**7**	$HSiCl_3$	*Markó*	0.0015	RT	96	<10	50	50
8	**4**	$HSiCl_3$	*Markó*	0.0015	90	72	100	30	70
9	**4/7**	$HSiCl_3$	*Dötz*	0.04	RT	16	0[c]	0	0
10	**4/7**	$HSiCl_3$	*Pd-P1*	0.0050	RT	16	100	100	0
11	**4/7**	$HSiCl_3$	*Pd-P2*	0.0050	RT	16	100	100	0
12	**4/7**	$HSiCl_3$	*Pd-P3*	0.05	RT	4	100	100	0

[a] 5 drops of a xylene based solution (2% w/w of Pt); [b] 10 drops of a xylene based solution (2% w/w of Pt); [c] after 16 h at RT formation of huge amount of colloid, impossible to analyze.

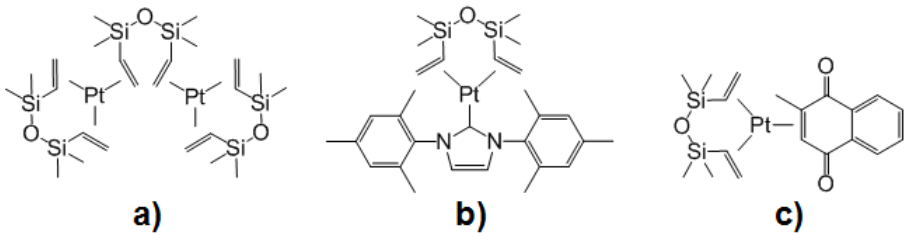

Scheme 9.9 *Different platinum based catalysts. (a) Karstedt's catalyst, (b) Markó's catalyst, (c) Dötz's catalyst.*

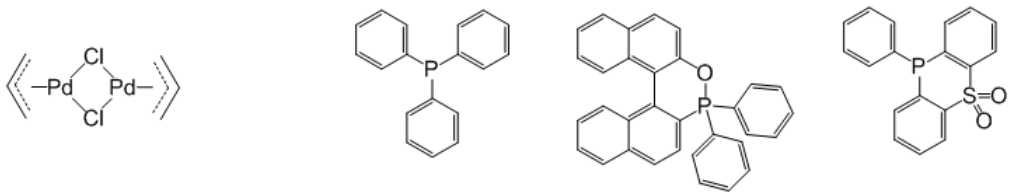

Scheme 9.10 *Catalyst precursor palladium allyl chloride to catalysts Pd-P1,2,3 (a) and the corresponding phosphorous based ligands P1 (b), P2 (c), P3 (d).*

Hydrosilylation of Styrenes with Chlorosilanes and Karstedt's Catalyst

Dichloro(4-dodecyloxyphenylethyl)methylsilane (β-7-$SiCl_2$) /
Dichloro(1-(4-dodecyloxyphenyl)ethyl)methylsilane (α-7-$SiCl_2$):

^{1}H NMR ($CDCl_3$, 300.13 MHz) δ = 0.62 (s, 1.7H, α-CH-Si-**CH_3**), 0.69 (s, 1.3H, β-CH_2-Si-**CH_3**), 0.88 (t, 3H, 3J = 6.75 Hz, CH_2-**CH_3**), 1.20 - 1.50 (m, 18H, CH_3-**CH_2**-CH_2, β-Si-**CH_2**), 1.51 (d, 1.3H, ^{3}J = 7.55 Hz, α-Si-CH-**CH_3**), 1.79 (m, 2H, O-CH_2-**CH_2**), 2.58 (q, 0.5H, ^{3}J = 7.55 Hz, α-Si-**CH**), 2.78 (m, 0.7H, β-Si-CH_2-**CH_2**), 3.93 (t, 2H, 3J = 6.60 Hz, O-**CH_2**), 6.83 (m, 2H, **Ph-H**), 7.10 (m, 2H, **Ph-H**).

See entry 1 in *Table 9.1.*

Dichloro(methyl)(3,4,5-tris(dodecyloxy)phenethyl)silane (β-4-$SiCl_2$):

^{1}H NMR ($CDCl_3$, 300.13 MHz) δ = 0.69 (s, 3H, β-CH_2-Si-**CH_3**), 0.88 (m, 9H, CH_2-**CH_3**), 1.20 - 1.60 (m, 56H, H-2, CH_3-**CH_2**-CH_2), 1.60 - 1.90 (m, 6H, O-CH_2-**CH_2**), 2.78 (m, 2H, β-Si-CH_2-**CH_2**), 3.98 (m, 6H, O-**CH_2**), 6.42 (s, 2H, **Ph-H**).

See entry 2 in *Table 9.1.*

Trichloro(3,4,5-tris(dodecyloxy)phenethyl)silane (β-4-$SiCl_3$) /
Trichloro(1-(3,4,5-tris(dodecyloxy)phenyl)ethyl)silane (α-4-$SiCl_3$):

^{1}H NMR ($CDCl_3$, 300.13 MHz) δ = 0.88 (m, 9H, CH_2-**CH_3**), 1.20 - 1.50 (m, 56H, β-Si-**CH_2**, CH_3-**CH_2**-CH_2), 1.58 (d, 0.9H, ^{3}J = 7.50 Hz, α-Si-CH-**CH_3**) 1.60-1.90 (m, 6H, O-CH_2-**CH_2**), 2.80 (m, 1.4H, β-Si-CH_2-**CH_2**), 3.98 (m, 6H, O-**CH_2**), 6.38 (s, 1.4H, β-**Ph-H**), 6.40 (s, 0.6H, α-**Ph-H**).

See entry 3 in *Table 9.1.*

Hydrosilylation of Styrenes with Chlorosilanes and Markó's Catalyst

Dichloro(1-(4-dodecyloxyphenyl)ethyl)methylsilane (α-7-$SiCl_2$):

^{1}H NMR after 120 h ($CDCl_3$, 300.13 MHz) δ = 0.69 (s, 0.9H, β-CH_2-Si-**CH_3**), 0.88 (t, 3H, 3J = 6.75 Hz, CH_2-**CH_3**), 1.20 - 1.50 (m, 18H, CH_3-**CH_2**-CH_2, β-Si-**CH_2**), 1.79 (m, 2H, O-CH_2-**CH_2**), 2.78 (m, 0.7H, β-Si-CH_2-**CH_2**), 3.96 (m, 2H, O-**CH_2**), 5.11 (dd, 0.6H, 2J = 0.90 Hz, 3J = 10.90 Hz, Sty-CH=**CH_2**), 5.60 (dd, 0.6H, 2J = 0.90 Hz, 3J = 17.60 Hz, Sty-CH=**CH_2**), 6.66 (dd, 0.6H, 3J = 10.90 Hz, 3J = 17.60 Hz, Sty-**CH**=CH_2), 6.85 (m, 2H, **Ph-H**), 7.12 (d, 0.7H, 3J = 8.70 Hz, **Ph-H**), 7.34 (d, 1.2H, 3J = 8.70 Hz, **Ph-H**).

See entry 4 in *Table 9.1.*

Trichloro(3,4,5-tris(dodecyloxy)phenethyl)silane (β-4-$SiCl_3$) /
Trichloro(1-(3,4,5-tris(dodecyloxy)phenyl)ethyl)silane (α-4-$SiCl_3$):

^{1}H NMR ($CDCl_3$, 300.13 MHz) δ = 0.88 (m, 9H, CH_2-**CH_3**), 1.20 - 1.50 (m, 56H, CH_3-**CH_2**-CH_2, β-Si-**CH_2**), 1.58 (d, 0.7H, ^{3}J = 7.50 Hz, α-Si-CH-**CH_3**) 1.60 - 1.90 (m, 6H, O-CH_2-**CH_2**), 2.80 (m, 1.4H, β-Si-CH_2-**CH_2**), 3.98 (m, 6H, O-**CH_2**), 6.38 (s, 1.3H, β-**Ph-H**), 6.40 (s, 0.7H, α-**Ph-H**).

See entry 8 in *Table 9.1.*

Hydrosilylation of Styrenes with Trichlorosilanes and Pd-based Catalysts (Pd-P1-3)

Trichloro(1-(3,4,5-tris(dodecyloxy)phenyl)ethyl)silane (α-4a-$SiCl_3$):

^{1}H NMR ($CDCl_3$, 300.13 MHz) δ = 0.88 (m, 9H, CH_2-**CH_3**), 1.2 - 1.5 (m, 54H, CH_3-**CH_2**-CH_2), 1.56 (d, 3H, 3J = 7.5 Hz, Si-CH-**CH_3**), 1.65 - 1.8 (m, 6H, O-CH_2-**CH_2**), 2.76 (m, 1H, Si-**CH**), 3.95 (m, 6H, O-**CH_2**), 6.38 (s, 2H, **Ph-H**).

See entry 10 - 12 in *Table 9.1*.

Trichloro(1-(3,4,5-tris(hexadecyloxy)phenyl)ethyl)silane (α-4b-$SiCl_3$):

^{1}H NMR ($CDCl_3$, 300.13 MHz) δ = 0.88 (m, 9H, CH_2-**CH_3**), 1.2 - 1.5 (m, 78H, CH_3-**CH_2**-CH_2), 1.56 (d, 3H, 3J = 7.5 Hz, Si-CH-**CH_3**), 1.65 - 1.8 (m, 6H, O-CH_2-**CH_2**), 2.76 (q, 1H, J = 7.6 Hz, Si-**CH**), 3.95 (m, 6H, O-**CH_2**), 6.38 (s, 2H, **Ph-H**).

See entry 10 - 12 in *Table 9.1*.

Trichloro(1-(4-dodecyloxy)phenyl)ethyl)silane (α-7a-$SiCl_3$):

^{1}H NMR ($CDCl_3$, 300.13 MHz) δ = 0.88 (t, 3H, 3J = 6.60 Hz, CH_2-**CH_3**), 1.2 - 1.5 (m, 18H, CH_3-**CH_2**-CH_2), 1.57 (d, 3H, 3J = 7.5 Hz, Si-CH-**CH_3**), 1.77 (m, 2H, O-CH_2-**CH_2**), 2.82 (q, 1H, J = 7.6 Hz, Si-**CH**), 3.92 (t, 2H, J = 6.6 Hz, O-**CH_2**), 6.85 (d, 2H, 2J = 8.8 Hz, **Ph-H**), 7.13 (d, 2H, 2J = 8.5 Hz, **Ph-H**).

See entry 10 - 12 in *Table 9.1*.

Trichloro(1-(4-hexadecyloxy)phenyl)ethyl)silane (α-7b-$SiCl_3$):

^{1}H NMR ($CDCl_3$, 300.13 MHz) δ = 0.88 (t, 3H, 3J = 6.60 Hz, CH_2-**CH_3**), 1.2 - 1.5 (m, 26H, CH_3-**CH_2**-CH_2), 1.57 (d, 3H, 3J = 7.5 Hz, Si-CH-**CH_3**), 1.77 (m, 2H, O-CH_2-**CH_2**), 2.82 (q, 1H, J = 7.6 Hz, Si-**CH**), 3.92 (t, 2H, J = 6.6 Hz, O-**CH_2**), 6.85 (d, 2H, 2J = 8.8 Hz, **Ph-H**), 7.13 (d, 2H, 2J = 8.5 Hz, **Ph-H**).

See entry 10 - 12 in *Table 9.1.*

9.2.5 Silicon Based Polymers

9.2.5.1 Coupling of Chlorosilane Monomers with neat Sodium Metal

Neat metallic Na was cut in small pieces under paraffin oil and subsequently washed in hexane, ethanol and dry toluene. 10 mmol of Na in dry toluene were vigorously stirred under reflux conditions until a homogeneous dispersion was obtained. To this dispersion a solution of 1 mmol of the corresponding monomer in dry toluene was added drop wise. After 6 h of reflux the reaction mixture was cooled to room temperature and filtered using a previously dried syringe filter. The solvent was evaporated and the residue dissolved in a small amount of DCM. Subsequently the polymer was precipitated in cold methanol. The precipitate was separated by centrifugation at 4000 rpm and dried in vacuum.

9.2.5.2 Coupling of Chlorosilane Monomers with neat Potassium Metal

Neat metallic K was cut in small pieces and soaked in dry toluene in a glove-box. For the coupling reactions 2 and 3 mmol were used for dichloro- and trichlorosilanes, respectively. The mixture was stirred vigorously under reflux until a homogeneous dispersion was obtained. To this dispersion a solution of 1 mmol of the corresponding monomer in dry toluene was added drop wise. After 6 h of reflux the reaction mixture was cooled to room temperature and filtered using a previously dried syringe filter. The solvent was evaporated and the residue dissolved in a small amount of DCM. Subsequently the polymer was precipitated in cold methanol. The precipitate was separated by centrifugation at 4000 rpm and dried in vacuum.

9.2.5.3 Coupling of Chlorosilane Monomers with Potassium Intercalated in Graphite

The C_8K intercalation compound was synthesized in big amounts and stored in a glove-box for further use. For that reason 10g (0.83 mol) graphite were dried n a *Schlenk*-tube and after cooling 4 g (0.10 mol) of K were added. This mixture was tempered under mechanical stirring at 170 °C. A smooth bronze colored powder was obtained.

For the polymerization reactions the powder was soaked in dry THF (2 and 3 mmol were used for coupling of dichloro- and trichlorosilanes, respectively). To this mixture a solution of 1 mmol of the corresponding monomer in dry THF was added drop wise. The reaction was quenched after different reaction times with dry methanol. The residual solids were separated by centrifugation at 8000 rpm. The solvent was evaporated and the residue dissolved in a small amount of DCM. Subsequently the polymer was precipitated in cold methanol. The precipitate was separated by centrifugation at 4000 rpm and dried in vacuum.

The analytical data of the polymerization products is presented and discussed in *Section 6.4*.

10 Appendix

10.1 List of Publications

10.1.1 Poster

F. Mögele, P. Heinz; B. Rieger; Nanopatterned Surfaces by Molecular Self Assembly – A STM Study; Macromolecular Systems for Nanoscience – Chemistry, Physics and Engineering Aspects; Kloster Irsee, Germany, Sep 2007

P. Heinz, B. Rieger; Self Assembled Structures of Oligosiloxanes with Mesogenic Side Groups; 5th European Silicon Days, Vienna, Austria, Sep 2009

P. Heinz, B. Rieger; Self Assembled Structures of Oligosiloxanes with Mesogenic Side Groups; 43rd Silicon Symposium, St. Louis, USA, May 2010

10.1.2 Articles

P. Heinz, K. Hindelang, A. Golosova, C.M. Papadakis, B. Rieger, *ChemPhysChem* **2011**, 12, 3591

P. Heinz, K. Hindelang, F. Fumagalli, G. Ceccone, H. Rauscher, B. Rieger, *in preparation*

11 References

[1] A. F. Hollemann, E. Wiberg, *Lehrbuch der Anorganischen Chemie*; 101st ed.; Walter de Gruyter: Berlin, 1995.

[2] http://hyperphysics.phy-astr.gsu.edu/hbase/tables/elabund.html.

[3] http://minerals.usgs.gov/minerals/pubs/commodity/silicon/mcs-2011-simet.pdf.

[4] http://www.wacker.com/cms/media/documents/investor-relations/factbook_2011.pdf.

[5] J. Bardeen, *Phys. unserer Zeit* **1983**, *14*, 187.

[6] E. Spenke, *Elektrische Halbleiter*; Springer Verlag: Berlin, Göttingen, Heidelberg, 1955.

[7] http://www1.eere.energy.gov/solar/pdfs/solar_timeline.pdf.

[8] C. Biswas, Y. H. Lee, *Adv. Funct. Mater.* **2011**, *21*, 3806

[9] J. Lehn, *Science* **1993**, *260*, 1762.

[10] J. W. Steed, J. L. Atwood, *Supramolecular Chemistry*; Wiley: Weinheim, 2000.

[11] H.-J. Schneider, A. Yatsimirsky, *Principles and Methods in Supramolecular Chemistry*; John Wiley & Sons, LTD: Chirchester, 2000.

[12] G. A. Jeffrey, *An Introduction to Hydrogen Bonding*; Oxford University Press: Oxford, 1997.

[13] C. A. Hunter, J. K. M. Sanders, *J. Am. Chem. Soc.* **1990**, *112*, 5525.

[14] A. Ben-Naim, *Hydrophobic Interactions*; Plenum Press: New York, 1980.

[15] J.-M. Lehn, *Science* **2002**, *295*, 2400.

[16] D. Iwanowski, *Izv. Imp. Akad. Nauk* **1892**, *35*, 67.

[17] A. Mayer, *Die Landwirtschaftlichen Versuchs Stationen* **1886**, *32*, 451.

[18] http://www.biologie.uni-hamburg.de/b-online/d35/35.htm.

[19] http://www.uni-stuttgart.de/impulse/imp/alles.php?id=7.

[20] D. Philip, J. F. Stoddart, *Angew. Chem.* **1996**, *108*, 1242.

[21] D. Myers, *Surfactant Science and Technology*; 2nd ed.; VCH Publishers: New York, 1992.

[22] J.-H. Fuhrhop, J. Köning, *Molecular Assemblies: The Synkinetic Approach*; The Royal Society of Chemistry: Cambridge, 1994.

[23] http://www.nano.psu.edu/labtour/stmd.htm.

[24] P. Zell, F. Mögele, U. Ziener, B. Rieger, *Chem. Eur. J.* **2006**, *12*, 3847.

[25] V. Percec, D. A. Wilson, P. Leowanawat, C. J. Wilson, A. D. Hughes, M. S. Kaucher, D. A. Hammer, D. H. Levine, A. J. Kim, F. S. Bates, K. P. Davis, T. P. Lodge, M. L. Klein, R. H. DeVane, E. Aqad, B. M. Rosen, A. O. Argintaru, M. J. Sienkowska, K. Rissanen, S. Nummelin, J. Ropponen, *Science* **2010**, *328*, 1009.

[26] K. Borisch, S. Diele, P. Göring, H. Kresse, C. Tschierske, *J. Mater. Chem.* **1998**, *8*, 529.

[27] M. J. Rosen, *Surfactants and Interfacial phenomena*; 2nd ed.; Wiley: New York, 1989.

[28] A. W. Adamson, *Chemistry of Surfaces*; 5th ed.; Wiley: New York, 1990.

[29] V. Malinova, S. Belegrinou, D. de Bruyn Ouboter, W. P. Meier In *Polymer Membranes / Biomembranes*; Meier, W. P., Knoll, W., Eds.; Springer-Verlag: Berlin Heidelberg, 2010; Vol. 224.

[30] A. Ulman, *An Introduction to Ultrathin Organic Films*; Academic Press: Boston, 1991.

[31] A. Ulman, *Chem. Rev.* **1996**, *96*, 1533.

[32] S. Krämer, R. R. Fuierer, C. B. Gorman, *Chem. Rev.* **2003**, *103*, 4367.

[33] R. G. Nuzzo, D. L. Allara, *J. Am. Chem. Soc.* **1983**, *105*, 4481.

[34] R. K. Smith, P. A. Lewis, P. S. Weiss, *Prog. Surf. Sci.* **2004**, *75*, 1.

[35] T. Wink, S. J. van Zuilen, A. Bult, W. P. van Bennekom, *Analyst* **1997**, *122*, 43R.

[36] J. Foisner, A. Glaser, T. Leitner, H. Hoffmann, G. Friedbacher, *Langmuir* **2004**, *20*, 2701.

[37] P. Zell, F. Mogele, U. Ziener, B. Rieger, *Chem. Commun.* **2005**, 1294.

[38] M. T. Räisänen, F. Mögele, S. Feodorow, B. Rieger, U. Ziener, M. Leskelä, T. Repo, *Eur. J. Inorg. Chem.* **2007**, *2007*, 4028.

[39] F. Mögele, D. Fantauzzi, U. Wiedwald, P. Ziemann, B. Rieger, *Langmuir* **2009**, *25*, 13606.

[40] H. Hoffmann, G. Ebert, *Angew. Chem. Int. Ed.* **1988**, *27*, 902.

[41] F. Reinitzer, *Monatsh. Chem.* **1888**, *9*, 421.

[42] O. Lehmann, *Z. Phys.Chem.* **1889**, *4*, 462.

[43] C. Tschierske, *J. Mater. Chem.* **1998**, *8*, 1485.

[44] R. Pardey, A. Zhang, P. A. Gabori, F. W. Harris, S. Z. D. Cheng, J. Adduci, J. V. Facinelli, R. W. Lenz, *Macromolecules* **1992**, *25*, 5060.

[45] V. Percec, A. Keller, *Macromolecules* **1990**, *23*, 4347.

[46] J. Ackermann, V. Damrath, *Chem. unserer Zeit* **1989**, *23*, 86.

[47] R. Schliebs, J. Ackermann, *Chem. unserer Zeit* **1987**, *21*, 121.

[48] F. S. Kipping, *J. Chem. Soc.* **1922**, *119*, 830.

[49] F. S. Kipping, *J. Chem. Soc.* **1924**, *125*, 2291.

[50] R. D. Miller, J. Michl, *Chem. Rev.* **1989**, *89*, 1359.

[51] S. W. Kantor, W. T. Grubb, R. C. Osthoff, *J. Am. Chem. Soc.* **1954**, *76*, 5190.

[52] W. Ziche, **2005**, *US 2006568132 A*.

[53] T. Tsudera, T. Kubota, A. Kiyomori, **2009**, *US 2007882335 A*.

[54] www.wacker.com.

[55] U. Schmidt, P. C. Zehetmaier, B. Rieger, *Macromol. Rapid Commun.* **2010**, *31*, 545.

[56] H. C. Kolb, M. G. Finn, K. B. Sharpless, *Angew. Chem. Int. Ed.* **2001**, *40*, 2004.

[57] R. H. Baney, M. Itoh, A. Sakakibara, T. Suzuki, *Chem. Rev.* **1995**, *95*, 1409.

[58] D. W. Scott, *J. Am. Chem. Soc.* **1946**, *68*, 356.

[59] A. R. Bassindale, H. Chen, Z. Liu, I. A. MacKinnon, D. J. Parker, P. G. Taylor, Y. Yang, M. E. Light, P. N. Horton, M. B. Hursthouse, *J. Organomet. Chem.* **2004**, *689*, 3287.

[60] G. Li, L. Wang, H. Ni, C. U. Pittman, *J. Inorg. Organomet. Polym.* **2001**, *11*, 123.

[61] J. R. Koe, D. R. Powell, J. J. Buffy, S. Hayase, R. West, *Angew. Chem. Int. Ed.* **1998**, *37*, 1441.

[62] F. Fehér, D. Schinkitz, J. Schaaf, *Z. Anorg. Allg. Chem.* **1971**, *383*, 303.

[63] N. Auner, C. Bauch, G. Lippold, R. Deltschew, **2008**, *DE 102006034061 A1 CAN*, 115:115263.

[64] R. G. Jones, W. K. C. Wong, S. J. Holder, *Organometallics* **1998**, *17*, 59.

[65] R. H. Cragg, R. G. Jones, A. C. Swain, S. J. Webb, *J. Chem. Soc. Chem. Commun.* **1990**, 1147.

[66] R. G. Jones, U. Budnik, S. J. Holder, W. K. C. Wong, *Macromolecules* **1996**, *29*, 8036.

[67] R. D. Miller, E. J. Ginsburg, D. Thompson, *Polym. J.* **1993**, *25*, 807.

[68] T. J. Cleij, L. W. Jenneskens, *Macromol. Chem. Phys* **2000**, *201*, 1742.

[69] T. W. Weidman, P. A. Bianconi, E. W. Kwock, *Ultrasonics* **1990**, *28*, 310.

[70] R. G. Jones, R. E. Benfield, R. H. Cragg, P. J. Evans, A. C. Swain, *Polymer* **1994**, *35*, 4924.

[71] K. Matyjaszewski, D. Greszta, J. S. Hrkach, H. K. Kim, *Macromolecules* **1995**, *28*, 59.

[72] S. Gauthier, D. J. Worsfold, *Macromolecules* **1989**, *22*, 2213.

[73] V. Chandrasekhar In *Inorganic and Organometallic Polymers*; Springer: Berlin, 2005.

[74] M. Cypryk, Y. Gupta, K. Matyjaszewski, *J. Am. Chem. Soc.* **1991**, *113*, 1046.

[75] R. West, *Angew. Chem. Int. Ed.* **1987**, *26*, 1201.

[76] K. Sakamoto, K. Obata, H. Hirata, M. Nakajima, H. Sakurai, *J. Am. Chem. Soc.* **1989**, *111*, 7641.

[77] D. N. Roark, G. J. D. Peddle, *J. Am. Chem. Soc.* **1972**, *94*, 5837.

[78] Y. Wang, Y. Xie, P. Wei, R. B. King, H. F. Schaefer, III, P. von R. Schleyer, G. H. Robinson, *Science* **2008**, *321*, 1069.

[79] S. S. Sen, A. Jana, H. W. Roesky, C. Schulzke, *Angew. Chem.* **2009**, *121*, 8688.

[80] C. Aitken, J. F. Harrod, E. Samuel, *J. Organomet. Chem.* **1985**, *279*, C11.

[81] J. Y. Corey In *Advances in Organometallic Chemistry*; Robert, W., Anthony, F. H., Eds.; Academic Press: 2004; Vol. Volume 51, p 1.

[82] J. Y. Corey, Z. Xiao-Hong, *J. Organomet. Chem.* **1992**, *439*, 1.

[83] H. G. Woo, T. D. Tilley, *J. Am. Chem. Soc.* **1989**, *111*, 8043.

[84] M. Minato, T. Matsumoto, M. Ichikawa, T. Ito, *Chem. Commun.* **2003**, 2968.

[85] R. West, *J. Organomet. Chem.* **1986**, *300*, 327.

[86] J. Michl, *Acc. Chem. Res.* **1990**, *23*, 127.

[87] P. A. Bianconi, T. W. Weidman, *J. Am. Chem. Soc.* **1988**, *110*, 2342.

[88] P. A. Bianconi, F. C. Schilling, T. W. Weidman, *Macromolecules* **1989**, *22*, 1697.

[89] D. A. Smith, C. A. Freed, P. A. Bianconi, *Chem. Mater.* **1993**, *5*, 245.

[90] D. A. Smith, S. J. Joray, P. A. Bianconi, *J. Pol. Res.* **2005**, *12*, 393.

[91] H. K. Kim, C. R. Hove, C. K. Ober, *J. Macromol. Sci. Part A Pure Appl. Chem.* **1992**, *29*, 787

[92] A. Watanabe, M. Nanjo, T. Sunaga, A. Sekiguchi, *J. Phys. Chem. A* **2001**, *105*, 6436.

[93] M. J. S. Dewar, D. H. Lo, C. A. Ramsden, *J. Am. Chem. Soc.* **1975**, *97*, 1311.

[94] H. Matsumoto, K. Higuchi, Y. Hoshino, H. Koike, Y. Naoi, Y. Nagai, *J. Chem. Soc. Chem. Commun.* **1988**, 1083.

[95] A. Sekiguchi, T. Yatabe, H. Kamatani, C. Kabuto, H. Sakurai, *J. Am. Chem. Soc.* **1992**, *114*, 6260.

[96] N. Wiberg, C. M. M. Finger, K. Polborn, *Angew. Chem. Int. Ed.* **1993**, *32*, 1054.

[97] A. Sekiguchi, T. Yatabe, C. Kabuto, H. Sakurai, *J. Am. Chem. Soc.* **1993**, *115*, 5853.

[98] A. Sekiguchi, S. Nagase, *Chem. Org. Sil. Comp.* **1998**, *2*, 119.

[99] S. Nagase, H. Teramae, T. Kudo, *J. Chem. Phys.* **1987**, *86*, 4513.

[100] K. Abersfelder, A. J. P. White, H. S. Rzepa, D. Scheschkewitz, *Science* **2010**, *327*, 564.

[101] V. Percec, G. Johansson, J. Heck, G. Ungar, S. V. Batty, *J. Chem. Soc. Perkin Trans. 1* **1993**, 1411.

[102] G. Johansson, V. Percec, G. Ungar, D. Abramic, *J. Chem. Soc. Perkin Trans. 1* **1994**, 447.

[103] *IUPAC Compendium of Chemical Terminology*, 2002; Vol. 74, 497.

[104] C. T. Imrie, P. A. Henderson, *Chem. Soc. Rev.* **2007**, *36*, 2096.

[105] A. Abe, M. Ballauf, *Liquid Crystallinity in Polymers: Principles and Fundamental Properties*; John Wiley & Sons, Inc.: New York, 1991.

[106] J. C. Dubois, P. Le Barny, M. Mauzac, C. Noel, *Acta Polym.* **1997**, *48*, 47.

[107] T. Kato, *Liquid Crystalline Functional Assemblies and their Supramolecular Structures*; Springer: Berlin Heidelberg, 2008.

[108] V. S. K. Balagurusamy, G. Ungar, V. Percec, G. Johansson, *J. Am. Chem. Soc.* **1997**, *119*, 1539.

[109] R. Brückner, *Reaktionsmechanismen*; Spektrum, Akademischer Verlag: Heidelberg, 2003; Vol. 2.

[110] A. Ramacciotti, R. Fiaschi, E. Napolitano, *Tetrahedron: Asymmetry* **1996**, *7*, 1101.

[111] H. Meier, H. C. Holst, *Adv. Synth. Catal.* **2003**, *345*, 1005.

[112] J. Wu, M. D. Watson, L. Zhang, Z. Wang, K. Müllen, *J. Am. Chem. Soc.* **2003**, *126*, 177.

[113] E. J. Corey, P. L. Fuchs, *Tetrahedron Lett.* **1972**, *13*, 3769.

[114] A. K. Ghosh, Y. Wang, *J. Am. Chem. Soc.* **2000**, *122*, 11027.

[115] H. Finkelmann, G. Rehage, *Makromol. Chem. Rapid Commun.* **1980**, *1*, 31.

[116] C. Tschierske, *J. Mater. Chem.* **2001**, *11*, 2647.

[117] M. Ibn-Elhaj, A. Skoulios, D. Guillon, J. Newton, P. Hodge, H. J. Coles, *Liq. Cryst.* **1995**, *19*, 373

[118] J. Newton, H. Coles, P. Hodge, J. Hannington, *J. Mater. Chem.* **1994**, *4*, 869.

[119] C. Keith, R. A. Reddy, A. Hauser, U. Baumeister, C. Tschierske, *J. Am. Chem. Soc.* **2006**, *128*, 3051.

[120] I. A. Rousseau, H. Qin, P. T. Mather, *Macromolecules* **2005**, *38*, 4103.

[121] Y. Zhang, U. Baumeister, C. Tschierske, M. J. O'Callaghan, C. Walker, *Chem. Mater.* **2010**, *22*, 2869.

[122] E. Corsellis, D. Guillon, P. Kloess, H. Coles, *Liq. Cryst.* **1997**, *23*, 235

[123] G. H. Mehl, A. J. Thornton, J. W. Goodby, *Mol. Cryst. Liq. Cryst.* **1999**, *332*, 455

[124] M. Redmond, H. Coles, E. Wischerhoff, R. Zentel, *Ferroelectrics* **1993**, *148*, 323

[125] F.-H. Kreuzer, D. Andrejewski, W. Haas, N. Häberle, G. Riepl, P. Spes, *Mol. Cryst. Liq. Cryst.* **1991**, *199*, 345

[126] T. J. Bunning, H. E. Klei, E. T. Samulski, W. W. Adams, R. L. Crane, *Mol. Cryst. Liq. Cryst.* **1993**, *231*, 163

[127] K. D. Gresham, C. M. McHugh, T. J. Bunning, R. L. Crane, H. E. Klei, E. T. Samulski, *J. Polym. Sci., Part A: Polym. Chem.* **1994**, *32*, 2039.

[128] R. Pachter, T. J. Bunning, R. L. Crane, W. W. Adams, E. P. Socci, B. L. Farmer, *Macromol. Theory Simul.* **1993**, *2*, 337.

[129] S. G. McNamee, T. J. Bunning, S. S. Patnaik, C. M. McHugh, C. K. Ober, W. W. Adams, *Liq. Cryst.* **1995**, *18*, 787

[130] D. J. Gardiner, C. J. Davenport, J. Newton, H. J. Coles, *J. Appl. Phys.* **2006**, *99*, 113517.

[131] D. J. Gardiner, H. J. Coles, *J. Appl. Phys.* **2006**, *100*, 124903.

[132] K. Merkel, A. Kocot, J. K. Vij, R. Korlacki, G. H. Mehl, T. Meyer, *Phys. Rev. Lett.* **2004**, *93*, 237801.

[133] H. Katayama, K. Taniguchi, M. Kobayashi, T. Sagawa, T. Minami, F. Ozawa, *J. Organomet. Chem.* **2002**, *645*, 192.

[134] T. J. Barton, J. Lin, S. Ijadi-Maghsoodi, M. D. Power, X. Zhang, Z. Ma, H. Shimizu, M. S. Gordon, *More Compelling Evidence That Silicon is Better Than Carbon: The Thermal Isomerization of Olefins to Carbenes*; Wiley-VCH Verlag GmbH, 2008.

[135] P. A. Tipler, *Physics for Scientists and Engineers*; Worth Publishers Inc.: New York, 1994.

[136] H. Kelker, R. Hatz, *Handbook of Liquid Crystals*; Verlag Chemie: Weinheim, 1980.

[137] M. Seitz, T. Plesnivy, K. Schimossek, M. Edelmann, H. Ringsdorf, H. Fischer, H. Uyama, S. Kobayashi, *Macromolecules* **1996**, *29*, 6560.

[138] G. R. Strobl, *The Physics of Polymers*; Springer: Berlin / Heidelberg, 1996.

[139] in *Collection of RIS Models, Rotational Isomeric State Models in Macromolecular Systems*, Vol. 131 –132 (Eds.: A. Abe, H.-J. Cantow, P. Corradini, K. Dusˇsek, S. Edwards, H. Fujita, G. Glçckner, H. Hçcker, H.-H. Hçrhold, H.-H. Kausch, J. Kennedy, J. Koenig, A. Ledwith, J. McGrath, L. Monnerie, S. Okamura, C. Overberger, H. Ringsdorf, T. Saegusa, J. Salamone, J. Schrag, G. Wegner), Springer Berlin/Heidelberg, 1997, pp. 19–476.

[140] A. Feigl, A. Bockholt, J. Weis, B. Rieger In *Adv. Polym. Sci.*; Muzafarov, A. M., Ed.; Springer Berlin / Heidelberg: 2011; Vol. 235, p 1.

[141] Q. Zhang, J.-Q. Huang, M.-Q. Zhao, W.-Z. Qian, F. Wei, *Chem. Sus. Chem.* **2011**, *4*, 864.

[142] *Advances in Silicon Science*; J. Matisons, Ed.; Springer: Heidelberg, 2009; Vol. 1.

[143] A. J. Chalk, J. F. Harrod, *J. Am. Chem. Soc.* **1965**, *87*, 16.

[144] J. F. Harrod, A. J. Chalk, *J. Am. Chem. Soc.* **1964**, *86*, 1776.

[145] I. E. Markó, S. Stérin, O. Buisine, G. Mignani, P. Branlard, B. Tinant, J.-P. Declercq, *Science* **2002**, *298*, 204.

[146] A. Hopf, K. H. Dötz, *J. Mol. Cat. A* **2000**, *164*, 191.

[147] H. J. Frohn, A. Lewin, V. V. Bardin, *J. Organomet. Chem.* **1998**, *570*, 255.

[148] A. Fürstner, *Angew. Chem. Int. Ed.* **1993**, *32*, 164.

[149] R. G. Jones, S. J. Holder, *Silicon Containing Polymers*; Kluwer Academic: Dordrecht, 2000, pp. 353.

[150] R. G. Jones, S. J. Holder, *Polym. Int.* **2006**, *55*, 711.

[151] T. Tamai, M. Watanabe, Y. Hatanaka, H. Tsujiwaki, N. Nishioka, K. Matsukawa, *Langmuir* **2008**, *24*, 14203.

[152] A. Feigl, **2011**, Dissertation; Technische Universität München.

[153] O. Kylián, H. Rauscher, B. Denis, L. Ceriotti, F. Rossi, *Plasma Processes Polym.* **2009**, *6*, 848.

[154] A. von Keudell, P. Awakowicz, J. Benedikt, V. Raballand, A. Yanguas-Gil, J. Opretzka, C. Flötgen, R. Reuter, L. Byelykh, H. Halfmann, K. Stapelmann, B. Denis, J. Wunderlich, P. Muranyi, F. Rossi, O. Kylián, N. Hasiwa, A. Ruiz, H. Rauscher, L. Sirghi, E. Comoy, C. Dehen, L. Challier, J. P. Deslys, *Plasma Processes Polym.* **2010**, *7*, 327.

[155] A. Schwabedissen, E. C. Benck, J. R. Roberts, *Phys. Rev. E* **1997**, *56*, 5866.

[156] S. V. Roth, R. Döhrmann, M. Dommach, M. Kuhlmann, I. Kröger, R. Gehrke, H. Walter, C. Schroer, B. Lengeler, P. Müller-Buschbaum, *Rev. Sci. Instrum.* **2006**, *77*, 085106.

[157] P. Busch, M. Rauscher, D.-M. Smilgies, D. Posselt, C. M. Papadakis, *J. Appl. Crystallogr.* **2006**, *39*, 433.

[158] D.-M. Smilgies, *J. Appl. Crystallogr.* **2009**, *42*, 1030.

[159] J. S. Gutmann, P. Müller-Buschbaum, D. W. Schubert, N. Stribeck, D. Smilgies, M. Stamm, *Physica B* **2000**, *283*, 40.

[160] H. J. Bestmann, H. Frey, *Liebigs Ann. Chem.* **1980**, *1980*, 2061.